Effect of heterochromatin (com)position on DNA replication timing

Effekt der Heterochromatin (Kom)position auf den DNA Replikationszeitpunkt
Vom Fachbereich Biologie der Technischen Universität Darmstadt zur Erlangung des akademischen Grades eines Doctor rerum naturalium
genehmigte Dissertation von Kathrin Sarah Heinz, M.Sc. aus Darmstadt
Tag der Einreichung: 31.08.2018, Tag der Prüfung: 26.10.2018
Darmstadt, Technische Universität Darmstadt

1. Gutachten: Prof. Dr. M. Cristina Cardoso
2. Gutachten: Prof. Dr. Bodo Laube

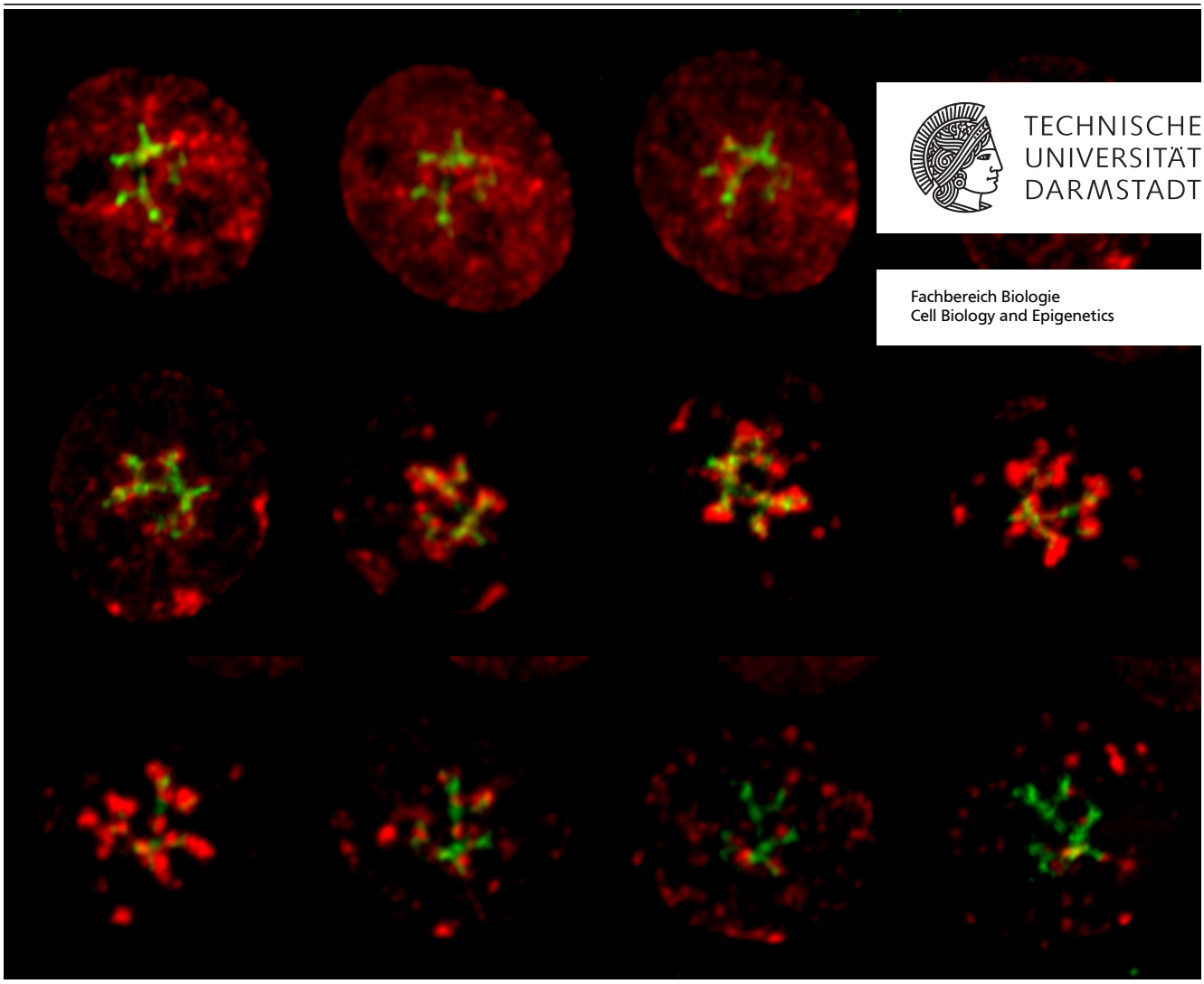

Effect of heterochromatin (com)position on DNA replication timing
Effekt der Heterochromatin (Kom)position auf den DNA Replikationszeitpunkt

Genehmigte Dissertation von Kathrin Sarah Heinz, M.Sc. aus Darmstadt

1. Gutachten: Prof. Dr. M. Cristina Cardoso
2. Gutachten: Prof. Dr. Bodo Laube

Tag der Einreichung: 31.08.2018
Tag der Prüfung: 26.10.2018

Darmstadt, Technische Universität Darmstadt

There are no problems, there are only challenges.

— H. D. H.

Summary

The accurate replication of the genome prior to each cell division is of upmost importance as mistakes are potentially transferred to subsequent generations but can also lead to genetic mutations, karyotype aberrations or to diseases that may result in cancer or cell death. Therefore, the duplication of the genome is one of the most crucial processes in any living organism and thus essential for development and reproduction.

The process of DNA replication is a highly organized process, both spatially and temporally, where specific genomic regions undergo DNA replication at distinct times during S-phase (Synthesis-phase). During development of an organism, DNA replication is a flexible process and several chromatin properties have been proposed as potential regulators thereof. Although a lot is known on the composition of the basic DNA replication machinery, it is mostly unclear, how its activity is regulated.

In the context of the present thesis, I made use of different targeting and manipulation approaches to elucidate the impact of potential regulators that control DNA replication dynamics in mammalian cells. To this end, I established and validated a novel targeting strategy to manipulate and reposition subcellular structures and molecules.

I first took advantage of constitutive heterochromatin as a prominent and well-characterized structure within the mammalian nucleus and repositioned it to the nuclear lamina to assess the nuclear position of DNA as one potential regulator of DNA replication dynamics. Using time-lapse microscopy, I was able to observe that constitutive heterochromatin, known to replicate during late S-phase, was replicated during mid S-phase when repositioned to the nuclear periphery. For this reason, I proposed that constitutive heterochromatin was activated in *trans* according to the domino model of origin activation by nearby (mid S) firing origins. This data provided a novel approach to reposition large genomic regions and to manipulate nuclear DNA position within the nucleus. Here, I established the nuclear position as a novel regulator of DNA replication timing.

Secondly, I made use of female *Microtus cabrerae* cells, which are characterized by their very prominent giant sex chromosomes with large coupled heterochromatic blocks. Again, I made use of a well-defined structure within the nucleus and manipulated the histone acetylation level as another potential regulator of DNA replication timing. First, I manipulated the global acetylation level by HDAC inhibition via drug-treatment and secondly, I specifically targeted a histone acetyltransferase to the inactive and active X chromosome. I elucidated the impact of histone acetylation level on DNA replication dynamics in the vole genome. I was able to show that both manipulation assays, global and site-directed, were sufficient to significantly increase the histone acetylation level, resulting in a prolongation of total S-phase duration and substage duration. The DNA replication onset of facultative heterochromatin was shifted toward early S-phase, as DNA content was further increased in early S-phase in treated samples. I was able to detect a negative effect of histone hyperacetylation on DNA replication fork speed. Here, I assessed the validity and reproducibility of DNA replication regulation by histone acetylation level across species.

Zusammenfassung

Die akkurate und fehlerfreie Duplikation des Genoms vor jeder Zellteilung ist von großer Bedeutung, da potenzielle Fehler an Nachfolgegenerationen weitergegeben werden können. Potenzielle Fehler können zu genetischen Mutationen, karyotypischen Aberrationen und Krankheiten wie Krebs oder zum Zelltod führen. Die Replikation des Genoms ist folglich einer der wichtigsten Prozesse in jedem lebenden Organismus und essentiell für dessen Entwicklung und Reproduktion. Der Prozess der DNA Replikation ist räumlich und zeitlich hoch organisiert, da spezifische genomische Regionen in festen Zeitfenstern während der S-Phase (Synthese-Phase) dupliziert werden. Während der Entwicklung ist die Duplikation des Genoms ein flexibler Prozess und verschiedenste epigenetische Eigenschaften des Chromatins wurden als potenzielle Regulatoren postuliert. Obwohl die grundlegende Maschinerie der DNA Replikation bekannt ist, ist die eigentliche Regulation ihrer Aktivität weitestgehend unbekannt.

Im Rahmen dieser Dissertation habe ich mich mit verschiedenen Targeting- und Manipulationsmethoden befasst, um gezielt verschiedene potenzielle Regulatoren der DNA Replikation in Säugerzellen zu manipulieren, um deren Effekt und Einfluss zu bewerten. Hierzu habe ich eine neue Targetingstrategie etabliert sowie validiert, um subzelluläre Strukturen und Moleküle zu manipulieren und zu repositionieren.

Somit habe ich mir zunächst die prominente und gut charakterisierte Struktur des konstitutiven Heterochromatins in Mauszellen zu Nutze gemacht und dieses an die nukleare Lamina transferiert. Diese Repositionierung vom Inneren des Zellkerns an die Peripherie wurde genutzt, um den Einfluss der Position von DNA auf ihren DNA Replikationszeitpunkt zu evaluieren. Mittels Lebendzellmikroskopie und Zeitrafferaufnahmen war ich in der Lage zu beobachten, dass repositioniertes konstitutives Heterochromatin, welches eigentlich erst in der späten S-Phase repliziert wird, durch die Repositionierung bereits in der mittleren S-Phase repliziert wird. Daher nahm ich an, dass die Replikation des transferierten konstitutiven Heterochromatins in *trans* aktiviert wurde, gemäß dem sogenannten Domino Model. Dieses Model postuliert die Aktivierung von feuernden Replikationsursprüngen durch naheliegende feuernde Startpunkte der mittleren S-Phase. Meine Ergebnisse indizieren nicht nur eine Aktivierung in *cis* entlang des Chromosoms, sondern auch in *trans* über verschiedene Chromosomen hinweg. Diese Daten validieren die Wirksamkeit der Methode, um die Position von DNA gezielt zu manipulieren und demonstrieren zudem den Einfluss der Lokalisation von DNA auf ihren Zeitpunkt der DNA Replikation.

Außerdem machte ich mir weibliche *Microtus cabrerae* Zellen zu Nutze, welche ebenfalls eine prominente Struktur aufweisen und zwar die der gigantischen Sexchromosomen, die große heterochromatische Blöcke haben. Ich manipulierte das Histonacetlyierungslevel als potenziellen Regulator der Organisation der DNA Replikation. Ich erhöhte global mittels HDAC Inhibitor und durch gezieltes Targeting einer Histonacetyltransferase an die Sexchromosomen das Histonacetylierungslevel in dieser Spezies. Ich war in der Lage zu demonstrieren, dass beide Methoden zu einer Hyperacetylierung führen und die Dauer der gesamten S-Phase sowie der einzelnen Subphasen verlängern. Dies ging einher mit einer Erhöhung der genomischen DNA bereits in der frühen S-Phase in behandelten Zellen. Dies zeigte eine verfrühte DNA Replikation des fakultativen Heterochromatins, das eigentlich erst in der mittleren S-Phase repliziert. Die globale Hyperacetylierung hatte außerdem einen negativen Effekt auf die Geschwindigkeit der Replikationsgabel. Mit dieser Studie demonstriere ich den spezies-übergreifenden Einfluss der Histonacetylierung als Regulator der DNA-Replikation.

Preface

This thesis is built up of three different manuscripts:

Chapter I: submitted to: Imaging Gene Expression: Methods and Protocols, Methods in Molecular Biology
Chapter II: Heinz et al. 2018, published in Nucleic Acid Research, 2018, Volume 46, No. 12
(Taken from https://doi.org/10.1093/nar/gky368)
Chapter III: in submission to Epigenetics and Chromatin

To link all individual chapters together, this thesis starts with a general introduction with common aspects, before the three individual chapters (chapter I-III) follow. Each chapter is composed of its own introduction, material and methods, results and discussion as well as its own bibliography. At the end I discuss and conclude all three chapters in relation to each other with a general perspective for further experiments.

List of Contributions

Chapter I: Targeted manipulation/ repositioning of subcellular structures and molecules

K. S. Heinz wrote the manuscript and prepared all of the figures and figure legends (I.1,I.2,I.3). M. C. Cardoso conceived and supervised the project, and revised the manuscript.

Chapter II: Peripheral re-localzation of constitutive heterochromatin advances its replication timing and impairs maintenance of silencing marks

K. S. Heinz wrote the manuscript and prepared all of the figures and figure legends (II.1, II.2, II.3, II.4, II.5, II.6, II.7, II.8, II.S1, II.S2, II.S3, II.S4, II.S5, II.S6, II.S7, II.S8, II.S10, II.S11, II.S12 - except II.S9). **K. S. Heinz** performed and analyzed all experiments. T. Török helped with pulse labeling, image acquisition therefor and time-lapse microscopy for figure II.4 and II.S4. A. Rapp wrote R script for analysis and provided expertise for figure II.5. A. Scholl performed western blot analysis for figure II.S2B. A. K. Ludwig helped with the Priithon script for user-independent image analysis and prepared figure II.S9. C. S. Casas-Delucchi and M. C. Cardoso conceived and supervised the project, and revised the manuscript.

Chapter III: DNA replication dynamics of vole genome and its epigenetic regulation

K. S. Heinz wrote the manuscript and prepared all of figures and figure legends (III.1, III.4, IIII.5, III.6, III.7, III.S1, III.S2, III.S3, III.S4, III.S5, III.S6 - except figures III.2,III.3). **K. S. Heinz** performed and analyzed all experiments (except figures III.1, III.2, III.3 and III.S1). I. Romero-Fernandez performed X-FISH for figure III.1A and performed immunostainings for figure III.S1. **K. S. Heinz** analyzed data for figure III.S1 and prepared figure III.S1. C. S. Casas-Delucchi performed pulse-chase experiments and time-lapse microscopy, analyzed the data for figure III.2 and IIII.3 and prepared the figures. A. Rapp wrote R script for analysis and provided expertise for figures III.8 and III.9. J. A. Marchal and M. C. Cardoso provided expertise, conceived the project and revised the manuscript.

List of Figures

List of Tables

Contents

1 Introduction

1.1 The most fundamental principle and its importance in cell biology

In 1855, Rudolf Virchow claimed that every cell arises from another cell: *Omnis cellula e cellula*. This postulation was one of the most important declarations in cell biology as it indicates that every cell is an offspring from another cell. Thus, a cell needs to divide to ensure its persistence. But, if a cell would simply divide over several cell cycles, it would dilute its genetic information over several generations and consequently loose its genetic information. Consequently, prior to mitosis a cell must ensure that its genetic information is precisely duplicated and subsequently distributed to its daughter cells equally. This fundamental biological process is conserved throughout all kingdoms of life. The procedure relies on the error-free and complete duplication of the genome before a cell can divide. If not, mistakes can lead to genetic mutations or karyotype aberrations that may result in diseases or cell death. The duplication of DNA is therefore one of the most crucial processes in any living organism and essential for development and reproduction.

1.2 The history of DNA replication

Half a century ago, with the discovery of the DNA double helix structure [1], the mechanism of its duplication was suggested as a semi-conservative [2] copying the nucleotide sequence into two daughter strands. With the first isolation of DNA polymerase by Kornberg [3], there was this fundamental question of how genomes are duplicated prior to cell division[4]. Combining genetics and *in vitro* biochemistry tools lead to the assumption that the fundamental features and components of DNA replication are well conserved throughout evolution from bacteria to mammals (reviewed in [4]). Microscopic observation of nuclei became a powerful tool to investigate the spatio-temporal organization of DNA replication within the context of nuclear architecture. Monitoring ongoing DNA synthesis provides a way to directly detect the sites of nuclear DNA replication after introducing labeled nucleotides into the cells. Initially, radioactive thymidine was used [5] and later, with the development of antibodies specifically detecting halogenated thymidine analogs [6, 7]. Immunofluorescence analysis of nuclear replication structures became reality [8–10]. More recently, live-cell analysis of progression of DNA replication was made possible by introducing fluorescently conjugated nucleotides or by the expression of fluorescent replication factors [4, 11, 12]. With the help of these approaches, DNA replication was found to occur at discrete subnuclear sites called replication foci, which accumulate multiple DNA replication factors and cell cycle proteins [11–13]. *In situ* visualization of active sites of DNA replication results in distinct replication patterns that change upon S-phase progression and are typically divided into early, mid and late S-phase patterns, based on their distinct morphological and topological features [10] (Figure 1.1).

These characteristic patterns are built by DNA replication foci, structures of approximately 120 nm in size that are stably maintained throughout the cell cycle [15]. Each focus of DNA replication represents a cluster of coordinately activated sites of replication that are in close spatial proximity. Today, studying the localization, composition and dynamics is feasible and studies are based on the elucidation of how DNA replication is regulated on a cellular level. Time-lapse microscopy of living mammalian cells over the progression of S-phase and even an entire cell cycle has shown that early S-phase immediately follows the onset of DNA replication [4]. In early S-phase a multitude of small DNA replication foci are distributed throughout the whole nucleus, excluding the nucleolus. During mid S-phase, the foci are uniformly larger and located at the nucl(eo)lar periphery. At the end of S-phase during late S-phase, the sites of DNA replication are consolidated into a smaller number of very large foci. These DNA replication dynamics are conserved from hydra to mammals [16, 17] and reflect the higher order 3D organization of chromatin in the nucleus [18, 19]. Early DNA replication foci correspond to euchromatic regions and R bands, characterized by a high gene density and mostly found in the interior of the nucleus, whereas mid foci represent facultative heterochromatin accommodated in the nucle(ol)ar periphery and late foci mark constitutive heterochromatin [20]. Early replication patterns represent actively transcribed euchromatin, whereas late replicating patterns are associated with transcriptionally inactive heterochromatic regions. The appearance of such distinct patterns demonstrates that clusters of replication origins are activated in a highly coordinated manner with some nuclear regions being specifically activated earlier than others. This conserved DNA replication mode raises the question of how specific replication origins are selected to fire in distinct S-phase stages.

1.3 Increasing genome complexity means increasing challenges

The site where DNA replication is initiated is called the origin of replication (ori). In prokaryotes the entire genome is replicated from one single replication origin in a timely fashion, whereas in mammals DNA replication becomes more

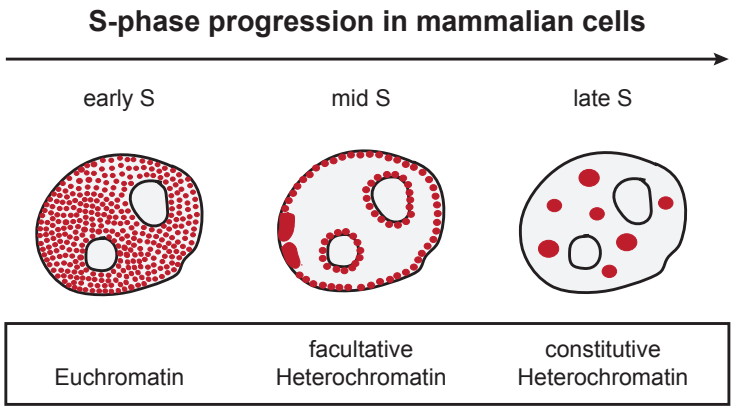

Figure 1.1.: Schematic representation of the spatio-temporal organization of DNA replication foci patterns (red) during S-phase progression within the mammalian cell nucleus. In early S-phase, when mostly euchromatin is replicated, a multitude of small replication foci are distributed throughout the whole nucleus. In mid S-phase, DNA replication foci are mostly concentrated at the nucle(ol)ar periphery and at the inactive X-chromosome(s). In this substage, mostly facultative heterochromatin is replicated. In late S-phase, replication foci mostly colocalize with constitutive heterochromatin. (Figure modified after [14]).

difficult, due to their larger genome size and complexity. When genome size and complexity increase, a fast enough DNA replication of the entire genome is more difficult to accomplish, resulting in the need of a larger number of DNA replication origins. For instance, the number of DNA replication origins in humans was estimated to be 50000 [21]. In some single cell eukaryotes, such as budding yeast, replication origins are known to be genetically defined by a consensus sequence and the time of origin firing is constant. But already in fission yeast, the definition of DNA replication origins is less stringent. When it comes to metazoan, no consensus sequence defining origins of replication has been identified, yet [22–26]. With more required sites of replication initiation, the regulation of their firing becomes an issue. First, a cell needs to ensure an error-free duplication of DNA in a timely fashion. Second, a re-replication of any genomic region has to be avoided, which might be a consequence of uncoordinated firing. And if that wasn't enough, the process of DNA replication needs to be coordinated with other chromatin-based processes, such as transcription and the concomitant chromatin remodeling [27], further underlining the importance of control and organization of origin firing.

1.4 The molecular process of DNA replication

With the help of prokaryotic and eukaryotic models the molecular factors and processes involved in DNA replication were identified *in vitro* [4, 28, 29]. These pioneer studies were the basis for the understanding of essential factors, their interactions and the enzymatic processes involved in DNA replication. The transition to an *in vivo* eukaryotic system was another milestone, when yeast genetic tools became available to study DNA replication [30, 31]. Studies in yeast are a powerful tool to dissect the differential biochemical components of the DNA replication process, which includes setting up the origin assembly, the process of origin firing and the synthesis of DNA itself. Nevertheless, when it comes to the spatio-temporal organization of DNA replication, there are major differences between yeast and metazoans that make it difficult to generalize conclusions arising from studies performed in yeast. But, as the biochemical components of these processes of initiation and replication are well conserved from yeast to mammals and seem to work along the same principle, these studies shed light into the regulation of this complex mechanism (reviewed in [32]). The procedure till a DNA replication origin can fire includes several steps, including origin licensing, activation and finally the initiation of DNA synthesis (Figure 1.2). These steps are described in more detail in the following.

1.4.1 Assembly of the pre-replicative complex (pre-RC)

Before DNA synthesis during S-phase starts, a cell determines where the next round of DNA replication can potentially start. Origins of replication are determined even before G1, at the end of mitosis. Therefore this happens in metazoans in the absence of a nuclear membrane.
First, the origin recognition complex (ORC) binds during telophase to potential DNA replication origins. The ORC is composed of six related proteins, conserved from yeast to human [33]. During the transition from mitosis to G1 the ORC recruits the initiation factors Cdc6 and Cdt1 (Figure1.2A). Cdc6, an AAA+ ATPase, modulate ORC binding to chromatin

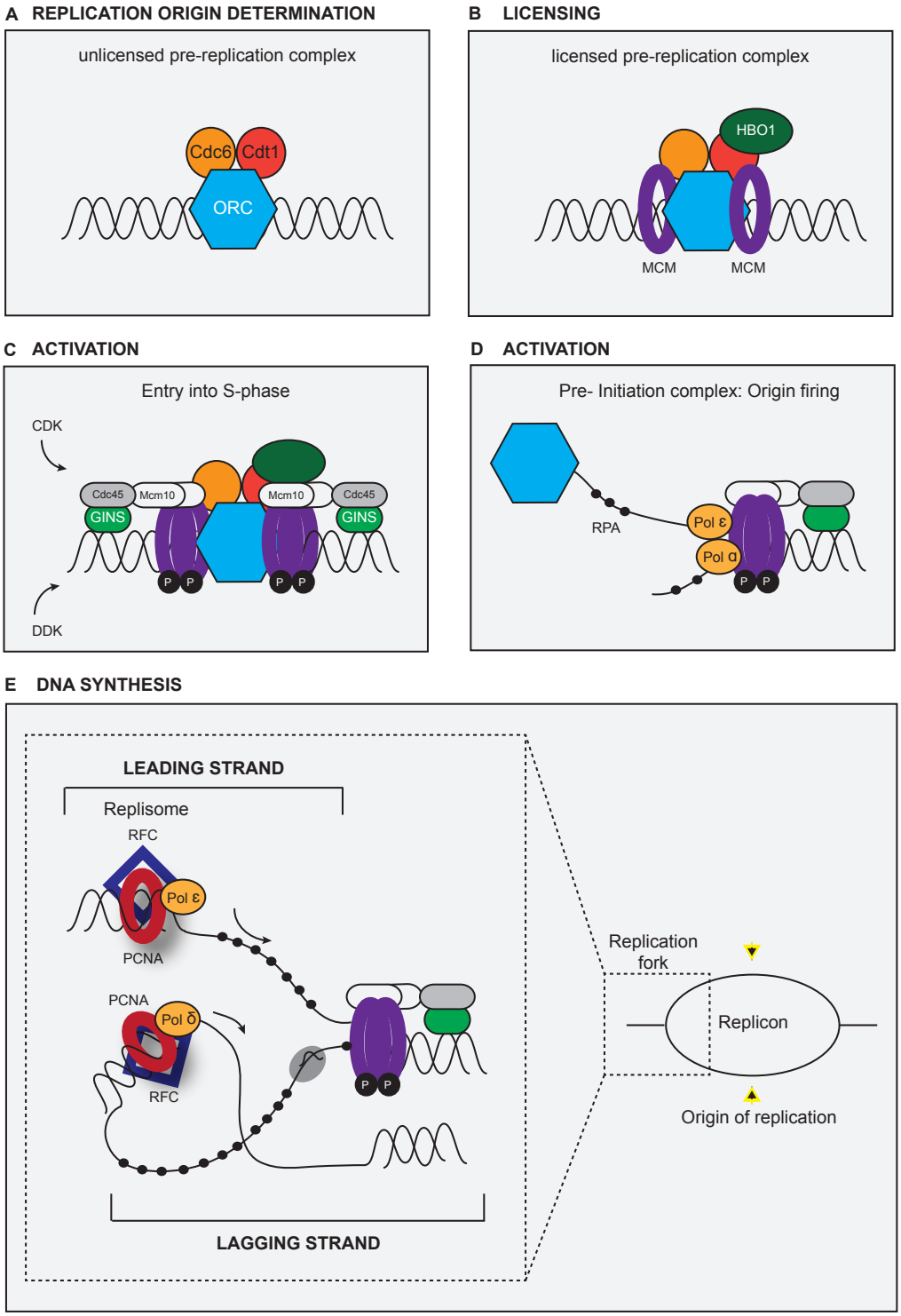

Figure 1.2.: Schematic representation of the multi-step process of DNA replication: from origin determination, licensing, activation to DNA synthesis (A-E). (A) Origin determination: The origin recognition complex (ORC) binds to chromatin during late S-phase and recruits Cdc6 and Cdt1. (B) Cdt1 binds to histone acetyltransferase HBO1, which is required for pre-RC licensing by MCM-loading. (C) Activities of DDK and CDK lead to the assembly of pre-IC (pre-initiation complex), including the binding of MCM10, Cdc45 and GINS. (D) The DNA double helix is unwound by the origin activation. The replication protein A (RPA) stabilizes single-stranded DNA and DNA polymerases α and ϵ are recruited. DNA polymerases α has also a primase activity, synthesizing RNA primers on single-stranded DNA. (E) Processive DNA synthesis is accomplished after a polymerase switch to DNA polymerase δ and the loading of the proliferating cell nuclear antigen (PCNA) sliding clamp by replication factor C (RFC). The duplication of the lagging strand happens in a discontinuous manner, with several rounds of Okazaki fragments, starting each with the synthesis of a new RNA primer. (Figure adapted from [32]).

[34] and inhibits ORC binding to non-specific DNA [35]. The main function of ORC, Cdc6 and Cdt1 is the loading of the Mcm2-7 complex (MCM) onto chromatin and to complete the licensed pre-replication complex (pre-RC). After MCM loading the ORC, Cdc6 and Cdt1 become dispensable for origin firing [36, 37]. Structural studies have shown that ORC and Cdc6 may function as a clamp loader complex for opening and closing MCM around DNA at origins [38]. Cdt1 recruits HBO1, a histone H4 acetyltransferase (HAT) to origins. The HAT activity of HBO1 is required for the loading of the MCM complex [39] (Figure 1.2B). MCM renders a licensed origin for the following S-phase. MCM has *in vitro* a helicase activity, therefore it is considered as the putative replicative helicase [40] able to unwind DNA replication origins [41]. But there are contradictory observations of the excess of nuclear MCM and its accumulation far from active replication foci and its proposed role as the replicative helicase [42, 43]. Nevertheless, it was shown that a fraction of MCM is colocalizing with sites of active DNA replication, supporting its role as replicative helicase [44].

1.4.2 Firing of origins: from pre-RC to the replication fork

Next, the pre-RC complex must be activated by cyclin-dependent kinase (CDK) and DBf4-dependent kinase (DDK) activities [45–48]. This phosphorylation of the pre-RC leads to the recruitment of Cdc45, Mcm10, Sld3 and GINS to DNA replication origins [49–51] (Figure 1.2C). These factors are required for initiation and for the unwinding of replication origins as well as for the recruitment of replicative DNA polymerases. As a consequence, a replication bubble is built containing two replication forks that progresses in opposite directions, when leading and lagging strands are replicated. The transition from pre-RC to elongation is initiated by interaction of Mcm10 with Orc2 and several Mcm2-7 subunits [52, 53]. Cdc45 is recruited to the complex [54, 55] and stimulates the helicase activity of the Mcm2-7 complex [56, 57]. The configuration containing single-stranded DNA is stabilized by replication protein A (RPA), which further stimulates the unwinding of DNA replication origins [41]. The binding of Cdc45 and RPA results in the recruitment of the core DNA replication machinery, including DNA polymerases ϵ and α to the now open replication origins [58], forming another complex, the so-called pre-initiation complex (pre-IC) (Figure 1.2D). DNA polymerase α, a primase, is the only known DNA dependent polymerase that is able to start *de novo* synthesis on single-stranded DNA and is, therefore, recruited to origins to synthesize short RNA primers for the leading and lagging strand. After the synthesis of a primer, DNA polymerases are exchanged and DNA polymerase α is replaced by DNA polymerase δ or ϵ, which have a higher processivity and a proofreading exonuclease activity [59]. The enhanced processivity involves the association to the proliferating cell nuclear antigen (PCNA), a homotrimeric ring, which serves as a loading platform for several elongation factors [60]. PCNA is loaded by the replication factor C (RFC) and moves with the replication fork at active sites of DNA replication. In addition, MCM, Cdc45 and GINS also move away from replication origins as part of the replication fork machinery [49], indicating a role in the elongation process besides their function in initiation.

1.4.3 Finally, ready for DNA synthesis

Unpon activation, DNA at licensed pre-RC is unwound, leading to the assembly of two replication forks, which progress in opposite directions, until they collide with a replication fork originating from a neighboring replication origin [61] (Figure 1.2E). The unit of DNA, which is replicated from one single replication origin, also called a replicon, is generally a symmetric structure with an origin located in the middle. The molecular machinery of DNA replication, which is in charge to replicate a replicon, is termed the replisome. At the chromatin fiber level, DNA replication is characterized by the location of replisomes (DNA synthetic complexes) on the DNA molecules. During DNA replication only a subset of potential origins of replication will be activated in an individual cell in the cell cycle [4, 62–64]. Each origin of replication, when activated, gives rise to two replication forks that travel along the template DNA. This initiation event of DNA synthesis at a particular origin of replication provides a functional definition of replicon as a chromosome segment. To ensure the duplication of the complete genome in a reasonable time frame, multiple replicons must be orchestrated together in parallel at any given time point during S-phase.

1.5 Organization of DNA replication in mammals

1.5.1 Replication origin definition: Of yeasts and men

In *Saccharomyces cerevisiae*, DNA replication origins were characterized as sequences that are able to replicate autonomously, when inserted into a plasmid, and therefore were called autonomous replicating sequences (ARS). They all share a ∼11 bp long conserved sequence, the autonomous consensus sequence (ACS) (reviewed in [65, 66]. But, ACS alone is not sufficient to predict a functional DNA replication origin. A region of helical instability close to ACS is also required for origin activity [67], indicating that sequence alone, even in yeast is not the only determinant for an active replication origin. In addition, replication origins in yeast have a binding site for the transcription factor Abf1, which

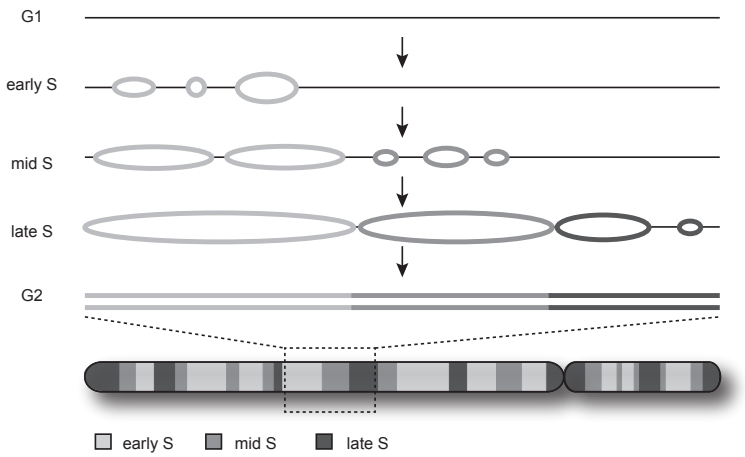

Figure 1.3.: Schematic representation of the Domino Model for the progression of genome replication. One replication cluster initiates DNA replication during early S-phase and DNA synthesis proceeds bidirectional as a replication bubble. According to the next-in-line activation, this activates the initiation of neighboring replicon clusters, which in turn activate DNA replication at later replicon clusters (dark grey) till the complete chromosome is duplicated in G2 phase. (Figure adapted from [4])

might promote origin activation [68]. Binding of Gcn5, a histone acetyltransferase (HAT), is associated with transcriptional activity [69], increasing DNA replication when tethered to an origin [70]. In metazoan no consensus sequence defining DNA replication origins has been found [24, 26]. In higher eukaryotes sequence elements defining DNA replication origins are much weaker. Indeed some potential DNA replication origins were found, but up until now, no sequence motif could be identified. This fact indicates that other potential regulators, such as DNA structure and chromatin might play a role in the regulation of DNA replication timing [71].

1.5.2 Propagation of DNA replication as a domino

Replication of a specific genomic region facilitates subsequent loading of new replication factors at neighboring sites, indicating that the act of DNA replication induces local changes in chromatin condensation, which in turn promotes the access, recruitment and initiation of additional replication units [4]. DNA replication starts at sites with an open chromatin conformation, resulting in a decondensation of adjacent regions, which would normally not support replication initiation. Replication helicases like MCM proteins promote local chromatin decondensation. Studies on the molecular dynamics of the replisome demonstrated that neighboring chromatin loci are not replicated by the same replication machinery, but rather a new replisome is assembled, preferentially nearby already active replication sites [72]. The observation that new sites of active DNA replication almost always appear in close proximity to active sites [12] has led to the idea of a domino model with a 'next-in-line' activation mechanism, determining the temporal order of origin activation [32]. On a genome-wide scale, the domino model (Figure 1.3) would lead to a simple, self-propagating mode by which the entire chromosome become fully duplicated by simply spreading the replication process using the 'next-in-line' principle [4, 72].
Stochastic firing [73] of the first origin clusters lead to a chain reaction of activation of later origin clusters, depending on the relative spatial distribution in the genome. This domino effect model is compatible with the increasing efficiency model [63, 74], which claims that origin firing efficiency increases when S-phase progresses, from early to late S-phase. Origins of early S-phase are quite inefficient at initiating DNA replication, in contrast to late S-phase origins, although occurring in a random manner, the relative firing efficiency was significantly higher [74]. This increased efficiency of late replication foci is not caused by polymerase recycling, but rather by the fact that upon S-phase progression, the likelihood increases that any given region of the genome is proximal to a site of DNA replication. Consequently, even origins located in hyper-condensed, later replicating regions such as constitutive heterochromatin become accessible as more of the surrounding chromatin undergoes replication [4]. It has been shown in human cells that the spatial continuity of replication foci correlated with their genomic continuity along chromosomes [75]. This model is supported by the fact that neighboring replication domains tend to initiate replication at similar time points on human chromosomes [76], as well as by the observation that the temporal order of DNA replication of distinct regions corresponds to their linear order in the genome [32, 77]. These 'replication waves' are most likely transmitted by the local destabilization or changes in the chromatin structure resulting from replication activity itself. Such structural changes, caused by active DNA replication

process, would render neighboring regions more prone to replication initiation and result in a self-propagation of DNA replication [32].

1.5.3 DNA replication as a flexible and non-static process

At a single origin level, the firing process is believed to be a stochastic one: not every potential origin fires in every cell cycle [73], but can vary in their firing efficiency [78]. Underlining the fact that DNA replication is not a static process [32]. Changes throughout development and with differentiation rather demonstrate that it is a quite flexible process [79–83]. During early embryogenesis, DNA replication starts at the same time, randomly distributed all over the nucleus. This mode of DNA replication results in a very short inter-origin distance (IOD) of around 15 kbp [82, 84]. During mid blastula transition, a re-arrangement of DNA replication occurs, which correlates with the onset of transcription and global changes in the structure of chromatin, leading to much longer IODs. Furthermore, the re-programming of mouse somatic cells to a pluripotent state is accompanied with a reduced size of replication domains [85]. These changes during the development of an organism, clearly demonstrate that DNA replication origins are not defined at a sequence level and their selection can adapt throughout differentiation. Interestingly, the described longer IODs in differentiated mammalian nuclei (around 100 kb) can be reprogrammed in Xenopus egg extract to shorter and more embryonic-like IODs of 15 kb, when conditioned in mitotic egg extracts [86]. This redistribution of replication origins comes along with a remodeling of loop size and correlate with the redistribution of ORC [87].
In mammalian cells, around 20% of the genome changes its DNA replication timing during induced differentiation of embryonic stem cells to neural progenitor cells [85]. The idea of DNA replication timing being controlled by a mechanism beyond the level of DNA sequence first appeared, when it was observed that in female mammalian cells, one of the X chromosomes is randomly inactivated and replicates with different dynamics than its active homolog [88]. This notion came up already in the 1960s, clearly showing that genetics alone cannot determine DNA replication timing. In metazoan there is a correlation between transcription, early DNA replication timing and open chromatin structure. Usually actively transcribed R-bands replicate early, while gene-poor G bands are late replicating [20, 89]. However, early DNA replication is not a straightforward consequence of transcriptional activity [81]. When DNA replication timing changes, this is not directly influenced by transcription or influence transcription, but this is rather a result from a level of higher-order organization of the genome, which in turn affects the competence of transcription [78, 89].
This developmental regulation shows that similar as for origin selection, replication dynamics cannot be defined at a sequence level, but rather suggests chromatin signature to play a role in the regulation of DNA replication timing [88]. These observations further propose the idea that open chromatin structure, allowing active transcription, is most likely involved in determining DNA replication timing by turning specific chromatin domains into favorable substrates for DNA replication. This might be a due to increased accessibility of chromatin to initiation factors, resulting in for example a preferential ORC binding [32, 90].
These developmental changes together with the unsuccessful search for a consensus sequence, defining origins in metazoans, support the idea that the regulation of DNA replication cannot be explained at a genetic level alone. Potential candidates to control DNA replication are epigenetic factors that influence the chromatin state of different genomic regions. These factors influences processes such as transcription and epigenetic modifications, including DNA methylation, histone modifications, non-coding RNAs, among others. These factors intrinsically define chromatin structure and potentially play a role in any chromatin-based event.

1.5.4 Epigenetic control of DNA replication dynamics

Over the last decade, correlations between epigenetic modifications and the particular replication timing of distinct genomic region have been demonstrated in different organism [91–94]. Types of chromatin, characterized by specific epigenetic modifications replicate during distinct times of S-phase (Figure 1.4). In early S-phase, euchromatin is replicated, which includes less condensed and transcriptional active regions. Euchromatin is determined by depletion of methylated DNA, an enrichment in specific methylated histones like H3K4, H3K36, H3K79 and a high level of histone acetylation [95]. Next, facultative heterochromatin is replicated, which corresponds to developmentally silenced regions that are enriched in H3K27 trimethylation (H3K27me3) with the inactive X chromosome in mammals as one of the most prominent examples [96–98]. In contrast, constitutive heterochromatin is replicated in late S-phase. This type of heterochromatin is enriched for a set of histone modifications like H3K9 and H4K20 trimethylation and histone hypoacetylation [99]. Ultimately, early origins correlate with actively transcribed genes, while late origins are located in non-transcribed regions [27, 100, 101]. Several studies proposed a correlation between transcription sites and replication origins. The presence of a promoter or a transcription factor affects the localization of replication origin and the activation in different systems [102–106], probably by the recruitment of chromatin remodeling complexes, by histone modifying complexes, or by direct interaction of transcription factors and pre-RC components [107]. In general, an open chromatin formation is considered to be a better substrate for transcription and DNA replication initiation: replication

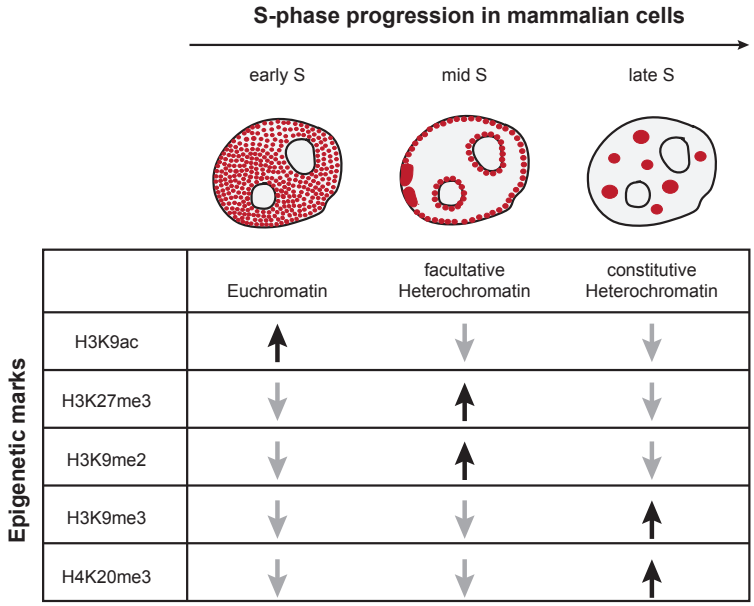

Figure 1.4.: Summary of epigenetic modifications, chromatin types and DNA replication timing. Schematic images depict DNA replication foci pattern (red) during S-phase progression in mammalian cell nucleus. In early S-phase, when mostly euchromatin is replicated, a multitude of small replication foci are distributed throughout the whole nucleus. In mid S-phase, DNA replication foci are mostly concentrated at the nucle(ol)ar periphery and at the inactive X-chromosome(s). In this substage, mostly facultative heterochromatin is replicated. In late S-phase, replication foci mostly colocalize with constitutive heterochromatin. Post-translational modifications of histones typical for the different chromatin types are indicated below. Less compacted euchromatin contains hyperacetylated histones. In contrast histones in heterochromatin are hypoacetylated and hypermethylated at the amino acid residues indicated. This is correlated with a more compacted structure and later DNA replication timing. (Figure taken from [14])

origins are usually enriched in open chromatin structures [108–110]. Promoters, which are transcriptionally active are usually hyperacetylated at histone H3/H4 [111], resulting in an open chromatin conformation and consequently making these regions as favorable substrates for DNA replication. In *Drosophila melanogaster*, *Xenopus laevis* and *Mus musculus* histone acetylation is a potential regulator of DNA replication [103, 112, 113].
In general, every epigenetic modification that discriminates between euchromatin and heterochromatin regions is a potential candidate responsible for differential DNA replication timing, ranging from DNA methylation, to histone modifications and higher order structure.

1.5.5 Manipulating epigenetic composition and DNA replication dynamics

The impact of epigenetic composition on the process of origin firing and its regulation, especially in mammals, is far from being completely understood. But, it has been shown that artificial manipulations of the chromatin state at defined regions result in altered DNA replication timing (Table 1.1).
In yeast, histone acetylation levels were manipulated by either knocking out HDAC Rpd3 or by HAT Gcn5 recruitment to a late origin, resulting in an earlier origin firing and concurrent Cdc45 binding [70]. Furthermore, it was shown that Sir HDACs are sufficient to reprogram an origin from early to late [92, 114] and that over 100 late origins are regulated by HDAC Rpd3L [115]. In addition, Crampton et al. 2008 demonstrated that HDAC Sir2 (H4K16 deacetylation) inhibits the assembly of pre-RC at late origins by promoting unfavorable structures and inhibiting MCM binding [116]. Unnikrishnan et al. 2010 [117], further strengthen the importance of histone acetylation by their finding that multiple acetylated residues are required for efficient origin activation. Also histone methylation has an effect in yeast as H3K36me1 together with histone acetylation advance the binding time of Cdc45 to replication origins, while H3K36me3 and histone deacetylation delay it [118].
In Drosophila, histone hyperacetylation has an effect on ORC binding at replication origins [112]. In addition, knocking down HP1 in Drosophila affects 5%-10% of the genome in its DNA replication timing, leading to an advanced replication of centromeric repeats, but a delayed duplication of unique sequences embedded in repeats (targets of HP1) [119]. Furthermore, Eaton et al. 2011 demonstrated that the chromatin environment in Drosophila does not regulate replication origins as a binary switch, but rather acts as a tunable rheostat to regulate replication initiation events [92]. These effects

of epigenetic manipulations were not only observed in yeast or Drosophila, but also in murine or human cells. Similarly to studies in Drosophila, treating human cells with the HDAC inhibitor trichostatin A (TSA) results in an early initiation of DNA replication of imprinted genes [120, 121]. In addition, treating murine cells with TSA leads to advanced DNA replication onset of constitutive heterochromatin [113]. Histone hypoacetylation was not only shown to be required to maintain the late DNA replication timing of constitutive heterochromatin, but also to play a role in controlling the replication dynamics of the inactive X chromosome. Thus, histone acetylation level has been proposed as possibly the best candidate to control DNA replication timing [100], since high levels of histone acetylation correlate with euchromatin, transcriptional activity and an open chromatin structure.
In human cells, Cdt1-mediated recruitment of HBO1, before the onset of S-phase, affects DNA replication by increasing H4 acetylation, chromatin decondensation and consequently enhancing the recruitment of MCM [122]. Knockdown of HBO1 leads to a decrease of DNA synthesis and affects the progression throughout S-phase. Importantly, the acetylating activity of HBO1 is necessary for MCM recruitment [39, 101]. The counterpart of this effect is HDAC11, an additional partner of Cdt1, which is active during S-phase. It prevents MCM recruitment and consequently avoids re-replication [122]. In human erythrocytes, the β-globin gene cluster is active, early replicating and histone hyperacetylated. In non-erythrocytes, β-globin is inactive, late replicating and histone hypoacetylated. When a histone deacetylase (HDAC) is tethered to its active promoter this leads to a shift to late DNA replication timing in erythrocytes. Whereas, when a histone acetylase (HAT) is targeted to the inactive promoter this results in an advanced DNA replication timing [123].
DNA methylation is another potential candidate to control DNA replication timing and, therefore, also a target for epigenetic manipulations. CpG islands at promoter regions are usually demethylated, whereas CpGs in silenced constitutive heterochromatin are characterized by high levels of DNA methylation [124]. The same can be found at promoter regions of the inactive X chromosome in female cells or at imprinted genes. All these regions show a characteristic replication pattern, differing from that of demethylated euchromatic regions. Studies on differential DNA replication at imprinted regions showed that treatment of cells with 5- azacytidine, a demethylating agent, does not change replication timing of imprinted loci in relation to earlier replication homologous regions [121]. In addition, it has been postulated that asynchronous replication of imprinted loci is independent of DNA methylation in murine embryonic stem cells, but dependent on differential subnuclear localization [125]. Moreover, DNA methylation alone was shown to be not sufficient to promote late DNA replication timing, as *in vitro* methylated DNA that was inserted into specific genomic sites, remained early replicating even though transcription was blocked [126]. Remarkably, induced hyperacetylation in human cells by TSA, a HDAC inhibitor, is unlike demethylation by 5-azacytidine, able to change DNA replication timing of imprinted regions, resulting in earlier replicating of normally late replicating loci, when compared with homologous active regions [121]. Late replicating constitutive heterochromatin become earlier replicating upon hyperacetylation, independently of the level of DNA methylation [113].
Within the present thesis, a new approach was developed to efficiently and reliable manipulate DNA replication timing by specifically changing the nuclear position of targeted DNA elements. Furthermore, the impact of histone acetylation was manipulated in two different ways to elucidate its validity and reproducibility of its epigenetic control on replication dynamics across species.

Table 1.1.: Overview of different studies manipulating epigenetic composition. Studies were categorized into classes of organisms and in the respective target of manipulation. The publication as well as the major outcome is indicated. Figure is modified and complemented from [32]

Studies manipulating epigenetic composition

Organism	Target	Puclication	Result
Yeast	Histone acetylation	Vogelauer et al. 2002	Knocking out HDAC Rpd3 or HAT Gcn5 recruitment to a late origin, lead to an earlier origin firing and concurrent Cdc45 binding.
		Zappulla et al. 2002	Sir HDACs are sufficient to reprogram an origin from early to late.
		Crampton et al. 2008	HDAC Sir 2, responsible for H4K16 deacetylation, inhibits the assembly at late origins by promoting unfavorable structures and by inhibiting MCM binding.
		Knott et al. 2009	HDAC Rpd3L regulates over 100 late origins.
		Unnikrishnan et al. 2010	Multiple acetylated residues are necessary for efficient origin activation.
	Histone methylation	Pryde et al. 2009	H3K36me1 together with histone acetylation advance the binding time of Cdc45 to replication origins, while H3K36me3 with histone deactylation delays it.
Drosophila	Histone acetylation	Aggarwal and Calvi, 2004	Histone hyperacetylation at origins affects ORC binding.
	HP1	Schwaiger et al. 2010	Knockdown of HP1 results in advanced replication of centromeric repeats, but in delayed replication of unique sequences located in repeats (= targets of HP1).
	Chromatin modifications	Eaton et al. 2011	Chromatin environment does not work as a binary switch in regulating replication origins, but rather acts as a tunable rheostat to regulate initiaton events.
Mouse	Histone acetylation/ histone methylation	Casas-Delucchi et al. 2012	Histone acetylation (and not histone methylation) is required to maintain late replication timing of constitutive heterochromatin.
	Histone methylation	Gribnau et al. 2003	Asynchronous replication of imprinted loci is independent of DNA methylation, but consistent with different subnuclear localization.
		Schubeler et al. 2010	DNA methylation is not enough to promote late DNA replication timing. *In vitro* methylated DNA that was inserted into specific genomic sites, remained early replicating.
Human	Histone acetylation	Bickmore et al. 1995	Induced hyperacetylation by HDAC inhibition leads to early initiation of of DNA replication of imprinted genes.
		Ilzuka et al. 2006	Knockdown of HBO1 leads to decrease of DNA synthesis, that is necessary for MCM recruitment.
		Goren et al. 2008	Tethering a HDAC to the active promoter of the beta-globin gene cluster leads to its late DNA replication. Targeting a HAT to its inactive promoter results in advanced DNA replication timing.
		Wong et al. 2010	Ctd1-mediated recruitment of human HBO1 (before S-phase), leads to an increase of H4 acetylation, chromatin decondensation and enhacing recruitment of MCM.
	Histone methylation	Bickmore et al. 1995	Treatment with demethylating agent did not affect DNA replication timing of imprinted foci.

2 Aims of this study

Up until now there is no consensus sequence of DNA replication origins identified in higher eukaryotes. Besides, there are striking examples of the flexibility of spatio-temporal organization of DNA replication dynamics during development of an organism, demonstrating that this complex process cannot be regulated at a genetic level alone. These observations rather emphasize the role of epigenetic mechanisms as potential candidates to regulate DNA replication timing or further point out the role of up until now unknown regulators. In this study, I attempt to elucidate the impact of different potential regulators of DNA replication dynamics in mammals by targeting and manipulation thereof.
Thus, I made use of a new targeting method based on the very strong interaction of GFP and GFP-binding nanobody. In chapter I, I will explain the setup and validation of this targeting approach and discuss potential applications. In chapter II, I made use of this strategy and repositioned constitutive heterochromatin to the nuclear lamina to evaluate the impact of nuclear position of DNA on its DNA replication timing. In chapter III, I targeted an active enzyme, a histone acetyltransferase to heterochromatic blocks and thereby increased the local histone acetylation level. Furthermore, I compared this site-directed targeting with a global drug-induced hyperacetylation. Here, I would like to elucidate the level of histone acetylation on DNA replication dynamics.

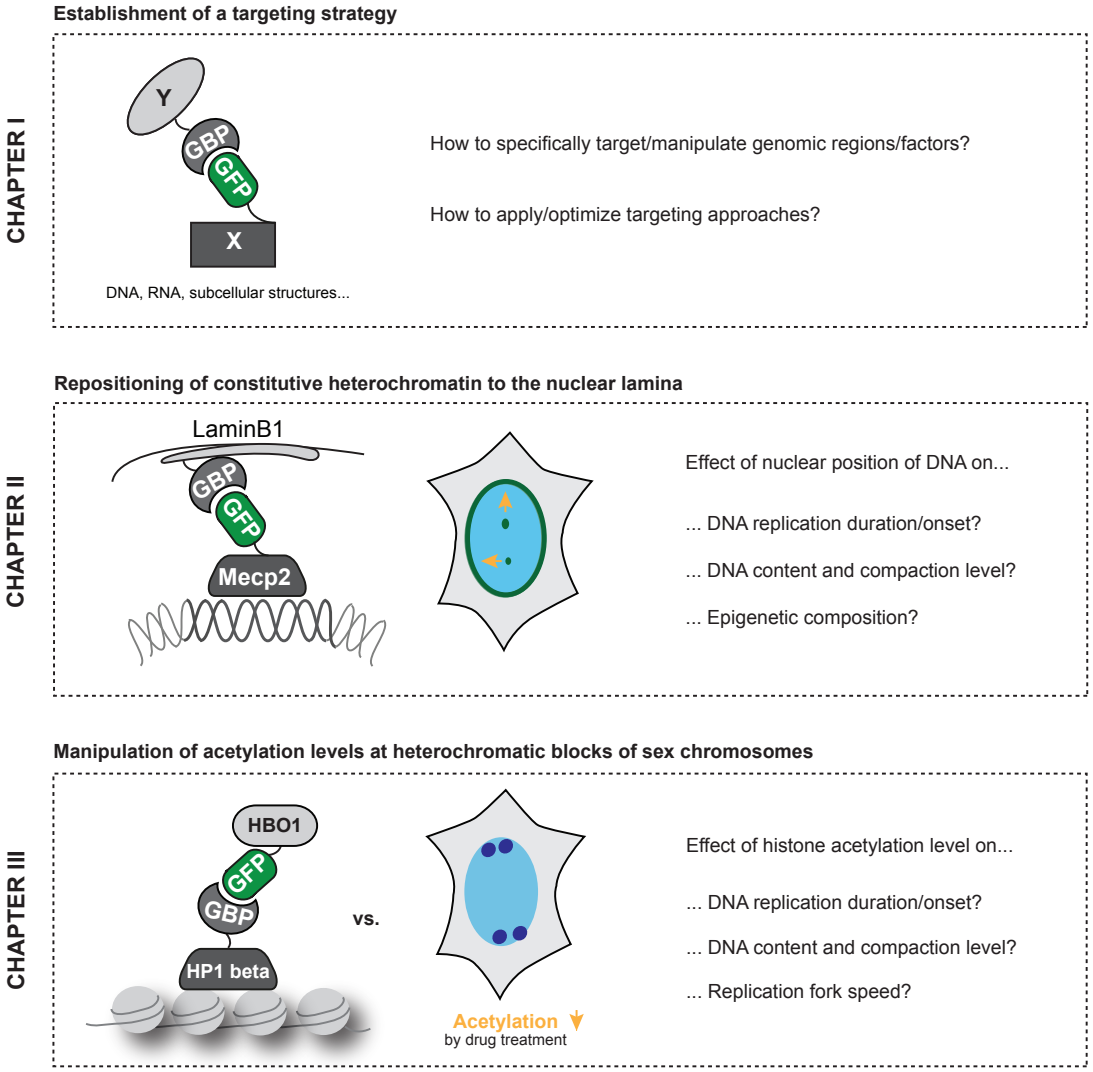

Figure 2.1.: Graphical overview of the aims of this study, from setting up an universal targeting strategy to two applications. In this step by step guide I give an overview of the key aspects from this thesis and how they work hand in hand in the quest for potential regulators of DNA replication timing.

3 Studies

I Targeted manipulation/repositioning of subcellular structures and molecules

I.1 Abstract

Technical advances in live-cell imaging have made cell biology into a highly dynamic field, allowing the visualization and quantification of complex processes in individual cells and in real time. To follow changes and to specifically manipulate factors potentially involved in processes like DNA replication, transcription or repair, we set up an universal targeting approach, allowing directed manipulation of subcellular structures and molecules therein. This strategy is based on the very strong and specific interaction of GFP and GFP-binding nanobody. We describe in detail how to set up the targeting approach with appropriate controls, as well as how to improve and validate its efficiency and finally provide exemplary applications.

I.2 Introduction

The visualization and quantification of processes in individual cells and in real time enables the tracking of spatio-temporal changes and evaluating their potential impact and function. To answer fundamental questions and understand the function of individual factors on multiplex processes it is important to be able to study the role of any factor X on any process Y. Thus, it is of major advantage to specifically manipulate DNA, RNA, proteins or even subcellular structures in a controlled and targeted manner. The manipulation of proteins localization via bait and prey type of approaches, such as fluorescence two/tri-hybrid assays [1, 2] amongst others, is a very useful tool to study protein-protein interactions. It would be of major advantage to use the same principles to manipulate the localization of entire subcellular structures and study complex questions like the effect of location on function.
Here, we describe a strategy that is based on the strong and highly specific interaction of GFP and GFP-binding protein (GBP). GBP is a recombinant 13-kDa GFP-binding fragment derived from a llama single chain V_HH antibody [3, 4] (Figure I.1). Because of the high affinity of GFP and GBP with a K_D in the subnanomolar range, it is possible to target any desired factor and even reposition large genomic regions when both factors are co-expressed in cells. The efficiency and strength of this targeting approach becomes obvious, since it is possible to even reposition constitutive heterochromatin in murine cells to the nuclear periphery to study the effect of nuclear position on basic cellular processes such as DNA replication and epigenetic composition [5].

In this chapter, we explain in detail how to design an individual and successful targeting assay and how to develop the appropriate controls. Depending on the question to be addressed, different control setups are possible (Figure I.2A). A control setup with no targeting or manipulation is achieved by transfection of X-GFP alone without the additional transfection of the GBP-carrying counterpart (Figure I.2A setup 1). To rule out any effect caused by the overexpression of factor Y one could remove the GBP part and simply transfect factor Y with X-GFP, leading to no interaction (Figure I.2A setup 2). Furthermore, the disruption of the targeting for a control setup can be achieved by replacing GFP by RFP, which does not interact with GBP (Figure I.2A setup 3). Lastly, it is possible to co-transfect X-GFP with a GBP- carrying an inactive form of protein Y (Figure I.2A setup 4). In case of enzymes one could inactivate the catalytic activity by site-directed mutagenesis and, thus, target an inactive version of the factor to the desired location. Furthermore, we present in detail how the validation of the targeting and control setup is accomplished (Figure I.2B). Different parameters need to be considered when optimizing the targeting approach, from the best ratio of both plasmid constructs during transfection, to incubation time after transfection up to validation of transfection efficiency.

This targeting strategy was successfully used to study the effect of nuclear position of DNA on its DNA replication timing. For this study constitutive heterochromatin was repositioned to the nuclear periphery into an environment of mid-replicating facultative heterochromatin [6]. MeCP2 as a methyl-cytosine binding protein [7] was used as X and tagged to GFP. MeCP2 binds methylated cytosines, which are highly abundant in constitutive heterochromatin. The latter forms micrometer sized aggregates in mouse cells termed chromocenters [8] . LaminB1, as a component of the nuclear lamina, was used as Y and was transfected without the GBP-counterpart to give normally localized GFP labeled chromocenters (Figure I.3A). To reposition constitutive heterochromatin, MeCP2-GFP and GBP-LaminB1 were co-expressed, leading to a clear green targeting ring at the nuclear periphery. With this approach constitutive heterochromatin was recognized, labeled and repositioned in different cells, including mouse embryonic fibroblasts (MEF [9]), embryonic stem cells (J1 [10]) and myoblasts (C2C12 [11]). Additionally, we were able to transport specific factors to a desired location. We transported factor Y (a histone acetylating enzyme) to the heterochromatin of the inactive X chromosome (Xi) with

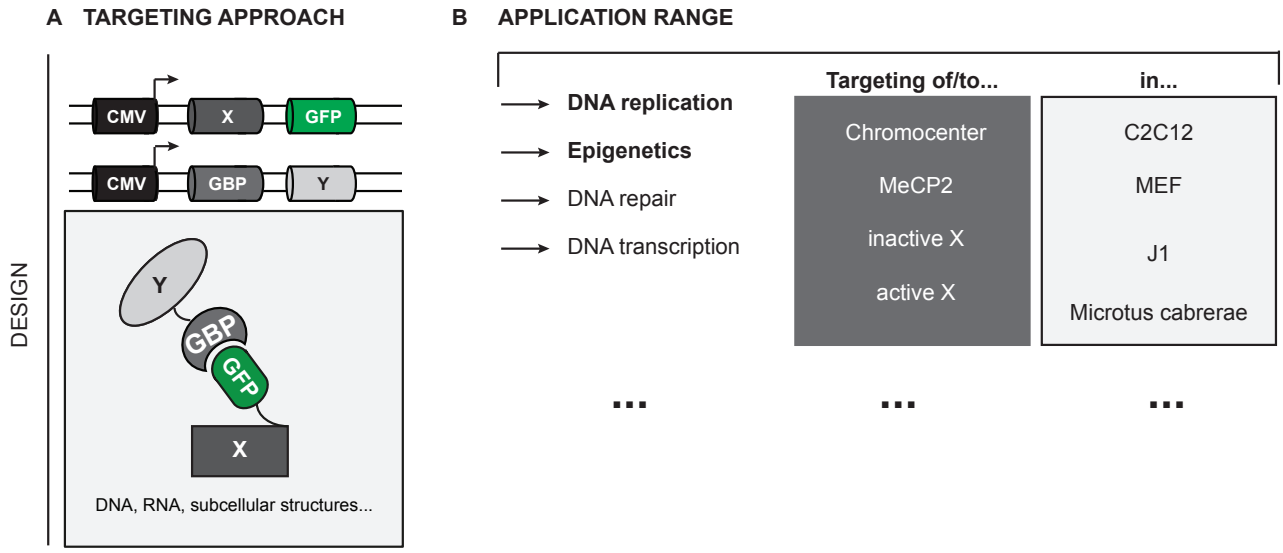

Figure I.1.: (A) Schematic representation of the targeted manipulation approach. The strategy is based on the strong interaction of GFP and GFP-binding protein (GBP). Both counterparts can be designed and cloned to any desired factor X and Y to target DNA, RNA or even subcellular structures. Upon co-expression of both constructs, the interaction of GFP with GBP is strong enough to even reposition large genomic regions. (B) The application range of the targeting approach is broad and potential processes include DNA replication, epigenetics, DNA repair and DNA transcription. Targeting of structures to reposition them is one application but also targeting of factors to a desired locus. Successful targeting can be achieved in different cell lines, depending on the factors used and processes under study.

the help of the macroH2a histone variant [12] and to the active X chromosome (Xa) with the help of HP1 beta [13, 14] in *Microtus cabrerae* [15] cells (Figure I.3B). For this purpose, an additional control should be added including the inactive form of the enzyme.
All in all, this experimental strategy enables specific tethering of any DNA, RNA, protein or even subcellular structures of interest to any desired location and lays the ground for controlled manipulation of factors such as epigenetic regulators, transcription factors, or ultimately subcellular localization of structures.

I.3 Materials

All materials and solutions used for cell culture, fixed cell studies and live-cell microscopy must be sterile.

1 Cell lines used for live-cell microscopy should be adherent cell cultures or be spun down on a support, such as glass coverslip. While the cell line to be used depends on the interest of the scientist, there are various considerations simplifying the data acquisition (see Note 1).
2 Culture medium: use the standard medium required for the particular cell line
3 Pre-warmed PBS containing 0.5 mM EDTA and 0.25% trypsin in PBS
4 0.2% gelatin for coating the microscopy dishes or coverslips
5 Plasmids: mammalian expression vectors coding for the setup of the targeting strategy of interest (one carrying the GBP counterpart and one carrying the GFP; (see Notes 2 and 3)). Additional fluorescent markers should be chosen according to the wavelengths that can be imaged using the microscope available.
6 Transfection reagents: nucleofection system from Amaxa (Lonza) or Neon nucleofection system (Thermo Fisher Scientific) [16], nucleofection solutions, cuvettes/tubes and pipettes (see Notes 4 and 5)
7 Microscopy dishes: form and size depends on the optical table inset available for the microscope. The bottom of the dish needs to be thin enough for higher magnification immersion lenses to be able to image through the sample. Material can be either glass or optical plastic (see Note 6). Glass lids are recommended for optimal contrast images.
8 Microscope: for imaging of live cells and fixed cells, we recommend the use of a spinning disc confocal microscope, characterized by high-speed acquisition and low level of phototoxicity to cells. The stage should be motorized to allow the acquisition of 3D stacks at several time points and several stage positions in one experiment.

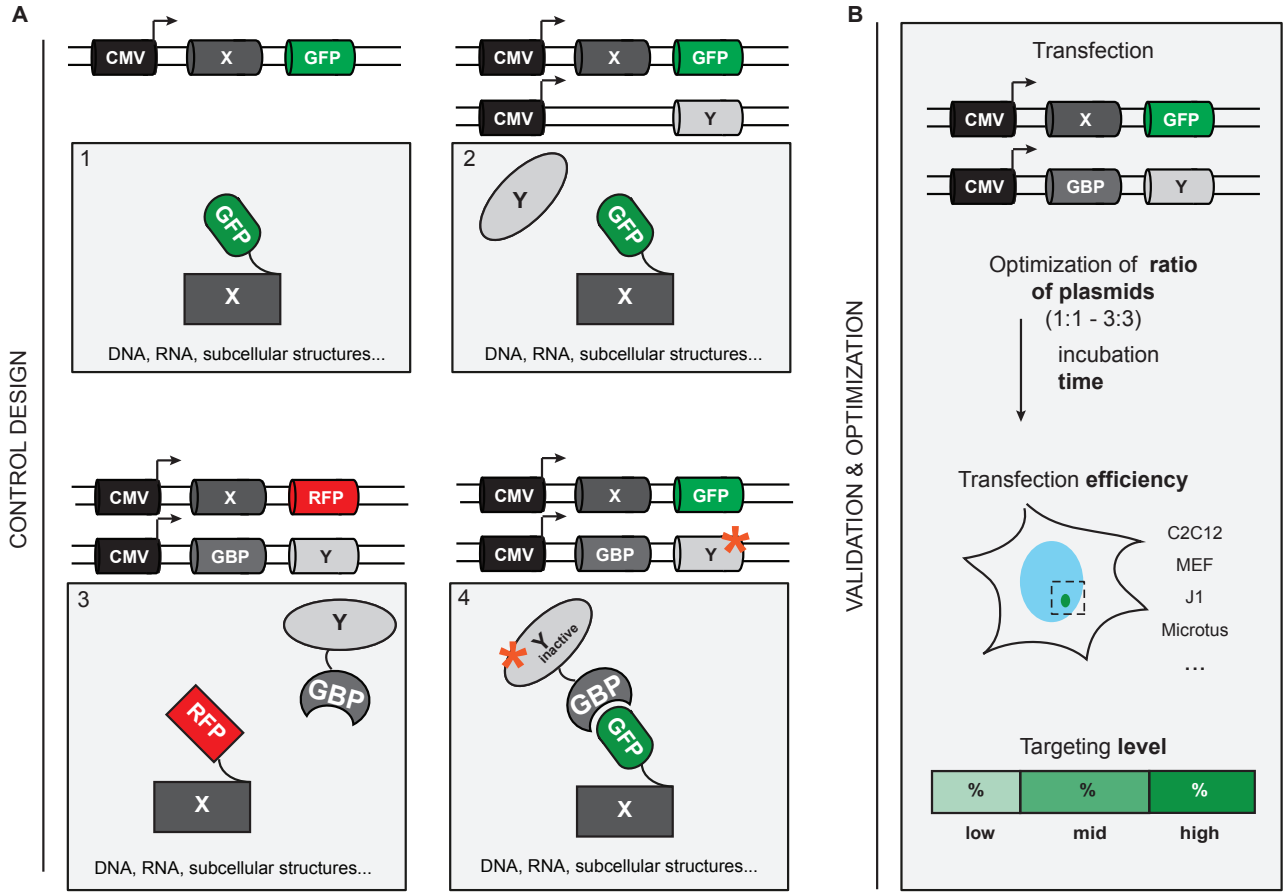

Figure I.2.: Schematic representation of the design of appropriate controls and the validation thereof. (A) The design of appropriate controls is flexible and dependent on the question to be answered. Here, we show different strategies to disrupt targeting, leading to a control setup. First, an untargeted state is achieved by transfecting only the X-GFP part without any interaction partner (setup 1). Furthermore, the X-GFP is transfected with Y alone, without the GBP part, which is required for interaction of both constructs. One advantage of this method is to elucidate, whether the over-expression of Y alone already leads to an effect on the investigated process (setup 2). Another strategy to achieve an untargeted control state, especially when targeting a factor to a desired locus, is the inactivation of factor Y. If Y is an enzyme, one could inactivate the catalytic activity by point mutation (setup 4). As GBP interacts with GFP but not with RFP, another strategy includes the design of an RFP-tagged X, which no longer interacts with the GBP-Y counterpart (setup 3). (B) After successful design of controls, the validation thereof as well as of the targeting is of upmost importance. The first step is to transfect cells with the appropriate constructs and validate the perfect ratio of plasmids to achieve a targeting signal. The incubation time after transfection needs also to be optimized. When cells show a targeted signal, the transfection efficiency can be determined, meaning the percentage of cells expressing the constructs and showing the desired targeted signal. The power of targeting could be categorized into different levels, e.g., low, mid and high targeting to check which level is the most desired one and depicting no toxic effects. Control and targeted cells should show their characteristic morphology to rule out toxic effects, which can lead to cell death.

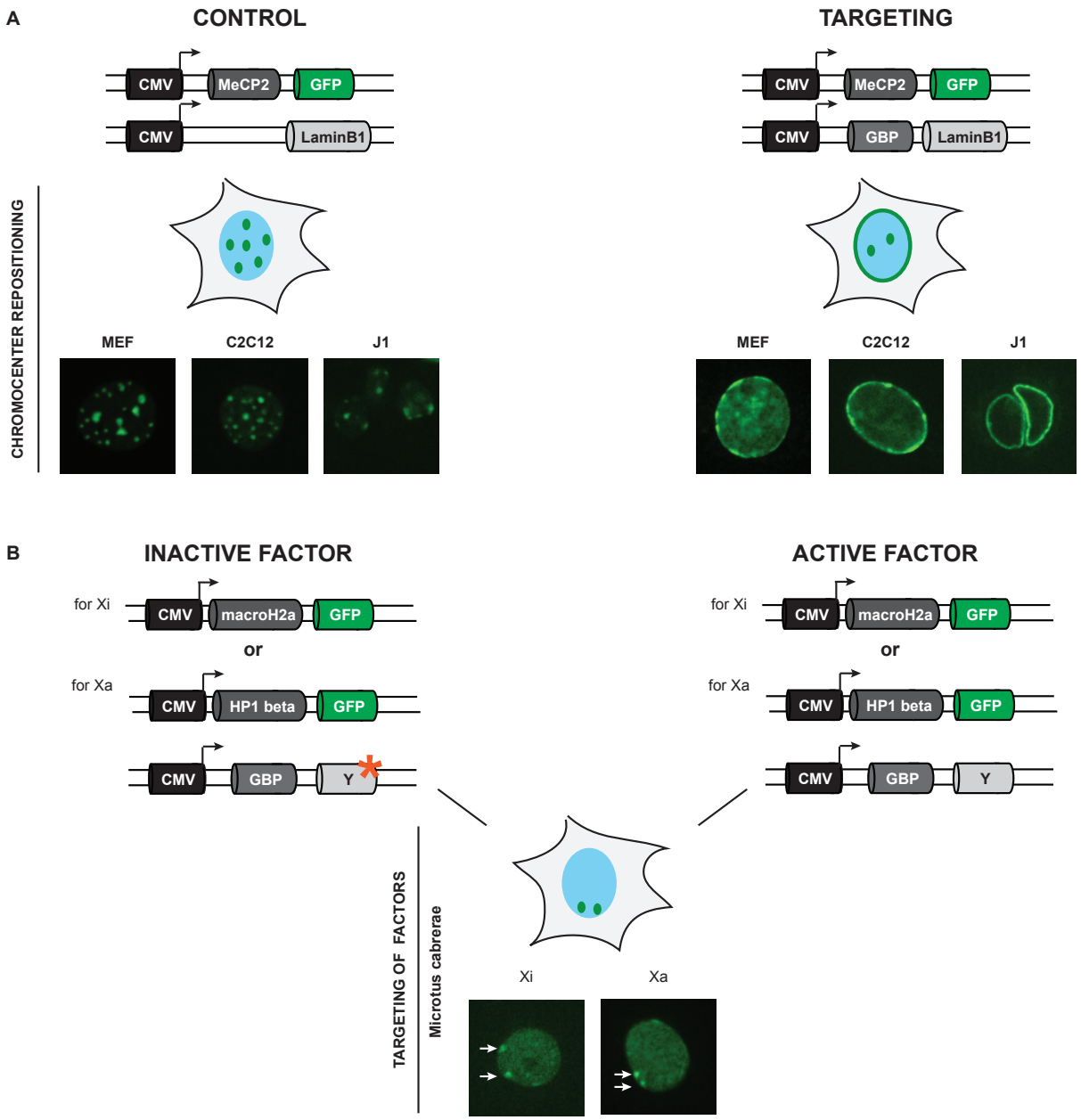

Figure I.3.: Application of the targeting approach to constitutive and facultative in different cell lines and species. (A) Repositioning of constitutive heterochromatin in various cell lines. MeCP2-GFP was co-expressed with LaminB1 without the GBP. No interaction of both targeting parts took place and thus constitutive heterochromatin was distributed throughout the whole nucleus. Upon co-expression of MeCP2-GFP and GBP-LaminB1, constitutive heterochromatin was repositioned to the nuclear lamina, resulting in a clear peripheral targeting ring. The targeting strategy was performed in different somatic and embryonic mouse cell lines: MEF, C2C12 and J1. (B) Macro-H2a and HP1-beta were tagged to GFP to either recognize the heterochromatin of the inactive X chromosome (Xi) or the active X chromosome (Xa) in *Microtus cabrerae* female fibroblasts. Upon co-expression with GBP-Y, where Y is any desired factor, Y is transported to the Xi or Xa. For the control setup, factor Y could be inactivated by, e.g., point mutation.

I.4 Methods

Here, we present a detailed protocol to target, manipulate or reposition specific factors and genomic regions to any desired location. The protocol is adapted to image fixed cells on glass coverslips or to image living cells in a 35 mm diameter glass-bottomed dish:

1 Pre-warm growing medium and PBS/EDTA to 37 °C and trypsin as well as transfection solutions to room temperature.
2 Prepare the dish where transfected cells will be seeded by coating for 20 minutes with 0.2% gelatin. Wash twice with pre-warmed medium to fully remove gelatin and add the final volume of growing medium (2 ml for a 35 mm diameter dish) and keep it in an incubator so that the medium reaches 37 °C and CO_2 diffuses into it.
3 Use 3 x 10^5 adherently growing cells of a 10 cm diameter plate (see Note 7). Remove growing medium and wash carefully with 5 ml PBS/EDTA, avoiding detaching cells from the surface. Add 0.5 ml trypsin and incubate at 37 °C for 2-5 minutes. Check cell detachment under a microscope. When most of the cells have detached from the substrate and are separated from each other, stop the enzymatic reaction by adding 4.5 ml growing medium. If cells are clumped together, carefully break up the cell clumps by pipetting up and down a couple of times. Centrifuge the cells for 6 minutes at 300 x g.
4 Prepare 100 μl of transfection solution with the appropriate and optimized amount of plasmid DNA (see Notes 8 and 9).
5 Once the cells are pelleted, discard the supernatant and carefully resuspend in transfection solution. Transfer the cell suspension into an electroporation cuvette/tube. Make sure to avoid bubbles and that the solution is clear without phenol red, because this can cause error messages during the electroporation process. Immediately perform the electroporation using the appropriate program for your cells (see Note 5). Use the previously prepared dish from the incubator and seed cells into the dish. Carefully shake the plate to homogenously distribute the cell suspension and return it into the incubator. Incubate overnight (see Notes 10 and 11).
6 On the next day, remove the medium and wash twice with prewarmed medium to remove dead cells, debris and add fresh medium.
7 For fixed cell studies, cells are fixed with 4% formaldehyde for 10 minutes, permeabilized for 20 minutes with 0.5% Triton X-100/PBS prior to immunostainings with the desired antibodies (see Note 12).
8 In case of live-cell imaging make sure that your incubation chamber is ready: 37 °C, 5% CO_2 and over 40% humidity level.
9 Place the dish with the transfected cells on the microscope. Allow the dish to acclimatize to new conditions prior to starting imaging. Slight changes in temperature may affect the material in such a way that the focal plane can change dramatically during the first 10-20 minutes.
10 Look for transfected cells by using short exposure times to minimize phototoxicity. Select cells that express the minimal amount of the fluorescent proteins that can be imaged properly. Too high expression levels may lower the chances that transfected cells will pass normally through S-phase and/or increases the chances that the cells undergo apoptosis.
11 Set up the imaging conditions finding a compromise between phototoxicity and undersampling. The ideal conditions depend strongly on the cell line, since some cells are more sensitive to transfection and phototoxicity, as well as of course on the transfection strategy you have set up. In general, acquiring z-stacks at a time interval of 20 minutes is usually enough to follow changes of, e.g., S-phase. The minimal amount to acquire an entire cell cycle depends on how fast the cells divide (see Note 3). Under normal conditions cells can be kept on the microscope stage and be imaged over two days.

I.5 Notes

1 Factors to consider when choosing a cell line to perform targeted manipulation and live-cell imaging of the targeting approach:
   - How well the cells can be transfected (transfection and expression rate),
   - How the cells can tolerate imaging-derived phototoxicity,
   - How much the cells move, which makes long term imaging difficult,
   - How fast cells divide and how they handle targeting in the subsequent cell cycles.
2 Factors to consider when setting up your targeting approach:
   - Which factor is targeted?
   - Where is the factor targeted?
   - Are the target and/or the location specific enough for a manipulation?
3 We always suggest linking the GBP to the leading part of the targeting assay and the targeted factor to the GFP. With this setup you are directly able to check by eye whether your factor is targeted by visual inspection of the GFP signal.

4 While a good transfection rate is a factor to consider when choosing your transfection method, when following cell cycle progression at a single cell level, it is more important to achieve a moderate expression level. We recommend the nucleofection system from Amaxa (Lonza) for somatic cells and Neon Nucleofection (Thermo Fisher) for embryonic stem cells, although other methods can be used.

5 We suggest for myoblasts and fibroblasts the B-032 program (e.g. C2C12, *Microtus cabrerae* fibroblasts) and for mouse embryonic fibroblasts the A-024 program (e.g. MEF) of the Amaxa machine. For mouse embryonic stem cells like J1 we suggest to use the Neon nucleofection system with a transfection setup of 1250 Volt, 20 ms width and two pulses.

6 Irrespective of whether you use your targeting approach for fixed cell studies or live-cell imaging we highly suggest to coat glass surfaces with gelatin as this improved the fast attachment of transfected cells and increased the general transfection efficiency.

7 Cell density is a key factor for live-cell imaging and to provide enough cells prior to transfection as a higher amount of cells is dying during the process of electroporation. While a too high density can result in cell contact inhibition, preventing cells from cycling, a too low density can result in cells moving more freely along growing surface, making it extremely hard to keep them in frame over several hours. In case of low transfection efficiency the likelihood of having enough cells for your studies is further decreased. The optimal cell density depends on the cell line used: mouse myoblasts and fibroblasts tend to move and a rather high density is recommended. In case of embryonic stem cells like for J1 for instance, a lower density makes more sense to avoid large colonies of cells, further complicate the imaging and validation of targeting in single cells.

8 The optimal ratio of both plasmids is of upmost importance. Therefore we suggest ratio measurements before starting experiments. We always used combinations (in μg) from 1:1 up to 3:3, changing for every plasmid to make sure to achieve the perfect combination, resulting in healthy cells with typical morphology but an efficient targeting with high transfection efficiency.

9 Further optimization is needed when you want to combine your targeting approach with e.g. a PCNA transfection to label active replication sites. We checked triple transfections as well as quadruple transfections, both is suitable, but requires further optimization step. As already indicated, use as less plasmid as possible to do not harm the cells too much, but still enough to have an appropriate targeting efficiency.

10 During optimization we recommend to check for the perfect incubation time after transfection. Too high expression levels may lower the chances that transfected will pass normally through S-phase and/or increases the chances that the cells undergo apoptosis. High targeted cells often appear right fast after nucleofection, but also die quite fast, thus make sure to estimate the right level of targeting for your experiments. For imaging and reliable cell cycle studies, cells with low or mid expression rate are preferable. These cells appear slightly later after transfection process.

11 During the establishment of different targeting strategies in different cell lines we always incubated in a range in between 20 and 24 hours for first cell cycle studies and up to 49 hours for second cell cycle studies. But these numbers strongly depend on the cell line you are using and its doubling time.

12 When targeted cells are used for fixed cell studies, like FISH, pulse labeling setups or immunostainings in general, we suggest when the GFP signal is very weak to boost the signal with an additional GBP (1 mg/ml) incubation step prior to DAPI staining. We suggest a step of one hour at room temperature.

I.6 Acknowledgments

We thank H. Leonhardt (LMU-Munich, Germany) for providing plasmids and the C2C12 and MEF cell lines stably expressing RFP-PCNA. We thank Juan Alberto Marchal (University of Jaen, Spain) for the *Microtus cabrerae* fibroblasts and all present and past members of the laboratory for their contributions over the years. The laboratory of M. Cristina Cardoso is supported by grants of the German Research Foundation (DFG).

I.7 References

1. Zolghadr, K., Rothbauer, U. & Leonhardt, H. The fluorescent two-hybrid (F2H) assay for direct analysis of protein-protein interactions in living cells. *Methods Mol Biol* **812,** 275–82 (2012).
2. Herce, H. D., Deng, W., Helma, J., Leonhardt, H. & Cardoso, M. C. Visualization and targeted disruption of protein interactions in living cells. *Nat Commun* **4,** 2660 (2013).
3. Rothbauer, U. *et al.* Targeting and tracing antigens in live cells with fluorescent nanobodies. *Nat Methods* **3,** 887–9 (2006).
4. Rothbauer, U. *et al.* A versatile nanotrap for biochemical and functional studies with fluorescent fusion proteins. *Mol Cell Proteomics* **7,** 282–9 (2008).

5. Heinz, K. S. *et al.* Peripheral re-localization of constitutive heterochromatin advances its replication timing and impairs maintenance of silencing marks. *Nucleic Acids Res* **46,** 6112–6128 (2018).
6. Casas-Delucchi, C. S. & Cardoso, M. C. Epigenetic control of DNA replication dynamics in mammals. *Nucleus* **2,** 370–82 (2011).
7. Brero, A. *et al.* Methyl CpG-binding proteins induce large-scale chromatin reorganization during terminal differentiation. *J Cell Biol* **169,** 733–43 (2005).
8. Vissel, B. & Choo, K. H. Mouse major (gamma) satellite DNA is highly conserved and organized into extremely long tandem arrays: implications for recombination between nonhomologous chromosomes. *Genomics* **5,** 407–14 (1989).
9. Peters, A. H. *et al.* Loss of the Suv39h histone methyltransferases impairs mammalian heterochromatin and genome stability. *Cell* **107,** 323–37 (2001).
10. Li, E., Bestor, T. H. & Jaenisch, R. Targeted mutation of the DNA methyltransferase gene results in embryonic lethality. *Cell* **69,** 915–26 (1992).
11. Yaffe, D. & Saxel, O. Serial passaging and differentiation of myogenic cells isolated from dystrophic mouse muscle. *Nature* **270,** 725–7 (1977).
12. Abbott, D. W., Chadwick, B. P., Thambirajah, A. A. & Ausio, J. Beyond the Xi: macroH2A chromatin distribution and post-translational modification in an avian system. *The Journal of biological chemistry* **280,** 16437–45 (2005).
13. Nielsen, A. L. *et al.* Heterochromatin formation in mammalian cells: interaction between histones and HP1 proteins. *Mol Cell* **7,** 729–39 (2001).
14. Cheutin, T. *et al.* Maintenance of stable heterochromatin domains by dynamic HP1 binding. *Science* **299,** 721–5 (2003).
15. Fernandez, R. *et al.* Molecular and cytogenetic characterization of highly repeated DNA sequences in the vole Microtus cabrerae. *Heredity (Edinb)* **87,** 637–46 (2001).
16. Kim, J. A. *et al.* A novel electroporation method using a capillary and wire-type electrode. *Biosens Bioelectron* **23,** 1353–60 (2008).

II Peripheral re-localization of constitutive heterochromatin advances its replication timing and impairs maintenance of silencing marks

II.1 Abstract

The replication of the genome is a highly organized process, both spatially and temporally. Although a lot is known on the composition of the basic replication machinery, how its activity is regulated is mostly unknown. Several chromatin properties have been proposed as regulators, but a potential role of the nuclear DNA position remains unclear. We made use of the prominent structure and well-defined heterochromatic landscape of mouse pericentric chromosome domains as a well-studied example of late replicating constitutive heterochromatin. We established a method to manipulate its nuclear position and evaluated the effect on replication timing, DNA compaction and epigenetic composition. Using time-lapse microscopy, we observed that constitutive heterochromatin, known to replicate during late S-phase, was replicated in mid S-phase when repositioned to the nuclear periphery. Out-of-schedule replication resulted in deficient post-replicative maintenance of chromatin modifications, namely silencing marks. We propose that repositioned constitutive heterochromatin was activated in *trans* according to the domino model of origin firing by nearby (mid S) firing origins. In summary, our data provide, on the one hand, a novel approach to manipulate nuclear DNA position and, on the other hand, establish nuclear DNA position as a novel mechanism regulating DNA replication timing and epigenetic maintenance.

II.2 Introduction

The duplication of the genome is a highly complex process organized in a spatial and temporal manner (reviewed in [1]). On a cytological level, DNA replication is detectable as discrete sub-nuclear foci, where each focus corresponds to a cluster of coordinately activated replication forks [2–5], which can be resolved using superresolution light microscopy [6–8]. During S-phase progression, the spatial distribution of these foci changes 'following' chromatin condensation level and leading to distinct nuclear patterns associated with early (euchromatin), mid (facultative heterochromatin) and late replicating (constitutive heterochromatin) chromosomal regions This spatio-temporal organization of DNA replication is intrinsically related to the coordination of origin firing at distinct chromatin and nuclear regions, reflecting the higher order packing of the genome (reviewed in [9–11]. The plasticity of DNA replication timing is not sequence driven, as up until now no consensus origin sequence was identified in higher eukaryotes [12–15]. Even in budding yeast, where replication origins are defined at the sequence levels, excising them from their endogenous locus can result in changes in their timing of firing during S-phase [16]. On the other hand, DNA and histone modifications have been identified to play a central role in the definition of chromatin structure and replication progression (reviewed in [17]). Several lines of evidence support the idea that DNA replication timing is dictated by the chromatin structure as specific chromatin modifications correlate with DNA replication timing, such as histone acetylation with early replication in Drosophila [18] and H3K9 trimethylation (H3K9me3) or H4K20 trimethylation (H4K20me3), which are associated with late DNA replication [19–22]. Moreover, disrupting chromatin modifications can lead to changes in DNA replication timing [19, 23–26] indicating a possible interplay between chromatin state and DNA replication timing. However, the mechanisms by which chromatin composition regulates the timing of origin firing and, vice-versa, how replication timing affects chromatin state, remain unclear. Circumstantial evidence correlates the spatial reorganization of chromatin at the end of mitosis / beginning of G1 phase of the cell cycle with the setup of the replication program [27]. In budding yeast, an early firing origin was artificially tethered to the nuclear envelope [28] to study a regulatory effect of sub-nuclear position on its DNA replication timing. The peripheral positioning was not sufficient to delay the firing of this early origin. Hence, the available evidence does not provide an answer to whether nuclear architecture and positioning of chromatin, chromatin state and replication timing depend on each other.

Here, we set up a targeting strategy to investigate the effect of sub-nuclear localization of DNA within the mammalian nucleus on its replication timing and chromatin state. We made use of constitutive heterochromatin as it exhibits a distinct chromatin landscape characterized by high levels of DNA methylation, H3K9 trimethylation and histone hypoacetylation. In mice, these regions assemble into higher order aggregates known as chromocenters [29], composed of $\sim 10^5$ major satellite DNA repeats that can be visualized by staining the DNA as round, highly condensed, prominent structures in the nucleus [30]. We manipulated the nuclear localization of late replicating chromocenters by juxtaposing them next to mid replicating facultative heterochromatin at the nuclear periphery to elucidate the impact of nuclear position of DNA

on its replication timing and composition. We were able to observe an advanced DNA replication timing of repositioned chromocenters accompanied by a decondensation of repositioned constitutive heterochromatin, as well as a progressive loss of silencing histone marks. We, therefore, conclude that the nuclear position plays a role in regulating DNA replication timing in mammalian cells.

II.3 Materials and methods

II.3.1 Expression plasmids

Expression vector encoding the complete rat Mecp2 ORF fused in frame to the NH2 terminus of the enhanced GFP to construct the Mecp2-GFP (pc=plasmid collection number, pc1121) was described before [31] and was used here to detect methylated cytosines abundant at chromocenters. The second element of the targeting strategy was a GBP-Lamin B1 (pc1467), an expression vector encoding the sequence of the GFP-binding V_HH domain [32–34] fused to the human Lamin B1 coding sequence. As a control for the targeting assay the GFP-binding V_HH domain was removed by restriction with XhoI and SacII enzymes, followed by a treatment with Klenow polymerase large fragment to create blunt ends and re-ligation, to establish an expression vector with human Lamin B1 alone (pc2809). For sequence-specific chromocenter recognition by binding major satellite (ms) DNA, we performed double-transfections with GBP-Lamin B1 or Lamin B1 alone in combination with either msTALE (pc3086) [35], msPZF (pc1803) [36] or triple transfection with msCRISPR/dCas9 (pc3147, pc2942) [37] (Figure II.S1).

II.3.2 Cell culture and transfection

C2C12 mouse myoblasts [38] were grown at 37 °C, 5% CO_2, in Dulbecco's modified Eagle's medium (DMEM) supplemented with 20% fetal calf serum and 1 μM gentamycin. Mouse embryonic fibroblasts (MEF) [39] were grown at 37 °C, 5% CO_2, in DMEM supplemented with 10% fetal calf serum and 1 μM gentamycin. Cell lines stably expressing mRFP-PCNA were kindly provided by the Leonhardt laboratory (LMU, Munich, Germany). These cell lines were established using an expression vector encoding a mRFP-tagged fusion of human PCNA (pc2729). For creation of this expression vector, a CMV-driven mRFP-tagged PCNA encoding mammalian expression vector [40] (pc1054) was used to amplify the mRFP-PCNA part with the following primers including restriction sites for XhoI and AflII enzymes (forward: XhoI 5'-GCGCCTCGAGGATCTTGGTGGCGTGAAACTC; reverse: AflII 5'- GCGCGCCTTAAGCCAAACTCACCCTGAAGTTCTC. This amplicon was digested with the corresponding restriction enzymes and ligated to a similarly cut CAG promoter containing mammalian expression vector to generate a mRFP-PCNA fusion gene under the control of the CAG promoter (pc2729). The resulting vector was used to transfect C2C12 and MEF cells. Positive clones were selected using 0.75 μg/ml puromycin (Figure II.S2). Transient transfections of C2C12 and MEF cells were performed using nucleofection (Amaxa NucleoFector II, Lonza Ltd., Basel, Switzerland) with either 1 μg DNA per plasmid (pc1121, pc1467, pc2809, pc1803) or 2 μg per plasmid (pc3086, pc3147, pc2942).

II.3.3 Immunofluorescence

Cells were grown on gelatinized glass coverslips, which were coated for 20 minutes with 0.2% gelatine from porcine skin (in ddH_2O, Sigma-Aldrich, Steinheim, Germany, Cat #: G2500). Cells were fixed in 4% formaldehyde (10 minutes at room temperature (RT)), permeabilized for 20 minutes at RT in 0.5% Triton X-100/PBS and unspecific binding sites were blocked with 4% BSA/PBS for 30 minutes at RT. Immunofluorescence stainings were performed in 4% BSA/PBS for 2 hours at RT (primary antibodies) and for 1 hour at RT (secondary antibodies). The following primary antibodies were used: rabbit anti-H3K9ac (1/200, Upstate, Lake Placid, USA, Cat #: 06-942), mouse anti-H3K27me3 (1/100, Active Motif, Carlsbad, USA, Cat #: 39535), rabbit anti-H3K27me3 (1/200, Active Motif, Carlsbad, USA, Cat #: 39155), rabbit anti-H3K9me2 (1/200, Biomol, Hamburg, Germany, Cat #: 07-212), mouse anti-H3K9me3 antibody (1/200, Active Motif, Carlsbad, USA, Cat #: 39285), rabbit anti-H3K9me3 (1/200, Upstate, Lake Placid, USA, Cat #: 07-442), rabbit anti-H4K20me3 (1/500, Abcam, Cambridge, UK, Cat #: ab9053), rabbit anti-Lamin A/C (1/200, kind gift of Ricardo Bastos, Institute Jacques Monod, Paris, France), mouse anti-Lamin B (undiluted, Progen Biotechnik GmbH Heidelberg, Germany, Cat #: 65147C) and mouse anti-Nup153 (1/200, Abcam, Cambridge, UK, Cat #: ab24700). For Lamin B staining, samples were fixed 10 minutes at RT with ice-cold methanol and were dehydrated prior to standard protocol. The following secondary antibodies were used: donkey-anti-mouse IgG-Cy3 and donkey-anti-rabbit IgG-Cy3 (1/200, Jackson Immuno Research, Baltimore, USA, Cat #: 715-166-151/ 711-165-152). Nuclear DNA was visualized by 4,6-diamidino-2-phenylindole (DAPI, 1 μg/ml, Sigma-Aldrich, Steinheim, Germany, Cat #: D9542). Cells were mounted in Mowiol 4-88 (Sigma-Aldrich, Steinheim, Germany, Cat #: 81381).

II.3.4 *In situ* replication labeling

For the visualization of replicating DNA, C2C12 mouse myoblasts were pulse labelled for 30 minutes with 100 μM 5-bromo-2'-deoxyuridine, BrdU (Sigma-Aldrich, Steinheim, Germany, Cat #: 59-14-3) and/or 10 μM 5'-ethynyl-2'-deoxyuridine, EdU (Invitrogen, Carlsbad, USA, Cat #: C10339). For a pulse-chase-pulse experimental setup a 200 μM thymidine chase (Sigma-Aldrich, Steinheim, Germany, Cat #: T1895) was performed in between both pulses. Incorporated BrdU was detected with a rat anti-BrdU antibody (1/200, AbD Serotec, Oxford, UK, Cat #: OBT0030CX) combined with 10 $\mu g/\mu l$ DNaseI (Sigma-Aldrich, Steinheim, Germany, Cat #: D5025) for 1 hour at 37 °C in 4% BSA/PBS. Cells were then washed with 0.5% BSA/1mM EDTA/PBS + 0.01% Tween to stop DNaseI digestion. EdU was detected using ClickIT chemistry (Invitrogen, Carlsbad, USA, Cat #: C10639) as described in [41] with Alexa Fluor 594 (1/300). DNA was counterstained with 1 μg/ml DAPI (Sigma-Aldrich, Steinheim, Germany, Cat #: D9542) for 10 min at RT and cells were mounted in Mowiol.

II.3.5 Major satellite DNA-FISH

For mouse major Satellite DNA-FISH, DNA probes were generated by PCR using biotinylated nucleotides (forward primer: 5'-GCGAGAAAACTGAAAATCAC, reverse primer: 5'-TCAAGTCGTCAAGTGGATG). Briefly, transfected C2C12 cells grown on gelatinized coverslips for 20 hours or 49 hours post-transfection were washed with PBS and fixed with 4% formaldehyde for 10 minutes at room temperature. After permeabilization with 0.5% Triton-X100 in PBS for 20 minutes, cells were treated with 0.1 M HCl (for 15 minutes at RT). After washing with PBS, cells were again permeabilized for 15 minutes and incubated for 20 minutes with 50% formamide/saline sodium citrate (SSC) (Carl Roth, Karlsruhe, Germany, Cat #: P040/3957/3580). For FISH probe precipitation, biotinylated probe was incubated with fish sperm DNA (Sigma-Aldrich, Steinheim, Germany,Cat #:74782), 3 M sodium acetate (Carl Roth, Karlsruhe, Germany, Cat #: 6773) and 100% ice-cold ethanol at -80 °C for 50 minutes. After centrifugation for 45 minutes at 13000 rpm and 4 °C, supernatant was removed and the probe was incubated with ice-cold 70% ethanol. The FISH probe was centrifuged for 30 minutes, the supernatant discarded and the pellet dried for at least 60 minutes. The dried pellet was dissolved in a hybridization solution, containing 50% formamide, 2x SSC, 10% dextran sulfate pH 7 (Applichem, Darmstadt, Germany, Cat #: A4970) and was incubated for 45 minutes at 37 °C shaking at 300 rpm. After denaturation for 8 minutes at 80 °C the probe was immediately cooled on ice and put on the fixed and permeabilized cells. The samples were put in a humidified chamber, incubated for 5 minutes at 80 °C and over night at 37 °C. Coverslips were washed for 15 minutes at 45 °C in 50% formamide/SSC followed by 10 minutes in 2x SSC. After blocking in 1% BSA/4x SSC for 45 minutes at RT, probes were detected by streptavidin-Cy5 (1/500, Amersham Biosciences, Piscataway, USA, Cat #: PA45001) for 45 minutes at RT. Nuclear DNA was visualized with DAPI and cells were mounted in Mowiol as described above.

II.3.6 Light microscopy

Confocal images were obtained using an UltraVIEW VoX spinning disc system (PerkinElmer, Massachusetts, USA) on a Nikon Ti microscope equipped with an oil immersion Plan-Apochromat x60/1.45 numeric aperture objective lens (pixel size in XY= 112 μm, Z-step 0.3 – 1 μm). Excitation was done using the following laser lines: 405 nm, 488 nm, 561 nm and 640 nm. Images were taken with the appropriate filters for the respective dyes: DAPI: emission wavelength (em): 415-475 nm; GFP: em: 505-549 nm; RFP: em: 580-650 nm and Cy5: em: 664-754 nm. Z stacks and montages were created using ImageJ (http://rsb.info.nih.gov/ij/). For live-cell microscopy stable C2C12 and stable MEF cell line expressing RFP-PCNA were transfected and plated on a glass bottom p35 dish and grown under standard conditions for at least 20 hours. Time-lapse experiments were carried out in a closed live-cell microscopy chamber (ACU control, Olympus) heated to 37 °C, with 5% CO_2 and 60% humidity. Z-stacks were acquired with 20 minutes intervals with a Hamamatsu C9100-50 EMCCD camera.

II.3.7 Image analysis and quantification

The frequency of DNA replication patterns was quantified from the light microscopy images by visual classification of C2C12 cells into early, mid and late S-phase patterns (described in [3]) followed by calculating the respective percentages. An early S-phase pattern is characterized by DNA replication foci distributed homogenously throughout the nucleus with exclusion of the nucle(ol)ar periphery, whereas a mid S-phase pattern is identifiable by well-organized foci at the nucle(ol)ar periphery. Late S-phase is clearly recognizable due to the appearance of fewer but larger clusters of DNA replication foci, colocalizing with chromocenter.
The onset of DNA replication timing of chromocenters in C2C12 and MEF control and targeted cells was analyzed by the colocalization of DNA replication (RFP-PCNA) and chromocenters signal (Mecp2-GFP) and quantified with the Hcoeff [42]. For the calculation of mean post-translational modifications (PTM) levels at pericentric heterochromatin

of control and targeted C2C12 and MEF cells, routines were written in the programming language python (http://-code.google.com/p/priithon/).

II.3.8 DNA content analysis

C2C12 cells were imaged using the Operetta High Content imaging system (Perkin Elmer, Massachusetts, USA), equipped with a 40x 0.95 numeric aperture air objective. For imaging constant exposure times and appropriate filter sets (DAPI: ex: 360-400 nm; em: 410-480 nm; GFP: ex: 460-490 nm; em: 500-560 nm; RFP: ex: 560-580 nm; em: 590-640 nm) were used. Cell segmentation and quantification of nuclear intensities was performed using Harmony (Perkin Elmer, Massachusetts, USA). Subsequently, cells were manually staged for early, mid or late S-phase based on their PCNA pattern as well as assigned whether the cells showed a targeted pattern.
Based on this classification, the total DNA intensity (DAPI) per cell nucleus was plotted for all cells from each replicate. Based on the histogram of all cells per replicate, the DAPI intensity of each cell was normalized to the corresponding G1 and G2 peaks obtained by density fitting. This allowed pooling of the four replicates. Next, the normalized DAPI intensity per nucleus was classified first into non-targeted and targeted pools and, then, in the corresponding S-phase substages.

II.4 Results

II.4.1 Manipulating the nuclear position of constitutive heterochromatin

Expression vector encoding the complete rat Mecp2 ORF fused in frame to the NH2 terminus of the To study the impact of chromatin position on DNA replication, we developed a system to change the sub-nuclear localization of mouse pericentric heterochromatin. Late replicating chromocenters were juxtaposed next to mid replicating facultative heterochromatin to the nuclear periphery. We chose these regions as they have a well-defined epigenetic landscape and form large supra-chromosomal structures, which can be visualized by DNA staining and are a prominent landmark within the nucleus. Our targeting system consisted of two fusion proteins: a chromocenter recognizer (Figure II.S1A) and either Lamin B1 alone or GFP-binding protein (GBP) tagged-Lamin B1 (Figure II.1 and II.2). Mecp2-GFP [31] binds strongly to pericentric heterochromatin due to its high levels of DNA methylation. As a control for possible effects of Mecp2-GFP-binding and Lamin B1 over-expression on the replication timing or chromatin constitution of chromocenters, we used cells over-expressing Mecp2-GFP and untagged Lamin B1 (Figure II.1) as reference. In these cells, chromocenters showed their typical round structure and position within the nucleus.
In a targeted state, Lamin B1 fusion protein is incorporated into the nuclear lamina like untagged Lamin B1, while its GBP domain [32, 33] causes it to interact with Mecp2-GFP (Figure II.2). This interaction resulted in the recruitment of Mecp2, and concomitantly of the pericentric heterochromatin to which Mecp2 was bound, to the nuclear periphery. Major satellite DNA-FISH confirmed that the GFP signal overlapped with pericentric heterochromatin, demonstrating a successful re-localization of chromocenters to the nuclear periphery. Some cells still exhibited a subpopulation of internal chromocenters. This feature was very useful as an internal control, as it allow us to look at differences between peripheral and internal pericentric heterochromatin within the very same cell. After targeted cells went through mitosis, the chromocenters underwent further rearrangements, resulting in their clustering at the top/bottom of the nucleus and forming a star-like cluster (Figure II.2, lower middle row). This secondary rearrangement allowed us to reliably distinguish between cells undergoing the first and second cell cycle after repositioning of chromocenters. After several days of cultivation, whether cells stayed in the targeting mode with star-shaped cluster or whether they exhibited normally localized chromocenters like in control cells, seemed to depend on the transfection efficiency and amount of GBP-LaminB1, which is diluted over the cell cycles.
As shown by these data, our targeting strategy allowed us to manipulate the sub-nuclear localization of pericentric heterochromatin from the nuclear interior to the nuclear periphery. Next, we moved on to use this novel tool to ask whether these position re-arrangements would affect heterochromatin structure, DNA replication timing and epigenetic composition.

II.4.2 Repositioning constitutive heterochromatin does not affect global organization of lamina and nuclear pores

Having demonstrated that our system is proficient to target constitutive heterochromatin to the nuclear lamina, we wanted to evaluate the effect on general nuclear organization. Several lines of evidence support the idea of a relationship between heterochromatin, lamins and nuclear pore complexes (NPC) [43, 44].
First, we addressed the question whether the nuclear lamina is affected by the repositioning. For this reason, we performed immuno-detection with antibodies against Lamin A/C and B (Figure II.3A). We did not observe differences in the lamin organization in the first cell cycle, comparing control and targeted cells. Whereas in the second cell cycle, the

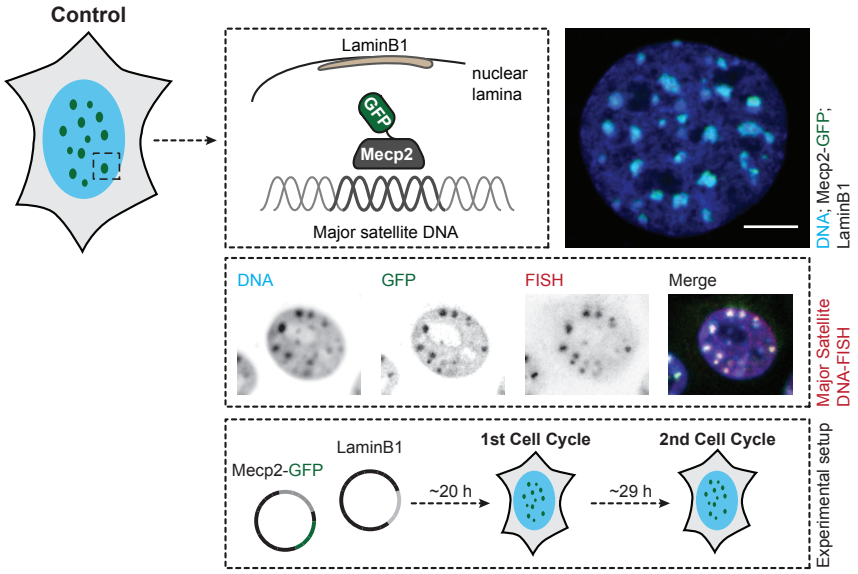

Figure II.1.: Control setup and its validation by major satellite DNA-FISH. In an untargeted state, the fusion protein composed of a chromocenter recognizer Mecp2 and GFP was visible as multiple green fluorescent spots throughout the nucleus, corresponding to constitutive heterochromatin (top section) and colocalized with DAPI dense structures. Untagged Lamin B1, a key component of the nuclear lamina, did not interact with Mecp2-GFP leading to original localized chromocenters throughout the whole nucleus. Mid section of fixed nuclei of an untargeted cell is shown: DAPI stained DNA in blue, Mecp2-GFP in green and untagged Lamin B1. The efficiency of this targeting approach was validated by major Satellite DNA-FISH (middle row), demonstrating a strong colocalization of the green targeting signal and the major satellite DNA-FISH signal: DAPI stained DNA in blue, Mecp2-GFP in green, major satellite DNA-FISH in red and the overlay of all channels (merge). The experimental setup (bottom row) implied the transient transfection of two plasmids: Mecp2-GFP and Lamin B1 followed by an incubation time of either 20 hours for first cell cycle studies or 49 hours for second cell cycle studies. Scale bar = 5 µm.

peripheral lamina was mostly unaffected in both control and targeted cells but a fraction of the LaminB colocalized with the star-shaped constitutive heterochromatin cluster of the second cell cycle. Likely, the over-expression of Lamin B1 is involved in the genesis of the star-shaped cluster in the second cell cycle as the Lamin B1 antibody signal colocalized with the targeted chromocenters.

To test whether NPCs are distribution was altered, we performed immuno-detection with antibodies against Nup153, which is an essential component for the anchoring of NPCs (Figure II.3B and Table II.S1). The data showed no differences between control and targeted cells and no colocalization between NPCs and targeted chromocenters as additionally assayed by measuring the H_{coeff} [42]. In this coefficient, particles that exclude each other show an H_{coeff} lower than 1, if particles are randomly distributed with respect to each other, the H_{coeff} is 1 and if they interact, this factor has a value above 1.

As shown by these data, our targeting strategy allowed us to manipulate the sub-nuclear localization of pericentric heterochromatin from the nuclear interior to the periphery without major disruption of the general nuclear organization. Therefore, we used this novel tool to ask whether these position re-arrangements would affect DNA replication timing and/or chromatin composition.

II.4.3 Targeting constitutive heterochromatin to the nuclear periphery increases mid S-phase length

We next asked whether this repositioning would be accompanied by changes in DNA replication timing from late to mid S-phase of the now peripherally located constitutive heterochromatin. If this were the case, we would expect an increase in the percentage of mid S-phase replication patterns due to an increase of mid S-phase duration. To test this hypothesis, we added thymidine analogs for a 30-minute pulse to proliferating populations of C2C12 control and targeted cells (Figure II.4A). In S-phase cells, which are actively replicating DNA, the thymidine analogs are incorporated into newly synthesized DNA. After detection, S-phase patterns were visually assessed and categorized into early, mid and late S-phase patterns. In control C2C12 cells, about 44% of the S-phase cells exhibited a late S-phase pattern (large labeled structures of constitutive heterochromatin), whereas 24% of cells were identified as mid replicating (perinuclear and perinucleolar

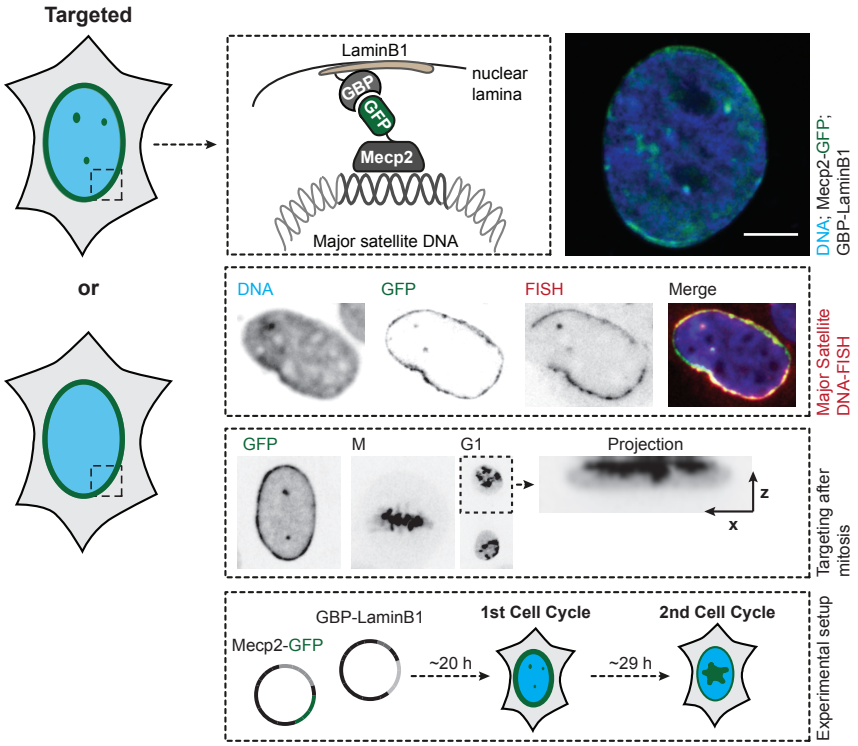

Figure II.2.: Targeting strategy to reposition chromocenters to the nuclear periphery and its validation by major satellite DNA-FISH. Schematic representation of the targeting approach in a C2C12 targeted cell (bottom section). Upon co-expression of Mecp2-GFP and Lamin-tagged GFP-binding protein (GBP), tagged chromocenters were repositioned to the nuclear periphery (top row). GBP, a camelidae-derived nanobody, acts as the key component of the targeting strategy. Because of the strong interaction of GFP and GBP in a subnanomolar range, chromocenters were repositioned to the nuclear periphery, clearly visible as a green targeting ring with or without internal chromocenters (two phenotypes possible). The functionality of the targeting was validated by major satellite DNA-FISH (upper middle row), resulting in a strong colocalization of the green targeted chromocenter signal and the major satellite DNA-FISH signal: DAPI stained DNA in blue, Mecp2-GFP and GBP-Lamin B1 in green, major satellite DNA-FISH in red and the overlay of all channels (merge). The efficiency and nontoxicity of this targeting approach was demonstrated by the fact that targeted C2C12 cells were able to undergo mitosis and replicated in a second cell cycle and even further cell cycles (lower middle row). After mitosis the green targeting ring signal no longer appeared as a targeting ring but rather as a 'star'-shaped topologically associated chromocenter cluster. For a better spatial visualization of the star-shaped cluster as a bulk of DNA distributing from the periphery into the inside of the nucleus, a xz projection of the GFP signal is shown. The xz-projection of targeted chromocenters of the 2nd cell cycle showed indeed that these topologically associated chromocenters were still repositioned and localized at the nuclear periphery. The experimental setup (bottom row) required a transient double transfection of Mecp2-GFP and GBP-Lamin B1 followed by an incubation time of either 20 hours for the first cell cycle studies or 49 hours for second cell cycle studies. Scale bar = 5 µm.

Taken from https://doi.org/10.1093/nar/gky368

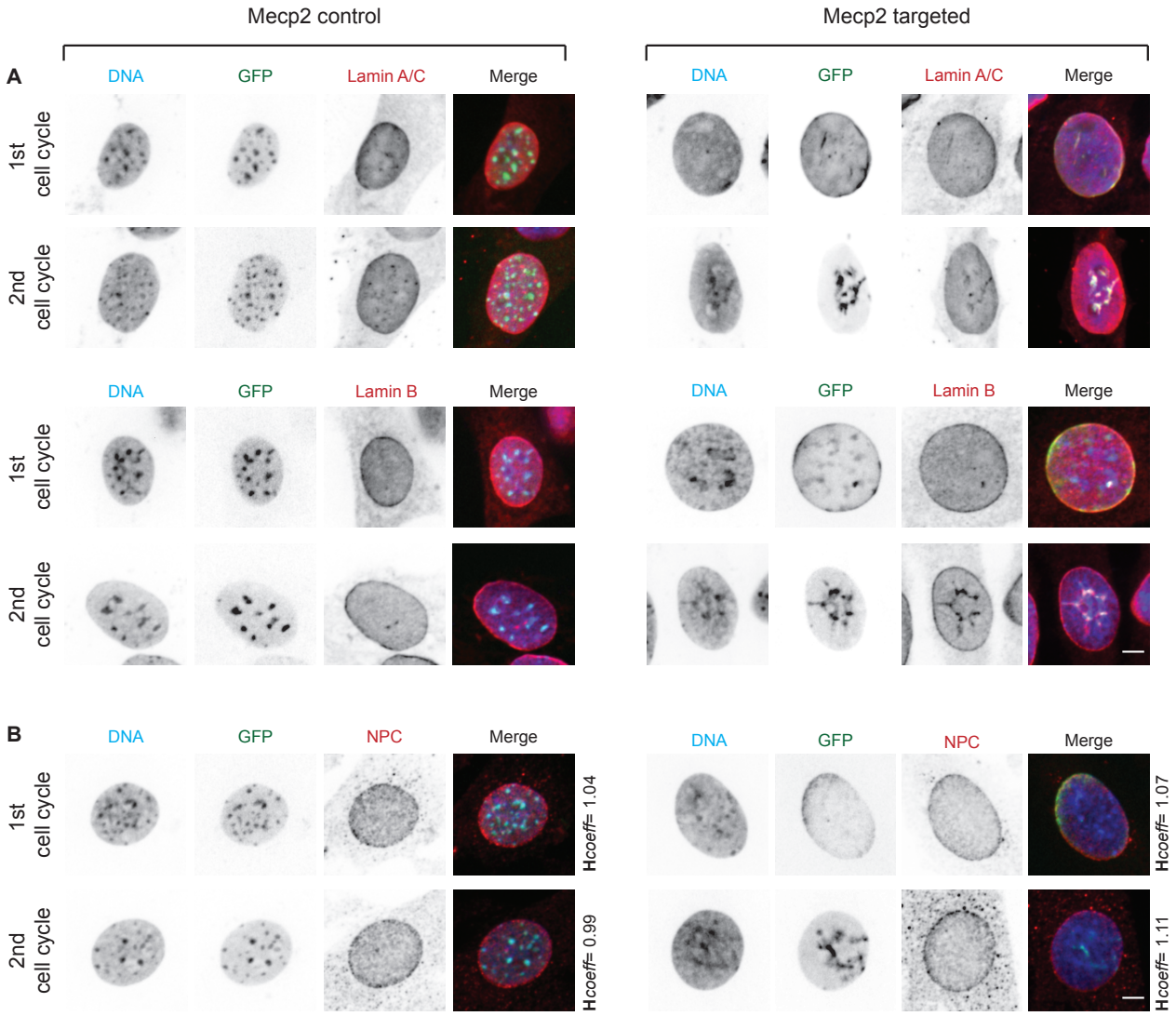

Figure II.3.: Organization of Lamin A/C, Lamin B and NPCs in control and targeted C2C12 cells. (A) C2C12 control and targeted cells were transfected with the appropriate constructs and were either incubated for 20 hours for first cell cycle studies or for 49 hours for second cell cycle studies. Immunostainings for Lamin A/C and Lamin B were performed. DAPI stained DNA (far left), Mecp2-GFP (mid-left), respective immunostaining (mid right) and merge of all channels (far right). No effect on lamin distribution is detectable, comparing control and targeted C2C12 cells. Only in the second cell cycle, Lamin B1 is colocalizing with the star- shaped chromocenter cluster. Scale bar = 5 µm. (B) Transfected C2C12 control and targeted cells in the first and the second cell cycle were stained for Nup153. DAPI stained DNA (far left), Mecp2-GFP (mid-left), NPCs (mid right) and merge of all channels (far right). No effect on the NPC distribution is measurable. Values of H_{coeff} colocalization analysis are indicated next to the respective merge. Scale bar = 5 µm.

foci of facultative heterochromatin). Upon repositioning of constitutive heterochromatin, targeted cells showed a decrease in late S-phase patterns to 33% along with an increase of mid S-phase patterns to 32%.
To test whether the increased frequency of mid S-phase patterns was the result of a prolonged mid S-phase duration, indicating more time required to replicate the extra major satellite DNA repositioned to the nuclear periphery, we set up a replication labeling with two pulses and a variable chase in between (Figure II.4B and Table II.S2). Again, thymidine analogs (BrdU and EdU) were added to proliferating populations of C2C12 control and targeted cells prior to fixation in a pulse-chase-pulse experimental protocol. We chose chases of 210 and 240 minutes as we knew from our S-phase distribution measurements that mid S-phase duration in C2C12 cells lasts around three hours and, hence, at least in control cells, we expected complete progression through mid S-phase during these chase times. We selected all cells that were undergoing mid S-phase during the first pulse (BrdU) and asked whether they stayed in mid S-phase (referred as mid/mid S) or whether they had transitioned into late S-phase after the different chase times. For simplification, we only plotted the percentage of cells that show in both pulses a mid S-phase pattern. Indeed, after a chase of 210 minutes most control C2C12 cells transitioned from mid S-phase to late S-phase, only a small percentage of cells still persisted in mid S-phase. After a chase of 240 minutes nearly all untargeted cells exhibited a late S-phase pattern in the second pulse. In contrast, targeted cells did not exhibit this clear decrease of mid S-phase patterns over the same time. After a chase of 210 minutes there were significantly more cells in mid S-phase (mid/mid S) than in control cells, demonstrating a prolonged duration of mid S-phase patterns detectable in targeted cells. This longer prevalence of mid S-phase patterns suggests that repositioning the normally late replicating constitutive heterochromatin to the nuclear periphery advanced their replication timing to mid S-phase.

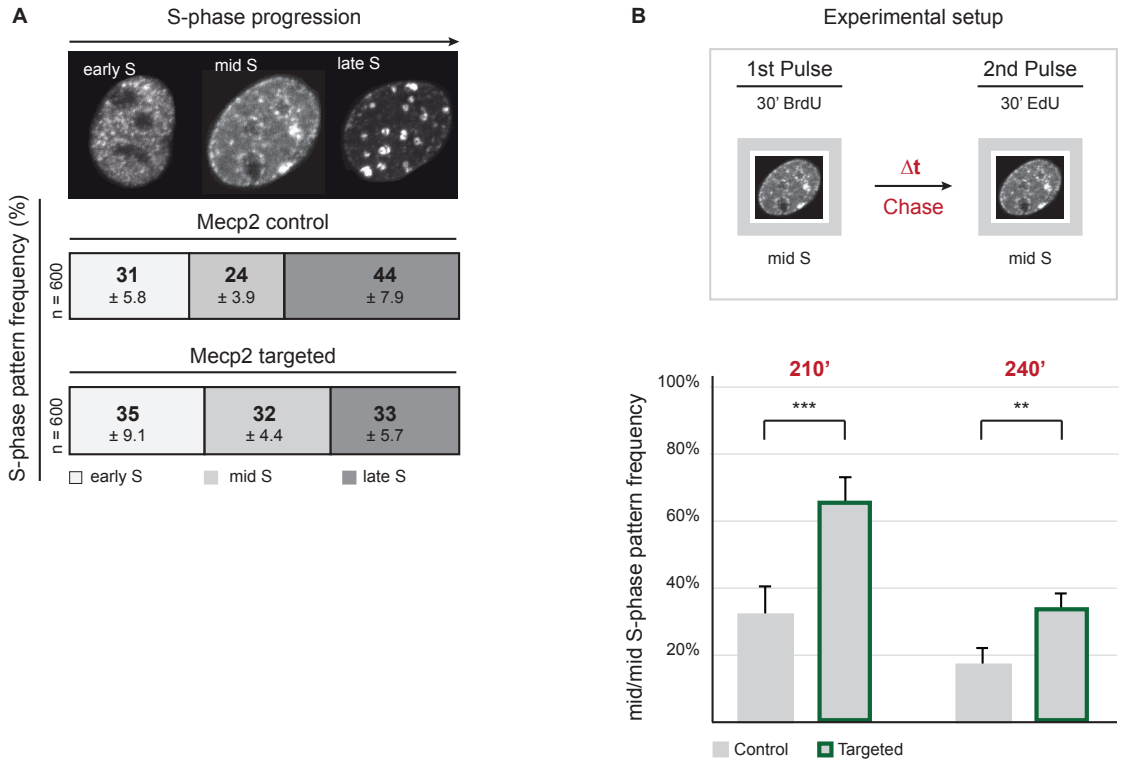

Figure II.4.: Effect of heterochromatin repositioning on mid S-phase pattern frequency and duration. (A) Modified thymidine analogs (BrdU or EdU) were given to the cells for 30 minutes prior to fixation. Detection thereof and fluorescence microscopy allowed the quantification of early, mid and late DNA replication patterns. Exemplary images of S-phase patterns were depicted to illustrate the categorization into early, mid and late S-phase stages. In C2C12 control cells about 44% of replicating cells showed a late S-phase pattern. In contrast, in targeted cells the frequency of late S-phase replication pattern decreased to 33% with a corresponding increase of mid S-phase replication patterns. Sample sizes are indicated on the left-hand side. Standard deviations of replicates are shown below the numbers in the boxes. (B) Schematic representation of the experimental setup to estimate the mid S-duration in C2C12 control and targeted cells. For the quantification, modified thymidine analogues (BrdU and EdU) were added to the culture medium in a pulse-chase-pulse experimental setup. Between 30 minutes pulses a variable thymidine chase of either 210 or 240 minutes was performed. Plotted was the percentage of cells that show in the second pulse (EdU) still a mid S-phase pattern (referred as mid/mid). Error bars represent standard deviations of replicates. Statistical significance was tested using the t-test, comparing control and targeted C2C12 cells. $**P$ <0.005; $***P$ <0.001.

II.4.4 Targeting constitutive heterochromatin to the nuclear periphery increases DNA content of targeted cells during mid S-phase

As a next step, we directly measured the amount of genomic DNA synthesized throughout the S-phase of control and targeted cells in C2C12 cells stably expressing RFP-PCNA. We visually categorized replicating cells by PCNA staining pattern in early, mid and late S-phase and in non S-phase cells. We analyzed the integrated DAPI intensity in individual nuclei and normalized all cells of one replicate to the G1 peak intensity (Figure II.5A) (for details see [7]). To investigate whether more DNA was replicated during mid S-phase due to repositioning of constitutive heterochromatin to the nuclear periphery, we plotted the relative DNA content (as G1 equivalents) (Figure II.5B and Table II.S1). Over time the DNA content increased from G1 towards G2 when cells duplicated their genome. We were able to show that the amount of genomic DNA is significantly increased in mid S-phase in targeted cells. This result is consistent with our previous finding that mid S-phase duration is prolonged in targeted cells, indicating that the repositioned normally late replicating constitutive heterochromatin replicates concomitantly with mid replicating facultative heterochromatin. To test this hypothesis we performed time-lapse microscopy to identify the DNA replication onset of repositioned chromocenters.

II.4.5 Manipulating the sub-nuclear heterochromatin position advances the onset of its DNA replication

To directly analyze the DNA replication onset of repositioned chromocenters, as well as the total duration of S-phase we assessed changes in the timing of peripheral and internal chromocenters in the first and the second cell cycle. For these experiments, we made again use of C2C12 cells stably expressing RFP-PCNA to label active DNA replication sites and co-transfected these cells with Mecp2-GFP to label chromocenters and either Lamin B1 or GBP-Lamin B1. We started the time-lapse imaging either 20 or 49 hours post-transfection for analysis of the first and second cell cycle respectively. The combination of fluorescent labels allowed us to measure colocalization of chromocenters (Mecp2-GFP) and DNA replication (RFP-PCNA) signals *in vivo* throughout S-phase. Images were collected every 20 minutes intervals for up to 16 hours, allowing us to unequivocally identify early, mid and late S-phase patterns in the same cell. We used these images to perform three steps of analysis: visual inspection of time-lapse images, line profile intensity measurements and H_{coeff} colocalization analysis [42]. We made use of the H_{coeff} to quantify colocalization of signals from chromocenters and DNA replication (Figure II.6 and Table II.S1).
Mecp2 control cells (Figure II.6A, Figure II.S13 and Figure II.S16) showed clear colocalization of chromocenter and replication signals during late S-phase only. The H_{coeff} analysis confirmed these findings with a value above 1 in late S-phase cells. In targeted cells (Figure II.6B, Figure II.S14 and Figure II.S17) two regions of interest (ROI) were chosen for the line intensity plot analysis: an untargeted chromocenter (as an internal control) and a peripheral chromocenter. As a consequence of repositioning to the periphery, we observed colocalization of targeted chromocenters and DNA replication already during mid S-phase, in parallel to facultative heterochromatin (shortly after the inactive X chromosome, Figure II.S3). In contrast, in control or internal chromocenters, we detected very little colocalization between chromocenters and sites of mid S-phase DNA replication. Conversely, these chromocenters showed a strong correlation of both signals in late S-phase. Time-lapse microscopy analysis also showed that the total S-phase length of targeted cells is not significantly affected by the repositioning (Figure II.6B).
As Mecp2 is known to recruit other proteins like histone deacetylases, by itself it could have an effect on DNA replication timing. For this reason, we used alternative targeting strategies to exclude that the effects we observed were due to the Mecp2 dependent targeting of chromocenters. To this end, we performed an equivalent set of experiments with DNA sequence-specific chromocenter binders: msTALE, msPZF, msCRISPR/dCas9 (Figures II.S4 and Table II.S2) with a similar outcome, i.e., earlier onset of DNA replication of constitutive heterochromatin. The fact that all four targeting systems to manipulate the position of constitutive heterochromatin resulted in similar effects on DNA replication strengthens our conclusions that the localization of DNA in the nucleus is involved in promoting earlier replication onset of chromocenters.
Next, we addressed the impact of DNA repositioning to the nuclear periphery on the second cell cycle (Figure II.6C, II.S5, Figure II.S15 and Figure II.S18). As described above, we observed that after mitosis, upon nuclear envelope reformation, in 100% of the cells the chromocenters adopted a star-shaped cluster at the nuclear periphery of the nucleus. We took advantage of this star-shaped chromocenter cluster to ensure that targeted cells were in the second cell cycle and followed them throughout the following S-phase. The effects on DNA replication timing of repositioned chromocenters in the second cell cycle proved to be even more dramatic than in the first cell cycle. The complete DNA replication of the star-shaped chromocenter cluster took place during mid S-phase, in parallel to the inactive X chromosome (Figure II.S5), as observable in the time-lapse images, by line intensity plot analysis and quantifiable using the H_{coeff}. Mid S-phase was followed by a very short late S-phase with only a few small active DNA replication sites no longer colocalizing with constitutive heterochromatin, also confirmed by the $H_{\text{coeff}} < 1$. The total S-phase duration in the second cell cycle of targeted cells was not dramatically altered (Figure II.6B). A slight increase of total S-phase duration in subsequent cell cycles is a known phenomenon due to mild phototoxicity of fluorescent protein imaging over long periods of time. Nevertheless targeted cells in the second cell cycle showed a further increase of mid S-phase duration accompanied with a

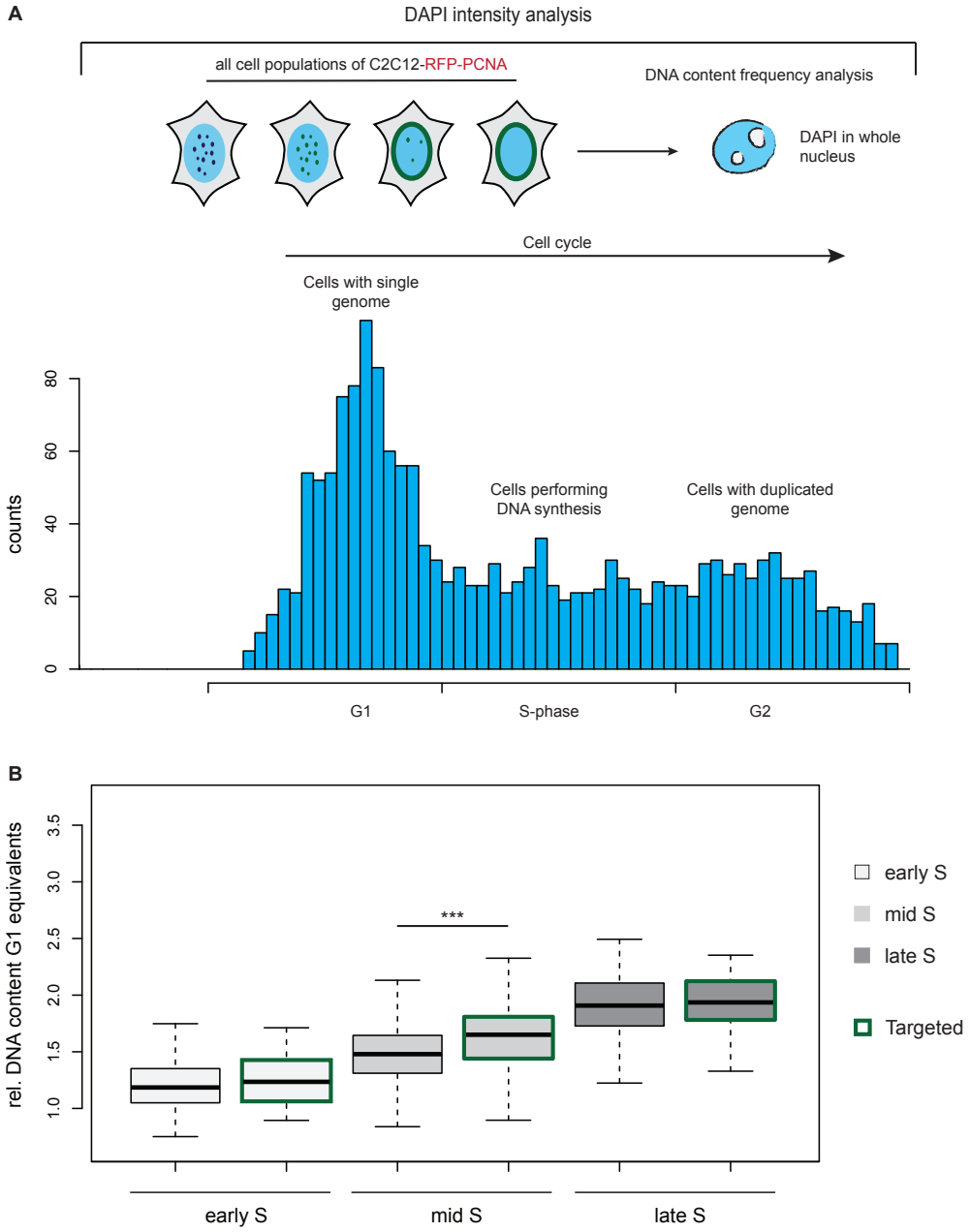

Figure II.5.: Increase of DNA content in mid S-phase in targeted relative to control cells. (A) DNA content frequency analysis throughout the cell cycle. Cells from each replicate (n>1,000) are binned by the integrated DNA content (DAPI signal) with the x-axis showing the DNA content of bins in arbitrary units. The first peak represents G1 cells exhibiting a single genome, whereas the second peak corresponds to cells in G2 phase with a duplicated genome. The ratio between the two peak maxima was measured to be 1.93. S-phase cells were manually scored into early, mid and late S-phase. (B) Cells from four replicates were normalized to the corresponding G1 peak (set to DNA content of 1) as described in the methods. Box plots depict S-phase substages from early to late for both control and targeted cells. The DNA content of targeted cells in mid S-phase is significantly increased in comparison to non-targeted cells. Statistical significance was tested using the Wilcoxon test, comparing control and targeted C2C12 cells. $***P$ <0.001.

Taken from https://doi.org/10.1093/nar/gky368

further decrease of late S-phase duration, shown by time-lapse experiments. To demonstrate that our previous findings are not C2C12 mouse myblasts specific, we performed the targeting strategy and analysis in addition in mouse embryonic fibroblasts (MEFs), which resulted in the same outcome of earlier DNA replication onset of peripheral constitutive heterochromatin (Figure II.S6 and Table II.S2).
In summary, our *in vivo* data demonstrated that, when repositioned to the nuclear periphery, constitutive heterochromatin shifted its replication timing towards mid S-phase and is replicated concomitantly to facultative heterochromatin. These changes in replication timing might be mediated by, result in or be independent of any changes in the composition of pericentric heterochromatin, as defined by post-translational histone modifications. Hence, we next investigated the chromatin marks of the repositioned constitutive heterochromatin.

II.4.6 Histone methylation marks are progressively lost at repositioned constitutive heterochromatin

The nuclear periphery is a region normally occupied by mid S-phase replicating, facultative heterochromatin. Therefore, peripheral targeting of pericentric heterochromatin could potentially change its epigenetic composition to mimic that of facultative heterochromatin. Such changes could in turn be responsible for the earlier onset of DNA replication. We hypothesized three different scenarios: 1) repositioning of chromocenters to the nuclear periphery causes epigenetic changes, which in turn advance DNA replication onset; 2) after replicating out-of-schedule, pericentric heterochromatin changes its typical epigenetic landscape; 3) nuclear position and DNA replication timing change without affecting the epigenetic composition of chromocenters. To test these different hypotheses, we analyzed the effect of peripheral repositioning on the levels of DNA condensation and different histone modifications during the first and second cell cycle.
First, we assessed the condensation level of peripheral chromocenters by analyzing the DNA (DAPI) signal at peripheral versus internal chromocenters in C2C12 cells. We were able to detect a significant decondensation of DNA at peripheral chromocenters in comparison to the internal ones (Figures II.7A and Table II.S1).
Next, we tested the effect of nuclear localization on the epigenetic composition of pericentric heterochromatin. To this end, we measured the levels of its characteristic chromatin marks by immuno-detection of various post-translational modifications (PTMs). This allowed us to quantify any changes in the levels of the respective epigenetic modification within chromocenters. The modifications investigated included H3K9 acetylation (H3K9ac), H3K27 trimethylation (H3K27me3), H3K9 dimethylation (H3K9me2), H3K9 trimethylation (H3K9me3) and H4K20 trimethylation (H4K20me3) (Figures II.7B, II.S7, II.S8 and Table II.S1). For this purpose, we developed a user-independent routine measuring the mean PTM levels at pericentric chromatin (for details see Figure II.S9). We made use of the internal chromocenters of partially targeted cells as control to quantify potential differences in the levels of PTMs for the first cell cycle and control cell chromocenters for the second cell cycle measurements.
H3K9ac, a mark of transcriptionally active chromatin, was enriched in euchromatic regions. In both, control and targeted cells, this mark was excluded from DAPI dense regions as well as from GFP-labeled chromocenters, corresponding to constitutive heterochromatin regions. Mean H3K9ac levels showed a mild decrease at peripheral chromocenters in contrast to internal chromocenters (Figure II.7B) and this was also the case in MEFs as well as when using sequence specific chromocenter binders (Figures II.S10, II.S11 and Table II.S2). Thus, we conclude that earlier onset of replication was not caused by increased histone acetylation upon nuclear repositioning.
We then investigated the distribution patterns of four epigenetic marks characteristic of heterochromatin, two enriched at facultative heterochromatic regions, usually found at the nuclear periphery, and two enriched in constitutive heterochromatin. Both H3K27me3 and H3K9me2 as markers for facultative heterochromatin were increased at the nucle(ol)ar periphery as well as, in the case of H3K27me3, on the inactive X chromosome(s) of the female cells. Due to the quasi-tetraploidy of C2C12 cells [23], two inactive X chromosomes were stained in control and targeted cells. However, neither of these modifications colocalized with constitutive heterochromatin, even when it was targeted to the nuclear periphery. The level of H3K27me3 stayed the same in control and targeted cells, whereas the level of H3K9me2 decreased over the second cell cycle in comparison to control cells. Prominent marks for constitutive heterochromatin like H3K9me3 and H4K20me3 showed a strong signal overlapping with DAPI-positive regions and GFP-stained chromocenters in control cells and partially also in targeted cells. Altogether, the level of these constitutive heterochromatin marks decreased over subsequent cell cycles in contrast to the control cells, indicating a progressive loss of the typical histone methylation marks. To rule out any change caused by the targeting strategy via Mecp2 binding or specific to C2C12 cells, we performed these experiments also for targeted cells via sequence-specific targeting (Figure II.S10) as well as with MEF cells (Figure II.S11). Typical constitutive heterochromatin marks were decreased for the sequence-specific binding, whereas in MEF cells H3K9me3 was more stable and only H4K20me3 was lost over time.

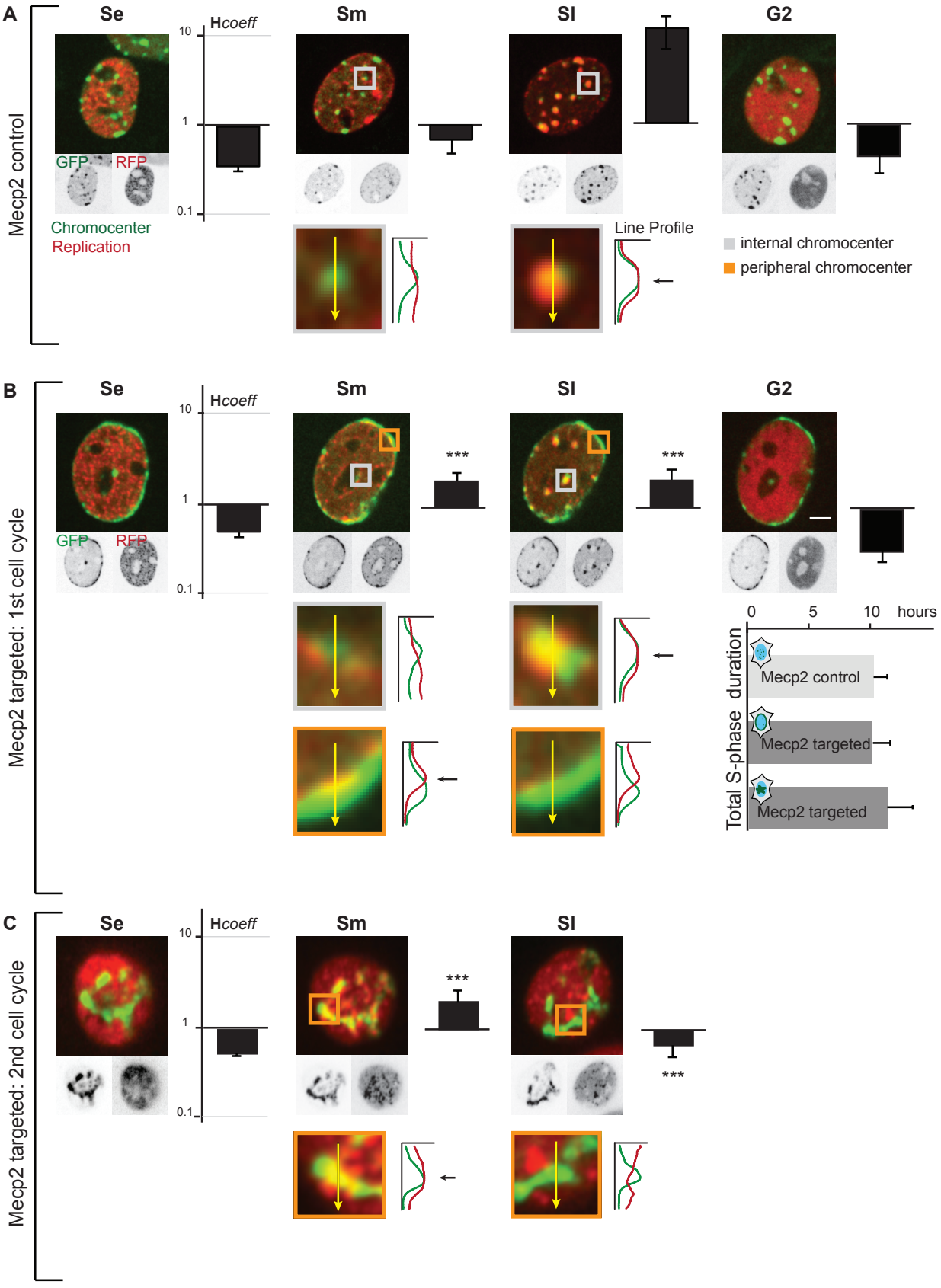

Figure II.6.: Advanced DNA replication onset in first and second cell cycles in targeted cells, but no effect on total S-phase duration. C2C12 cells stably expressing RFP-PCNA were transfected with Mecp2-GFP and either Lamin B1 (= control) or GBP-Lamin B1 (= targeted) and were incubated for 20 hours (A,B) or 49 hours (C) and subjected to live-cell time lapse microscopy. (A) Representative images depict the different DNA replication patterns in a C2C12 control cell over time. Line intensity plots of DNA replication (red) and chromocenters (green) with a selected ROI of control chromocenter in mid and late S-phase were shown. Control chromocenters showed an increased anti-correlation of DNA replication in mid S-phase, this changed in late S-phase towards high colocalization demonstrating the underlying DNA replication timing of control chromocenters. Colocalization of DNA replication foci and chromocenters was quantified with the H_{coeff} and plotted with bar graphs. H_{coeff} value >1 demonstrated the colocalization of DNA replication foci and control chromocenters in late S-phase. (B) Targeted peripheral chromocenters (orange ROI) showed an increased correlation of DNA replication (red) and chromocenters (green) already during mid S-phase, while internal chromocenters (grey ROI) still exhibited an anti-correlation. However, DNA replication of internal chromocenters in a targeted cell took place according to control chromocenters in late S-phase. Scale bar = 5 µm. Increased correlation of DNA replication and targeted chromocenters was verified by an H_{coeff} > 1 already in mid S-phase and only a mild increase was observed in late S-phase of internal chromocenters, whereas there was no correlation at all in early S-phase and G2 cells. Analysis of total S-phase duration from time lapse experiments of Mecp2 control and targeted cells revealed no significant differences in the first and second cell cycles. Error bars represent standard deviations of replicates. Statistical significance was tested using the Wilcoxon test, comparing control and targeted C2C12 cells in the first cell cycle. $***P$ <0.001. (C) DNA replication timing of targeted C2C12 cells in the 2nd cell cycle. The star-shaped chromocenter cluster started DNA replication during mid S-phase and also completed its DNA replication during mid S-phase. There was only colocalization between DNA replication and chromocenters during mid, whereas there was anti-correlation during late S-phase when only some small foci excluded from chromocenters were replicated. Error bars represent 95 Cl. Statistical significance was tested using the Wilcoxon test, comparing control and targeted C2C12 in the second cell cycle. $***P$ <0.001.

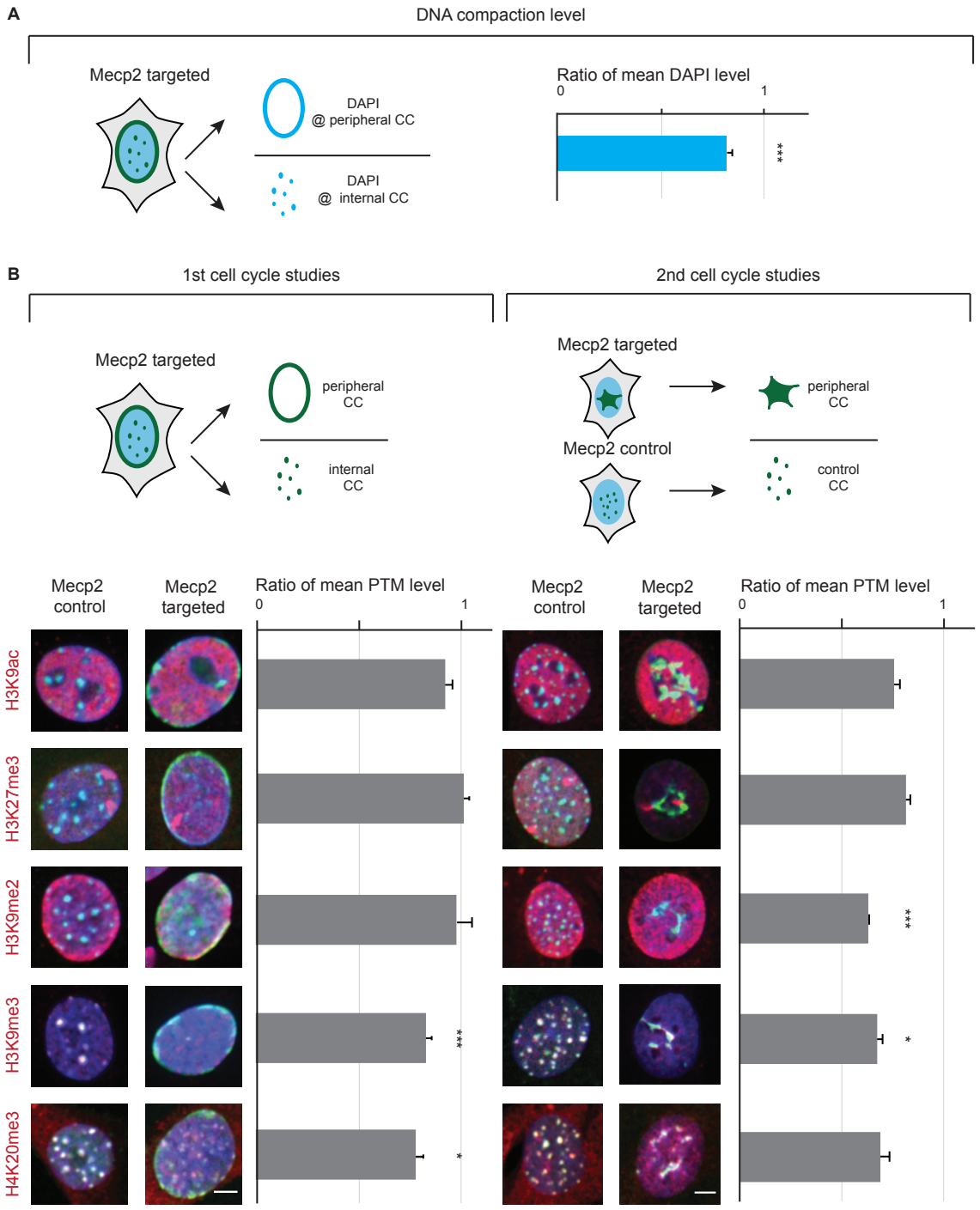

Figure II.7.: Distribution of prominent chromatin marks in control and targeted C2C12 cells. (A) DNA density was measured in Mecp2 targeted cells with the help of a user-independent analysis. The mean DAPI level was measured at peripheral versus internal chromocenters to estimate their compaction level. Bar graphs demonstrate the ratio of mean DAPI levels of peripheral versus internal chromocenters, indicating a significant decrease of condensation level of peripheral ones. Error bars represent 95 CI. Statistical significance was tested using the Wilcoxon test, comparing peripheral and internal chromocenters. $***P$ <0.001. (B) Prominent chromatin marks were analyzed by immunostainings: H3K9ac (euchromatin), H3K27me3 (facultative heterochromatin), H3K9me2 (marker for chromatin at the nuclear periphery), H3K9me3 and H4K20me3 (constitutive heterochromatin). Top row depicts the rationale of the user-independent analysis and the normalization of mean PTM values. Exemplary images show merges of all channels: DAPI stained DNA (blue), Mecp2-GFP (green), post-translational modification (PTM, red). Scale bar = 5 µm. Bar graphs demonstrate the ratio of mean PTM levels at peripheral versus internal chromocenters. Error bars represent 95 CI. Statistical significance was tested using the t-test, comparing control or internal chromocenters and targeted chromocenters. $*P$ <0.05; $***P$ <0.001.

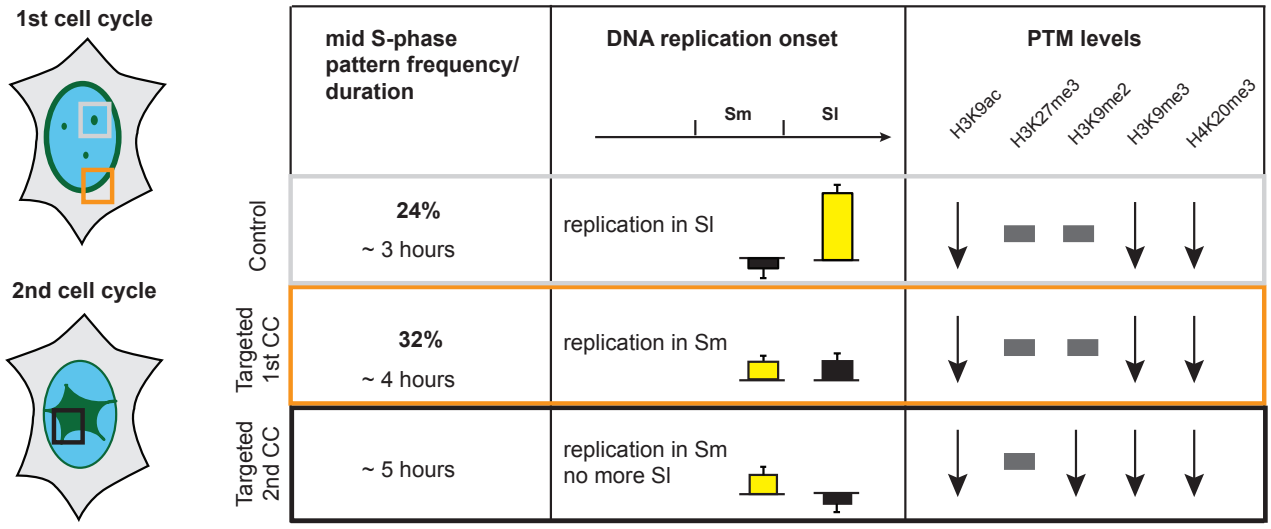

Figure II.8.: Summary of the effects of DNA position on its replication timing and epigenetic composition. Repositioning of constitutive heterochromatin resulted in advanced DNA replication onset of peripheral constitutive heterochromatin. In targeted cells the mid S-phase pattern frequency was increased, going hand in hand with a prolongation of mid S-phase duration, even more dramatic in the second cell cycle. Whereas control chromocenters replicated in late S-phase (colocalization indicated by yellow bar) and only in late S-phase, there was a shift towards mid S-phase in targeted cells. Peripheral chromocenters were replicated during mid S-phase, whereas internal chromocenters still replicated during late S-phase, indicated by H_{coeff} values over 1 in mid and late S-phase. Changes in the PTM level were indicated with arrows and no changes are illustrated by the grey rectangles. Chromocenters known to be hypoacetylated and enriched in H3K9me3 and H4K20me3, still showed these characteristic marks, only in decreased levels in comparison to control or internal chromocenters. The repositioning affected the reestablishment of the proper levels of the most characteristic histone marks leading to their progressive loss over subsequent cell cycles. The characteristic epigenetic marks for peripheral chromatin were not added *de novo* to the relocated constitutive heterochromatin.

In this study, we developed strategies to change the position of constitutive heterochromatin within the murine nucleus. Our targeting approach, based on the strong interaction between GFP and GBP, provides a very potent tool, suitable to tether different chromatin regions of interest to specific regions within the nucleus. Our assay, therefore, provides the novel opportunity to study the effect of nuclear position on a variety of genomic processes. By combining this approach with quantitative microscopy, we were able to study nuclear position as a potential regulator of DNA replication timing (Figure II.8). We show that repositioning chromocenters to the nuclear periphery and thereby transferring late replicating constitutive heterochromatin into a mid S-phase replicating environment, results in an earlier onset of replication of repositioned chromocenters. This effect was associated with a higher mid S-phase pattern frequency and a longer mid S-phase length. Furthermore, we were able to demonstrate that the DNA content is increased in targeted cells in mid S-phase. This result is consistent with the notion that more time in mid S-phase is required to replicate this out-of-schedule DNA at the nuclear periphery. These data suggest that the total number of active origins at any given time remains constant, in accordance to a limiting factor model (reviewed in [45]). The fact that repositioned chromatin adopts the replication timing of the neighboring facultative heterochromatin supports the idea that adjacent active origins of facultative heterochromatin triggered the earlier DNA replication onset of repositioned chromocenters. According to the domino effect model [46], stochastic activation of the first origin clusters leads to a chain reaction of activation of later origin clusters depending on the relative spatial distribution in the genome within the nucleus (Figure II.S12). Hence, we propose that the concentration of (regulatory) replication factors at the nuclear periphery during mid S-phase creates a microenvironment that enhances the firing efficiency/probability of origins in the nearby, repositioned constitutive heterochromatin. Upon targeting two parameters influencing origin firing are likely coming together: a high local concentration of DNA at the periphery as well as a high concentration of replisomes loaded on facultative heterochromatin. This hypothesis would also explain why chromocenters originally located in inner nuclear regions, surrounded by early replicating chromatin, are not generally triggered to fire earlier in S-phase. In an early replicating nucleus, euchromatin is distributed throughout the whole nucleus and, consequently, concentrations of DNA and replisomes are generally low. This is in contrast to

the situation when chromocenters are repositioned to the nuclear periphery where facultative heterochromatin is highly concentrated and replisomes are locally enriched in mid S-phase. Thus, we propose that normally late replicating origins of repositioned chromocenters were triggered by mid replicating origins in a domino-like manner, working not only in *cis* along the chromosome fiber, but rather also in *trans* across different chromosomes within the 3D nuclear space. One important consideration is that the effects on DNA replication timing are not targeting method specific (Figure II.S4) or cell line specific (Figure II.S6), generalizing the regulatory role of nuclear position of DNA on its DNA replication timing. Finally, we tested whether the epigenetic composition of chromocenters was affected by the repositioning to the nuclear periphery and whether this is a cause or a consequence thereof. The peripherally located chromocenters did exhibit a decrease in the normal levels of the histone methylation marks characteristic for constitutive heterochromatin. These marks were progressively lost over subsequent cell cycles. This suggests that the advanced DNA replication that results from the repositioning of chromocenters to the nuclear periphery affects the re-establishment of chromatin modifications after replication. Conversely, the characteristic epigenetic marks of peripheral facultative chromatin were not added *de novo* to the relocated constitutive heterochromatin. Moreover, the low levels of histone acetylation at chromocenters were maintained regardless of their nuclear location. Previous studies have shown that histone hypoacetylation is the main regulator of the late replication timing of chromocenters and neither H3K9me3 nor large-scale chromatin decondensation were directly involved in defining the late replication timing of constitutive heterochromatin [19]. The latter strongly suggests that the advanced replication timing we observed is not a result of changes in the chromatin marks on pericentric heterochromatin.

Shang et al. [47] set up a repositioning assay in *cis* along the chromosome. They developed a chromosome engineering system in chicken DT40 cells that allowed the efficient excision of the native centromere and the selection of chromosomes with neocentromeres. When a neocentromere was introduced into an early or early/mid replicating domain this resulted in a shift of the surrounding regions, which were previously early replicating, to a later DNA replication timing. When introducing the neocentromere into a late replicating domain, the replication timing of the domain was not altered. This study demonstrated that the insertion of a neocentromere seems to have affected the DNA replication timing of the surrounding domain in cis. It is though not clear whether this is due to impact of the neocentromere insertion in the chromatin state of the domain where it was inserted or on transcriptional activity of the domain. It is also unclear whether the 3D spatial nuclear distribution of the domain was altered upon neocentromere insertion. Whereas in Shang et al. [47] the receiving chromatin domain adopts the replication timing of the inserted neocentromere, in our study, positioning of constitutive heterochromatin in a facultative heterochromatin environment in *trans*, affected rather the replication timing of the repositioned chromatin.

Taken together, we propose that the nuclear position directly affects DNA replication timing of peripheral chromocenters, independently of changes in histone modifications. Furthermore, the changed position and replication timing of constitutive heterochromatin impairs post-replicative establishment of chromatin marks.

II.6 Acknowledgments

We thank H. Leonhardt for providing the C2C12 and MEF cell lines stably expressing RFP-PCNA and plasmid constructs as well as Irina Solovei for providing antibodies to Nup153. We are indebted to A. K. Ludwig for the Priithon script for user-independent image analysis; A. Scholl for cell line characterization help and A. Lehmkuhl for cell line characterization and excellent technical work.

II.7 Funding

This work was supported by the German Research Foundation (grant number DFG CA198/9-1 and 9-2 to M.C.C.) and by the Grant Agency of Czech Republic (P302/12/G157). Funding for open access charge: German Research Foundation.

Conflict of interest statement.

None declared.

II.8 References

1. Chagin, V. O., Stear, J. H. & Cardoso, M. C. Organization of DNA replication. *Cold Spring Harb Perspect Biol* **2,** a000737 (2010).
2. Jackson, D. A. & Pombo, A. Replicon clusters are stable units of chromosome structure: evidence that nuclear organization contributes to the efficient activation and propagation of S phase in human cells. *J Cell Biol* **140,** 1285–95 (1998).

3. Leonhardt, H. *et al.* Dynamics of DNA replication factories in living cells. *J Cell Biol* **149,** 271–80 (2000).
4. Nakamura, H., Morita, T. & Sato, C. Structural organizations of replicon domains during DNA synthetic phase in the mammalian nucleus. *Exp Cell Res* **165,** 291–7 (1986).
5. Fox, M. H., Arndt-Jovin, D. J., Jovin, T. M., Baumann, P. H. & Robert-Nicoud, M. Spatial and temporal distribution of DNA replication sites localized by immunofluorescence and confocal microscopy in mouse fibroblasts. *J Cell Sci* **99,** 247–53 (1991).
6. Baddeley, D. *et al.* Measurement of replication structures at the nanometer scale using super-resolution light microscopy. *Nucleic Acids Res* **38,** e8 (2010).
7. Lob, D. *et al.* 3D replicon distributions arise from stochastic initiation and domino-like DNA replication progression. *Nat Commun* **7,** 11207 (2016).
8. Chagin, V. O. *et al.* 4D Visualization of replication foci in mammalian cells corresponding to individual replicons. *Nat Commun* **7,** 11231 (2016).
9. Casas-Delucchi, C. S. & Cardoso, M. C. Epigenetic control of DNA replication dynamics in mammals. *Nucleus* **2,** 370–82 (2011).
10. Pope, B. D. & Gilbert, D. M. The replication domain model: regulating replicon firing in the context of large-scale chromosome architecture. *J Mol Biol* **425,** 4690–5 (2013).
11. Farkash-Amar, S. *et al.* Global organization of replication time zones of the mouse genome. *Genome Res* **18,** 1562–70 (2008).
12. Hyrien, O. Peaks cloaked in the mist: the landscape of mammalian replication origins. *J Cell Biol* **208,** 147–60 (2015).
13. Gilbert, D. M. Making sense of eukaryotic DNA replication origins. *Science* **294,** 96–100 (2001).
14. Cayrou, C. *et al.* New insights into replication origin characteristics in metazoans. *Cell Cycle* **11,** 658–67 (2012).
15. Cayrou, C. *et al.* Genome-scale analysis of metazoan replication origins reveals their organization in specific but flexible sites defined by conserved features. *Genome Res* **21,** 1438–49 (2011).
16. Raghuraman, M. K., Brewer, B. J. & Fangman, W. L. Cell cycle-dependent establishment of a late replication program. *Science* **276,** 806–9 (1997).
17. Aladjem, M. I. Replication in context: dynamic regulation of DNA replication patterns in metazoans. *Nat Rev Genet* **8,** 588–600 (2007).
18. Schwaiger, M. *et al.* Chromatin state marks cell-type- and gender-specific replication of the Drosophila genome. *Genes Dev* **23,** 589–601 (2009).
19. Casas-Delucchi, C. S., Becker, A., Bolius, J. J. & Cardoso, M. C. Targeted manipulation of heterochromatin rescues MeCP2 Rett mutants and re-establishes higher order chromatin organization. *Nucleic Acids Res* **40,** e176 (2012).
20. Jorgensen, H. F. *et al.* The impact of chromatin modifiers on the timing of locus replication in mouse embryonic stem cells. *Genome Biol* **8,** R169 (2007).
21. O'Keefe, R. T., Henderson, S. C. & Spector, D. L. Dynamic organization of DNA replication in mammalian cell nuclei: spatially and temporally defined replication of chromosome-specific alpha-satellite DNA sequences. *J Cell Biol* **116,** 1095–110 (1992).
22. Wu, R., Singh, P. B. & Gilbert, D. M. Uncoupling global and fine-tuning replication timing determinants for mouse pericentric heterochromatin. *J Cell Biol* **174,** 185–94 (2006).
23. Casas-Delucchi, C. S. *et al.* Histone acetylation controls the inactive X chromosome replication dynamics. *Nat Commun* **2,** 222 (2011).
24. Kemp, M. G., Ghosh, M., Liu, G. & Leffak, M. The histone deacetylase inhibitor trichostatin A alters the pattern of DNA replication origin activity in human cells. *Nucleic Acids Res* **33,** 325–36 (2005).
25. Schwaiger, M., Kohler, H., Oakeley, E. J., Stadler, M. B. & Schubeler, D. Heterochromatin protein 1 (HP1) modulates replication timing of the Drosophila genome. *Genome Res* **20,** 771–80 (2010).
26. Vogelauer, M., Rubbi, L., Lucas, I., Brewer, B. J. & Grunstein, M. Histone acetylation regulates the time of replication origin firing. *Mol Cell* **10,** 1223–33 (2002).
27. Dimitrova, D. S. & Gilbert, D. M. The spatial position and replication timing of chromosomal domains are both established in early G1 phase. *Mol Cell* **4,** 983–93 (1999).
28. Ebrahimi, H. *et al.* Early initiation of a replication origin tethered at the nuclear periphery. *J Cell Sci* **123,** 1015–9 (2010).

29. Jones, K. W. Chromosomal and nuclear location of mouse satellite DNA in individual cells. *Nature* **225,** 912–5 (1970).

30. Vissel, B. & Choo, K. H. Mouse major (gamma) satellite DNA is highly conserved and organized into extremely long tandem arrays: implications for recombination between nonhomologous chromosomes. *Genomics* **5,** 407–14 (1989).

31. Brero, A. *et al.* Methyl CpG-binding proteins induce large-scale chromatin reorganization during terminal differentiation. *J Cell Biol* **169,** 733–43 (2005).

32. Rothbauer, U. *et al.* A versatile nanotrap for biochemical and functional studies with fluorescent fusion proteins. *Mol Cell Proteomics* **7,** 282–9 (2008).

33. Rothbauer, U. *et al.* Targeting and tracing antigens in live cells with fluorescent nanobodies. *Nat Methods* **3,** 887–9 (2006).

34. Kirchhofer, A. *et al.* Modulation of protein properties in living cells using nanobodies. *Nat Struct Mol Biol* **17,** 133–8 (2010).

35. Thanisch, K. *et al.* Targeting and tracing of specific DNA sequences with dTALEs in living cells. *Nucleic Acids Res* **42,** e38 (2014).

36. Lindhout, B. I. *et al.* Live cell imaging of repetitive DNA sequences via GFP-tagged polydactyl zinc finger proteins. *Nucleic Acids Res* **35,** e107 (2007).

37. Anton, T., Bultmann, S., Leonhardt, H. & Markaki, Y. Visualization of specific DNA sequences in living mouse embryonic stem cells with a programmable fluorescent CRISPR/Cas system. *Nucleus* **5,** 163–72 (2014).

38. Yaffe, D. & Saxel, O. Serial passaging and differentiation of myogenic cells isolated from dystrophic mouse muscle. *Nature* **270,** 725–7 (1977).

39. Peters, A. H. *et al.* Loss of the Suv39h histone methyltransferases impairs mammalian heterochromatin and genome stability. *Cell* **107,** 323–37 (2001).

40. Sporbert, A., Domaing, P., Leonhardt, H. & Cardoso, M. C. PCNA acts as a stationary loading platform for transiently interacting Okazaki fragment maturation proteins. *Nucleic Acids Res* **33,** 3521–8 (2005).

41. Salic, A. & Mitchison, T. J. A chemical method for fast and sensitive detection of DNA synthesis in vivo. *Proc Natl Acad Sci U S A* **105,** 2415–20 (2008).

42. Herce, H. D., Casas-Delucchi, C. S. & Cardoso, M. C. New image colocalization coefficient for fluorescence microscopy to quantify (bio-)molecular interactions. *J Microsc* **249,** 184–94 (2013).

43. Maeshima, K. *et al.* Cell-cycle-dependent dynamics of nuclear pores: pore-free islands and lamins. *J Cell Sci* **119,** 4442–51 (2006).

44. Shimi, T. *et al.* The A- and B-type nuclear lamin networks: microdomains involved in chromatin organization and transcription. *Genes Dev* **22,** 3409–21 (2008).

45. Rhind, N. & Gilbert, D. M. DNA replication timing. *Cold Spring Harb Perspect Biol* **5,** a010132 (2013).

46. Sporbert, A., Gahl, A., Ankerhold, R., Leonhardt, H. & Cardoso, M. C. DNA polymerase clamp shows little turnover at established replication sites but sequential de novo assembly at adjacent origin clusters. *Mol Cell* **10,** 1355–65 (2002).

47. Shang, W. H. *et al.* Chromosome engineering allows the efficient isolation of vertebrate neocentromeres. *Dev Cell* **24,** 635–48 (2013).

Taken from https://doi.org/10.1093/nar/gky368

A

Targeting mode (X)	Mecp2	msTALE	msPZF*	msCRISPR/dCas9
Operating mode	binds mCpG	binds DNA sequence (TGGCGAGAAAAACTGAAAAT)	binds DNA sequence (GGCGAGGAA)	binds via guide RNA (GCAAGAAAACTGAAAATCA)

* control is not fixable

B

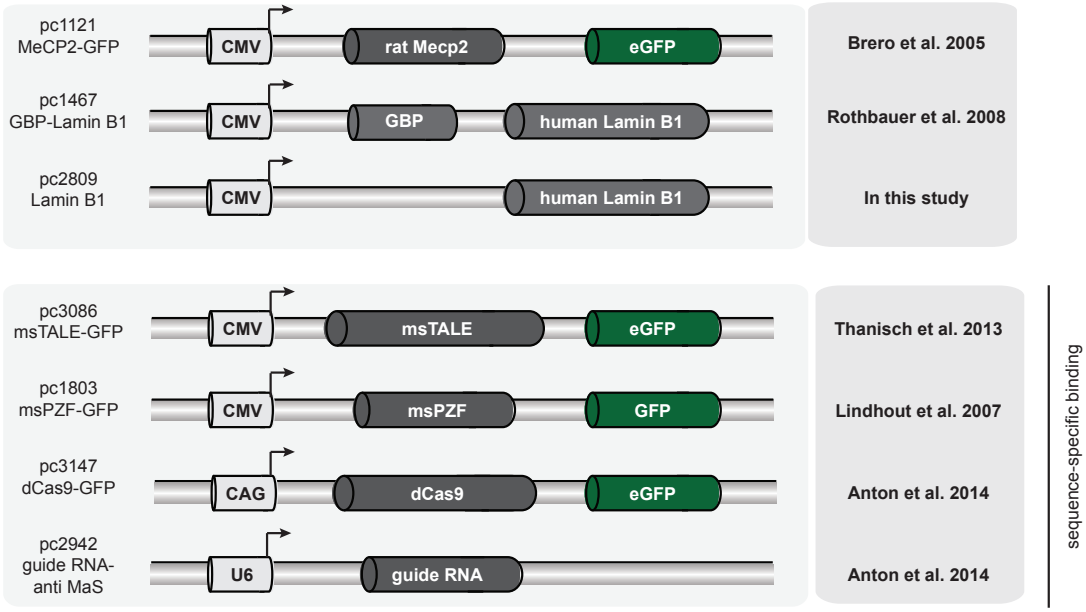

C

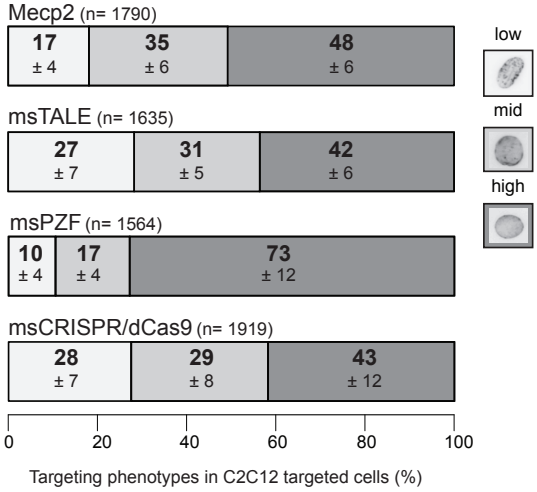

D

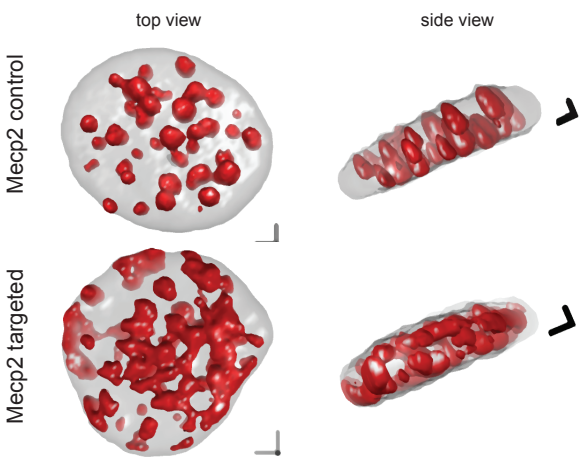

E

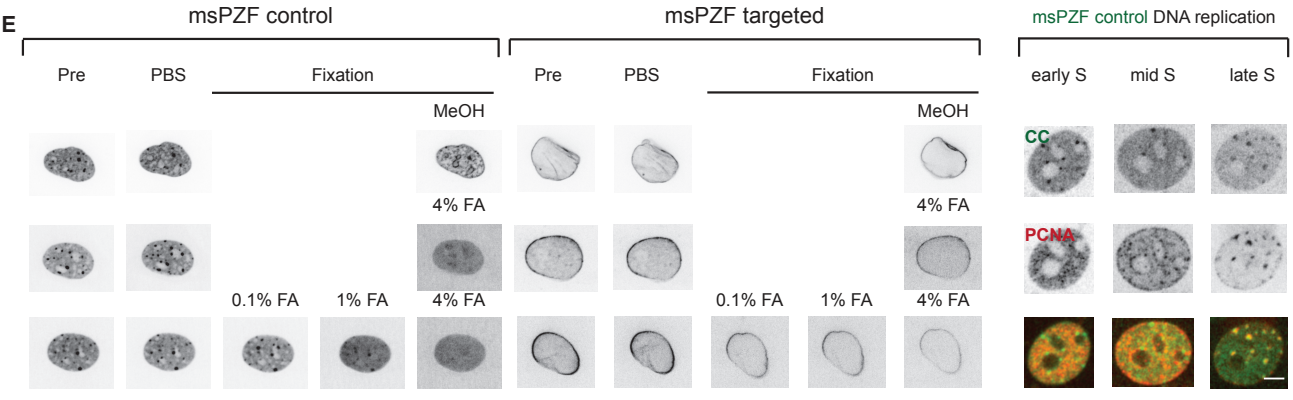

Figure II.S1.: Different targeting strategies to reposition chromocenters to the nuclear periphery: targeting mode, targeting efficiency and application
(A) Different chromocenter recognizers (X-GFP) were used to reposition chromocenters to the nuclear periphery. Recognizers either bound highly methylated DNA of chromocenters, like Mecp2 (1), or they detected, in a sequence-specific manner, major satellite DNA. Sequence-specific chromocenter detection was obtained by the usage of a major satellite specific zinc finger protein (2), a major satellite specific TALE (3) or with a major satellite specific guide RNA by CRISPR/d-Cas9 targeting (4). These constructs were either double transfected with Lamin B1 (pc2809) (control) or GBP-Lamin B1 (pc1467) (targeted) in combination with msPZF (pc1803), msTALE (pc3086) or triple transfected with msCRISPR/dCas9 (pc3147, pc2942). Potential chromocenter recognizers are listed with the respective binding motifs. (B) Relevant parts of expression constructs for either indirect binding (upper box) or sequence-specific binding (lower box). On the right side the corresponding reference of the plasmids are shown. Drawings are not to scale.
(C) Overview of targeting efficiencies of different targeting strategies. Evaluated by their status of chromocenter repositioning C2C12 targeted cells were classified into three categories: low, mid and high targeting efficiency. A multitude of internal chromocenters and a very weak targeting ring at the nuclear periphery characterized the low level of targeting. Mid level targeted C2C12 cells showed internal chromocenters with an additional targeting ring at the nuclear periphery and a strong fluorescence GFP signal. High level targeted C2C12 cells did no longer show any internal chromocenters; instead they only showed a clear and complete targeting ring. For this study, we were mostly interested in the mid-targeted phenotype, as this level allowed the direct evaluation of the impact of nuclear position in the same cell. As the Mecp2-based targeting strategy showed the highest percentage of the mid-targeted level, we used this targeting strategy for most experiments.
(D) 3D reconstruction of mouse nuclei (grey) transfected with Mecp2-GFP and Lamin B1 (top) or Mecp2-GFP and GBP-Lamin B1 (bottom). Major satellite DNA-FISH was performed to label major satellite repeats at pericentromeric heterochromatin (red). Control chromocenters are homogenously distributed throughout the nucleus. Top and side views of a Mecp2 targeted cell demonstrate that the recruitment of Mecp2-GFP to the nuclear periphery is accompanied with a re-localization of the highly methylated heterochromatic regions, resulting in the disruption and displacement of chromocenters.
(E) Overview of C2C12 cells transfected with msPZF-GFP and Lamin B1 (control) or with msPZF-GFP and GBP-Lamin B1 (targeted). Control cells transfected with the respective zinc finger constructs were not fixable, neither with methanol nor with different formaldehyde fixation protocols. More likely because of its high mobility and low affinity of binding (2). Only targeted msPZF-GFP samples were fixable, indicating the decrease of dynamic binding of msPZF-GFP by the interaction with the GBP-containing counterpart. C2C12 control cells transfected with msPZF-GFP and Lamin B1 were only used for time lapse microscopy live-cell experiments.

Taken from https://doi.org/10.1093/nar/gky368

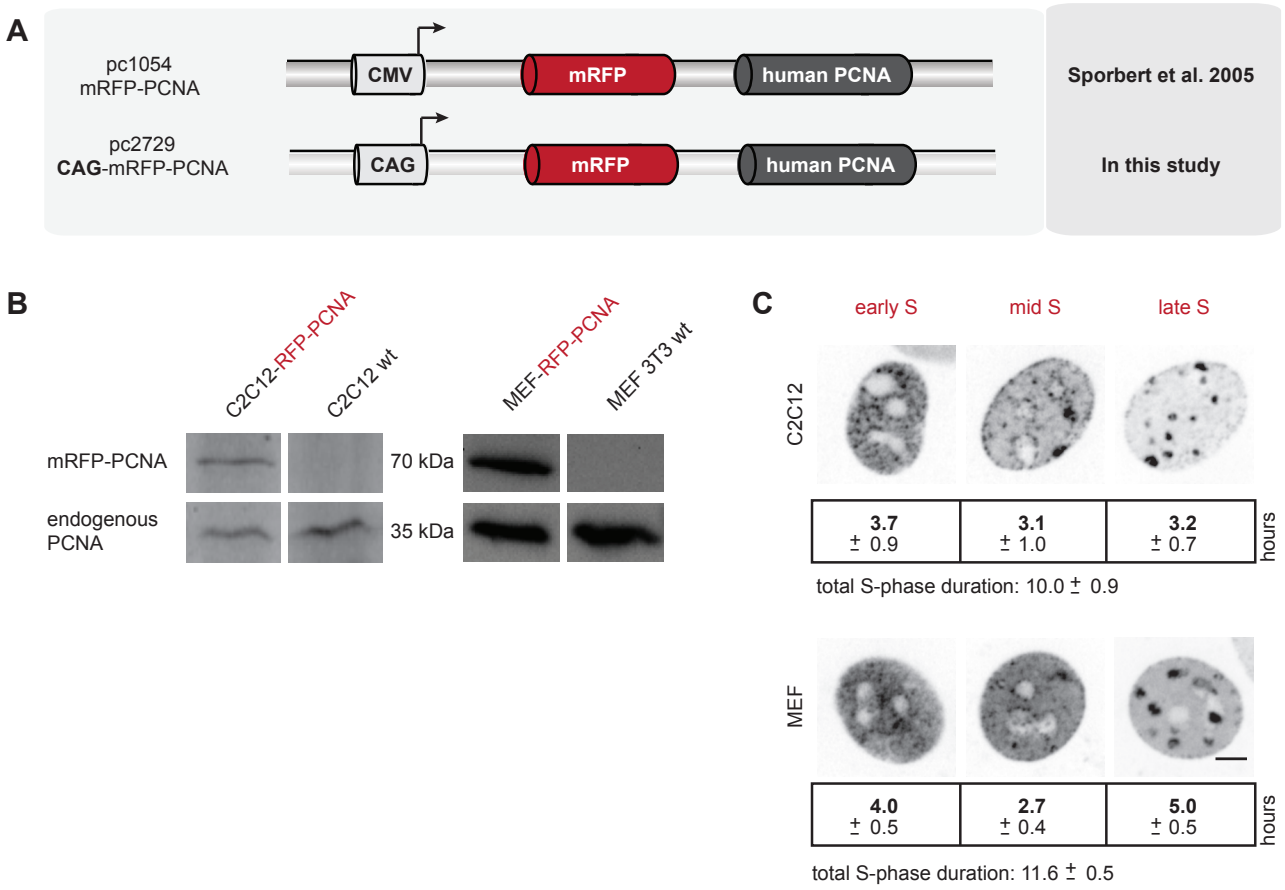

Figure II.S2.: Characterization of cell lines stably expressing RFP-PCNA.
(A) Relevant parts of expression constructs needed for stable cell line generation. mRFP-PCNA from pc1054 was cloned into a backbone expression vector carrying the CAG-promoter. The resulting construct (pc2729) was used for transfection of C2C12 and MEF cells to generate cells with stable expression of RFP-tagged PCNA.
(B) For the PCNA protein characterization via Western Blot C2C12 and MEF cells, either wild type or stably expressing RFP-PCNA were cultured to >70% confluence for harvesting. Cells were lysed in 4x SDS loading buffer by resuspending with a syringe. Whole protein lysates were blotted on a nitrocellulose membrane (GE Healthcare, Munich, Germany). Visualization of immunoreactive bands was achieved by ECL plus Western Blot detection reagent (GE Healthcare, Munich, Germany). The following antibodies were used: mouse anti-PCNA (1/2000, Santa Cruz, Dallas, USA, Cat #: sc-56) over night at 4 °C and sheep anti-mouse IgG HRP (1/5000, GE Healthcare, Munich, Germany, Cat #:NA931) for one hour at room temperature. Upper row shows positive mRFP-PCNA band (70 kD) in RFP-PCNA expressing cell lines, whereas no equivalent size band is detectable in the respective wildtype. Lower row shows positive endogenous PCNA bands in all cell lines.
(C) Depiction of S-phase replication patterns in C2C12 and MEF cell line stably expressing RFP-PCNA. Images demonstrate typical distribution of replication foci during all substages of S-phase. Total S-phase and substage durations obtained from following individual cells in time lapse microscopy experiments are indicated in the boxes below with the respective standard deviations. Scale bar = 5 µm.

Taken from https://doi.org/10.1093/nar/gky368

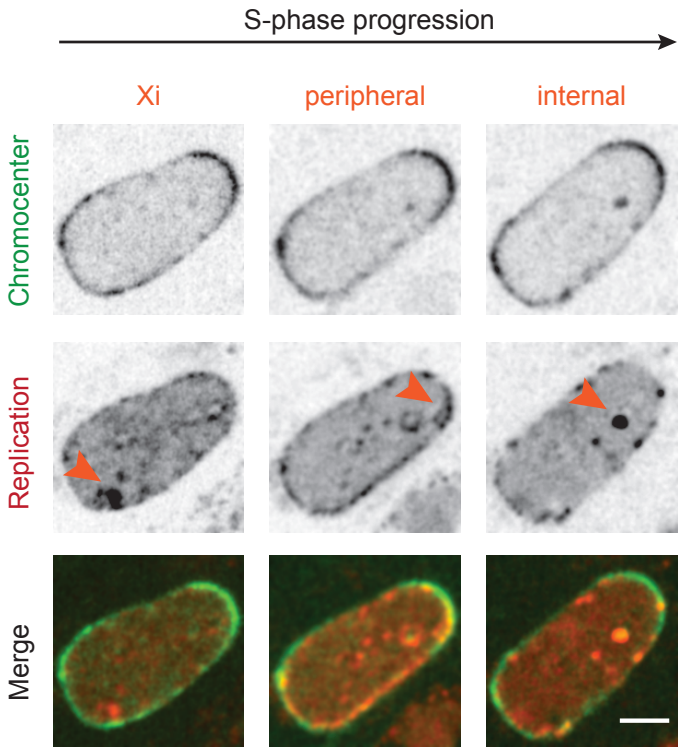

Figure II.S3.: Temporal order of DNA replication in a targeted cell.
Depiction of a C2C12 cell stably expressing RFP-PCNA transfected with Mecp2-GFP and GBP-Lamin B1 throughout mid and late S-phase. Chromocenters in green, DNA replication in red and the merge as an overlay of both channels. Arrows depict the temporal order of DNA replication in targeted C2C12 cells: first the inactive X chromosome (Xi) is replicated, followed by the peripheral targeting ring and finally DNA replication of internal control chromocenters that were not repositioned. Scale bar = 5 µm.

Taken from https://doi.org/10.1093/nar/gky368

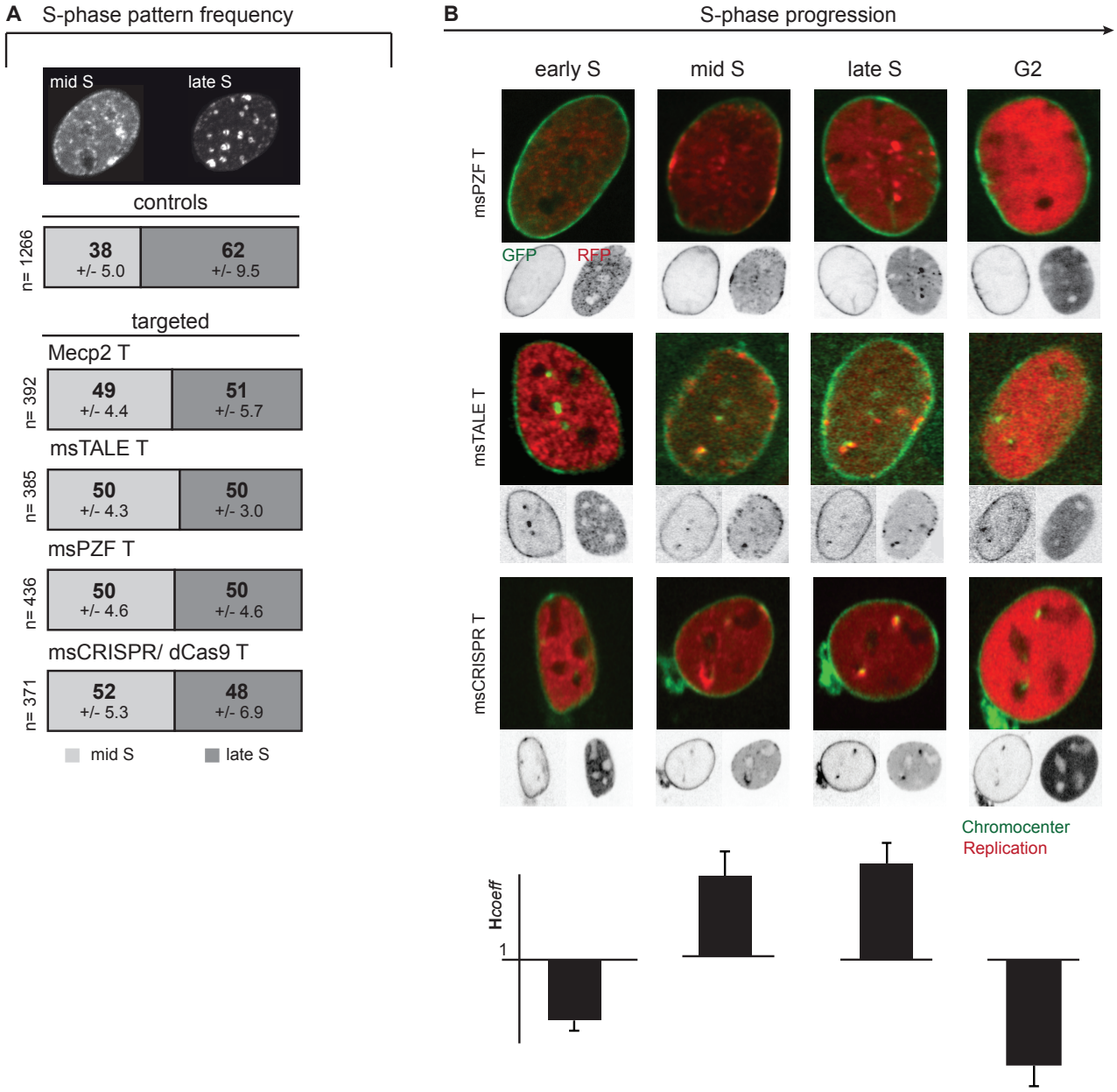

Figure II.S4.: Sequence-specific targeted cells show an increased mid S-phase pattern frequency and earlier DNA replication onset of chromocenters.
(A) Modified thymidine analogs (BrdU or EdU) were given to the cells for 30 minutes prior to fixation. Detection thereof and fluorescence microscopy allowed the quantification of mid versus late DNA replication patterns. Exemplary images of mid and late S-phase pattern were depicted to illustrate the categorization into mid and late S-phase stages. The distribution of mid versus late S-phase replication patterns is shown. In C2C12 control cells (n= 1266 cells) about 62% of replicating cells were in late S-phase. Targeted cells, irrespective of the targeting mode, showed a decrease in frequency of late S-phase replication pattern with a corresponding increase of mid S-phase replication patterns. Sample sizes are indicated on the left. Standard deviations of different replicates are shown.
(B) C2C12 cells stably expressing RFP-PCNA were transfected with either msPZF, msTALE or msCRISPR/dCas9 and GBP-Lamin B1. Representative images depict the different DNA replication patterns in C2C12 targeted cells over time. Colocalization of DNA replication foci and chromocenters was quantified with the H_{coeff} and plotted with bar graphs. Values >1 demonstrated the colocalization of DNA replication foci and chromocenters already in mid S-phase for peripheral chromocenters, but also in late S-phase for internal chromocenters. Error bars represent 95 CI.

Taken from https://doi.org/10.1093/nar/gky368

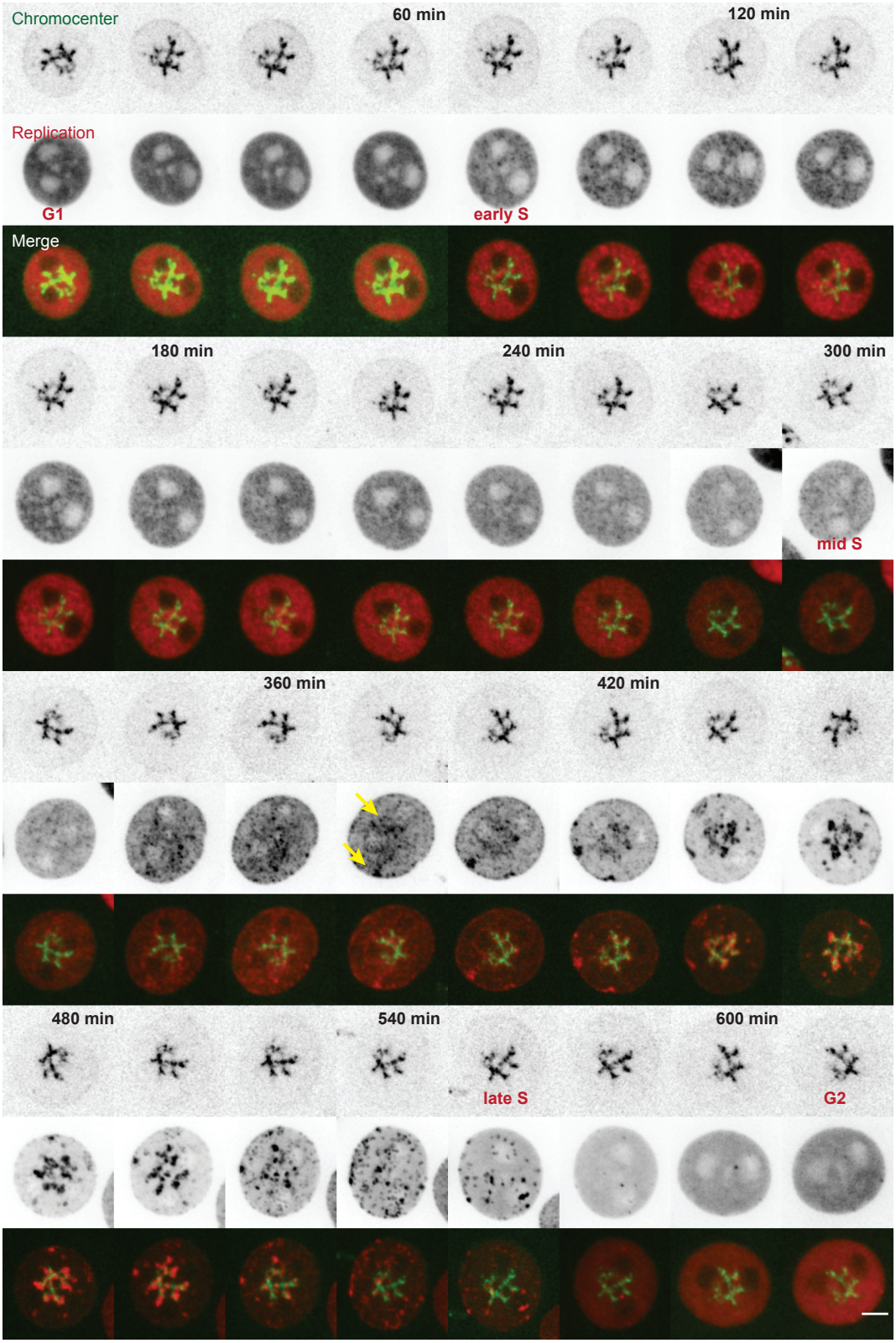

Figure II.S5.: Gallery of Mecp2 targeted cell throughout second cell cycle.
Gallery of images of time lapse experiment of a Mecp2 targeted cell in the second cell cycle: DNA replication (red), chromocenters (green) and overlay of both channels (merge). Scale bar = 5 µm. Yellow arrows indicate the concomitant DNA replication of the inactive X chromosome (hallmark of mid S-phase in female cells) and the star-shaped chromocenter cluster. Depicted Mecp2 targeted cell progressed from G1 to G2 phase.

Taken from https://doi.org/10.1093/nar/gky368

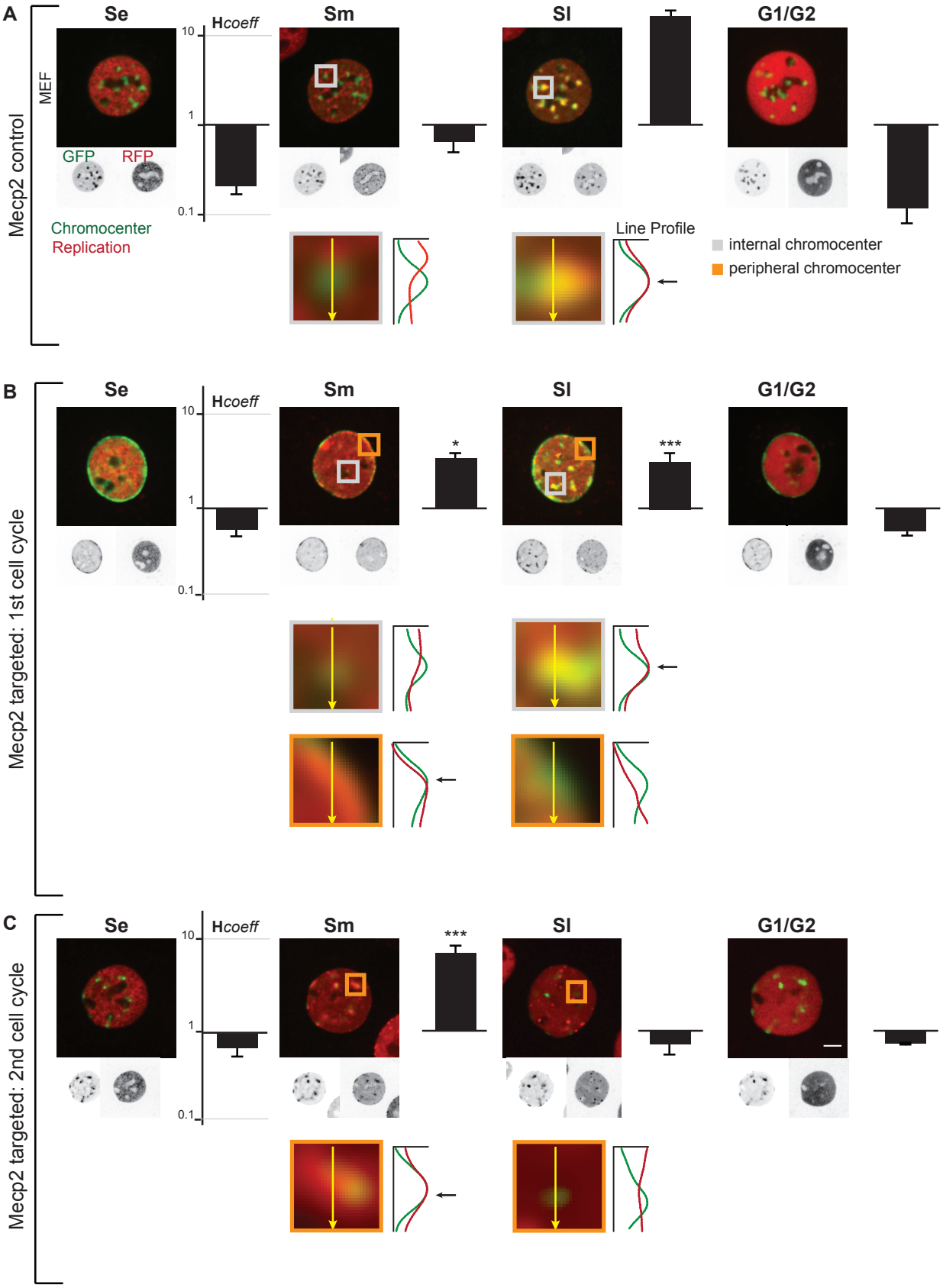

Figure II.S6.: DNA replication timing onset of MEF control and targeted cells in the 1st and 2nd cell cycle. MEF cells stably expressing RFP-PCNA were transfected with Mecp2-GFP and either Lamin B1 (= control) or GBP-Lamin B1 (= targeted) and were incubated for 20 hours (A,B) or 49 hours (C) and subjected to live-cell time lapse microscopy.
(A) Representative images depict the different DNA replication patterns in a MEF control cell over time. Line intensity plots of DNA replication (red) and chromocenters (green) with a selected ROI of control chromocenter in mid and late S-phase were shown. Control chromocenters showed an increased anti-correlation of DNA replication in mid S-phase, this changed in late S-phase towards high colocalization demonstrating the underlying DNA replication timing of control chromocenters. Colocalization of DNA replication foci and chromocenters was quantified with the H_{coeff} and plotted with bar graphs. H_{coeff} value >1 demonstrated the colocalization of DNA replication foci and control chromocenters in late S-phase. Error bars represent 95 CI.
(B) Targeted peripheral chromocenters (orange ROI) showed an increased correlation of DNA replication (red) and chromocenters (green) already during mid S-phase, while internal chromocenters (grey ROI) still exhibited an anti-correlation. However, DNA replication of internal chromocenters in a targeted cell took place according to control chromocenters in late S-phase. Increased correlation of DNA replication and targeted chromocenters was verified by an H_{coeff} > 1 already in mid S-phase and only a mild increase was observed in late S-phase of internal chromocenters, whereas there was no correlation at all in early S-phase and G1/G2 cells. Error bars represent 95 CI. Statistical significance was tested using the Wilxocon test, comparing DNA replication of control and targeted chromocenters in the first cell cycle. $*P$ <0.05; $***P$ <0.001.
(C) DNA replication timing of targeted MEF cells in the 2nd cell cycle. The star-shaped chromocenter cluster started DNA replication already during mid S-phase and also completed it during mid S-phase. There was only colocalization between DNA replication and chromocenters during mid, whereas there was anti-correlation during late S-phase when only some small foci excluded from chromocenters were replicated. Error bars represent 95 CI. Statistical significance was tested using the Wilxocon test, comparing DNA replication control and targeted chromocenters in the second cell cycle. $***P$ <0.001. Scale bar = 5 μm.

Taken from https://doi.org/10.1093/nar/gky368

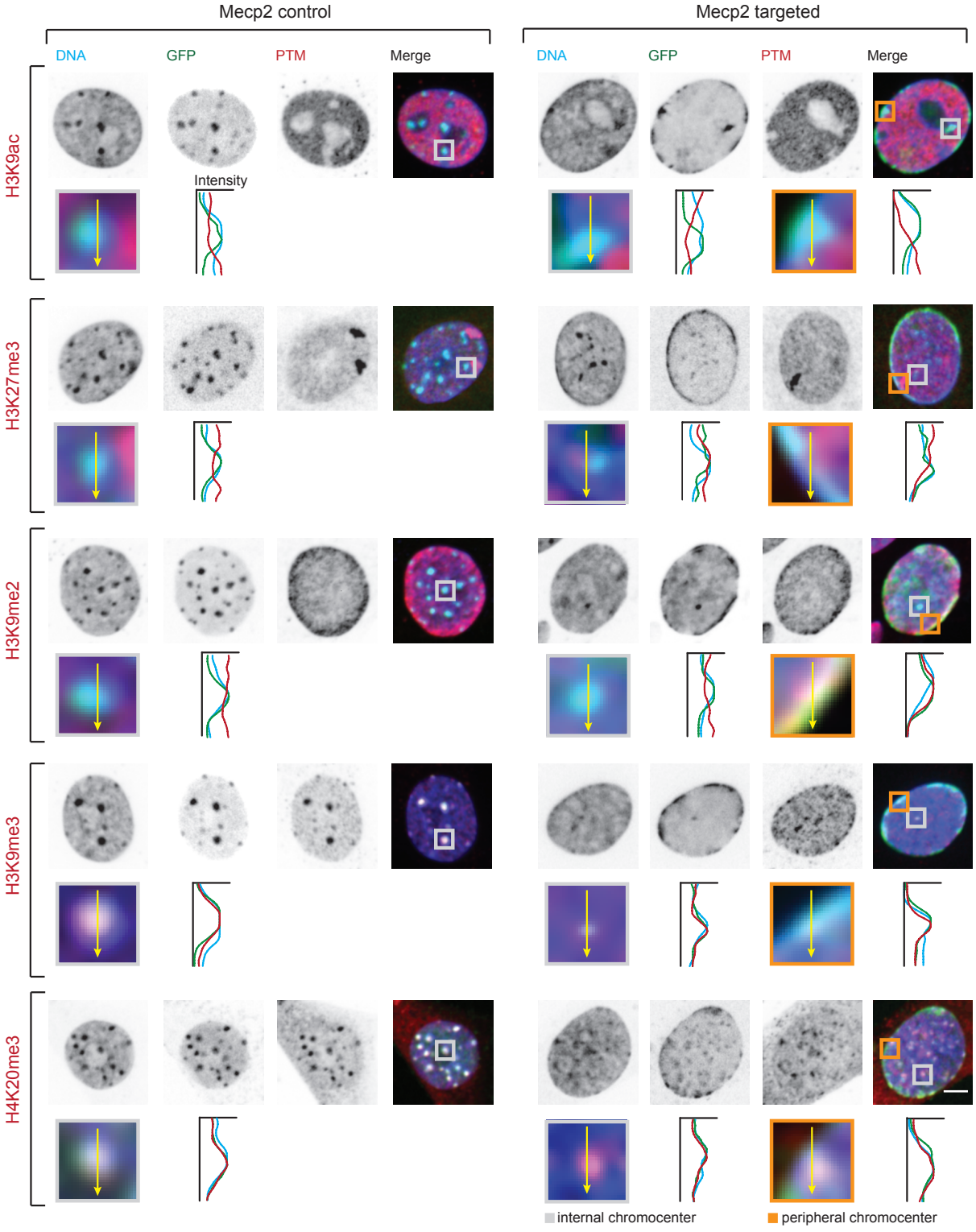

Figure II.S7.: Epigenetic composition of chromocenters in the first cell cycle.
C2C12 control and targeted cells were analyzed by immunostainings against H3K9ac (euchromatin), H3K27me3 (facultative heterochromatin), H3K9me2 (marker for nuclear periphery) and against H3K9me3 and H4K20me3 (constitutive heterochromatin). DAPI stained DNA (far left), Mecp2-GFP (mid-left), post-translational modification (PTM, mid right) and merge of all channels (far right) are depicted. A ROI around an internal (and a peripheral) chromocenter was selected and a line intensity plot analysis was performed: DNA (blue), chromocenters (green) and PTM (red). Scale = 5 µm.

Taken from https://doi.org/10.1093/nar/gky368

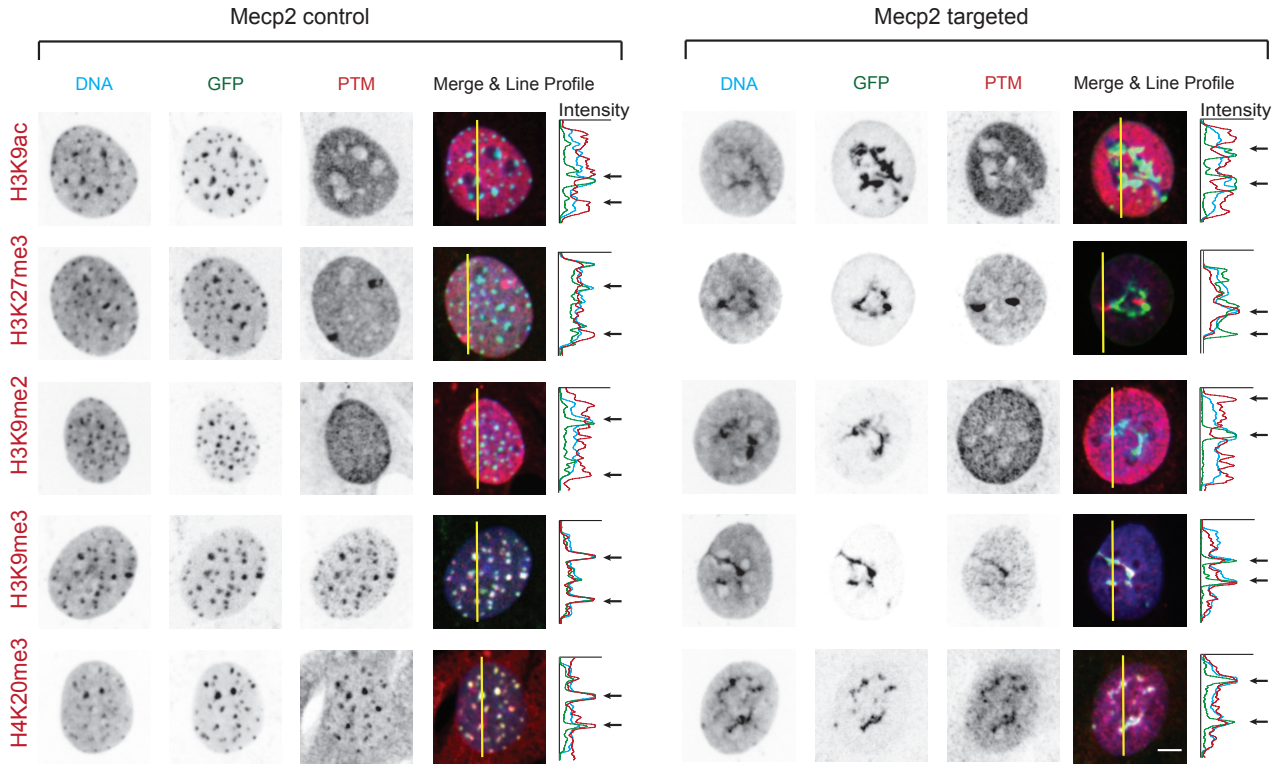

Figure II.S8.: Epigenetic composition of chromocenters in the second cell cycle.
C2C12 control and targeted cells were transfected with the appropriate constructs and incubated for 49 hours. Cells were analyzed by immunostainings against H3K9ac (euchromatin), H3K27me3 (facultative heterochromatin), H3K9me2 (marker for nuclear periphery) and against H3K9me3 and H4K20me3 (constitutive heterochromatin). DAPI stained DNA (far left), Mecp2-GFP (mid-left), post-translational modification (PTM, mid right) and merge of all channels (far right) are depicted. A ROI through the whole cell was selected and a line intensity plot analysis was performed: DNA (blue), chromocenters (green) and PTM (red). Scale = 5 µm.

Taken from https://doi.org/10.1093/nar/gky368

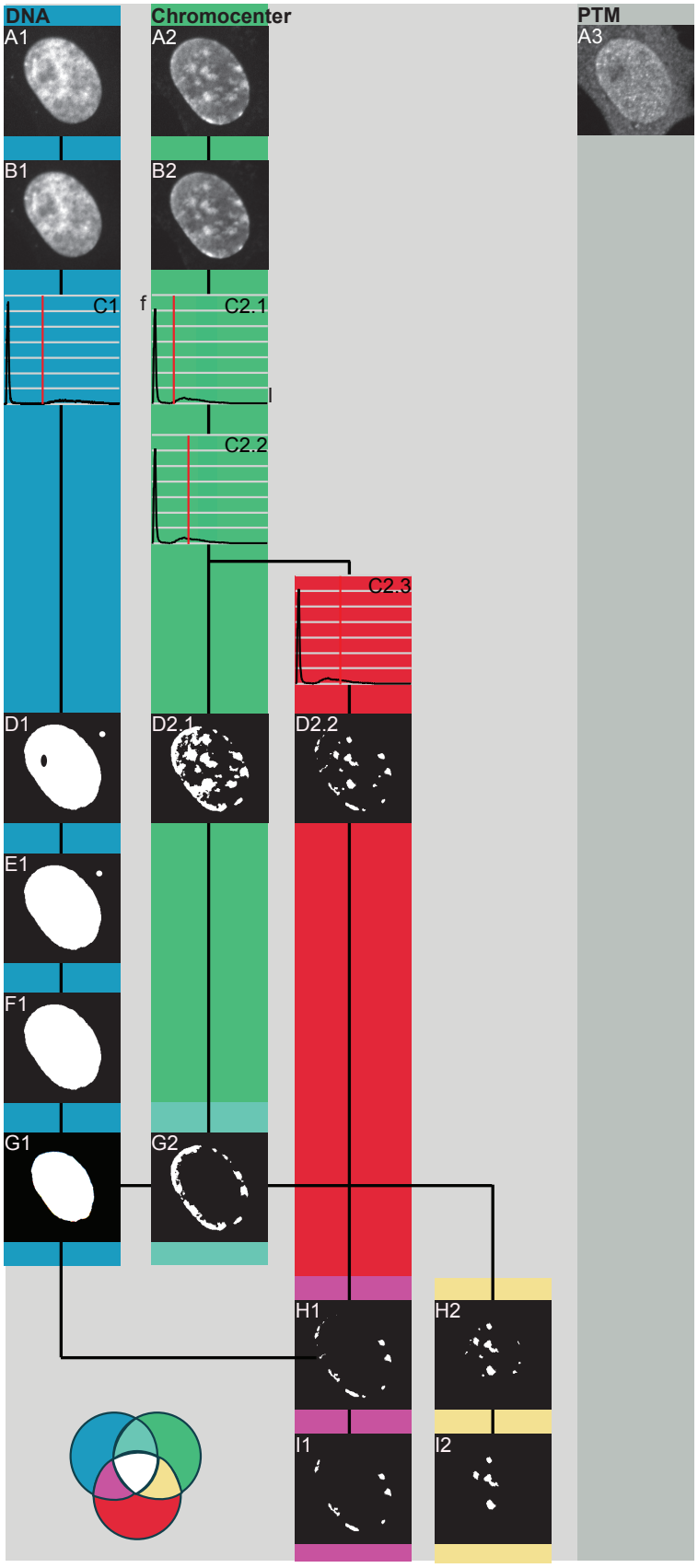

A: Confocal images
microscope: spinning disc
magnification: 60x
pixel size: 0.12 x 0.12 µm
maximum projection

B: Filtered images
B1: median filter; radius 3
B2: median filter; radius 3

C: Threshold calculation
C1: basic; B1>0
C2.1: basic; B2>0
C2.2: basic; B2>C2.1
C2.3: basic; B2>C2.2

D: Binary masks
D1: pixels>C1 = 1; pixels<C1 = 0
D2.1: pixels>C2.2 = 1; pixels<C2.2 = 0
D2.2:pixels>C2.3 = 1; pixles< C2.3 = 0

E: Mask optimization
E1: D1 after 'fill holes' algorithm

F: Final nucleus mask
F1: E1 after 'watershed' algorithm

G: Auxiliary masks
G1: F1 after 'erosion' algorithm
G2: D2.1-G1

H: Preliminary chromocenter masks
H1: D2.2-G1
H2: D2.2-G2

I: Final chromocenter masks
I1: H1 after 'watershed' algorithm
I2: H2 after 'watershed' algorithm

I: Quantification of fluorescence signals derived from immunostained histone modifications

	whole nucleus	chromocenters at nuclear periphery	chromocenters within nucleus
total	sum(A3xF1)	sum(A3xI1)	sum(A3xI2)
mean	sum(A3xF1)/vol(F1)	sum(A3xI1)/vol(I1)	sum(A3xI2)/vol(I2)

Taken from https://doi.org/10.1093/nar/gky368

Figure II.S9.: Schematic rationale of single steps for mask generation used for quantification of nuclear PTM levels in control and targeted cells.
Confocal images were obtained using an UltraVIEW VoX spinning disc system (Perkin Elmer, Massachusetts, USA) on a Nikon Ti microscope equipped with an oil immersion Plan-Apochromat x60/1.45 numeric aperture objective lens (pixel size in XY= 112 µm, Z-step 0.3 µm). For the calculation of mean PTM intensities (H3K9ac, H3K27me3, H3K9me2, H3K9me3, H4K20me3) on chromocenters in control and targeted cells, mid-nuclear sections of the DAPI and GFP channel were used to generate nuclear and chromocenter masks, respectively. Images were processed using a median 3D filter and were threshold in four successive steps. For the generation of the binary masks, all pixels below the final threshold were set to 1, for both masks respectively. To further optimize the binary masks, holes were filled using the fill holes algorithm and touching objects were separated using the watershed algorithm. Total PTM level values overlapping with the chromocenter mask were calculated and divided by the total number of pixels corresponding to the area of the chromocenters. To automate this analysis procedure, a routine was written in the programming language python (https://-code.google.com/archive/p/priithon/). To evaluate the GFP signal at two different areas in the same cell, namely the interior of the cell versus its nuclear periphery, the chromocenter mask was further improved. With the help of the erosion algorithm (15 iterations) a smaller nuclear mask was generated, which served as an auxiliary mask and which was subtracted from the GFP signal, dividing the nucleus into an outer region and an inner one. Mean values were measured and normalized to either internal chromocenters (first cell cycle studies) or to control chromocenters (second cell cycle studies).

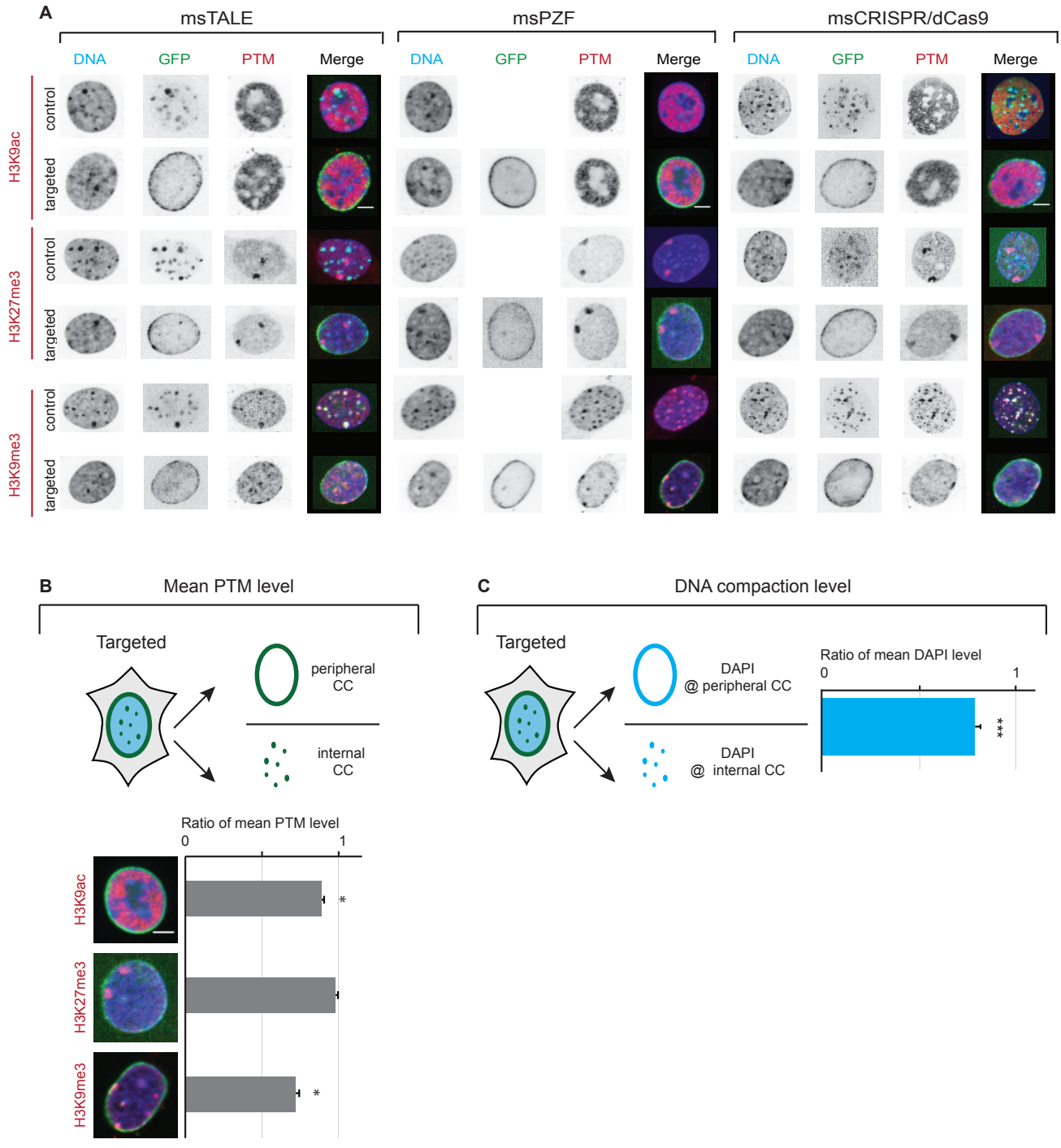

Taken from https://doi.org/10.1093/nar/gky368

Figure II.S10.: Effect of repositioning upon sequence-specific targeting on histone PTM levels and DNA compaction in C2C12 cells. (A) Distribution of prominent chromatin marks in C2C12 control and targeted cells with different sequence-specific targeting strategies. C2C12 control and targeted cells were analyzed by immunostainings against H3K9ac (euchromatin), H3K27me3 (facultative heterochromatin) and against H3K9me3 (constitutive heterochromatin). DAPI stained DNA (far left), X-GFP (mid-left), post-translational modification (PTM, mid right) and merge of all channels (far right) are depicted. msPZF controls are not fixable (see Figure II.S1E) and therefore no control images are shown. Scale bar = 5 µm. (B) Mean intensities of prominent chromatin marks in C2C12 targeted cells were measured with a user-independent analysis. Confocal images were processed and thresholded to generate binary masks of internal and peripheral chromocenter. Intensities of PTMs (H3K9ac, H3K27me3, H3K9me3) were validated, mean values were averaged and targeted PTM levels were normalized to internal chromocenters. Bar graphs demonstrate the ratios of intensities of prominent chromatin marks of chromocenters for all three sequence-specific targeting modes. Error bars represent 95 Cl. Statistical significance was tested using the t-test, comparing internal versus peripheral chromocenters. $*P$ <0.05. (C) Mean intensity of DNA levels were measured in C2C12 targeted cells. With the help of a user-independent analysis the mean DAPI signal was measured at peripheral versus internal chromocenters to estimate the compaction level of constitutive heterochromatin. Bar graphs demonstrate the ratio of mean DAPI signal of chromocenters, indicating a decrease of condensation level of peripheral chromocenters upon targeting with a sequence-specific targeting mode. Error bars represent 95 Cl. Statistical significance was tested using the t-test, comparing internal versus peripheral chromocenters. $***P$ <0.001.

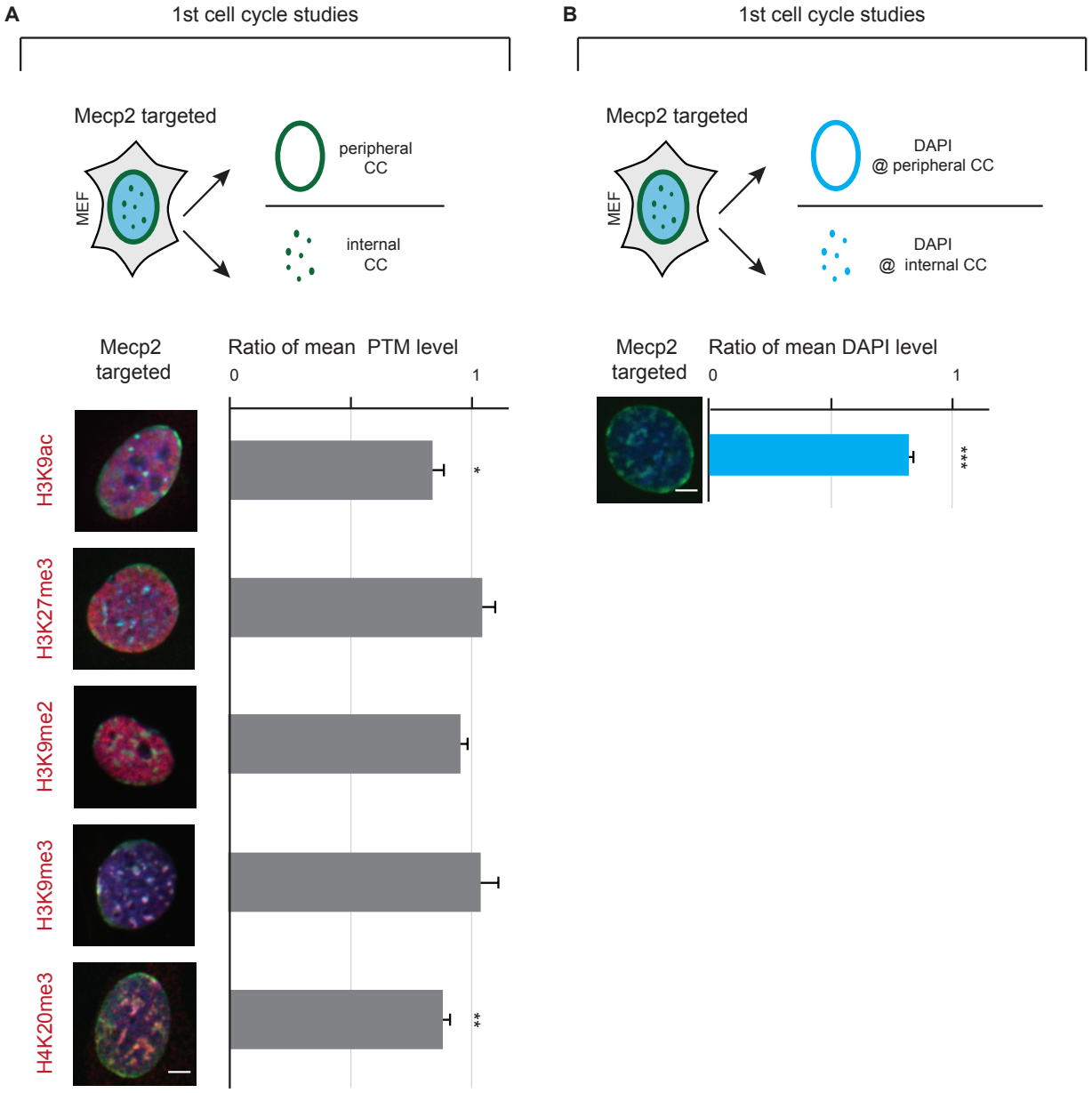

Figure II.S11.: Effect of repositioning on DNA compaction level and histone PTM levels in MEF cells.
(A) Mean intensities of prominent chromatin marks in MEF targeted cells were measured with a user-independent analysis. Confocal images were processed and threshold to generate binary masks of internal and peripheral chromocenter. Intensities of PTMs (H3K9ac, H3K27me3, H3K9me2, H3K9me3 and H4K20me3) were validated, mean values were averaged and targeted PTM levels were normalized to internal chromocenters. Bar graphs demonstrate the ratios of intensities of prominent chromatin marks of chromocenters for all three sequence-specific targeting modes. Error bars represent 95 CI. Statistical significance was tested using the t-test. *P <0.05; **P <0.005.
(B) Mean intensity of DNA levels were measured in MEF targeted cells. With the help of a user-independent analysis the mean DAPI signal was measured at peripheral versus internal chromocenters to estimate the compaction level of constitutive heterochromatin. Bar graphs demonstrate the ratio of mean DAPI signal of chromocenters, indicating a significant decrease of condensation level of peripheral chromocenters upon Mecp2 targeting. Error bars represent 95 CI. Statistical significance was tested using the Wilcoxon test, comparing internal and peripheral chromocenters. ***P <0.001.

Taken from https://doi.org/10.1093/nar/gky368

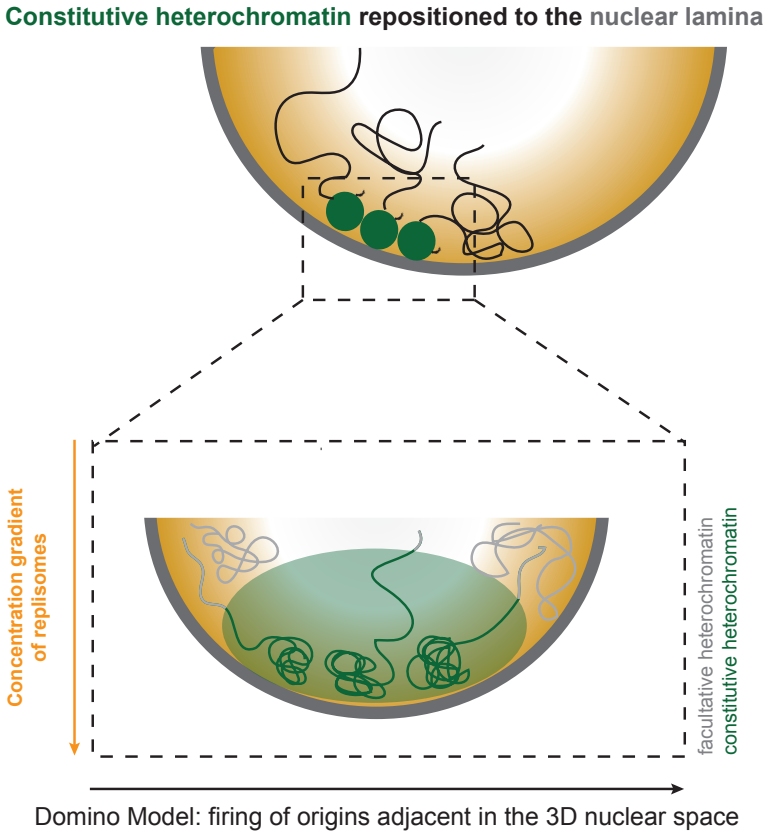

Figure II.S12.: Domino model of origin firing working in *trans* in the 3D nuclear space.
Schematic illustration of the domino effect model of adjacent firing origins in the 3D nuclear space. Constitutive heterochromatin (green) is repositioned to the nuclear lamina (grey). Magnification of pericentromeric region at the bottom (dashed-lined box). Constitutive heterochromatin is built up out of different chromosomes, juxtaposed upon repositioning next to facultative heterochromatin (grey). Because of the repositioning constitutive heterochromatin is repositioned into an environment with an increased local concentration of replisomes (orange gradient) triggering earlier firing of normally late-replicating constitutive heterochromatin. According to the domino effect model, activation of an origin cluster leads to a chain reaction of activation of later origin clusters depending on the relative spatial distribution of the genome within the nucleus. Normally late-replicating origins of repositioned chromocenters were triggered by mid-replicating origins in a domino-like manner, working not only in *cis* along the chromosome, rather in *trans* across different chromosomes.

Taken from https://doi.org/10.1093/nar/gky368

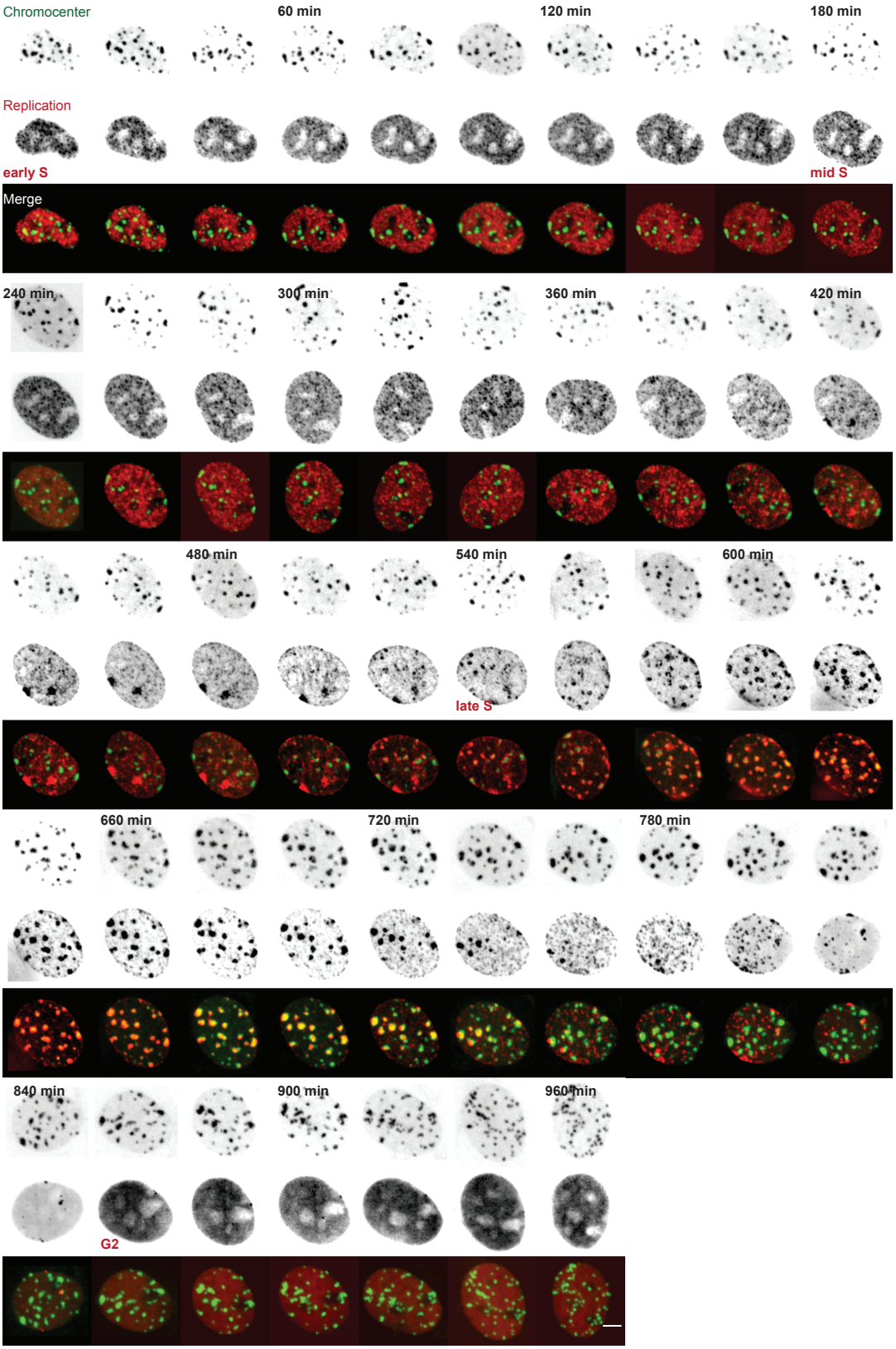

Figure II.S13.: Time-lapse figure of DNA replication in a C2C12 control cell in the first cell cycle. C2C12 cells stably expressing RFP-PCNA were transfected with Mecp2-GFP and Lamin B1 (control state) and Time-lapse confocal microscopy was performed 20 hours post-transfection. Stacks were acquired at 20 minutes intervals. Chromocenters (green), DNA replication (red) and merged images (overlay) are shown in left, middle and right, respectively in the movie. Channel labels are indicated on the bottom; S-phase substages are indicated on the upper middle, time intervals are shown on the upper right. Depicted C2C12 control cell progresses from early S to G2 phase. Scale bar = 5 µm.

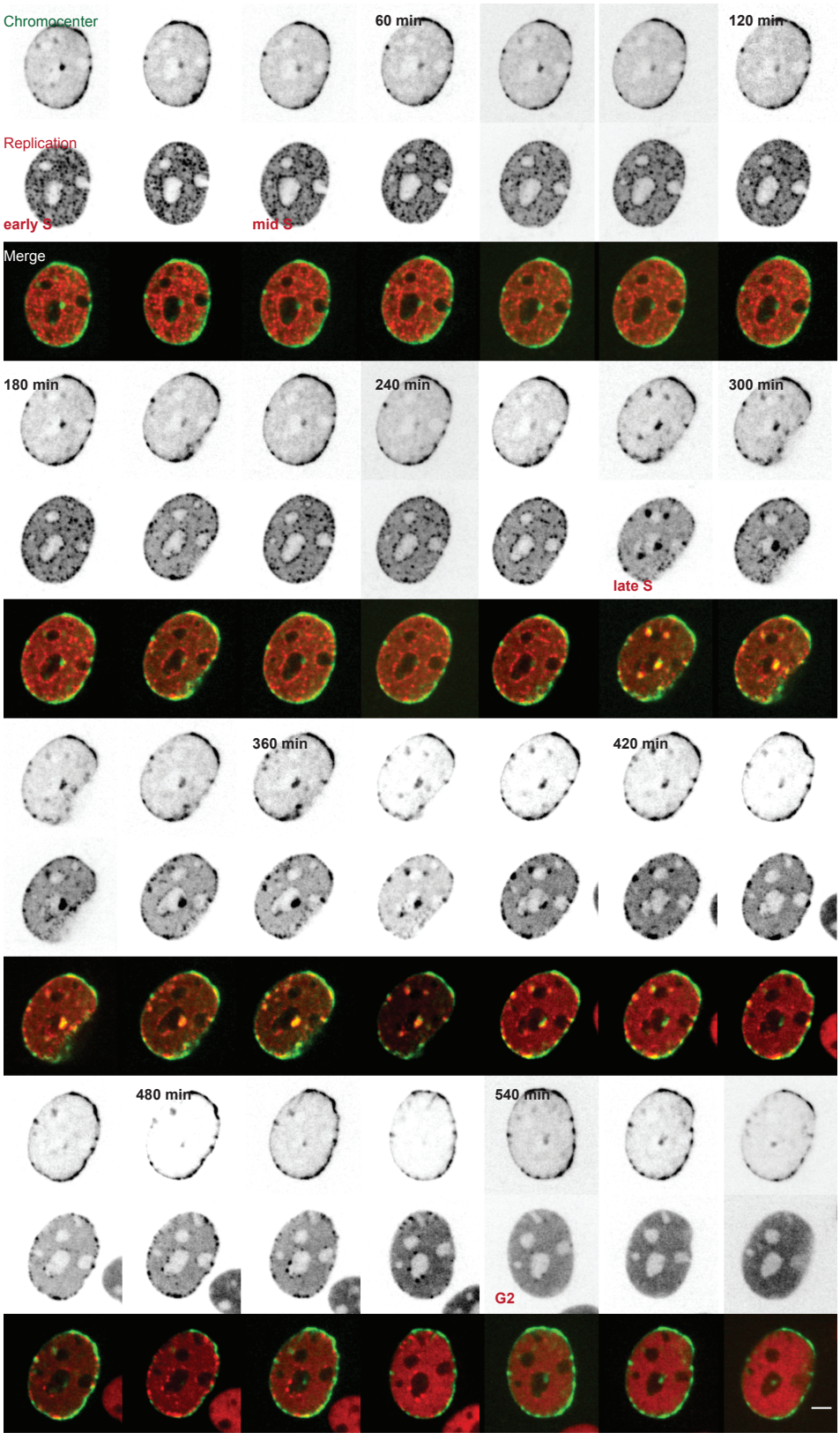

Figure II.S14.: Time-lapse figure of DNA replication in a C2C12 targeted cell in the first cell cycle. C2C12 cells stably expressing RFP-PCNA were transfected with Mecp2-GFP and GBP-Lamin B1 (targeted state) and time-lapse confocal microscopy was performed 20 hours post-transfection. Stacks were acquired at 20 minutes intervals. Channel labels are indicated on the bottom (Chromocenters in green, DNA replication in red). S-phase substages are indicated on the upper middle, the time intervals of 20 minutes are indicated on the upper right. Depicted C2C12 targeted cell progresses the first cell cycle from early S to mitosis. Scale bar = 5 µm.

Taken from https://doi.org/10.1093/nar/gky368

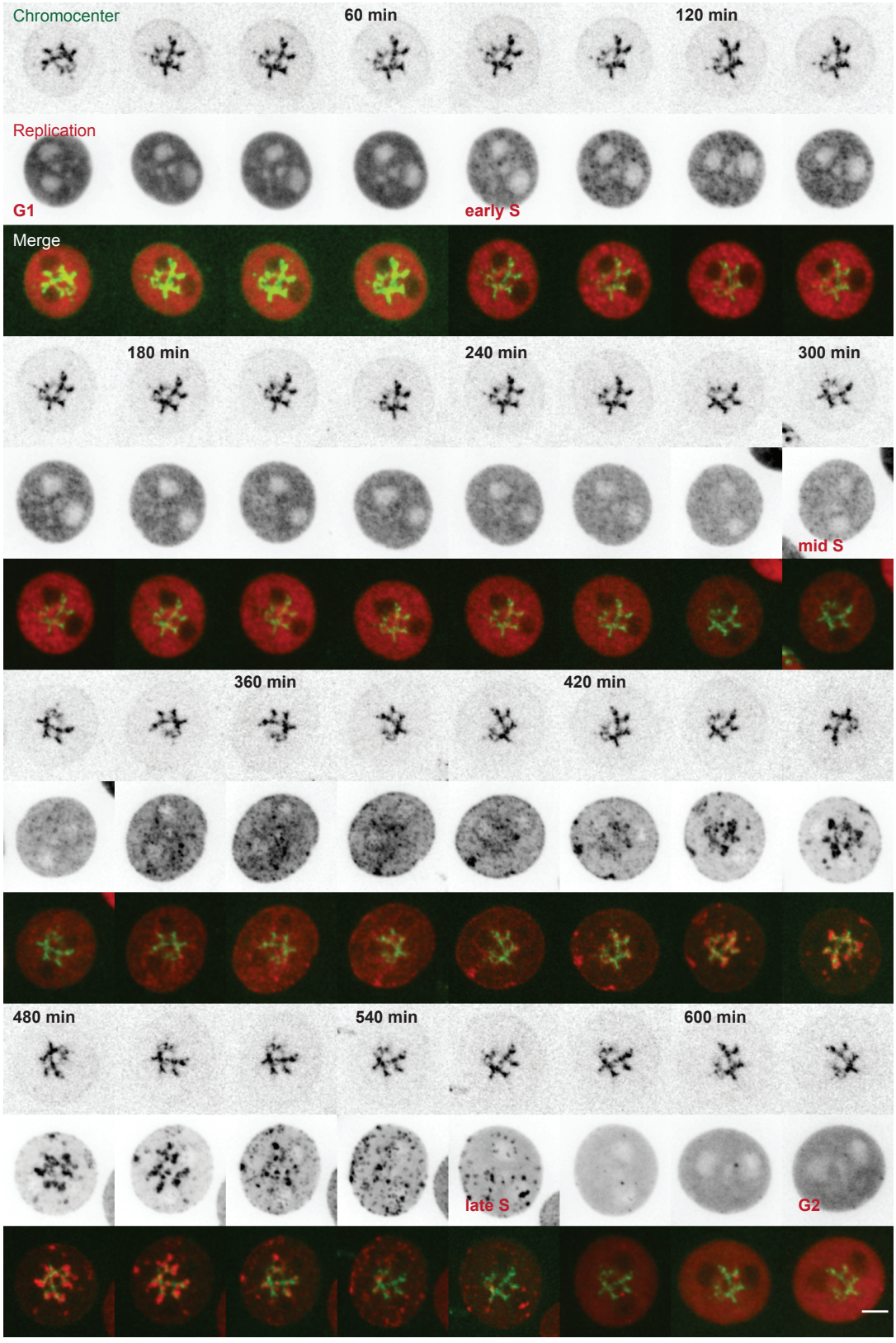

Figure II.S15.: Time-lapse figure of DNA replication in a C2C12 targeted cell in the second cell cycle. C2C12-RFP-PCNA cells were transfected with Mecp2-GFP and GBP-Lamin B1 (targeted) and incubated for 49 hours to ensure the cells entered the second cell cycle. Chromocenters are shown in green, DNA replication in red and the merge is an overlay of both channels. Labels are indicated on the bottom, whereas S-phase substage labels are shown on the upper middle. Time intervals are depicted at the upper right. Depicted C2C12 targeted cell progresses the second cell cycle from G1 to late S. Scale bar = 5 µm.

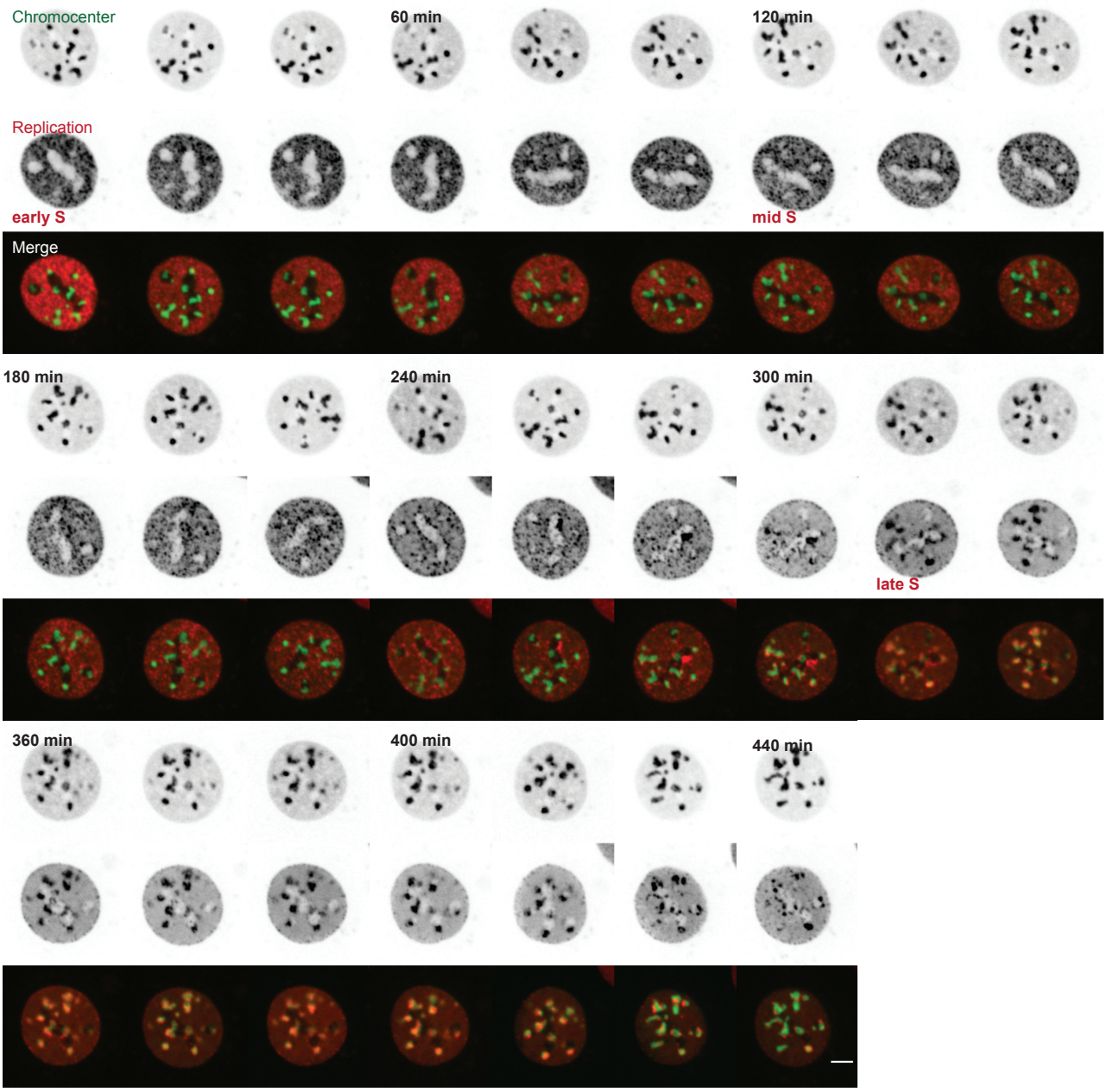

Figure II.S16.: Time-lapse figure of DNA replication in a MEF control cell in the first cell cycle. MEF cells stably expressing RFP-PCNA were transfected with Mecp2-GFP and Lamin B1 (untargeted state) and time-lapse confocal microscopy was performed 20 hours post-transfection. Chromocenters are shown in green, DNA replication in red and the merge is an overlay of both channels. Labels are indicated on the bottom, whereas S-phase substage labels are shown on the upper middle. Time intervals of 20 minutes are depicted at the upper right. Depicted MEF control cell progresses from early S to late S-phase. Scale bar = 5 µm.

Taken from https://doi.org/10.1093/nar/gky368

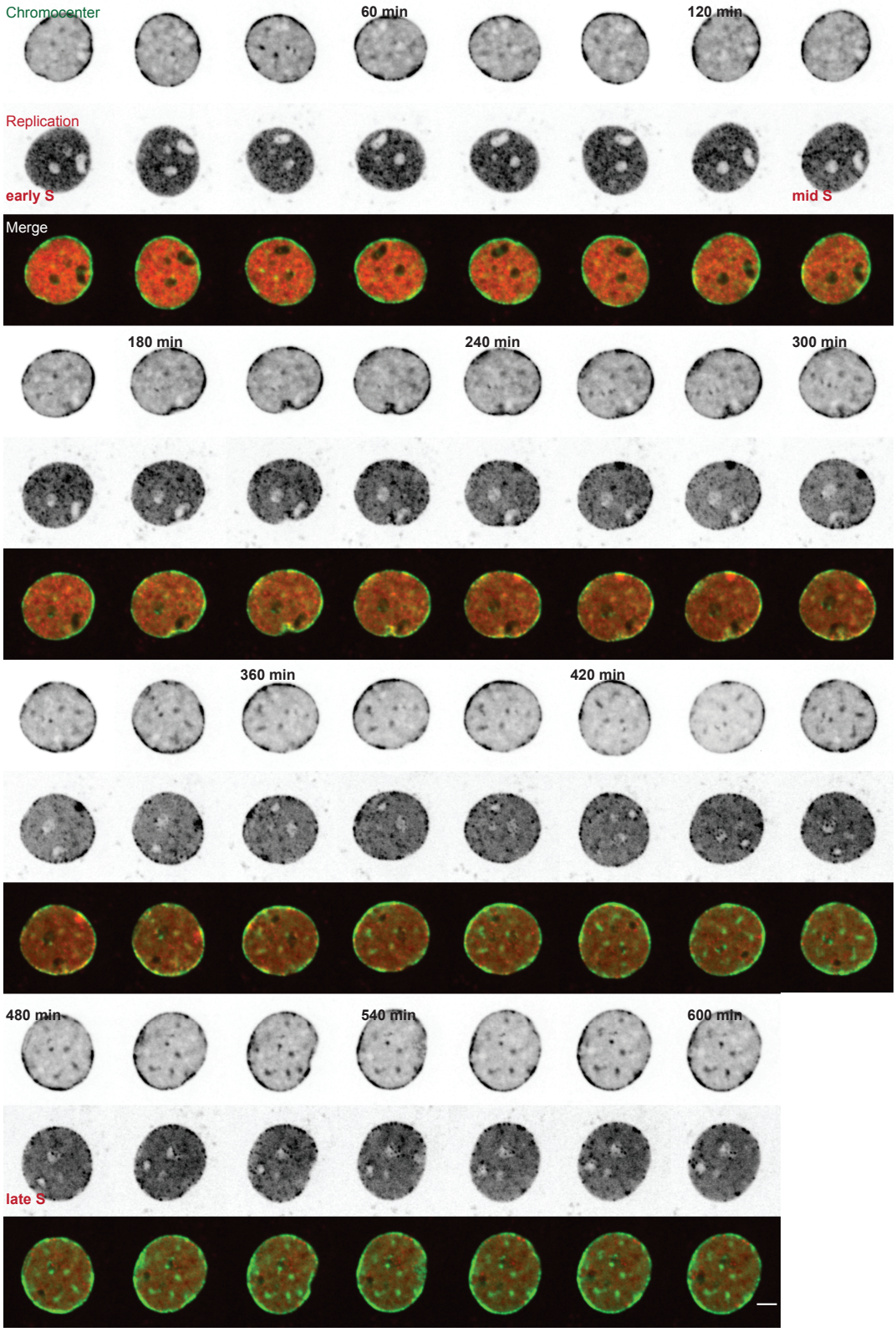

Figure II.S17.: Time-lapse figure of DNA replication in a MEF targeted cell in the first cell cycle. MEF cells stably expressing RFP-PCNA were transfected with Mecp2-GFP and GBP-Lamin B1 (targeted state) and time-lapse confocal microscopy was performed 20 hours post-transfection. Chromocenters are shown in green, DNA replication in red and the merge is an overlay of both channels. Labels are indicated on the bottom, whereas S-phase substage labels are shown on the upper middle. Time intervals of 20 minutes are depicted at the upper right. Depicted MEF targeted cell in the first cell cycle from early S to late S-phase is shown. Scale bar = 5 µm.

Taken from https://doi.org/10.1093/nar/gky368

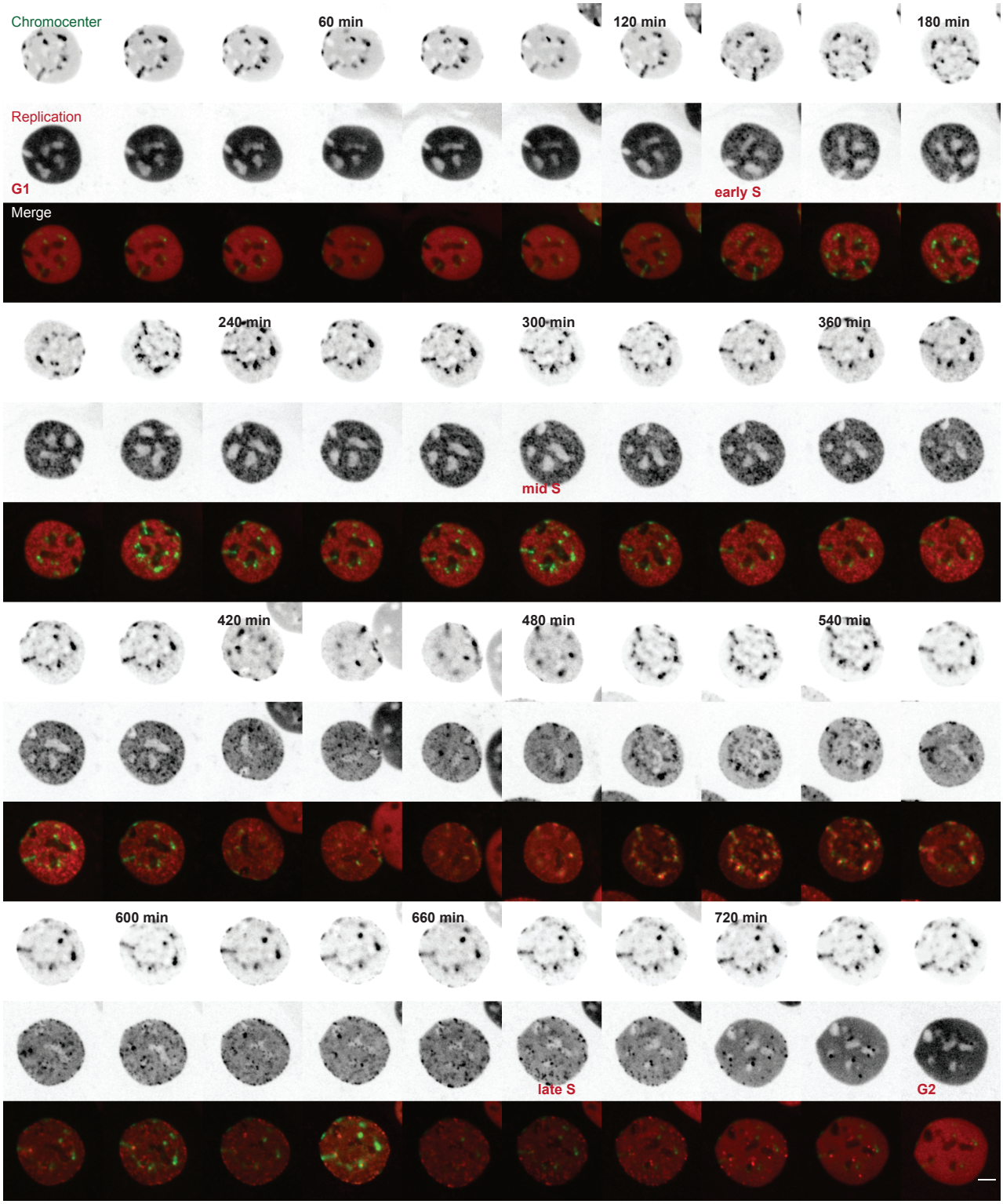

Figure II.S18.: Time-lapse figure of DNA replication in a MEF targeted cell in the second cell cycle. MEF cells stably expressing RFP-PCNA were transfected with Mecp2-GFP and GBP-Lamin B1 (targeted state) and time-lapse confocal microscopy was performed 49 hours post-transfection. Chromocenters are shown in green, DNA replication in red and the merge is an overlay of both channels. Labels are indicated on the bottom, whereas S-phase substage labels are shown on the upper middle. Time intervals of 20 minutes are depicted at the upper right. Depicted MEF targeted cell in the second cell cycle from G1 to late S-phase is shown. Scale bar = 5 µm.

Table II.S1.: Plot statistics chapter II (main figures)

Table S1. Plots statistics (main figures)

Figure	Sample	Mean	Stdev	n	95 CI	*P*
Figure 2						
NPCs	Control 1st CC	1.04	0.22	11	0.13	C/T: 0.73
	Targeted 1st CC	1.07	0.19	11	0.11	
	Control 2nd CC	0.99	0.07	20	0.03	C/T: 0.07
	Targeted 2nd CC	1.11	0.30	40	0.09	
Figure 3						
Duration	Control 210' chase	31	8.9	139	1.48	C/T: 0.001
	Targeted 210' chase	65	7.6	246	0.95	
	Control 240' chase	16	5.5	153	0.87	C/T: 0.008
	Targeted 240' chase	33	5.0	200	0.69	
Figure 4						
DNA content	Control, early S	1.28	0.41	390	0.04	C/T: 0.24
	Targeted, early S	1.44	0.65	48	0.19	
	Control, mid S	1.54	0.42	392	0.04	C/T: 0.0002
	Targeted, mid S	1.77	0.60	61	0.15	
	Control, late S	2.08	0.67	471	0.06	C/T: 0.54
	Targeted, late S	2.09	0.72	85	0.15	
Figure 5						
DNA replication	Control 1st, G1	0.45	0.25	31	0.09	
	Control 1st, early S	0.36	0.16	62	0.04	
	Control 1st, mid S	0.69	0.23	69	0.05	
	Control 1st, late S	11.73	9.10	107	1.73	
	Control 1st, G2	0.45	0.18	28	0.06	
	Targeted 1st, G1	0.65	0.06	9	0.04	
	Targeted 1st, early S	0.50	0.22	46	0.06	
	Targeted 1st, mid S	1.90	0.67	175	0.10	C/T: 5.6E-06
	Targeted 1st, late S	1.94	1.88	90	0.39	C/T: 4.33E-05
	Targeted 1st, G2	0.34	0.24	46	0.07	
	Targeted 2nd, G1	0.46	0.4	15	0.2	
	Targeted 2nd, early S	0.43	0.28	51	0.08	
	Targeted 2nd, mid S	2.59	1.24	75	0.28	C/T: 0.001
	Targeted 2nd, late S	0.64	0.26	16	0.13	C/T: 0.001
	Targeted 2nd, G2	0.70	0.11	5	0.10	
total S duration	Control 1st	10.16	1.10	67	0.28	
	Targeted 1st	10.13	1.38	73	0.33	
	Targeted 2nd	11.11	2.1	100	0.42	
Figure 6						
DNA compaction	Control/Targeted	0.81	0.12	82	0.03	C/T: 5.66E-05
PTMs						
H3K9ac	Control/Targeted	0.94	0.15	54	0.04	C/T: 0.09
H3K27me3	Control/Targeted	1.02	0.12	42	0.04	C/T: 0.65
H3K9me2	Control/Targeted	0.98	0.28	40	0.09	C/T: 0.89
H3K9me3	Control/Targeted	0.83	0.08	41	0.03	C/T: 0.001
H4K20me3	Control/Targeted	0.78	0.09	17	0.04	C/T: 0.01
H3K9ac, 2nd CC	Control/Targeted	0.92	0.02	75	0.01	C/T: 0.58
H3K27me3, 2nd CC	Control/Targeted	0.98	0.03	72	0.01	C/T: 0.07
H3K9me2, 2nd CC	Control/Targeted	0.77	0.18	101	0.03	C/T: 2.63E-05
H3K9me3, 2nd CC	Control/Targeted	0.82	0.08	108	0.02	C/T: 0.01
H4K20me3, 2nd CC	Control/Targeted	0.84	0.08	87	0.02	C/T: 0.6

C=Control; T=Targeted; "n" and "p" as indicated in the respective figure

Taken from https://doi.org/10.1093/nar/gky368

Table II.S2.: Plot statistics chapter II (supplementary figures)

Table S2. Plots statistics (supplementary figures)

Figure	Sample	Mean	Stdev	n	95 CI	*P*
Figure S4 C2C12 sequence-specific targeting	Targeted, early S	0.42	0.31	15	0.16	
	Targeted, mid S	3.16	2.39	41	0.73	
	Targeted, late S	3.98	3.06	29	1.11	
	Targeted, G2	0.23	0.08	4	0.08	
Figure S6 MEF DNA repl.	Control 1st, G1	0.25	0.14	4	0.12	
	Control 1st, early S	0.23	0.11	25	0.04	
	Control 1st, mid S	0.66	0.39	28	0.14	
	Control 1st, late S	14.06	6.03	37	1.94	
	Control 1st, G2	0.13	0.04	3	0.04	
	Targeted 1st, G1	0.59	0.10	9	0.07	
	Targeted 1st, early S	0.70	0.11	18	0.05	
	Targeted 1st, mid S	2.35	0.98	78	0.22	C/T: 0.006
	Targeted 1st, late S	2.23	0.88	35	0.29	C/T: 0.009
	Targeted 1st, G2	0.68	0.06	8	0.04	
	Targeted 2nd, G1	0.78	0.08	7	0.06	
	Targeted 2nd, early S	0.79	0.22	37	0.07	C/T: 0.02
	Targeted 2nd, mid S	3.77	1.72	47	0.49	C/T: 0.06
	Targeted 2nd, late S	0.80	0.36	23	0.15	
	Targeted 2nd, G2	0.81	0.01	6	0.01	
Figure S10						
H3K9ac	Control/Targeted	0.86	0.04	29	0.02	C/T: 0.01
H3K27me3	Control/Targeted	0.95	0.05	22	0.02	C/T: 0.88
H3K9me3	Control/Targeted	0.71	0.06	20	0.03	C/T: 0.05
DNA compaction	Control/Targeted	0.79	0.13	80	0.03	C/T: 2.16E-08
Figure S11						
H3K9ac	Control/Targeted	0.86	0.12	13	0.06	C/T: 0.03
H3K27me3	Control/Targeted	1.08	0.20	15	0.10	C/T: 0.50
H3K9me2	Control/Targeted	0.95	0.08	13	0.04	C/T: 0.57
H3K9me3	Control/Targeted	0.98	0.17	13	0.09	C/T: 0.78
H4K20me3	Control/Targeted	0.89	0.11	12	0.06	C/T: 0.01
DNA compaction	Control/Targeted	0.86	0.08	51	0.02	C/T: 0.00001

C=Control; T=Targeted; "n" and "p" as indicated in the respective figure

III DNA replication dynamics of vole genome and its epigenetic regulation

III.1 Abstract

The genome of some vole rodents exhibit large blocks of heterochromatin coupled to their sex chromosomes. The DNA content of these heterochromatin blocks has been studied, as well as their major epigenetic features and transcriptional activity, but little is known about their DNA replication dynamics. Here, we identified prominent marks of both heterochromatic blocks and we were able to dissect between the facultative and the constitutive heterochromatin blocks of the sex chromosomes. The facultative heterochromatic block located at the inactive X chromosome is enriched for macroH2a and H3K27me3, whereas the constitutive block at the active X chromosome is characterized by H3K9 trimethylation and HP1 beta enrichment. Furthermore, we found by *In situ* replication labeling and time-lapse microscopy that the heterochromatic block of the inactive X chromosome is replicated during mid S-phase, prior to the heterochromatic block of the active X chromosome, which is replicated during late S-phase. To test whether histone acetylation level was a potential regulator of their DNA replication timing, we induced either global hyperacetylation by HDAC inhibition or by targeting a HAT site-directed to the heterochromatic of the active X chromosome. Our data reveal a prolongation of total S-phase and sex chromatin replication duration, when histone acetylation level was increased. This result went hand in hand with a slower replication fork speed in treated samples. Furthermore, we found a stronger increase of genomic DNA already during early S-phase, when normally euchromatin is replicated, indicating a shift of DNA replication timing of facultative heterochromatin towards early S-phase. All in all, we identified major characteristics of epigenetic modifications controlling the structure of the heterochromatic blocks and identified histone acetylation level as a regulator of DNA replication kinetics in female *Microtus cabrerae* cells.

III.2 Introduction

In higher eukaryotes, the nuclear genome is compartmentalized into distinct chromatin territories to facilitate the regulation of complex processes like DNA repair, transcription and replication. The DNA replication process is highly regulated both spatially and temporally, resulting in the changing pattern of replication structures throughout S-phase. This temporal order of DNA replication reflects this higher order organization of the nuclear genome [1–3]. Euchromatin and heterochromatin, as major higher-order structures, are defined by a complex interplay between their condensation state, chromatin modifications, associated proteins as well as their transcriptional activity, all referred to as epigenetic marks [4–6]. These epigenetic properties of chromatic regions are potential determinants of their DNA replication timing [7–10]. In mammals, constitutive heterochromatin is mostly arranged at (peri)centromeric regions of the chromosome, whereas vole rodents (subfamily Arvicolinae) are a remarkable exception. In addition to this normal distribution at (peri)centromeric regions, a bulk of heterochromatin is also coupled to both sex chromosomes. Avicolidae is a rodent group, which is widely distributed and exhibits various interesting characteristics in their sex chromosomes as some species present enlarged, so called 'giant' sex chromosomes [11, 12].

Euchromatin includes less condensed transcriptional active regions, determined by a depletion of methylated DNA, an enrichment in specific methylated histones like H3K4, H3K36, H3K79 and a high level of histone acetylation [13]. Euchromatin is replicated in early S-phase, when the replication machinery is present as a multitude of small replication foci well distributed throughout the nuclear interior. Followed by the DNA replication of facultative heterochromatin, which corresponds to developmentally silenced regions that are enriched in H3K27 trimethylation (H3K27me3) with the inactive X chromosome in mammals as one of the most prominent examples [7, 14, 15]. This type of heterochromatin is replicated during the mid S-phase, when the replication foci become larger and are located around the nucle(ol)ar periphery. The second type of heterochromatin, namely constitutive heterochromatin, is replicated in the late S-phase stage. This type of heterochromatin is enriched for a set of histone modifications like H3K9 and H4K20 trimethylation and histone hypoacetylation [16]. H3K9 trimethylation is recognized and bound by a non-histone component named "chromodomain-containing heterochromatin protein" (HP1) [17], which is consequently accumulating at heterochromatic regions. Several lines of evidence support the idea of an interaction of epigenetic properties and DNA replication timing of a given genomic region. For instance, manipulations in yeast showed that the deletion of the histone deacetylase (HDAC) Rpd3 leads to an increased acetylation level at many replication origins and subsequently to an earlier onset of DNA replication [18]. Comparable are studies in human cells that were treated with the HDAC inhibitor trichostatin A (TSA) resulting in an early initiation of DNA replication of imprinted genes [19, 20]. Furthermore, manipulations

of epigenetic marks of the well-defined and prominent heterochromatic landscape of pericentromeric regions in mouse cells demonstrated that histone hypoacetylation is required to maintain the characteristic late DNA replication timing of constitutive heterochromatin [21]. In addition histone hypoacetylation is accredited to have a key role in controlling the DNA replication dynamics of the inactive X chromosome [7].
In this study, we assess the DNA replication dynamics in vole rodents to test the validity and reproducibility of the epigenetic control of replication dynamics across species. We made use of *Microtus cabrerae* female cells and their enlarged sex chromosomes to first determine their epigenetic constitution and second dissect the control mechanism of DNA replication at diverse chromatin states. Our study reveals that histone hypoacetylation and DNA demethylation are major epigenetic determinants of this sex heterochromatin. We distinguished between the Xi that is enriched in H3K27 trimethylation and macroH2a1, whereas the Xa exhibiting H3K9 trimethylation signal and HP1 accumulation. Furthermore, we showed that the synchronous Xi replication mode is conserved in mammals and therefore also observable at the sex heterochromatin of *Microtus cabrerae* female cells. To answer the question which factors might be involved in setting up the synchronous DNA replication process we used panobinostat to manipulate the Xi and Xa replication dynamics by inhibition of HDACs [22]. We showed that the increase in histone acetylation level affected DNA replication timing and lead to a prolongation of total S- and early- S-phase. We detected an increase of DNA content during early S-phase relative to control and untreated cells. This was due an earlier onset of DNA replication of facultative sex chromatin. Finally, we found a global decrease of fork speed in hyperacetylated cells explaining the prolongation of S-phase.

III.3 Material and methods

III.3.1 Expression plasmids

Expression vectors (Figure III.S2) encoding human PCNA were either tagged to CFP (pc922, [23], GFP (pc595, [1]) or to mRFP (pc1054, [24] to visualize active replication sites. For the detection of the heterochromatic block of the inactive X eGFP- tagged macroH2a1 (pc2101) was constructed with cDNA of human cells, amplified by PCR (macroh2a1-forward EcoR1: 5'-AAGAATTCAATGTCGAGCCGCGGTGGG; macroh2a1-reverse Not1: AAGCGGCCGCTAGTTGGCGTCCAGCTTGG) and cloned into pEGFP-C1. DsRedHP1 beta was transfected to identify the active X chromosome (pc1225, [25]). For site-directed targeting of HBO1 to the heterochromatic block of the inactive and active X chromosomes different plasmids were generated. A construct encoding human HBO1 was fused to C-terminal GFP of EGFP-C1 (pc852) (Clontech) (gift by B. Stillman). To detect the heterochromatic blocks of the inactive X chromosome a plasmid encoding GBP-macroH2a1 (pc2883) was constructed. The amplification of GBP was performed via PCR from GBP-MaSat (pc2469) [9]: (GBP-forward AgeI: 5'-ATACCGGTATGGCCGATGTGC; GBP-reverse XhoI: ATCACTCGAGATGAGGAGACG). GFP-macroH2a1 (pc2101) was used as a backbone and was cut with AgeI and XhoI to create the final plasmid GBP-macroH2a1 (pc2883). To detect the heterochromatic block of the active X chromosome a construct encoding GBP-HP1 beta (pc3357) was created. MacroH2a1 was removed from GBP-macroH2a1 (pc2883) by restriction with EcoRI and BamHI and replaced by HP1beta from DsRed-HP1beta (pc1225, [25]). As a control, HBO1 was catalytically inactivated by site-directed mutagenesis PCR. GFP-HBO1 (pc852) was manipulated with a primer (ATGCCTCAGTACATGAGACAGGCCTATGGCAAGATGCTTA) and a reverse complement thereof to get HBO1 G485A. Site-directed mutation results in a StuI restriction site, which was used to validate successful mutagenesis.

III.3.2 Cell culture, transfection and HDAC inhibitor treatment

M. cabrerae female cells [26] were cultured in Dulbecco's Modified Eagle's Medium (DMEM) supplemented with 10% fetal calf serum and 1 μM gentamycin in 5% CO_2 atmosphere at 37° C. Cells used for immunofluorescence experiments were plated and grown on gelatinized glass coverslips. Transient transfections of *Microtus cabrerae* female cells were performed using nucleofection (Amaxa NucleoFector II, Lonza Ltd., Basel, Switzerland) with 1 μg per plasmid. For HDAC inhibition treatment 50 nM panobinostat (= LBH-589, Selleckchem, Houston, USA, Cat #: S1030) in PBS was added 24 hours after seeding cells or nucleofection to the culture medium and incubated for at least 24 hours prior to fixation or live cell experiments.

III.3.3 Immunofluorescence and X-chromosome FISH

Cells were grown on gelatinized glass coverslips, fixed in 4% paraformaldehyde (10 minutes at room temperature (RT)) and permeabilized for 20 minutes at RT in 0.5% Triton X-100/PBS. Immunofluorescence stainings were performed in 4% BSA/PBS for 1 h at RT (primary antibodies) and in 4% BSA/PBS for 45 minutes at RT (secondary antibodies). The following primary antibodies were used: rabbit anti-H3K9ac (1/200, Upstate, Lake Placid, USA, Cat #: 06-942), rabbit anti-H4K8ac (1/200, Upstate, Lake Placid, USA, Cat #: 07-328) rabbit anti-H3K4me2 (1/800, Biomol, Hamburg,

Germany, Cat #: BPS-25255), rabbit-anti H3K27me3 (1/200, Upstate, Lake Placid, USA, Cat #: 07-449) and rabbit anti-H3K9me3 (1/200, Upstate, Lake Placid, USA, Cat #: 07-442), mouse-anti-H3K9me3 (1/100, Active Motif, Carlsbad, USA, Cat #: 39285). Secondary antibodies were goat-anti-rabbit-IgG Alexa Fluor 488 (1/200, Invitrogen, Carlsbad, USA, Cat #: A-11008) or donkey-anti-mouse IgG-Cy3 (1/200, The Jackson Laboratory, Bar Harbour, USA, Cat #: 715-166-151). Nuclear DNA was visualized by 4,6-diamidino-2-phenylindole (DAPI, 1 μg/ml, Sigma Aldrich, Steinheim, Germany, Cat #: D9542). Cells were mounted in Vectashield antifade (Vector Laboratories, Burlingame, USA, Cat #: H-1000). Mitotic preparations and FISH analyses in *Microtus cabrerae* cell cultures followed standard protocols previously described in [27, 28]. A painting probe from the X chromosome was prepared by micro dissection combined with DOP-PCR labeling method (Figure III.1).

III.3.4 *In situ* replication labeling

For the visualization of replicating DNA and epigenetic marks of heterochromatic blocks, *Microtus cabrerae* female cells were transiently transfected with CFP-PCNA and were pulse labeled for either 20 or 30 minutes with 10 μM 5'-ethynyl-2'-deoxyuridine (EdU) (Invitrogen, Carlsbad, USA, Cat #: C10337) followed by a 1 h or 2.5 h chase prior fixation with 4% paraformaldehyde. EdU was detected with the ClickIT system (Invitrogen) and AlexaFluor488 followed by an immunostaining with rabbit-anti H3K27me3 (1/200, Upstate, Lake Placid, USA, Cat #: 07-449) and with mouse-anti-H3K9me3 (1/100, Active Motif, Carlsbad, USA, Cat #: 39285). The following secondary antibodies were used: donkey-anti-mouse IgG-Cy3 (1/200, The Jackson Laboratory, Bar Harbour, USA, Cat #: 715-166-151) and donkey-anti-rabbit IgG-Cy5 (1/200, The Jackson Laboratory, Bar Harbor, USA, Cat #: 711-175-152). DNA was counterstained with 1 μg/ml DAPI for 10 minutes at RT and cells were afterwards mounted in Vectashield antifade (Vector Laboratories) (Figure III.2).

III.3.5 Microscopy

Confocal images were obtained using an UltraVIEW VoX spinning disc system (Perkin Elmer, Massachusetts, USA) on a Nikon Ti microscope equipped with an oil immersion Plan-Apochromat x60/1.45 NA objective lens (pixel size in XY= 112 μm, Z-step 0.3 – 1 μm). Excitation was done using the following laser lines: 405, 488, 561 and 640 nm. Images were taken with the appropriate filters for the respective dyes: DAPI: emission wavelength (em): 415–475 nm; GFP: em: 505–549 nm; RFP: em: 580–650 nm and Cy5: em: 664–754 nm. RGB stacks and montages were created using ImageJ (http://rsb.info.nih.gov/ij/). For live-cell microscopy transfected *Microtus cabrerae* female cells were plated on a glass bottom p35 dish and were grown and HDACi treated under standard conditions. Time-lapse experiments were carried out in a closed live-cell microscopy chamber (ACU control, Olympus, Tokio, Japan) heated to 37°C, with 5% CO_2 and 60% air humidity. Stacks were acquired at 20 minutes intervals and taken with a CCD camera. Immunofluorescence images of fixed cells were also captured with an Axiovert200 microscope (Carl Zeiss, Jena, Germany) with a 63/1.4 Plan-Achromatic oil objective lens (Carl Zeiss, pixel size in XY= 104 μm). Greyscale images were pseudocolored and merged using Image J. For nucleotide incorporation rate measurements and DNA content analysis, cells were imaged using the Operetta High Content imaging system (Perkin Elmer, Massachusetts, USA), equipped with a 40 $\times$ 0.95 numeric aperture air objective.

III.3.6 Image analysis and quantification

For the quantification of histone acetylation levels (H3K9ac, H4K8ac), the mean values of acetylation were measured in the whole nucleus, at the sex chromosomes and in the whole nucleus excluding the X chromosomes (Figures III.4, III.5, III.7, III.S3. Cells treated with HDACi were normalized to untreated samples. Quantification thereof was performed using a custom written software in the Priithon image analysis platform ((http://code.google.com/p/ priithon/). Images were processed using a 3D median filter. Filtered images were threshold and then used to calculate the mean intensity of DAPI compaction, acetylation and methylation level. Analysis of total S, S substage and Xi/Xa replication duration was performed by counting live cell data time points and categorizing cells into early, mid or late S-phase stage according to their PCNA pattern. An early S-phase pattern is characterized by DNA replication foci distributed homogenously throughout the nucleus with exclusion of the nucle(ol)ar periphery, whereas a mid S-phase pattern is identifiable by more organized foci at the nucle(ol)ar periphery and the replication of the inactive X chromosome(s). Late S-phase is clearly recognizable due to the appearance of larger DNA replication foci of the heterochromatic block of the active X chromosome(s) (Figure III.6).

III.3.7 Ratiometric analysis of nucleotide incorporation rate

Modified thymidine analogs (EdU) were given to the cells for 10 min prior to fixation. EdU was detected with the ClickIT system (Invitrogen) followed by an immunostaining with mouse-anti-PCNA (1/100, Dako, Santa Clara, USA,

Cat #: M0879) and detection with donkey-anti-mouse IgG-Cy3 (1/200, The Jackson Laboratory, Bar Harbour, USA, Cat #: 715-166-151). DNA was counterstained with 1 μg/ml DAPI for 10 minutes at RT and cells were afterwards mounted in Vectashield antifade (Vector Laboratories). Detection thereof and fluorescence microscopy allowed the identification of early, mid and late DNA replication patterns. *Microtus cabrerae* cells were imaged using the Operetta High Content imaging system. Cell segmentation and quantification of nuclear intensities was performed using Harmony (Perkin Elmer, Massachusetts, USA). Whereas EdU shows the synthesized DNA (incorporated nucleotide), PCNA represents the replication machinery and thus active replisomes. For the calculation of nucleotide incorporation rate, the ratio of EdU (incorporated nucleotides) and PCNA (replication machinery) was estimated, as a proxy for the fork speed (Figure III.8). If the ratio shows a value = 1, this means a complete overlap of both signals (EdU and PCNA) and indicates a slow replication fork speed and thus slower replication forks. The higher the ratio of the total intensity, the higher the amount of DNA synthesized per replisome within the pulse and so the faster the fork speed.

III.3.8 DNA content analysis and genome duplication rate

Microtus cabrerae cells were imaged using the Operetta High Content imaging system. For imaging constant exposure times and appropriate filter sets (DAPI: ex: 360–400 nm; em: 410–480 nm; GFP: ex: 460–490 nm; em: 500–560 nm; RFP: ex: 560–580 nm; em: 590–640 nm) were used. Cell segmentation and quantification of nuclear intensities was performed using Harmony (Perkin Elmer, Massachusetts, USA). Subsequently, cells were manually staged for early, mid or late S-phase based on their PCNA pattern. Based on this classification, the total DNA intensity (DAPI) per cell nucleus was plotted for all cells from each replicate (Figure III.9). Based on the histogram of all cells per replicate, the DAPI intensity of each cell was normalized to the corresponding G1 and G2 peaks obtained by density fitting. This allowed pooling of the three replicates. Next, the normalized DAPI intensity per nucleus was classified in the corresponding S-phase substages for untreated and HDACi treated samples. To directly measure the amount of genomic DNA synthesized in each substage we analyzed the maximal % of DAPI in each substage normalized to G1 and estimated how much DNA in total gets synthesized during the respective substage. When dividing this value by the duration of replication of each substage, we achieved the % of the genome per hour, indicating the speed of DNA replication.

III.4 Results and discussion

III.4.1 Subnuclear distribution of euchromatin and heterochromatin marks in *Microtus cabrerae* female fibroblasts

In order to investigate the localization of the heterochromatic blocks coupled to the sex chromosomes in *Microtus cabrerae* cells, we prepared metaphase chromosomes and hybridized with a specific painting probe for the X chromosome (Figure III.1A)[27]. The hybridization on *Microtus cabrerae* chromosomes with this probe showed an intense signal on the whole heterochromatic region of this chromosome, except the centromere. Furthermore, we observed four giant sex chromosomes, demonstrating the tetraploidy of this cell line. Next, we characterized the epigenetic composition of the heterochromatic blocks coupled to the giant sex chromosomes of *Microtus cabrerae* female fibroblasts. Thus, we analyzed immunostainings using antibodies to specific histone variants and modifications. This analysis allowed us to determine the pattern of enrichment/depletion for each specific mark at the heterochromatic blocks. The marks investigated included two facultative heterochromatin marks, H3K27me3, macroH2a1, and two constitutive heterochromatin marks, H3K9me3 and HP1beta (Figure III.1B). In addition, we investigated euchromatic marks, previously identified in male *Microtus agrestis* and *Microtus cabrerae* [29], like H3K4 dimethylation (H3K4me2), H4K8 acetylation (H4K8ac), H3K9 acetylation (H3K9ac), but also other heterochromatic markers such as HP1 alpha and DNA methylation (Figure III.S1). As shown before, the heterochromatic blocks of sex chromosomes are easily identifiable by eye with a simple DAPI staining for DNA and were located at the nuclear periphery. These blocks were depleted for euchromatic marks and were hypoacetylated, but were enriched for marks characteristic for heterochromatin. Here, we discriminated between marks typical for facultative heterochromatin and for constitutive heterochromatin in female cells. First, we checked for facultative mark H3K27me3 via immunodetection and transiently transfected GFP-tagged histone variant macroH2a1, which is enriched at the inactive X chromosome in female cells. A clear colocalization in all three channels was detected. This DAPI dense region was enriched for both facultative marks and was identified as the heterochromatic block at the inactive X chromosome (Xi). Furthermore, we checked whether we got two distinct patterns, when we combined one mark for facultative heterochromatin (H3K27me3) and one mark for constitutive heterochromatin (H3K9me3). We distinguished four different blobs, two for the inactive X chromosome (s) and two for the active X chromosome(s). Immunostaining for H3K9me3 and transient transfection with HP1beta demonstrated that the heterochromatic blocks at the active X chromosomes showed typical pattern for constitutive heterochromatin and a strong signal overlapping on the heterochromatic blocks visualized by DAPI. The marks of the facultative heterochromatic blocks at the inactive X chromosome(s) and the constitutive hterochromatic blocks at the active X chromosome(s) are summarized in Figure III.1C.

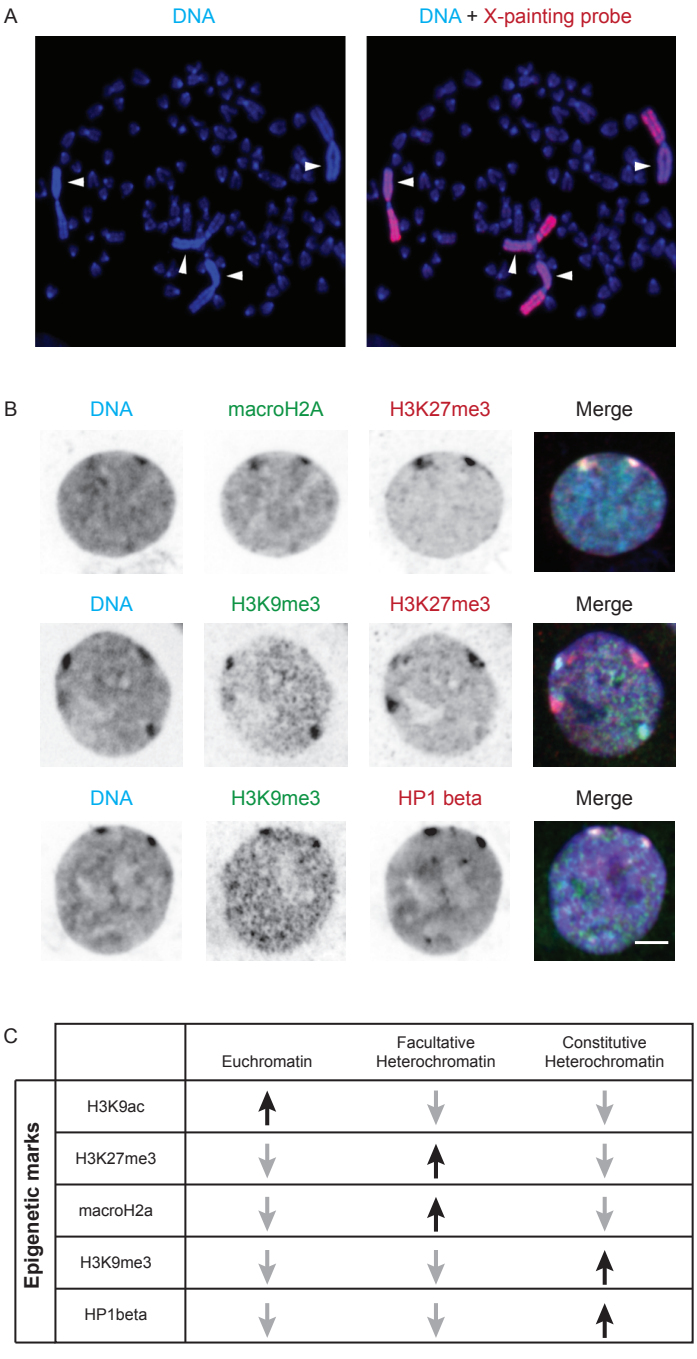

Figure III.1.: Subnuclear distribution of facultative and constitutive heterochromatin marks in *Microtus cabrerae* female fibroblasts. (A) Metaphase chromosomes from *Microtus cabrerae* female cell line were analyzed with a painting probe from the X chromosome. Arrow points to the heterochromatic block, which occupies the whole short arm of the X chromosome. (B) Prominent chromatin marks were analyzed by transient transfections and immunostainings. MacroH2a1 and H3K27me3 signals were simultaneously visualized by transient transfection with GFP-macroH2a1 and immunostaining using anti-H3K27me3 antibody (upper row). H3K9me3 and H3K27me3 marks, typical for constitutive and facultative heterochromatin, were simultaneously analyzed by double immunostaining (middle row). HP1beta and H3K9me3 signals were simultaneously visualized by transient transfection with DsRed-HP1beta and immunostaining against H3K9me3 (lower row). DNA was counterstained with DAPI. Protein and merge signals of all channels are shown. Single optical sections acquired on a spinning disc confocal microscope are shown. Scale bar: 5 µm. (C) Overview of subnuclear distribution of facultative and constitutive heterochromatin marks in *Microtus cabrerae* female cell line. Euchromatin is enriched for euchromatic marks like H3K9ac and H4K8ac, but depleted for heterochromatin marks like H3K27me3 and H3K9me3. Facultative heterochromatin is enriched for H3K27 trimethylation and macroH2a1. The constitutive heterochromatin is characterized by marks like H3K9me3 and HP1 beta accumulation.

III.4.2 Heterochromatic blocks coupled to sex chromosomes were replicated in distinct time frames

In order to dissect the DNA replication dynamics of facultative and constitutive heterochromatin in *Microtus cabrerae* female cells we transiently transfected the fibroblasts with a construct encoding for CFP-PCNA to label active replication sites and performed *In situ* replication labeling in combination with immunodetection of the previously characterized histone marks (Figure III.2). Modified nucleotides (EdU) were added to proliferating populations of *Microtus cabrerae* cells prior to fixation. We used pulses of either 20 or 30 minutes and a chase of either one or 2.5 hours (to distinguish between the DNA replication of the heterochromatic blocks coupled to the inactive (Xi) or the active (Xa) sex chromosome). We identified the facultative heterochromatin by immunostaining against H3K27me3 and the constitutive heterochromatin by immunostaining against H3K9me3 as well as ongoing DNA replication at the point of fixation by CFP-PCNA. After a chase of 1 hour (Figure III.2A), we detected an overlap of EdU and H3K27me3 in the first pulse, but at the time point of fixation there was only colocalization of H3K9me3 and PCNA left. This result indicated the order of sex chromosome replication, first the replication signal colocalized with facultative heterochromatin marks and later on with constitutive heterochromatin marks. When EdU was incorporated for 30 minutes and cells were chased for 2.5 hours (Figure III.2B), there was only colocalization left for PCNA and the active X chromosome, demonstrating that the active X chromosome replicated in this time frame and facultative heterochromatin was already replicated before (Figure III.2C).

III.4.3 Spatio-temporal progression of DNA replication in *Microtus cabrerae* female cells

To study the spatio-temporal progression of DNA replication in *Microtus cabrerae* female cells, we performed time-lapse microscopy of cells, triple-transfected with constructs encoding for CFP-PCNA, GFP-macroH2a1 and DsRed-HP1beta (Figure III.3, S2). With the help of PCNA we identified DNA replication patterns, macroH2a1 was used to detect the facultative heterochromatin and with HP1beta we spotted the constitutive heterochromatin. Visual inspection thereof allowed the unequivocal identification of three distinct S-phase patterns in *Microtus cabrerae* female cells. In early S-phase a multitude of small replication foci was distributed throughout the whole nucleus, excluding the nucleoli. This pattern was clearly comparable to the first S-phase pattern in other mammals, when euchromatin is replicated and chromatin is decondensed and hyperacetylated. With S-phase progression, another pattern arose, which showed more organized replication foci localized perinuclearly. The first big blob appeared in this phase, colocalizing with macroH2a1, indicating the DNA replication of facultative heterochromatin. After additional three hours there was no longer a colocalization of PCNA with macroH2a1, indicating the progression from mid to late S-phase. Now, there was a strong colocalization of HP1beta and PCNA within two big perinuclear blobs as a third distinct pattern of S-phase. As this structure colocalized with HP1 beta, we identified this structure as constitutive heterochromatin. From these three distinct patterns, we concluded that the chromatin state followed the DNA replication timing. First, euchromatin, next facultative heterochromatin and last constitutive heterochromatin were duplicated. When S-phase progressed smaller foci appeared simultaneously with the active X chromosome(s) before the cell transited toward G2 phase without any replication foci visible.

III.4.4 Manipulation of chromatin constitution by HDAC inhibition

Next, we tested histone acetylation level as a potential regulator of DNA replication dynamics in the vole rodent. Several studies have shown that histone acetylation level has an impact on DNA replication dynamics. Histone acetylation level controls the DNA replication dynamics of the inactive X chromosome [7] and is required to maintain the late DNA replication timing of constitutive heterochromatin [9]. As we identified the heterochromatic blocks to be both hypoacetylated, we tested whether, similarly to mouse cells, this mark regulated DNA replication timing. Thus, we manipulated the global acetylation level of cells and investigated whether this affects DNA compaction, histone acetylation level and consequently DNA replication onset of heterochromatic blocks of sex chromosomes (Figure III.4A). Cells were either treated with HDACi (LBH, panobinostat [22]) for 24 hours or with DMSO only. Cells were afterwards subjected to either immunofluorescence or to live cell imaging. To first answer the question, whether it is possible to successfully induce global hyperacetylation to *Microtus cabrerae* female cells, we treated cells with either HDACi or DMSO only and stained for DAPI and acetylation signal. We made use of a self-written analysis protocol (Figure III.S3) to measure the mean DNA compaction level and mean acetylation level in the whole nucleus (Figure III.4B). We detected a significant decrease of DAPI signal in hyperacetylated samples, leading to the assumption that the DNA compaction level is decreased and, consequently, the chromatin is more opened and accessible. Furthermore, we assessed the acetylation level in the whole nucleus of *Microtus cabrerae* female cells and we found a significant increase of acetylation level, demonstrating an efficient induction of global hyperacetylation in *Microtus cabrerae* cells.

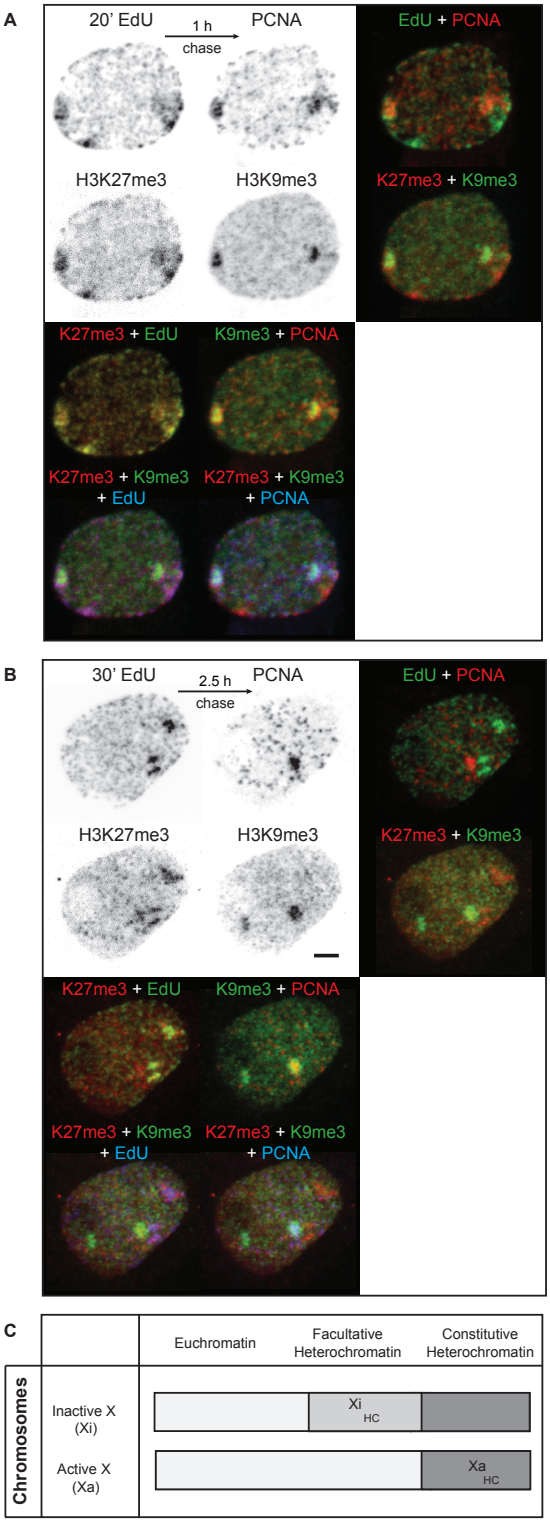

Figure III.2.: DNA replication dynamics and epigenetic constitution of facultative and constitutive heterochromatin in *Microtus cabrerae* female fibroblasts. Asynchronously growing *Microtus cabrerae* female cells were transfected with CFP-PCNA plasmid and pulse labeled with 10 µM EdU for either 20 min (A) or 30 min (B), followed by a 1 h (A) or 2.5 h (B) chase before fixation with 4% paraformaldehyde and methanol. EdU was detected with the ClickIT system with Alexa488 followed by immunostaining against H3K27me3 (facultative heterochromatin), H3K9me3 (constitutive heterochromatin) and PCNA to visualize ongoing replication at the time of fixation. Maximum intensity projections of confocal images are shown. Scale bar: 5 µm. (C) Schematic representation of sex chromosomes with corresponding heterochromatic blocks with either facultative heterochromatin (Xi) or constitutive heterochromatin (Xa). (Contribution of C. S. Casas-Delucchi to the manuscript.)

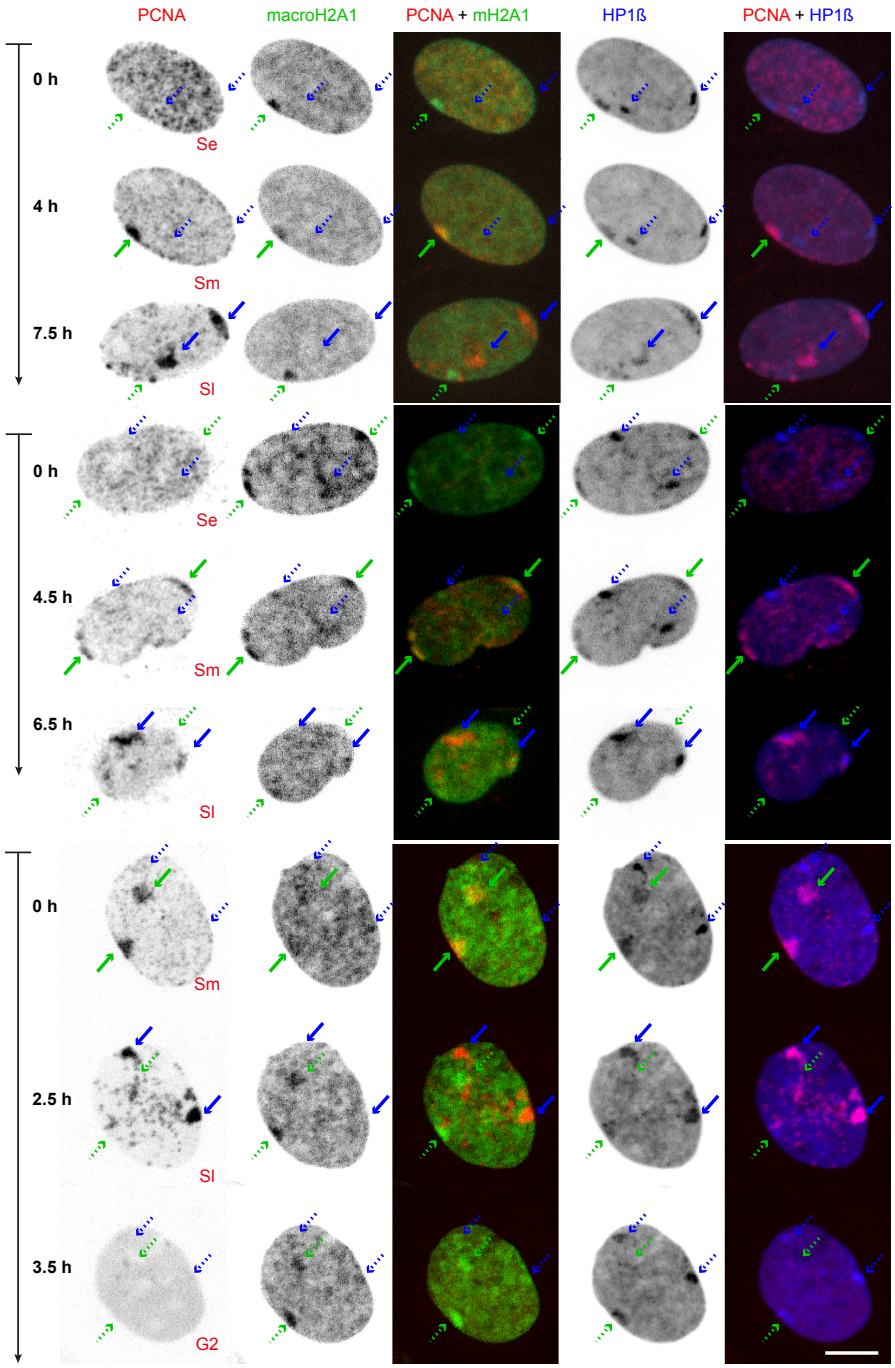

Figure III.3.: Time-lapse analysis of facultative and constitutive heterochromatin replication with their respective marks in *Microtus cabrerae* female fibroblasts. Live images from *Microtus cabrerae* female cells triple transfected with CFP-PCNA, GFP-macroH2a1 and DsRedHP1beta. Maximum intensity projection of z-stacks acquired on a spinning disc confocal microscope at 20 min time intervals. Green arrows: inactive X (Xi), blue arrows: active X (Xa). Solid lines denote ongoing replication of the chromosome. Exemplary images depict three distinct PCNA patterns, which can be assigned to three different types of chromatin. In early S-phase a multitude of small replication foci is distributed throughout the whole nucleus, excluding the nucleolus, when euchromatin is replicated. In mid S-phase the replication foci become more organized and a perinuclear pattern arises with foci at the nucle(ol)ar periphery. A first big blob is identified and supposed to be the facultative heterochromatic block of the inactive X-chromosome (Xi), which is enriched for macroH2a1. Whereas in late S-phase replication foci are consolidated together in large blobs supposed to correlate to the constitutive heterochromatic block of the active X-chromosome (Xa). This block is enriched for constitutive heterochromatin mark HP1 beta. Both heterochromatic blocks are replicated later than euchromatin. Scale bar: 10 µm. (Contribution of C. S. Casas-Delucchi to the manuscript.)

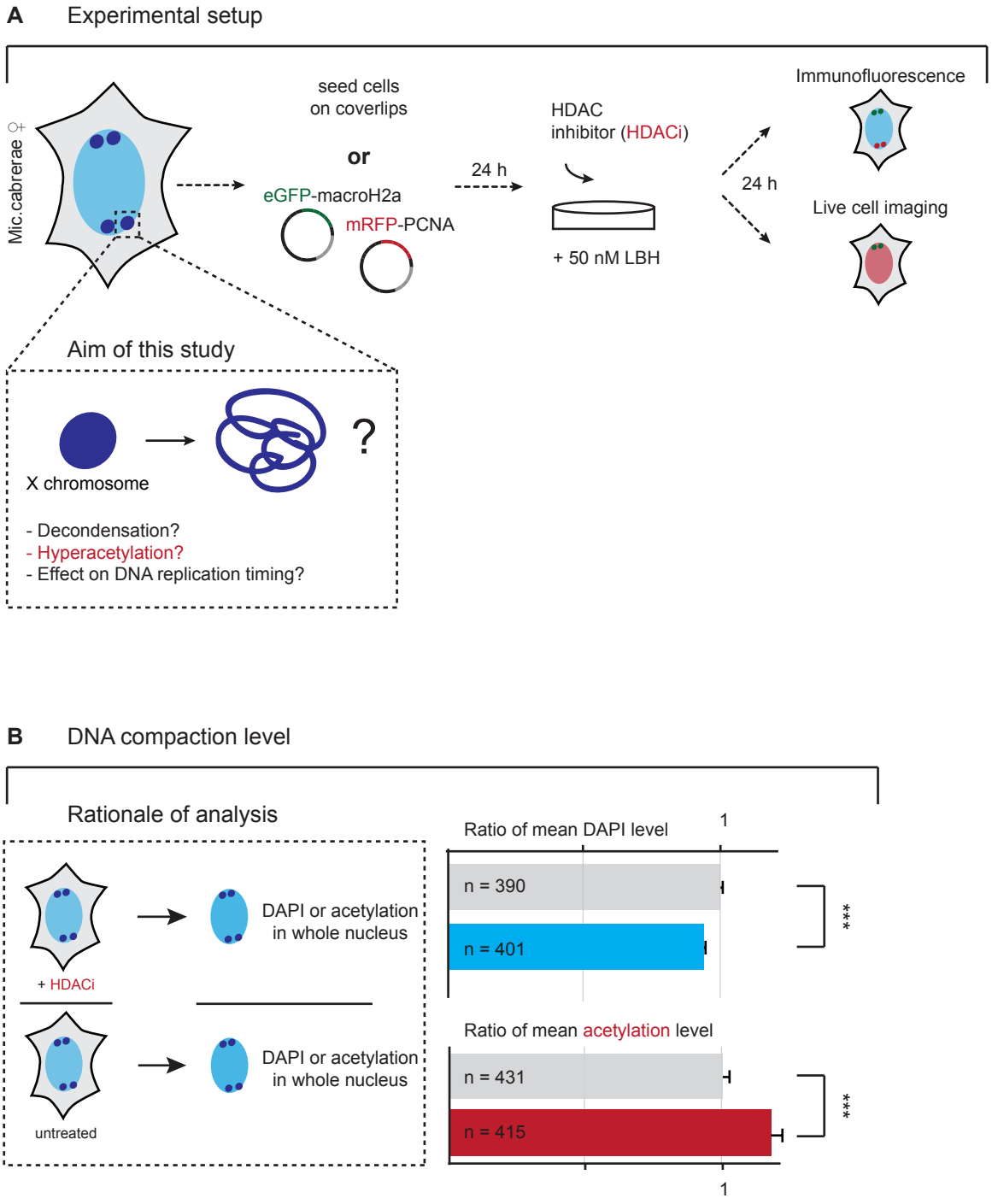

Figure III.4.: Manipulation of heterochromatic blocks' constitution by HDAC inhibitor. (A) Schematic representation of the experimental setup to manipulate the heterochromatic blocks' constitution of *Microtus cabrerae* cells by HDACi LBH. LBH as a panHDACi was expected to increase histone acetylation level and potentially lead to decondensation and a potential effect on DNA replication timing. Cells were either seeded or transfected with the corresponding constructs (GFP-macroH2a1, RFP-PCNA) and incubated for 24 hours. 50 nM LBH was added to the medium and cells were again incubated for 24 hours. Control cells were treated with DMSO only. Afterwards cells were either fixed and subjected to immunostainings or used for live-cell imaging with a spinning disc confocal microscope. (B) Untreated and HDACi treated female *Microtus cabrerae* fibroblasts were analyzed with a user-independent analysis to measure DNA compaction level and acetylation level in the whole cell nucleus. Bar graphs indicate the DAPI signal as well as the acetylation level in untreated cells and HDACi treated cells. Sample sizes are indicated in the bars. Grey bars demonstrate the normalized control. Statistical significance was tested using the t- test, comparing untreated and HDACi treated cells. Error bars demonstrate 95 CI. $***P < 0.001$.

III.4.5 Treatment with HDAC inhibitor leads to induced hyperacetylation globally and at the heterochromatic blocks of the sex chromosomes

In order to investigate whether the treatment with the HDAC inhibitor was sufficient to manipulate the heterochromatic blocks of the sex chromosomes, we analyzed the histone acetylation level directly at the heterochromatic blocks (Figure III.5). During the setup of this approach, we recognized that Trichostatin A, a commonly used HDACi, was not sufficient to hyperacetylate these heterochromatic blocks, although the global acetylation was increased (Figure III.S4). In fact the global histone acetylation level was increased but not the level of histone acetylation at the heterochromatic blocks of Xi or Xa. Normally concentrations of 20 nM over 72 hours were sufficient to lead to an efficient histone hyperacetylation even at very condensed structures. After incubation over several days *Microtus cabrerae* cells did not show any increase of acetylation level at heterochromatic blocks at Xi or Xa. To test whether LBH as a panHDACi was efficient to induce hyperacetylation at the heterochromatic blocks, we used a self-written user-independent analysis protocol (Figure III.S3) and estimated the acetylation level directly at the facultative heterochromatin (H3K27me3) and constitutive heterochromatin (H3K9me3). We measured two different histone acetylation marks H3K9ac and H4K8ac, which were normally depleted from the heterochromatic blocks (Figure III.S1). We observed for facultative and constitutive heterochromatin that both acetylation marks were significantly increased in contrast to untreated cells. In addition and potentially as a consequence of hyperacetylation, histone methylation marks typical for facultative heterochromatin (H3K27me3) and for constitutive heterochromatin (H3K9me3) were significantly decreased (Figure III.5). Only LBH as a panHDACi, which affects all four HDAC classes (Figure III.S4), was proficient to lead to induced hyperacetylation not only in the whole nucleus, but also at the heterochromatic blocks of Xi and Xa. Furthermore, this effect was already achieved after an incubation of only 24 hours, shortening the experimental setup.

III.4.6 Induced hyperacetylation leads to prolonged substage and total S-phase duration

After setting up a manipulation approach sufficient to manipulate the histone acetylation level of the heterochromatic blocks, we next asked whether this global hyperacetylation affects the length of total S-phase, substages as well as the duration of sex chromosome replication. To test this, we first analyzed images from live-cell imaging experiments of several hours to unequivocally distinguish between the three different substages of S-phase (Figure III.6A). By counting time-points, where each time point was a 20 minutes interval, we estimated the total S-phase duration, substage durations and sex chromatin replication duration in untreated and treated *Microtus cabrerae* cells. Total S-phase duration was significantly prolonged from 9.4 up to 12.6 hours in treated cells. In addition, the duration of early S-phase increased from 3.4 hours up to 5.1 hours, as well as of mid and late S-phase, too. With the help of double transfections of constructs encoding RFP-PCNA and either GFP-macroH2a1 or GFP-HP1beta, we further calculated the duration of DNA replication the heterochromatic blocks at the heterochromatic blocks of the Xi and the Xa (Figure III.6B). Not only the total S-phase duration and the substages were affected by the global hyperacetylation, but also the duration of DNA replication of the two heterochromatic blocks was prolonged. Xi and Xa were both replicated in a time frame of approximately 1.9 hours, but after HDACi treatment the duration of Xi replication increased up to 2.7 hours and the duration of Xa up to 2.2 hours.

III.4.7 Site-directed targeting of histone acetyltransferase increases histone acetylation level and prolongs DNA replication duration of the constitutive heterochromatin

Having demonstrated that our manipulation system is proficient to increase global acetylation level and to detect effects on the DNA replication onset and duration, we still do not know whether histone acetylation alone lead to these effects. So far, we also detected a decrease of DNA compaction as well as a decrease of histone methylation marks. To further elucidate the effect of histone acetylation on the DNA replication dynamics of a distinct region, we set up a targeting approach to specifically target HBO1, a histone acetyltransferase (HAT), to the heterochromatic block of the active X chromosome (Figure III.7). Our targeting system consisted of two fusion proteins: GFP- tagged histone acetyltransferase (HBO1) and a GFP-binding protein linked HP1beta for the recognition of the constitutive heterochromatin of the active X chromosome. In a targeted state, HP1beta binds to the constitutive heterochromatin of the active X chromosome, while its GBP domain causes it to interact with GFP-HBO1. This interaction resulted in the recruitment of HBO1 to the constitutive heterochromatin (Figure III.7A). For an untargeted state, we manipulated by site-directed mutagenesis the catalytic activity of HBO1, resulting in an inactive enzyme.
To confirm the successful site-directed targeting, we stained for H3K9me3 as a hallmark of the constitutive heterochromatin. Detection thereof showed a strong colocalization of the targeting signal and H3K9me3. As a next step, we elucidated the effect of this specific HBO1 targeting on the DNA compaction, H3K9me3 level and histone acetylation level. First, we directly analyzed the signals at the heterochromatic blocks using the H3K9m3 signal as a mark. We did not observe any effect on DNA compaction level, but significant decrease of H3K9 trimethylation and significant increases of the acetylation level at the constitutive heterochromatin (Figure III.7B). To demonstrate that our targeting is specific,

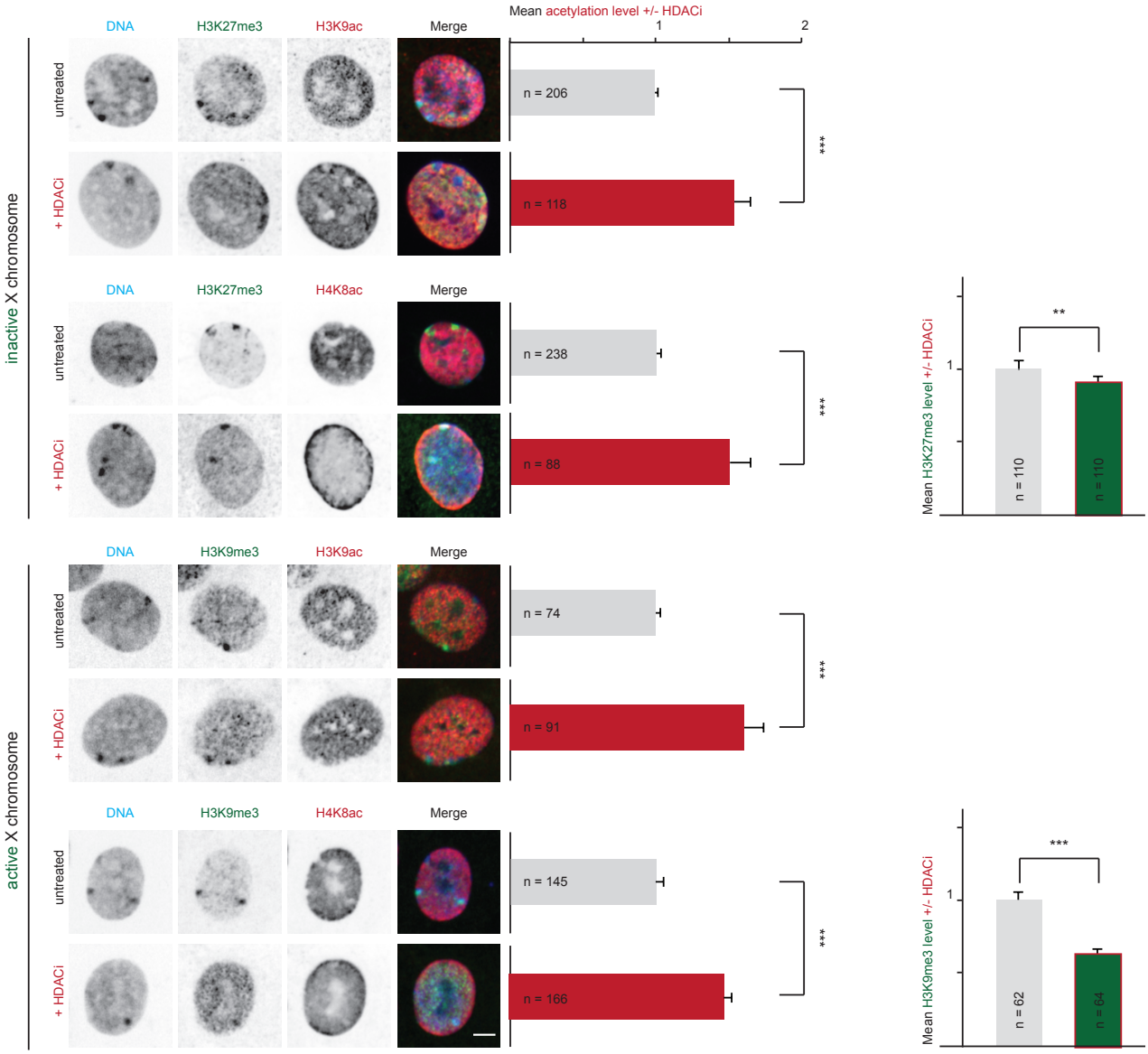

Figure III.5.: Treatment with HDAC inhibitor leads to hyperacetylation of heterochromatic blocks at sex chromosomes and decrease of methylation marks. Distribution of euchromatic marks H3K9ac and H4K8ac were analyzed by immunofluorescence staining. *Microtus cabrerae* female cells were treated with or without HDACi LBH (50 nM) for 24 hours prior to fixation. Acetylation levels were measured with a user-independent analysis: DNA (DAPI, blue), Xi/Xa (H3K27me3/H3K9me3, green), acetylation (H3K9ac or H4K8ac, red). Mean acetylation signals for untreated cells (grey bar) and HDACi treated cells (red bar) are shown. Sample sizes are indicated in the bar. Mean methylation levels are plotted for untreated cells (grey bar) and for HDACi treated cells (green bar, red-framed). Scale bar: 5 µm. Error bars demonstrate 95 CI. $***P <$ 0.001.

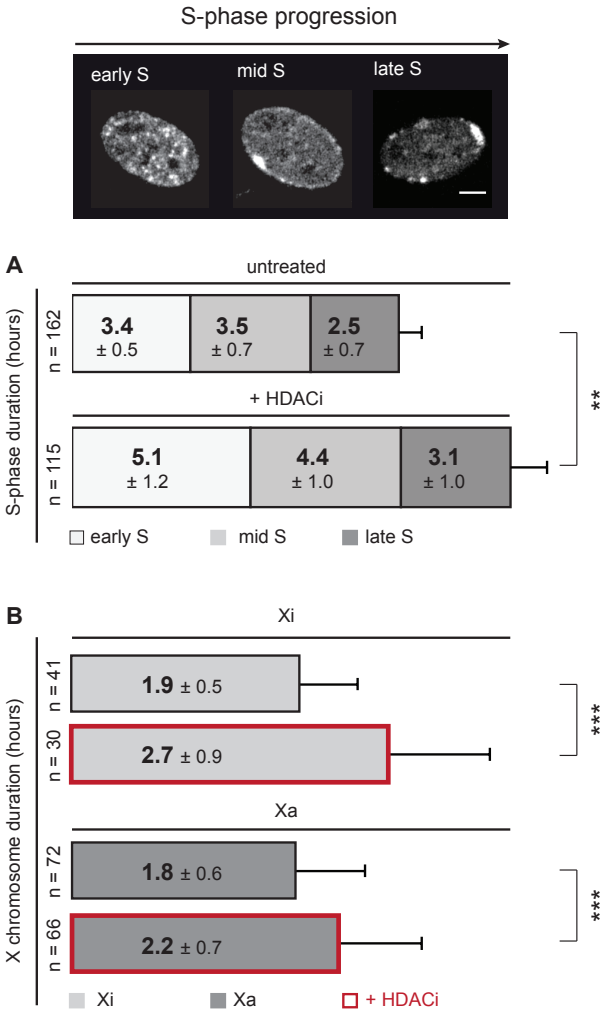

Figure III.6.: Hyperacetylation prolongs S-phase duration in total, of substages and of sex chromosomes. (A) Exemplary images of S-patterns were depicted to illustrate the categorization into S-phase substages. *Microtus cabrerae* cells were transiently transfected with a plasmid encoding PCNA (either RFP or GFP-tagged) and either GFP-macroH2a1 or DsRed-HP1beta. Cells were treated with DMSO or LBH according to the experimental setup in Figure III.4A and analyzed by live cell imaging. In HDACi treated cells the total S-phase duration is significantly increased. Early S-phase duration increased from 3.4 up to 5.1 hours, as well as mid S-phase, which is prolonged by approximately one hour. Sample sizes are indicated on the left-hand side. Statistical significance was tested using the t-test, comparing the total S- phase duration and S-substage duration in untreated and treated samples. Standard deviations of replicates are shown in the boxes. $**P <$ 0.01.

we performed a second analysis and created a binary mask, excluding the heterochromatic block signal measuring only the remaining part of the nucleus. Now, we did not see any effects on DNA compaction, histone acetylation or histone methylation level, supporting our approach of site-directed targeting specifically to the constitutive heterochromatin (Figure III.7C). Next, we wanted to elucidate the impact of site-directed targeting of HBO1 to the constitutive heterochromatin on its DNA replication duration. To this end, we transfected *Microtus cabrerae* cells with constructs encoding for RFP-PCNA, for GFP-HBO1 and GBP-HP1beta to visualize active replication sites and HAT targeting. With the help of time-lapse microscopy, we elucidated the duration of sex chromosome duration as described above. We observed a significant prolongation of the DNA replication duration of the heterochromatic block of the active X chromosome. Instead of 1.8 hours the constitutive heterochromatin was replicated in a time frame of 3.2 hours, when HBO1 was targeted. Moreover, no effect was measured in the duration of the inactive X chromosome, further confirming the specific increase of histone acetylation level only at the active X chromosome (Figure III.7D).
With this additional approach we ruled out the effect of DNA composition on DNA replication timing. The effect on DNA replication timing stayed the same and was even more dramatic, when targeted with HBO1. This fact demonstrated that the manipulation of all HDACi classes via LBH lead to more dramatic side effects. Whereas targeting with HBO1 did not affect the DNA compaction level as a more mild manipulation assay, but still a very efficient one. Although HBO1 is known as a H4 specific histone acetyltransferase, we did not only observe an effect on H4K8ac, but also on H3K9ac, indicating an interaction of HBO1 and histone H3, too. Studies have shown an interaction of HBO1 and H3K14ac [30], indicating interactions also with histone H3. Upon HAT targeting, we also achieved a loss of H3K9 trimethylation mark, similarly to our results by global hyperacetylation. Previous studies have shown that a loss of H3K9me3 was not sufficient to change replication timing of constitutive heterochromatin [9]. These data therefore suggest that the level of histone acetylation at a given genomic region is a major factor in its determination of DNA replication kinetics. We concluded that the observed H3K9me3 decrease was more likely a side effect of histone hyperacetylation, but had no direct effect on DNA replication kinetics.
The targeting of the inactive X chromosome, using GBP-macroH2a1 and GFP-HBO1 was less effective. The difference between both targeting assays was that HP1beta only needed to bind H3K9 trimethylated nucleosomes, whereas macroH2a1 as a histone variant needed to incorporate into the nucleosomes. Upon Xi targeting we achieved a prolongation of DNA replication of the facultative heterochromatin (Figure III.S5), but not at the constitutive heterochromatin, supporting our previous data of HAT targeting to the heterochromatic block of the active X chromosome.

III.4.8 Slower nucleotide incorporation rate in hyperacetylated *Microtus cabrerae* cells

We next asked, whether the strong increase on the duration of total S-phase, substages and sex chromosomes in treated samples was a consequence of slower fork speed and, thus, more time was needed to replicate the genome. To answer this question, we used again the global inhibition of HDACs and analyzed its effect on DNA replication timing in whole *Microtus cabrerae* cells to understand the mechanism behind the prolongation of DNA replication. We incorporated modified nucleotides for 10 minutes to treated and untreated cells, fixed cells and stained for nucleotides and PCNA. We analyzed the fork speed of untreated and treated samples with the help of total intensities of signals and ratiometric analysis of nucleotide incorporation rate. While PCNA is part of the DNA replication machinery and is therefore proportional to the amount of active replisomes, the amount of incorporated nucleotides is proportional to both the number of active replisomes and the replication fork speed. By calculating the ratio of the total nucleotide signal to the total PCNA signal, we assessed changes in the relative replication fork speed in treated and untreated samples. If the value of the normalized ratio of EdU/PCNA = 1, this meant a complete overlap of both signals (EdU and PCNA) and indicated a slow replication fork speed and thus slower replication forks (Figure III.8A, III.S6). If the value of the ratio of both signals was >1, this indicated more synthesized DNA and consequently faster replication forks and a faster fork speed. We plotted the nucleotide incorporation rate as box plots over S-phase progression from early S to mid and late S-phase (Figure III.8B). In untreated samples the nucleotide incorporation rate clearly increased over time approximately 1.4 times from early S to mid and late S. In treated samples there was no increase. When comparing early S-phase in treated versus untreated samples, we detected a significant decrease of nucleotide incorporation rate about 0.9. Comparing mid S and late S in treated versus untreated samples, the fold change was about 0.6, indicating a significant decrease on nucleotide incorporation rate and consequently slower fork speed in treated samples.

III.4.9 Hyperacetylation cells show more DNA during early S-phase pattern and have decreased genomic duplication rate

Next, we wanted to address the question, whether the onset of DNA replication was affected by the histone hyperacetylation by HDAC inhibition. As euchromatin is hyperacetylated and known to replicate during early S-phase, we tested whether this hyperacetylation advances the DNA replication onset of heterochromatin. To test this hypothesis, we plotted the relative DNA content (as G1 equivalents) from early S- to late S-phase. For this reason, thymidine analog was incor-

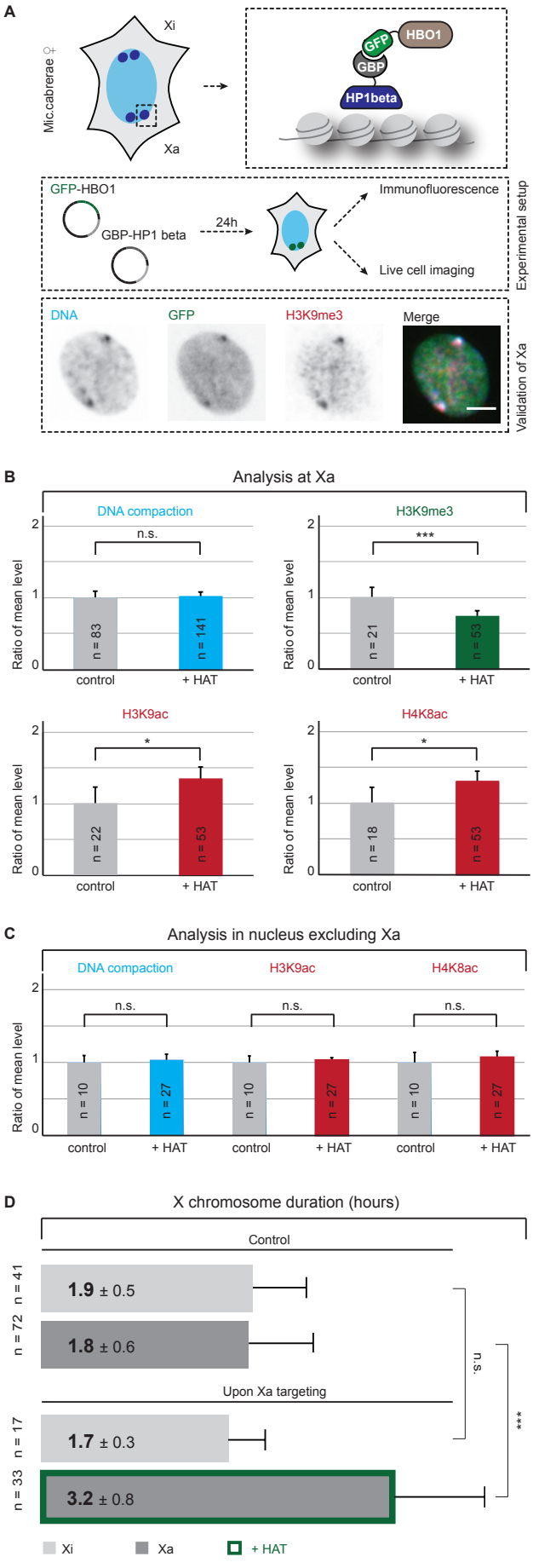

Figure III.7: Site-directed targeting of histone acetyltransferase leads to hyperacetylation and increase of DNA replication duration of constitutive heterochromatin. (A) Schematic representation of the targeting approach in a *Microtus cabrerae* cell. HBO1, a histone acetyl transferase, was tagged to GFP and HP1-beta was tagged to GBP, a GFP-binding nanobody. Upon co-expression of both and because of their strong interaction HBO1 is specifically targeted to the active X chromosome. The experimental setup (middle box) implied the transient transfection of two plasmids: GFP-HBO1 and GBP-HP1beta, followed by an incubation time of 24 hours. The functionality of the targeting was validated by antibody detection of H3K9me3, a marker of constitutive heterochromatin, resulting in a strong colocalization of DAPI stained DNA in blue, GFP-HBO1 and GBP-HP1beta in green and H3K9me3 in red. The merge shows an overlay of all three channels. Scale bar = 5 µm. (B) Untargeted and targeted female *Microtus cabrerae* fibroblasts were analyzed with a user-independent analysis to measure DNA compaction level, H3K9me3 and acetylation level at the active X chromosome. Bar graphs indicate the ratio of the mean levels, where greyish bars represent the normalized control and colored bars the respective targeted sample. Statistical significance was tested using the t- test, comparing untargeted and targeted cells. Error bars demonstrate 95 CI. $***P < 0.001$. (C) Untargeted and targeted female *Microtus cabrerae* fibroblasts were analyzed with a user-independent analysis to measure DNA compaction level, H3K9me3 and acetylation level in the whole nucleus excluding the active X chromosome. Bar graphs indicate the ratio of the mean levels, where greyish bars represent the normalized control and colored bars the respective targeted sample. Statistical significance was tested using the t- test, comparing untargeted and targeted cells. Error bars demonstrate 95 CI. (D) The duration of X chromosome replication was estimated out of live-cell imaging data. Error bars demonstrate the standard deviation. Statistical significance was tested using the t-test, comparing the duration of replication of Xi and Xa in untargeted and targeted samples. $***P < 0.001$.

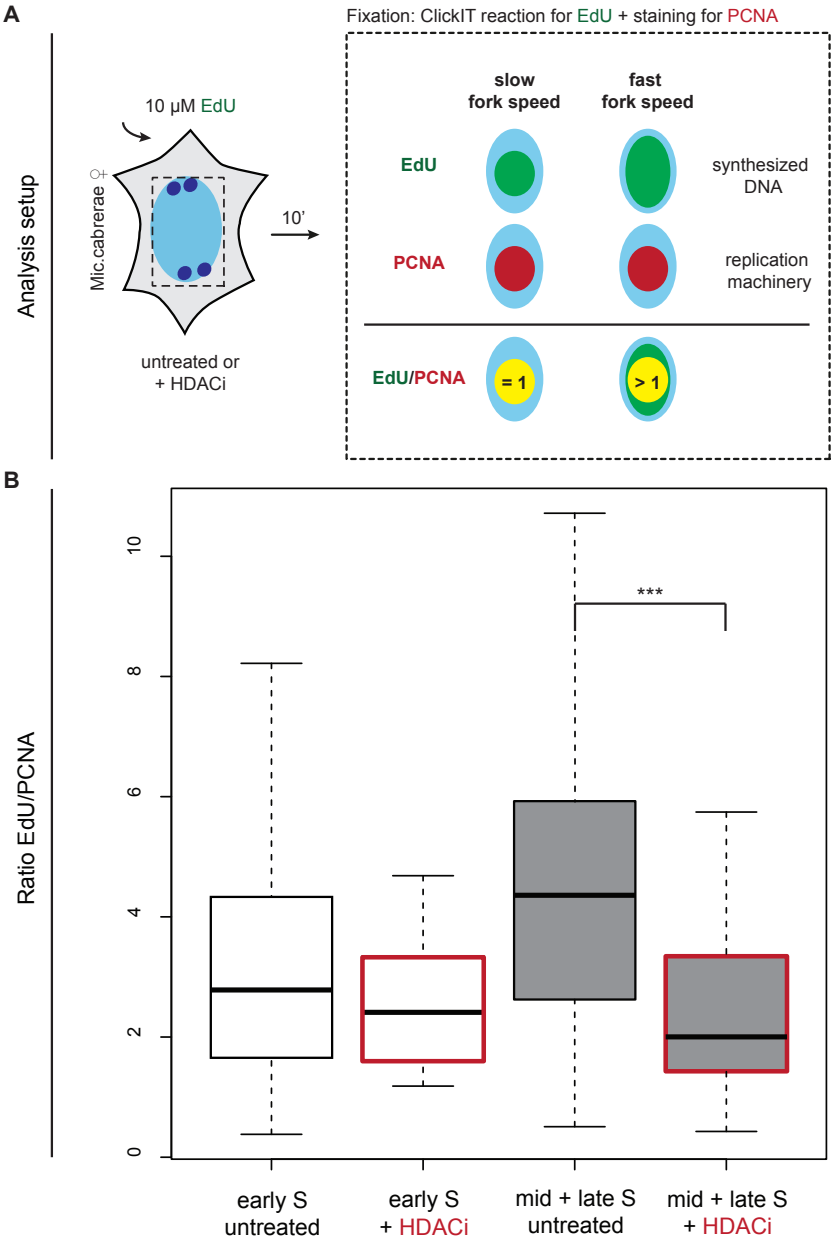

Figure III.8.: Induced hyperacetylation leads to a decrease of nucleotide incorporation rate and a slower fork speed. (A) Schematic representation of the calculation of relative nucleotide incorporation rate. Modified thymidine analog EdU was added for 10 minutes to *Microtus cabrerae* cells that were treated or untreated with HDACi prior to fixation. EdU was detected with ClickIT chemistry and endogenous PCNA via antibody detection. Whereas EdU represents the amount of synthesized DNA (incorporated nucleotides), PCNA reflects the replication machinery and thus active forks. For the estimation of nucleotide incorporation rate the ratio of EdU (incorporated nucleotides) total intensity and PCNA (replication machinery) total intensity was estimated, as a marker for the speed of replication forks. If the ratio shows a value = 1, this means a complete overlap of both signals (EdU and PCNA) and indicates a slow replication fork speed and thus slower replication forks. If the ratio of both signals is >1 this means that there was more DNA synthesized, indicating faster replication forks and hence a faster fork speed. (B) The ratio of EdU and PCNA signals was plotted as box plots. Cells were categorized by visual inspection of the EdU signal into early (light grey box) and mid+late cells (dark grey box). HDACi treated samples are indicated by the red-framed box. In untreated cells the nucleotide incorporation rate increases over time, demonstrating an increase of fork speed from early to mid+late cells. In contrast to untreated cells, HDACi treated samples show a significantly lower ratio of EdU/PCNA signal, indicating a slower nucleotide incorporation rate and thus a slower fork speed. Error bars demonstrate standard deviation. Statistical significance was tested using the Wilcoxon test, comparing untreated and HDACi treated *Microtus cabrerae* cells. $***P < 0.001$.

porated to replicating *Microtus cabrerae* cells for 10 minutes and cells were fixed and stained. We visually categorized replicating cells by replication signal (EdU) in early, mid and late S-phase as well as in non-S-phase cells (Figure III.9A). We analyzed the integrated DAPI intensity in individual nuclei and normalized all cells of one replicate to the G1 peak intensity [31]. Upon DNA replication, the DNA content increases from G1 to G2 over time (Figure III.9B). We showed that the amount of genomic DNA was significantly increased in early S-phase, when cells were hyperacetylated. This result was consistent with our previous finding that early S-phase was prolonged in treated cells, indicating that the facultative heterochromatin known to replicate during mid S-phase was shifted towards early S-phase.

Furthermore, we estimated the genome duplication rate in untreated and treated cells. For this we elucidated the per-

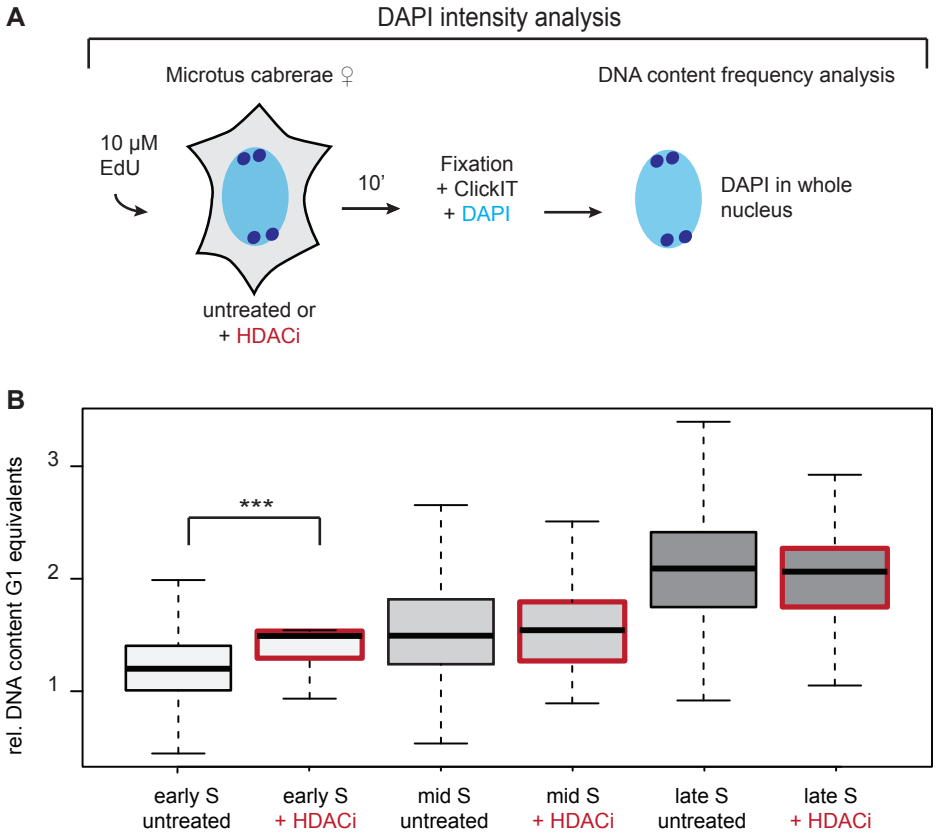

Figure III.9.: Hyperacetylated *Microtus cabrerae* cells show a stronger increase of genomic DNA in early S-phase. (A) Schematic representation of the experimental setup. 10 µM EdU was added to cultures of HDACi treated and untreated cells for 10 minutes prior to fixation. EdU was detected via ClickIT reaction and cells were DAPI stained for 10 minutes. The DNA content frequency analysis was performed by DAPI intensity measurements in treated and untreated cells, which were categorized into their respective S-phase substage according to their replication pattern. (B) Boxplots depict S-phase substages from early S to late S for both untreated and treated samples. HDACi treated samples are indicated by the red-framed box. The DNA content of treated cells is in early S-phase significantly increased in comparison to untreated cells. Statistical significance was tested using the Wilcoxon test, comparing untreated and HDACi treated *Microtus cabrerae* cells. $***P < 0.001$.

centage of increase of the genome by DNA content in every S-phase substage (Figure III.10A). In line with our previous outcome, we observed that 50% of the genome in treated cells was already replicated in early, whereas in untreated cells only 37% replicated during early S-phase. There was a clear shift from percentage of the genome replicating in mid towards early in treated samples. Consequently, the percentage of the genome replicating in mid S-phase was decreased in HDACi treated cells, further supporting our hypothesis that facultative heterochromatin was replicated in advance concomitantly with euchromatin during early S-phase. Finally, we combined these findings from the genome duplication rate analysis with data from live cell imaging experiments on substage durations to calculate the percentage of the genome replicated per hour as an indicator of genome duplication speed (Figure III.10B). This analysis matched the data from the nucleotide incorporation rate (Figure III.8B) indicating that the replication speed is slower in treated samples. Whereas

in untreated samples 10.9% of the genome was replicated per hour in early S-phase, only 9.8% of the genome was duplicated in treated samples. The difference was even more dramatic in mid S-phase, when only 5.4% of the genome was replicated during one hour in contrast to the untreated cells where 10.9% of the genome was replicated per hour.
All in all, we demonstrated that histone acetylation level is a potential regulator of DNA replication timing. Upon induc-

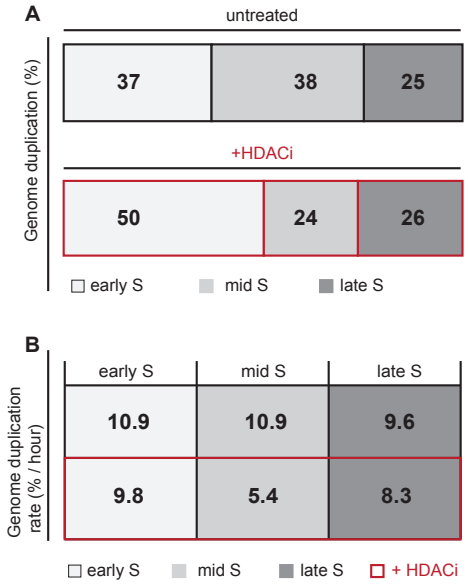

Figure III.10.: Hyperacetylation affects the genome duplication rate. (A) The genome duplication time was calculated from DNA content data (Figure III.9). As after S-phase 100% of the DNA is replicated, the genome duplication per substage can be estimated. In treated cells (red-framed box) 50% of the genome was already replicated during early S-phase, whereas only 37% of the genome was replicated in early S in control samples. 38% of the genome was replicated in mid S-phase in control cells. In contrast, only 24% of the genome were replicated in mid S-phase in HDACi treated cells. (B) When combining these genome duplication data with the measured DNA replication substage durations of Figure III.6A, we were able to measure the % of genome increase per hour, an indicator of replication speed. The values showed that the % of genome replicated in one hour were decreased in treated samples, in particular, in facultative heterochromatin.

tion of hyperacetylation, irrespective of global induction by drug treatment or by specific HAT targeting, we observed an increase of DNA replication duration. As the mean H4K8 acetylation level of the heterochromatic block of the inactive X chromosome was much higher in comparison to the active X chromosome, we concluded that hyperacetylation thereof lead to the shift from mid to early S-phase. Furthermore, the general prolongation of DNA replication suggests that the total number of active origins at any given time point remains constant in accordance to a limiting factor model (reviewed in [32]) and that there are not more origins firing to counterbalance the prolongation of S-phase. The fact that more DNA content is measurable during early S-phase, when normally euchromatin is replicated, is an indicator that mid replicating facultative heterochromatin was shifted towards early S replication.
Ultimately, DNA replication timing is defined by the timing, when DNA replication origins fire. The relative efficiency model of origin firing claims early origins to fire more efficiently, whereas late origins exhibit a lower efficiency at the beginning of S-phase, increasing over time when S- phase progresses, assuring the closure of potential gaps of unreplicated DNA in a timely fashion [33]. In this context, this study indicates that histone acetylation plays an important role in defining the efficiency of origins and concomitantly the DNA replication timing of distinct genomic regions like the heterochromatic blocks at the Xi or Xa. Several processes that lead to origin firing itself are known at which histone acetylation might regulate replication timing. In fission yeast the dynamic of origin firing could be a result of differences in the timing of ORC binding at different genomic regions [34]. The binding of limiting ORC factors is probably facilitated at acetylated and open chromatin. Another potential process being influenced and promoted by histone acetylation is the origin licensing, as HBO1-mediated histone acetylation in yeast has been shown to play a role in loading Mcm 2-7 complex [35], which itself is required for origin licensing [36]. The induction of hyperacetylation may promote origin licensing or is involved in the actual firing process by increasing accessibility by opening chromatin or by an increase of binding affinity to limiting factors such as Cdc45, respectively, [18, 37], which has been shown to increase the firing efficiency of inefficient origins [34]. Furthermore, it is known that an open chromatin state can promote origin firing, we were able to rule out that this is a major factor involved in the regulation of DNA replication dynamics in *Microtus cabrerae* cells.

However, we measured a very broad compaction level and cannot exclude decompaction at a lower level of nucleosomes. Nevertheless, upon site-directed HAT targeting to the heterochromatic blocks of inactive or active X chromosome, we achieved no effect on DNA compaction level, resulting in the same effects on DNA replication kinetics as observed before with global hyperacetylation.
Taken together, we propose that the histone acetylation level affects DNA replication timing of heterochromatic blocks of sex chromosomes, independently of changes in histone methylation marks or DNA compaction level. Importantly, histone acetylation level negatively regulates replication fork speed at a global level.

III.5 Conclusion

Our data, summarized in Figure III.11 reveal an impact of histone acetylation level on DNA replication timing in *Microtus cabrerae* cells. First, we showed that the heterochromatic blocks coupled to the inactive and active X chromosomes of female *Microtus cabrerae* cells showed typical marks for either facultative or constitutive heterochromatin. Moreover, we identified three distinct DNA replication patterns: early, mid and late. The heterochromatic block coupled to the inactive X chromosome was replicated during a narrow time frame of mid S-phase, whereas the heterochromatic block coupled to the active X chromosome was replicated during late S-phase. Our data also suggests histone acetylation as a major determinant of DNA replication timing, as global as well as site-directed histone hyperacetylation leads to prolongation of total S-phase and sex chromosome replication duration. Furthermore, we detected a slower fork speed, when chromatin was hyperacetylated going hand in hand with an increase of DNA content in early S-phase, indicating a shift from mid replicating facultative heterochromatin towards early S-phase, when euchromatin was replicated.

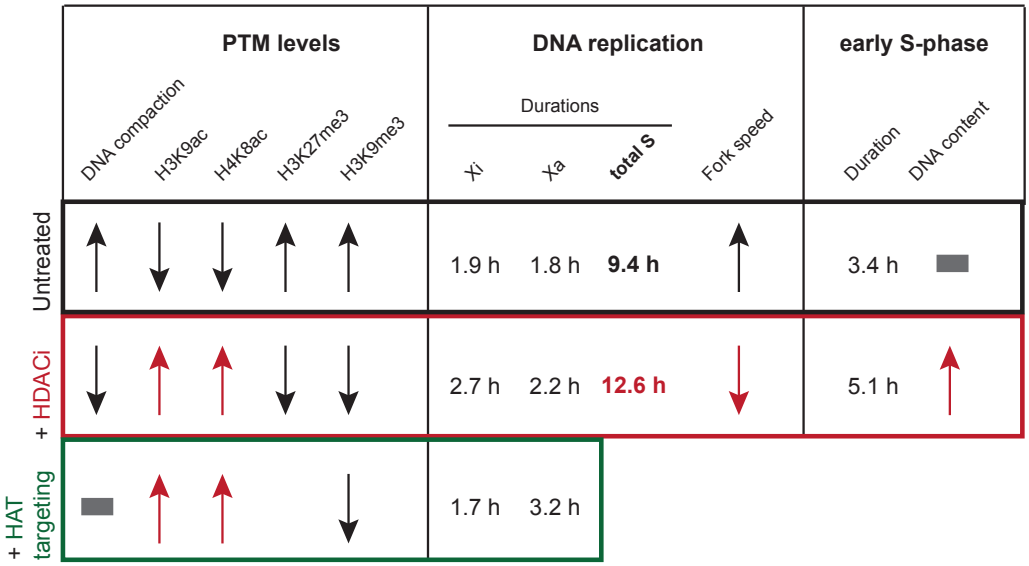

Figure III.11.: Summary of the effects of histone hyperacetylation on DNA replication timing. Untreated cells (black box) showed typical marks for heterochromatin. Both heterochromatic blocks were hypoacetylated, but enriched for either H3K27me3 (Xi, facultative heterochromatin) or H3K9me3 (Xa, constitutive heterochromatin). These cells replicate in 9.4 hours, where 1.9 hours was required for the DNA replication of the inactive X chromosome and 1.8 hours for the duplication of the active X chromosome. When cells were globally hyperacetylated with an HDAC inhibitor (red box), the histone acetylation level increases, but histone methylation marks decreased. The effect on DNA replication timing was dramatic, as the total S-phase duration was prolonged up to 12.6 hours. The heterochromatic block of the Xi was replicated in a time frame of 2.7 hours and constitutive heterochromatin of the Xa needed 2.2 hours for DNA duplication. This result going hand in hand with a strong increase of DNA content in early S-phase, indicating a shift from facultative heterochromatin, which is normally replicated during mid S-phase towards early S-phase. The duration of early S-phase was also prolonged, as a result of slower fork speed in treated samples. When constitutive heterochromatin was targeted with a HBO1 (green box), histone hyperacetylation is specifically increased, histone methylation marks were lost and DNA compaction level was not affected. Thus, I ruled out DNA compaction level as a potential regulator of DNA replication timing, as effects were observed with or without effects on DNA compaction level. The HAT targeting data confirmed the effect of histone hyperacetylation on DNA replication timing of genomic regions, as prolongation of constitutive heterochromatin replication is observed. The site-specificity of this targeting approach was demonstrated by the fact that the DNA replication of Xi was not affected upon Xa targeting.

III.6 References

1. Leonhardt, H. *et al.* Dynamics of DNA replication factories in living cells. *J Cell Biol* **149,** 271–80 (2000).
2. Fox, M. H., Arndt-Jovin, D. J., Jovin, T. M., Baumann, P. H. & Robert-Nicoud, M. Spatial and temporal distribution of DNA replication sites localized by immunofluorescence and confocal microscopy in mouse fibroblasts. *J Cell Sci* **99,** 247–53 (1991).
3. Nakamura, H., Morita, T. & Sato, C. Structural organizations of replicon domains during DNA synthetic phase in the mammalian nucleus. *Exp Cell Res* **165,** 291–7 (1986).
4. Richards, E. J. & Elgin, S. C. Epigenetic codes for heterochromatin formation and silencing: rounding up the usual suspects. *Cell* **108,** 489–500 (2002).
5. Francastel, C., Schubeler, D., Martin, D. I. & Groudine, M. Nuclear compartmentalization and gene activity. *Nat Rev Mol Cell Biol* **1,** 137–43 (2000).
6. Jost, K. L., Bertulat, B. & Cardoso, M. C. Heterochromatin and gene positioning: inside, outside, any side? *Chromosoma* **121,** 555–63 (2012).
7. Casas-Delucchi, C. S. *et al.* Histone acetylation controls the inactive X chromosome replication dynamics. *Nat Commun* **2,** 222 (2011).
8. Casas-Delucchi, C. S. & Cardoso, M. C. Epigenetic control of DNA replication dynamics in mammals. *Nucleus* **2,** 370–82 (2011).
9. Casas-Delucchi, C. S. *et al.* Histone hypoacetylation is required to maintain late replication timing of constitutive heterochromatin. *Nucleic Acids Res* **40,** 159–69 (2012).
10. Woodfine, K. *et al.* Replication timing of the human genome. *Hum Mol Genet* **13,** 191–202 (2004).
11. Jimenez, R., Carnero, A., Burgos, M., Sanchez, A. & Diaz de la Guardia, R. Achiasmatic giant sex chromosomes in the vole Microtus cabrerae (Rodentia, Microtidae). *Cytogenet Cell Genet* **57,** 56–8 (1991).
12. Marchal, J. A., Acosta, M. J., Bullejos, M., Diaz de la Guardia, R. & Sanchez, A. Sex chromosomes, sex determination, and sex-linked sequences in Microtidae. *Cytogenet Genome Res* **101,** 266–73 (2003).
13. Bartova, E., Krejci, J., Harnicarova, A., Galiova, G. & Kozubek, S. Histone modifications and nuclear architecture: a review. *J Histochem Cytochem* **56,** 711–21 (2008).
14. Lyon, M. F. Gene action in the X-chromosome of the mouse (Mus musculus L.) *Nature* **190,** 372–3 (1961).
15. Plath, K. *et al.* Role of histone H3 lysine 27 methylation in X inactivation. *Science* **300,** 131–5 (2003).
16. Kouzarides, T. Chromatin modifications and their function. *Cell* **128,** 693–705 (2007).
17. Kwon, S. H. & Workman, J. L. The heterochromatin protein 1 (HP1) family: put away a bias toward HP1. *Mol Cells* **26,** 217–27 (2008).
18. Vogelauer, M., Rubbi, L., Lucas, I., Brewer, B. J. & Grunstein, M. Histone acetylation regulates the time of replication origin firing. *Mol Cell* **10,** 1223–33 (2002).
19. Carothers, A. D. & Bickmore, W. A. Models of DNA replication timing in interphase nuclei: an exercise in inferring process from state. *Biometrics* **51,** 750–5 (1995).
20. Bickmore, W. A. & Carothers, A. D. Factors affecting the timing and imprinting of replication on a mammalian chromosome. *J Cell Sci* **108,** 2801–9 (1995).
21. Casas-Delucchi, C. S., Becker, A., Bolius, J. J. & Cardoso, M. C. Targeted manipulation of heterochromatin rescues MeCP2 Rett mutants and re-establishes higher order chromatin organization. *Nucleic Acids Res* **40,** e176 (2012).
22. Prince, H. M., Bishton, M. J. & Johnstone, R. W. Panobinostat (LBH589): a potent pan-deacetylase inhibitor with promising activity against hematologic and solid tumors. *Future Oncol* **5,** 601–12 (2009).
23. Zhang, P. *et al.* Methyl-CpG binding domain protein 1 regulates localization and activity of Tet1 in a CXXC3 domain-dependent manner. *Nucleic Acids Res* **45,** 7118–7136 (2017).
24. Sporbert, A., Domaing, P., Leonhardt, H. & Cardoso, M. C. PCNA acts as a stationary loading platform for transiently interacting Okazaki fragment maturation proteins. *Nucleic Acids Res* **33,** 3521–8 (2005).
25. Hayakawa, T., Haraguchi, T., Masumoto, H. & Hiraoka, Y. Cell cycle behavior of human HP1 subtypes: distinct molecular domains of HP1 are required for their centromeric localization during interphase and metaphase. *J Cell Sci* **116,** 3327–38 (2003).
26. Fernandez, R. *et al.* Molecular and cytogenetic characterization of highly repeated DNA sequences in the vole Microtus cabrerae. *Heredity (Edinb)* **87,** 637–46 (2001).

27. Marchal, J. A., Acosta, M. J., Bullejos, M., Diaz de la Guardia, R. & Sanchez, A. A repeat DNA sequence from the Y chromosome in species of the genus Microtus. *Chromosome Res* **12,** 757–65 (2004).

28. Marchal, J. A. *et al.* X chromosome painting in Microtus: origin and evolution of the giant sex chromosomes. *Chromosome Res* **12,** 767–76 (2004).

29. Romero-Fernandez, I. *et al.* Epigenetic modifications in sex heterochromatin of vole rodents. *Chromosoma* **124,** 341–51 (2015).

30. Kueh, A. J., Dixon, M. P., Voss, A. K. & Thomas, T. HBO1 Is Required for H3K14 Acetylation and Normal Transcriptional Activity during Embryonic Development. *Molecular and Cellular Biology* **31,** 845–860 (2011).

31. Lob, D. *et al.* 3D replicon distributions arise from stochastic initiation and domino-like DNA replication progression. *Nat Commun* **7,** 11207 (2016).

32. Rhind, N. & Gilbert, D. M. DNA replication timing. *Cold Spring Harb Perspect Biol* **5,** a010132 (2013).

33. Rhind, N. DNA replication timing: random thoughts about origin firing. *Nat Cell Biol* **8,** 1313–6 (2006).

34. Wu, P. Y. & Nurse, P. Establishing the program of origin firing during S phase in fission Yeast. *Cell* **136,** 852–64 (2009).

35. Miotto, B. & Struhl, K. HBO1 histone acetylase activity is essential for DNA replication licensing and inhibited by Geminin. *Mol Cell* **37,** 57–66 (2010).

36. Takahashi, T. S., Wigley, D. B. & Walter, J. C. Pumps, paradoxes and ploughshares: mechanism of the MCM2-7 DNA helicase. *Trends Biochem Sci* **30,** 437–44 (2005).

37. Aparicio, O. M., Stout, A. M. & Bell, S. P. Differential assembly of Cdc45p and DNA polymerases at early and late origins of DNA replication. *Proc Natl Acad Sci U S A* **96,** 9130–5 (1999).

III.7 Supplementary

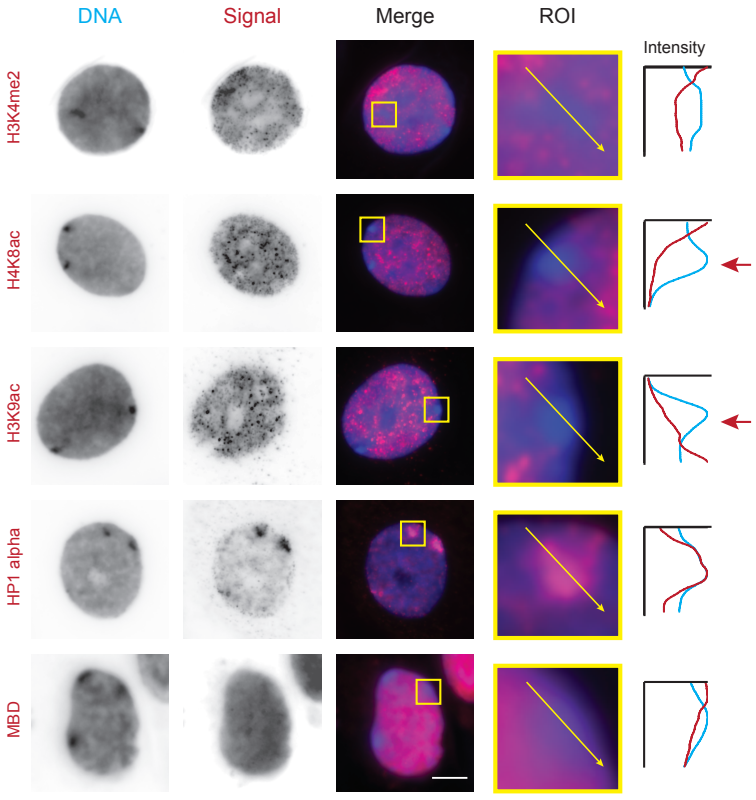

Figure III.S1.: Subnuclear distribution of facultative and constitutive heterochromatin marks in *Microtus cabrerae* female fibroblasts. Prominent chromatin marks were analyzed by immunostaining: H3K4me3, H3K9ac, H4K8ac (euchromatin), HP1 alpha (constitutive heterochromatin) and MBD (DNA methylation). DAPI stained DNA (blue), immunostaining (red) and merge of both channels are depicted. A ROI around one heterochromatic block was selected and a line intensity plot analysis was performed. Red arrows point to characteristic hypoacetylation of heterochromatic blocks. Scale Bar: 5 µm.

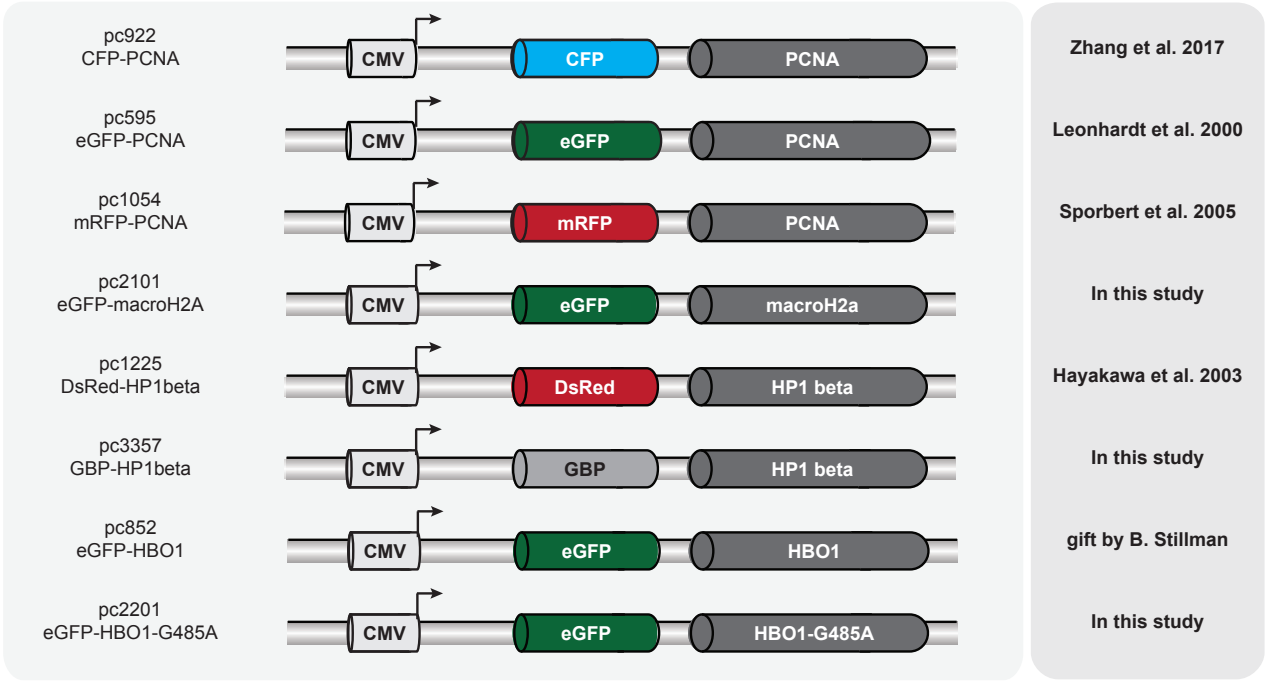

Figure III.S2.: Relevant parts of expression constructs used in this study. Schematic representation of relevant features of plasmids used in this study. Plasmid collection number (pc...), structure of the plasmid and on the right side the corresponding reference of the plasmids are shown. Drawings are not scaled.

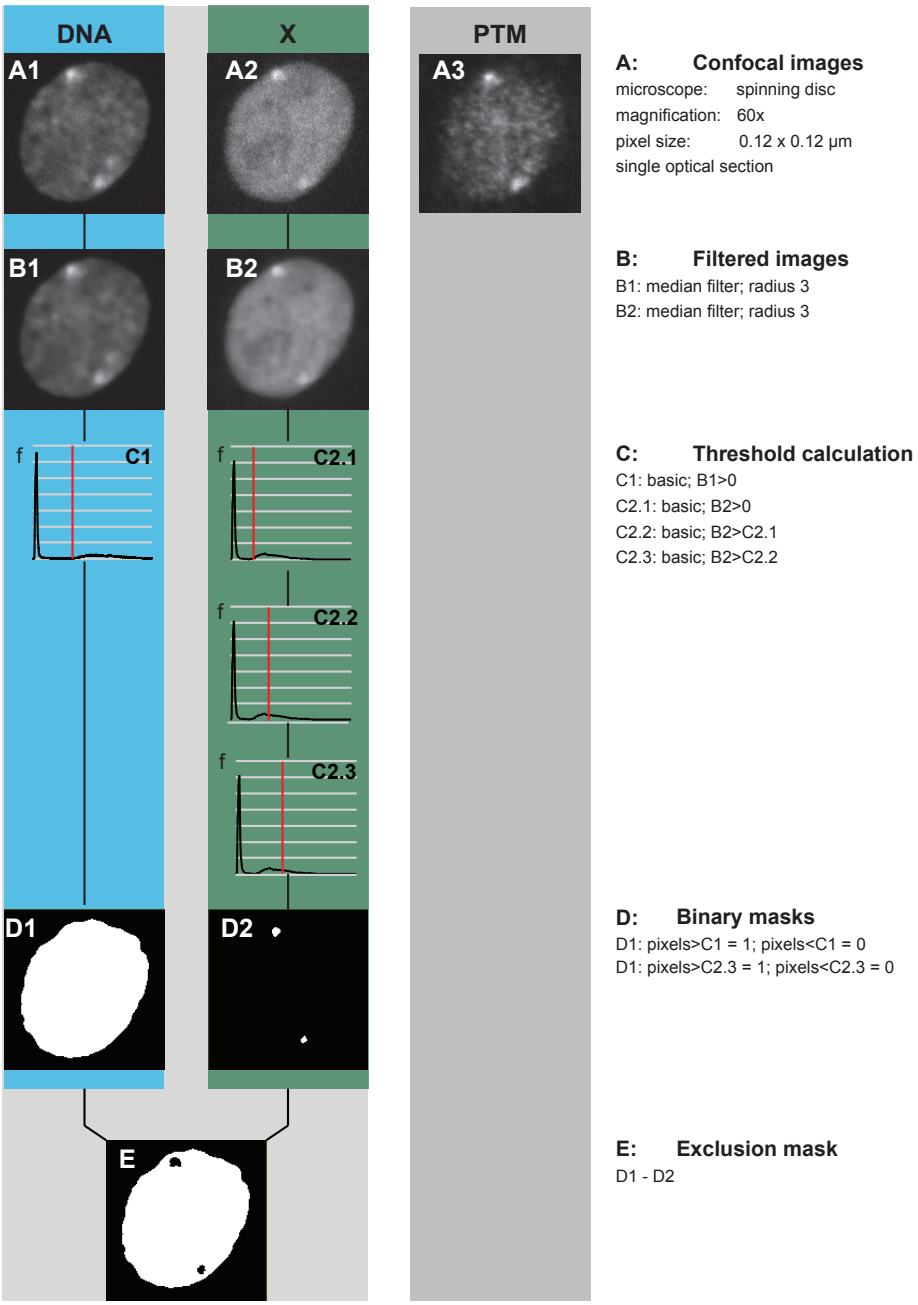

Quantification of fluorescence signals derived from immunostained histone modifications

	whole nucleus	X chromosome	Whole nucleus - X chromosome
total	sum(A3xD1)	sum(A3xD2)	sum(A3xE)
mean	sum(A3xF1)/vol(D1)	sum(A3xI1)/vol(D2)	sum(A3xE)/vol(E)

Figure III.S3.: Schematic rationale of single steps for mask generation used for quantification of nuclear PTM levels in untreated and treated/targeted cells. Confocal images were obtained using an UltraVIEW VoX spinning disc system (Perkin Elmer, Massachusetts, USA) on a Nikon Ti microscope equipped with an oil immersion Plan-Apochromat x60/1.45 numeric aperture objective lens (pixel size in XY= 112 µm, Z-step 0.3 µm). For the calculation of mean DAPI and mean PTM intensities (H3K9ac, H4K8ac, H3K27me3, H3K9me3) in the whole nucleus, at the heterochromatic block of the X chromosomes or in the whole nucleus excluding the X, mid nuclear sections of the DAPI and GFP channel were used to generate nuclear, X and exclusion masks, respectively. Images were processed using a median 3D filter and were threshold in four successive steps. For the generation of the binary masks, all pixels below the final threshold were set to 1, for both masks respectively. Total PTM level values overlapping with the respective mask were calculated and divided by the total number of pixels corresponding to the area of measurement. To automate this analysis procedure, a routine was written in the programming language python (https://code.google.com/archive/p/priithon/). Mean values were measured and normalized to either untreated or untargeted samples.

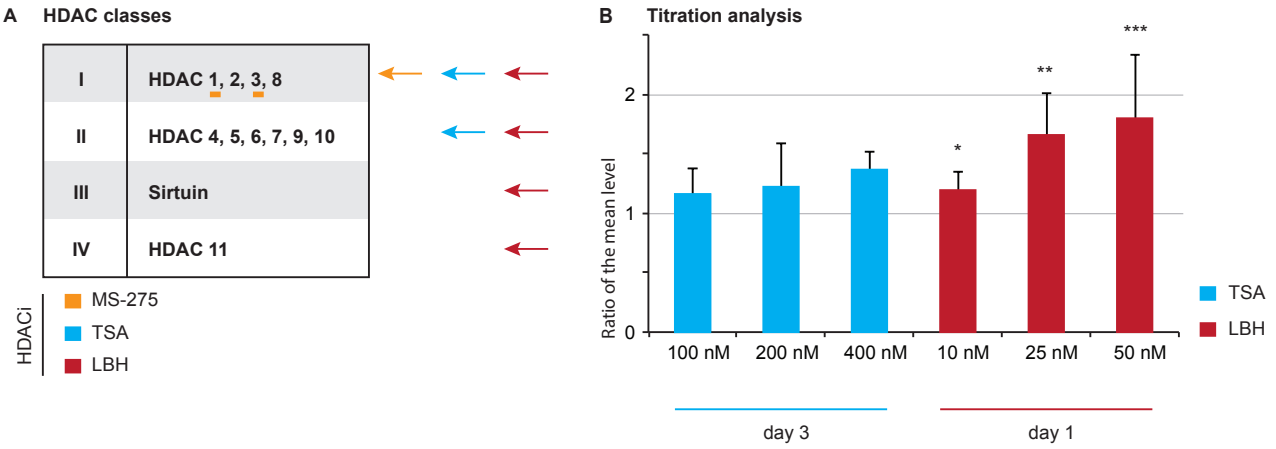

Figure III.S4.: Titration analysis of potential HDAC inhibitors. (A) Overview of different HDAC classes and corresponding HDAC inhibitors of each class. MS-275 only affects HDAC 1 and 3 of class I (orange), whereas TSA inhibits HDACs of class I and II (blue) and LBH as a pan-HDACi inhibits HDACs of all classes (red). (B) Titration analysis of different HDAC inhibitors in *Microtus cabrerae* female fibroblasts. Standard TSA treatment was performed over three days (72 hours). Casas-Delucchi et al. 2011 has shown that a concentration of 20 nM was sufficient to hyperacetylate very condensed constitutive heterochromatin in C2C12 mouse cells [113]. Here, the concentration of TSA was increased 5x, 10x and 20x without any significant increase of histone acetylation level at the heterochromatic blocks of the sex chromosomes. Over time and the higher the concentration of TSA, cells showed morphological changes and after a treatment with 800 nM TSA cells died. In contrast, LBH treatment leads to significant hyperacetylation already after 24 hours. To ensure a sufficient and stable hyperacetylation, cells were treated with 50 nM LBH for 24 hours. This treatment did not lead to morphological changes of cells or to increased cell death. MS-275 data is not shown as cells either showed same levels as control or died directly after treatment. Statistical significance was tested using the t- test, comparing untreated and HDACi treated cells. Error bars demonstrate 95CI. $***P < 0.001$.

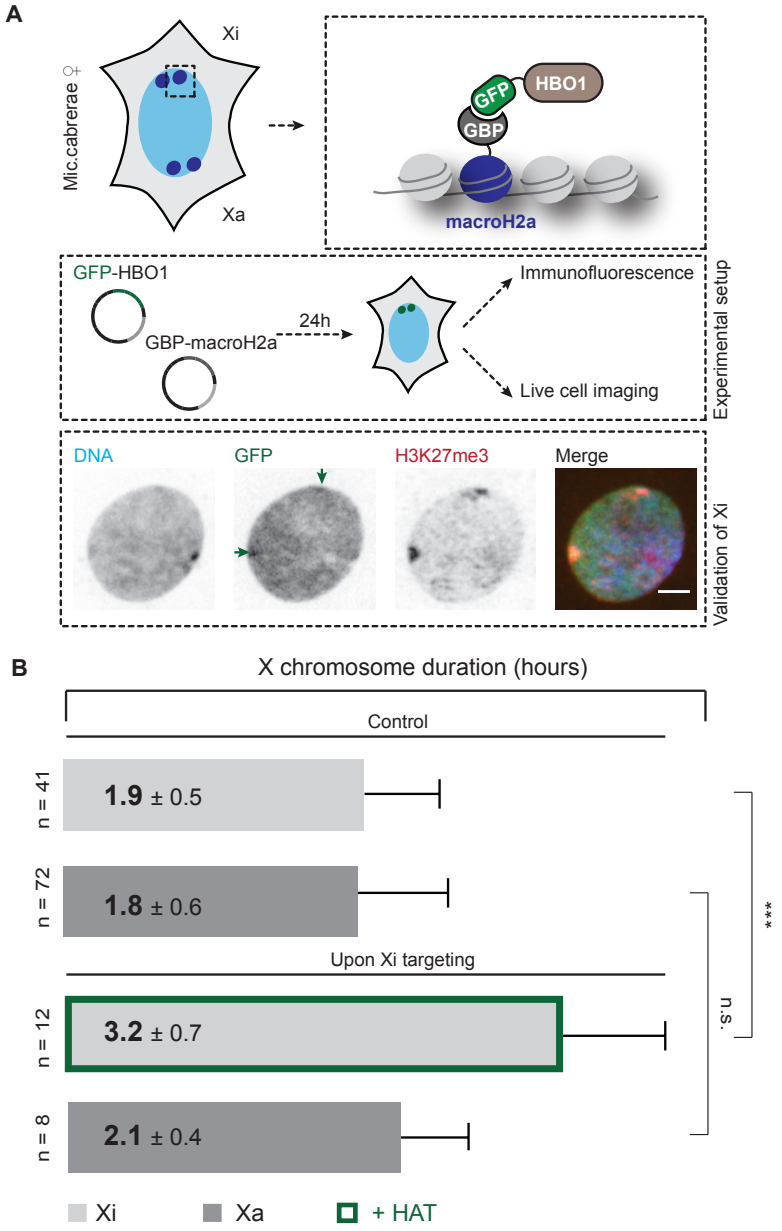

Figure III.S5.: HBO1 targeting to the heterochromatic block of the inactive X chromosome leads to prolongation of Xi DNA replication duration. (A) Schematic representation of targeting assay to specifically target HBO1 to the heterochromatic block of the inactive X chromosome. GFP-tagged HBO1 was transiently transfected with GBP-macroH2a. Upon co-expression of both, both counterparts of the targeting assay strongly interact, leading to the targeting of HBO1. Targeting was validated by immunostaining with H3K27me3 antibody as a hallmark of facultative heterochromatin. DNA (blue), GFP-HBO1 (green), H3K27me3 (red) and merge as an overlay of all three channels. Scale bar: 5 µm. (B) Site-directed targeting of HBO1 to the inactive X chromosome leads to significant prolongation of DNA replication duration of Xi. Specificity of the targeting approach was validated by the fact that there was no significant different between Xa upon Xi targeting and the Xa control.

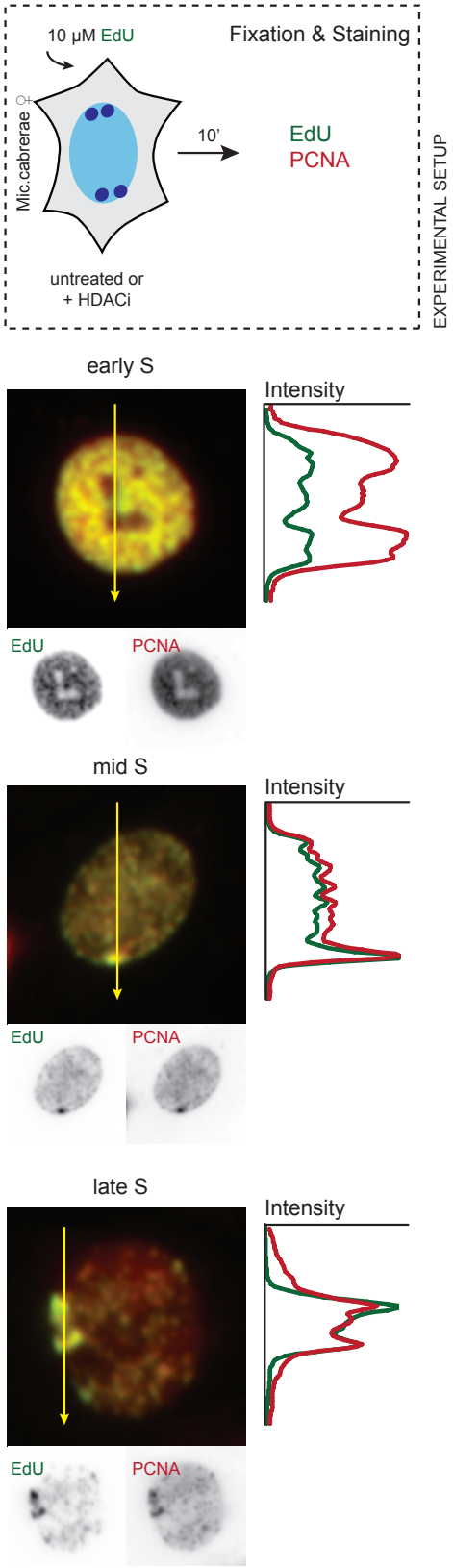

Figure III.S6.: Demonstration of ratiometric analysis of nucleotide incorporation rate in *Microtus cabrerae* control cell. Modified nucleotides were added to proliferating populations of *Microtus cabrerae* cells and were incorporated for 10 minutes. Cells were fixed and EdU was detected via ClickIT chemistry. PCNA was stained with an antibody. Exemplary images of an early S-, mid S- and late S-phase cell are shown: EdU (green), PCNA (red) and merge of both channels. Line profiles depict the ratio of EdU (synthesized DNA, green) and PCNA (DNA replication machinery, red). Scale bar: 5 µm.

Table III.S1.: Plot statistics chapter III (main figures)

Table S1. Plots statistics - Main Figures

Figure	Sample	Mean	Stdev	n	95 CI	*P*
Figure 4						
DNA compaction	Untreated	1	0.12	401	0.01	
	+ HDACi	0.93	0.09	390	0.01	6.36E-19
Acetylation	Untreated	1	0.33	431	0.03	
	+ HDACi	1.18	0.44	415	0.04	1.03E-11
Figure 5						
H3K9ac at Xi	Untreated	1	0.13	206	0.02	
	+ HDACi	1.54	0.06	118	0.11	8.17E-29
H4K8ac at Xi	Untreated	1	0.24	238	0.03	
	+ HDACi	1.51	0.65	88	0.14	1.24E-21
H3K27me3 at Xi	Untreated	1	0.33	110	0.06	
	+ HDACi	0.91	0.22	110	0.04	0.01
H3K9ac at Xa	Untreated	1	0.14	74	0.03	
	+ HDACi	1.60	0.69	91	0.14	1.42E-12
H4K8ac at Xa	Untreated	1	0.39	145	0.06	
	+ HDACi	1.47	0.35	166	0.05	3.26E-05
H3K9me3 at Xa	Untreated	1	0.24	62	0.06	
	+ HDACi	0.63	0.17	64	0.04	1.53E-17
Figure 6						
A total S duration	Untreated	9.41	0.64	162	0.10	
	+ HDACi	12.61	1.06	115	0.19	0.01
early S	Untreated	3.40	0.53	37	0.17	
	+ HDACi	5.09	1.16	15	0.59	2.08E-09
mid S	Untreated	3.45	0.70	33	0.24	
	+ HDACi	4.36	1.02	32	0.35	8.54E-05
late S	Untreated	2.55	0.70	92	0.14	
	+ HDACi	3.15	1.00	68	0.23	4.94E-06
B Xi duration	Untreated	1.92	0.50	41	0.15	
	+ HDACi	2.67	0.87	30	0.31	1.71E-05
Xa duration	Untreated	1.88	0.59	72	0.14	
	+ HDACi	2.24	0.70	66	0.17	0.001
Figure 7						
B DNA compaction	Untreated	1	0.47	83	0.10	
	+ HAT	1.02	0.45	141	0.07	0.8
H3K9me3	Untreated	1	0.35	21	0.15	
	+ HAT	0.73	0.31	141	0.08	0.0001
H3K9ac	Untreated	1	0.57	22	0.24	
	+ HAT	1.34	0.63	53	0.17	0.03
H4K8ac	Untreated	1	0.48	18	0.22	
	+ HAT	1.30	0.54	53	0.15	0.04
C DNA compaction	Untreated	1	0.15	10	0.10	
	+ HAT	1.04	0.21	27	0.08	0.61
H3K9ac	Untreated	1	0.15	10	0.09	
	+ HAT	1.04	0.08	27	0.03	0.36
H4K8ac	Untreated	1	0.23	10	0.14	
	+ HAT	1.07	0.21	27	0.08	0.36
D Xa targeting	Untreated	1.88	0.58	72	0.14	
	+ HAT	3.2	0.82	33	0.28	3.76E-05
	Xi control	1.92	0.49	41	0.15	
	Xi upon Xa targeting	1.71	0.33	17	0.16	0.11
Figure 8					lower; upper	
B early S	Untreated	3.15	1.86	102	3.87; 3.02	
	+ HDACi	2.83	2.02	17	0.80; 1.80	0.37
mid S + late S	Untreated	4.52	2.25	806	4.41; 4.63	
	+ HDACi	2.55	1.71	1645	3.27; 2.22	2.20E-16
Figure 9					lower; upper	
B early S	Untreated	1.21	0.30	806	1.21; 1.21	
	+ HDACi	1.45	0.31	17	1.41; 1.49	0.0016
mid S	Untreated	1.55	0.45	1073	1.55; 1.55	
	+ HDACi	1.58	0.42	52	1.57; 1.60	0.55
late S	Untreated	2.13	0.59	572	2.13; 2.13	
	+ HDACi	2.12	0.63	50	2.09; 2.14	0.71

"n" and "p" as indicated in the respective figure

Table III.S2.: Plot statistics chapter III (supplementary figures)

Table S2. Plots statistics - Supplementary Figures

Figure	Sample	Mean	Stdev	n	95 CI	*P*
Figure S3						
Titation analysis	Untreated	1	0.32	17	0.15	
	100 nM TSA, d3	1.16	0.27	6	0.21	0.29
	200 nM TSA, d3	1.22	0.46	6	0.37	0.22
	400 nM TSA, d3	1.24	0.17	6	0.14	0.10
	10 nM LBH, d1	1.20	0.43	29	0.15	0.03
	25 nM LBH, d1	1.37	0.66	13	0.36	0.005
	50 nM LBH d1	1.49	0.61	5	0.53	0.0007
Figure S4						
Xi targeting	Untreated	1.92	0.49	41	0.15	
	+ HAT	3.12	0.66	12	0.37	6.01E-09
	Xa control	1.88	0.58	72	0.14	
	Xa upon Xi targeting	2.12	0.43	8	0.30	0.052

"n" and "p" as indicated in the respective figure

4 Combined discussion and conclusion

4.1 Regulation of DNA replication timing by nuclear position of DNA and by histone acetylation level in mammalian cells

The spatio-temporal organization of DNA replication is conserved throughout metazoans and is developmentally regulated [80, 85, 127, 128]. Although the composition of the basic replication machinery was studied enormously, how its activity is regulated is mostly unknown. Up until now no consensus sequence of DNA replication origins was identified in higher eukaryotes. This fact in accordance with striking examples of the flexibility of the DNA replication process during development, further underlines that its regulation cannot be defined at a genetic level alone. These observations rather emphasize the role of several chromatin properties as potential regulators or even indicate the role of unknown regulators. To study the effects of potential regulators of DNA replication dynamics, I chose prominent examples of mammalian facultative and constitutive heterochromatin as targets for different targeted manipulations.
For this reason, I made use of a new universal targeting strategy (Chapter I) that is based on the strong and highly specific interaction of GFP and GFP-binding nanobody [129, 130]. In Chapter I, I explained how to set up, optimize and validate this approach and discussed potential applications. In Chapter II, I applied this strategy and repositioned constitutive heterochromatin to the nuclear periphery and evaluated the impact of nuclear position of DNA on its replication timing [14]. In Chapter III, I targeted an active enzyme, a histone acetyltransferase to heterochromatic blocks to increase the local level of histone acetylation and elucidated the effect on DNA replication timing. This site-directed targeting was evaluated side by side to a global drug-induced hyperacetylation.

4.1.1 Peripheral re-localization of constitutive heterochromatin advances its replication timing and impairs maintenance of silencing marks

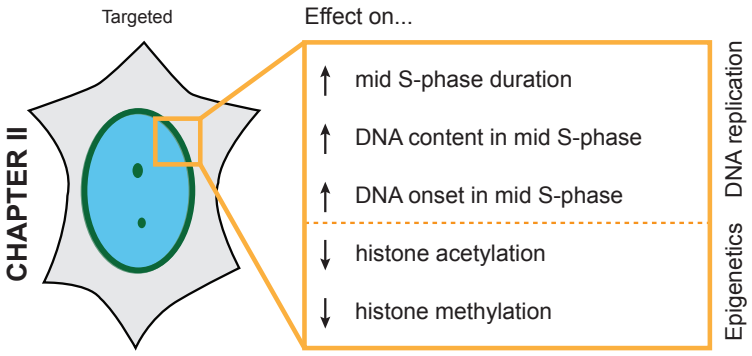

Figure 4.1.: Summary of the effects of nuclear position of DNA on its replication timing and epigenetic composition. In targeted cells, the mid S-phase duration was prolonged. The peripheral constitutive heterochromatin was replicated already during mid S-phase, in contrast to the non-repositioned internal one, which was still replicated during late S-phase. Constitutive heterochromatin, known to be hypoacetylated and enriched in H3K9me3 and H4K20me3, still showed these characteristic marks, although in decreased levels. The repositioning affected the re-establishment of proper levels of the most characteristic histone marks, resulting in their progressive loss over subsequent cell cycles. The epigenetic marks for peripheral facultative heterochromatin were not added *de novo* to the relocated constitutive heterochromatin [14].

In Chapter II, I identified the nuclear position as a potential regulator of DNA replication timing [14]. Time-lapse analysis demonstrated that constitutive heterochromatin known to replicate during late S-phase (Figure 1.1) was replicated during mid S-phase, when repositioned to the nuclear lamina (Figure II.6). This out-of-schedule DNA replication in a foreign mid-replicating environment went hand in hand with a higher mid S-phase pattern frequency and prolonged mid S-phase duration (Figure II.4). Interestingly, late S-phase length was shortened and no effect on total S-phase was measured during the first cell cycle (Figure II.6). The observation of increased DNA content in mid S-phase in targeted

cells in comparison to control cells, further strengthens the fact of advanced onset of DNA replication of constitutive heterochromatin (Figure II.5). Taken together, I was able to show that repositioned chromatin adopts the DNA replication timing of neighboring facultative heterochromatin.

The relative spatial distribution of replisomes and gradients of licensing and activation factors (Figure II.S12) enriched at the nuclear periphery during mid S-phase triggered earlier DNA replication onset of repositioned constitutive heterochromatin , localized upon targeting adjacent to mid-replicating facultative heterochromatin. The concentration of (regulatory) replication factors at the nuclear periphery during mid S-phase created a microenvironment, which enhances firing efficiency and probability of origins in the nearby, repositioned constitutive heterochromatin. As demonstrated by the domino model [72] (Figure 1.3) stochastic activation of origin clusters led to a chain reaction of activation of later replicating origin clusters. I expanded this model with this study to include not only a next-in-line activation in *cis* along the chromosome fiber, but rather also a next-in-line activation in *trans* within a 3D nuclear space (Figure 4.2) [14].

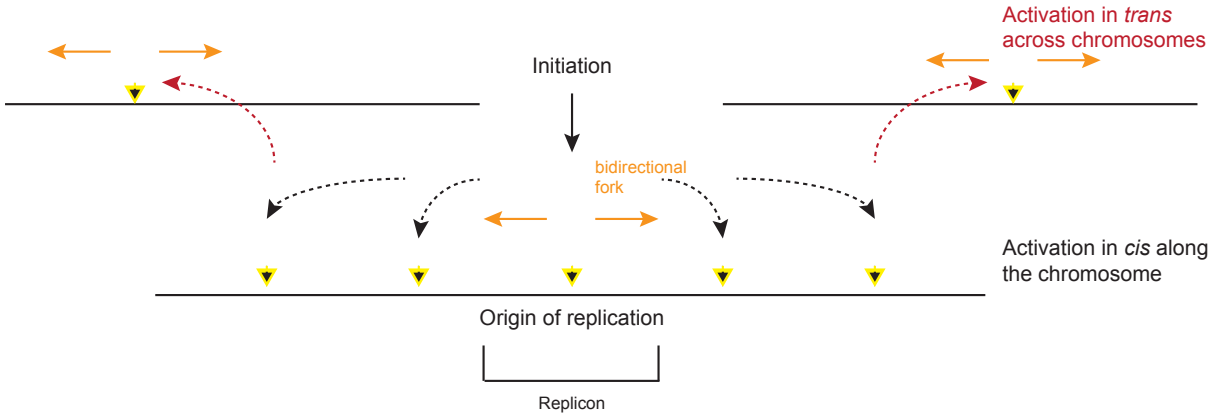

Figure 4.2.: Schematic representation of the domino model for the progression of genome duplication in *trans* across individual chromosomes. One origin of replication is activated and DNA synthesis proceeds bidirectional. According to the next-in-line activation, neighboring origins are activated, which in turn activate DNA replication at later replication clusters. This next-in-line principle does not need to work only in *cis* along the chromosome, but rather also across individual chromosomes to activate in *trans*.

4.1.2 DNA replication dynamics of the vole genome and its epigenetic regulation by histone acetylation level

The impact of histone acetylation on DNA replication timing was demonstrated by several studies manipulating its level, predominantly in yeast (Tabel 1.1). To study the reproducibility and validity of the impact of histone acetylation level on DNA replication timing in mammals, I manipulated the heterochromatic blocks, coupled to the giant sex chromosomes of *Microtus cabrerae* female cells [131, 132]. In Chapter III, I compared two different manipulation approaches to increase the global as well as the local level of histone acetylation (Figure III.4, III.7). First, I treated these cells with a pan-HDAC inhibitor that inhibits all classes of HDACs (Figure II.S4) and second, I made use of the targeting strategy (Chapter I) based on the very strong interaction of GFP and GFP-binding protein to target a histone acetyltransferase (HAT) to the heterochromatic blocks (Figure III.7, III.S5). As many other mammalian cells *Microtus cabrerae* cells exhibit three distinct DNA replication patterns: early, mid and late (Figure III.2, III.3). The heterochromatic block coupled to the inactive X chromosome(s) (Xi) replicated during a narrow time frame of mid S-phase, whereas the heterochromatic block of the active X chromosome(s) was replicated during late S-phase (Figure III.2, III.3). A measurably slower fork speed at hyperacetylated chromatin and a higher increase of DNA content in early S-phase, indicated a shift from mid replicating facultative heterochromatin towards early S-phase, normally a euchromatin replicated time domain (Figure III.9). As these manipulation approaches led to a prolongation of S-phase: Xi/Xa replication, substage duration and total S-duration, I further confirmed the impact of histone acetylation level on DNA replication timing in mammals (Figure III.6, III.S5).

4.1.3 Effects on DNA replication timing caused by targeted manipulations

Manipulations of either the nuclear position of DNA or of histone acetylation level led to effects on DNA replication timing (Figure II.6, II.S4, III.6, III.S5).

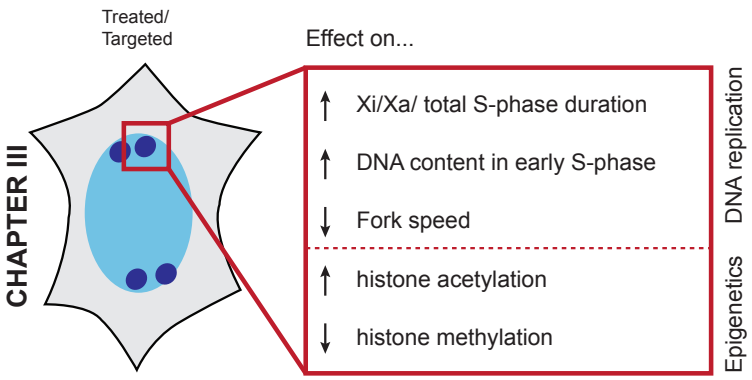

Figure 4.3.: Summary of the effects of histone hyperacetylation on DNA replication timing of heterochromatic blocks in *Microtus cabrerae* cells. Induced hyperacetylation led to a prolongation of replication of S-phase substages, of inactive X (Xi), active X chromosome (Xa) and total S-phase. This result went hand in hand with a negative effect on replication fork speed and a higher DNA content in early S-phase. When histone acetylation level increases, histone methylation marks decreased.

These observations demonstrated that the total number of active origins at any time point remains constant in accordance to a limiting factor model [88, 133, 134]. Otherwise, more origins could be activated to fire to counterbalance potential prolongations of S-phase. This was not the case upon any of the two targeted manipulations. Furthermore, upon repositioning (Chapter II) I detected a higher increase of DNA content in mid S-phase (Figure II.4) and upon histone hyperacetylation, I measured a higher increase of DNA content in early S-phase (Figure III.9). Both results indicated shifts in DNA replication timing of distinct regions towards another S-phase stage. In Chapter II, this shift was clearly visible in time-lapse analysis, where the targeting ring and facultative heterochromatin were replicated in parallel (Figure II.6). This phenomenon was even more dramatic in the second cell cycle, when repositioned chromocenters replicated concomitantly with the inactive X chromosome, the hallmark of mid S-phase in female cells (Figure II.6). Surprisingly, all manipulations did not disturb the order of their species specific DNA replication patterns.

4.1.4 Side effects and consequences for histone modifications

Studying potential regulators of DNA replication timing has been complicated due to the fact that epigenetic modifications seldom exert their influence on chromatin independently from each other and are often characterized by a strong crosstalk. Previous studies, where different histone modifications of constitutive heterochromatin were carefully assessed one after the other [113], pointed out a major impact of histone acetylation level on DNA replication timing. Furthermore, it was ruled out that effects on H3K9 trimethylation or large scale DNA decondensation have an impact on regulating DNA replication timing of constitutive heterochromatin. Even upon repositioning (Chapter II), constitutive heterochromatin was still hypoacetylated [14](Figure II.7). Typical hallmarks for constitutive heterochromatin, such as H3K9me3 and H4K20me3 were progressively lost over subsequent cell cycles (Figure II.7) and were not re-established. Upon DNA replication at the nuclear periphery, constitutive heterochromatin did not exhibit an increase of facultative heterochromatin marks, such as H3K27me3 or H3K9me2, ruling out a *de novo* addition of facultative heterochromatin marks [14]. In case of *Microtus cabrerae* cells, I was able to increase histone acetylation marks, like H3K9ac and H4K8ac, but this caused a loss of typical heterochromatic hallmarks (Figure II.5, II.7). H3K27me3 level at the inactive X chromosome as well as the H3K9me3 level at the active X chromosome were decreased as a side-effect of induced hyperacetylation. Global drug-induced hyperacetylation produced a more pronounced effect of hyperacetylation in comparison to the site-directed and local increase by HBO1-targeting. Even the loss of H3K9me3 was more dramatic upon global hyperacetylation, revealing a potential link between hyperacetylation and the loss of H3K9me3. This confirms previous studies [113, 135] and clearly demonstrates that a loss of H3K9me3 is not enough to explain advanced DNA replication timing.

4.2 Searching for "THE" limiting factor

4.2.1 Potential gradients of rate-limiting factors

The stochastic firing of replication origins in mammalian cells suggested their regulation by rate-limiting factors [23, 133, 134, 136, 137]. According to this limiting factor model (reviewed in[88]) the total number of active origins at any

time point is constant. The fact that upon both targeted manipulations S-phase durations were affected, this indicated no counterbalance by more activated origins to prevent disturption and prolongation of S-phase. Several studies were undertaken to find (the) limiting factor(s), but the search did not turn out as trivial.
For instance, varying the level of CDK affects the DNA replication timing in vertebrates [138–140]; the targeting of chromatin regulators next to an origin as well as the movement of an origin to a new chromatin context affects origin timing [70, 114, 123, 141, 142]. Models on DNA replication dynamics speculated that the existence of such a rate-limiting factor in addition to the differential firing efficiencies at distinct genomic regions are sufficient requirements to reconcile the contradicting phenomena of stochastic origin firing and the appearance of conserved DNA replication patterns [133, 134, 143, 144].
Ultimately, DNA replication timing is defined by the timing of origin firing. The complex multi-step process (for details see Figure 1.2) from origin determination, licensing up to origin firing provides multiple layers where limiting factors and histone acetylation level might play a role. For instance, the fact that there is no yeast homologue of HBO1 [39] could hint that the control mechanism of DNA replication timing in mammals is governed by its complex chromatin organization. As DNA replication origins fire with different efficiencies [136, 145] and high firing efficiency strongly correlates with early origin firing [146], this could be a consequence of a preferential binding to a limiting factor, involved in the process of origin activation [62]. The existence and role of such a rate-limiting factor was supported by a study in *Xenopus* egg extracts [147]. In this *in vitro* system all replication factors are present in excess. Besides, all DNA sequences replicate with approximately the same efficiencies. In accordance with this study, is a study in *Drosophila* and *Xenopus* embryos, where factors for origin determining, licensing and firing are present in excess and all available origins fire efficiently [71]. Consequently, it has been proposed that such a limiting factor would be recycled upon S-phase progression implying its release from early origins and its subsequent re-use [42].

Interestingly, the level of Cdc45 at particular origins was shown to reflect their firing efficiencies [148, 149]. Studies in budding yeast demonstrated that the timing of Cdc45 binding varies in early and late origins [54] or that Cdc45 overexpression advances DNA replication timing of some late origins [148]. Moreover, a study in fission yeast showed that ORC binds to early origins in mitosis earlier than to late origins [148]. Advancing pre-RC formation consequently lead to a preferential binding of pre-IC component Cdc45 to early regions [148]. Higher levels of MCM have been correlated with increased firing efficiency in budding yeast [150] and studies in *Xenopus* eggs have shown that the efficiency of replication of injected DNA increased with the size of injected DNA, which might be a consequence of longer DNA being able to bind more MCM [151].

One of the best potential candidates for such a rate-limiting factor is, therefore, the pre-IC factor Cdc45, which is in limited amount available in human cells and was later identified as (one) limiting factor in human cells [152, 153]. Köhler et al. 2016 showed that the limiting factor for DNA replication initiation in human is Cdc45. Upon co-expression of Cdc45 human cells fired at least twice as many origins as control cells [153]. However, these cells displayed an about 2-fold diminished fork elongation rate, a pronounced asymmetry of replication fork extension and an early S-phase arrest. This fact indicates that such a potential limiting factor could function as a control mechanism as unlimited excess would lead to inorganization and mistakes with dramatic consequences for a cell. However, other pre-IC components might also be available in limiting amounts, but the majority of remaining factors, in particular MCM proteins are found in large excess in the nucleus and are therefor unlikely to play a limiting role in origin firing [42].

Taken together, the limiting factor model for origin firing proposes the preferential binding of a limiting factor to early origins while late origins are bound only after release of this limiting factor from early origins. Repositioning late-replicating constitutive heterochromatin next to mid-replicating origins, increases the probability of activation by an adjacent recycled limiting factor. Probably, a higher affinity of a fraction of origins for such a limiting factor leads to the observed advanced DNA replication timing. This fact in accordance with the domino model working in *trans* would explain the earlier DNA replication onset of repositioned constitutive heterochromatin [14].

4.3 Still in the game: ratio HDAC/HAT

Histone acetylation has been shown to decrease the chromatin compaction level [154] and, therefore, might increase chromatin accessibility for different factors (Figure 4.4). This intrinsic link to chromatin condensation can be easily outbalanced at heterochromatic regions, where HDACS are actively recruited [155]. Thus, the local ratio of HDACs to HATs could function as an additional limiting factor in the regulation of origin firing efficiency. For instance, hyperacetylation mediated by TSA treatment equalized the origin firing efficiency at some human loci [156], while unfavorable nucleosome positioning was shown to inhibit origin firing. This fact further demonstrates that chromatin structure might be involved in origin selection [116, 157]. The tethering of a HDAC to an active promoter in human cells leads to a shift to late replication timing and in contrast, the targeting of a HAT to an inactive promoter results in advanced DNA replication timing [123] (Figure III.4, III.5, III.6, III.7, III.S5). This outcome underlines my findings in *Microtus cabrerae* cells, where

targeting of a HAT to heterochromatic blocks resulted in their advanced DNA replication timing. Similarly, the inhibition of HDACs, like knocking out HDACs or by targeting HATs to particular regions [70, 115], affects histone acetylation by changing the ratio of active HAT to HDACs globally or at specific loci. Furthermore, in human cells it was shown that increased H4 acetylation by HBO1 is a prerequisite for MCM loading [39].
I propose that increased histone acetylation level enhances the formation of pre-RC and licensing by increasing the access of pre-RC and pre-IC factors to chromatin. Such a preferential pre-RC formation would lead to an advantage for hyperacetylated origins when competing for any limiting pre-IC factor, leading to earlier origin firing ((Figure 4.4, III.9). Consequently, origins in hypoacetylated and condensed regions probably have slower RC-formation dynamics and would require more rounds of HBO1-mediated histone acetylation. Surprisingly, hyperacetylated regions, which are more open and decondensed indeed show an advanced DNA replication onset, but these regions are not faster replicated. TSA-mediated hyperacetylation of constitutive heterochromatin [113] replicated in advance, but the duration of its DNA replicaton was prolonged, in line with my data in *Microtus cabrerae* cells (Chapter III). This fact went hand in hand with a slower fork speed in treated samples (Figure III.9). Similarly, it was shown using knockdown systems or specific Hdacs1,2-selective inhibitors leads to a reduction in the replication fork speed [158] in mammalian cells. These observations lead to the fact, that earlier DNA replication onset is not directly linked with faster replication fork speed upon decondensation of chromatin.

Nonetheless, the mechanism of potential limiting factor(s) is far from being fully understood. Potentially, several factors are playing hand in hand and are orchestrated together in a complex mechanism. Already in budding yeast and fission yeast, initiation factors such as Cdc45, Sld2 and Sld3 and the Dbf4-dependent kinase Cdc7 (DDK) initiation kinase are limiting for origin firing. Overexpression of these factors increases the probability of origin firing, just like tethering them to specific loci can increase the firing of local origins [148, 159–161].
In summary, the search for limiting factor(s) for the organization and regulation of DNA replication timing is complex and the number of published studies are rapidly increasing with studies where down and/or overexpression of potential factors shed light into this multilayer mechanism. The identification of controlling factors presented in this thesis and the identification of limiting factor(s) regulating the organization of DNA replication timing will contribute to understand its dynamic regulation and will give rise to future studies manipulating new and up until now unknown regulators to fully understand the complex process of DNA replication.

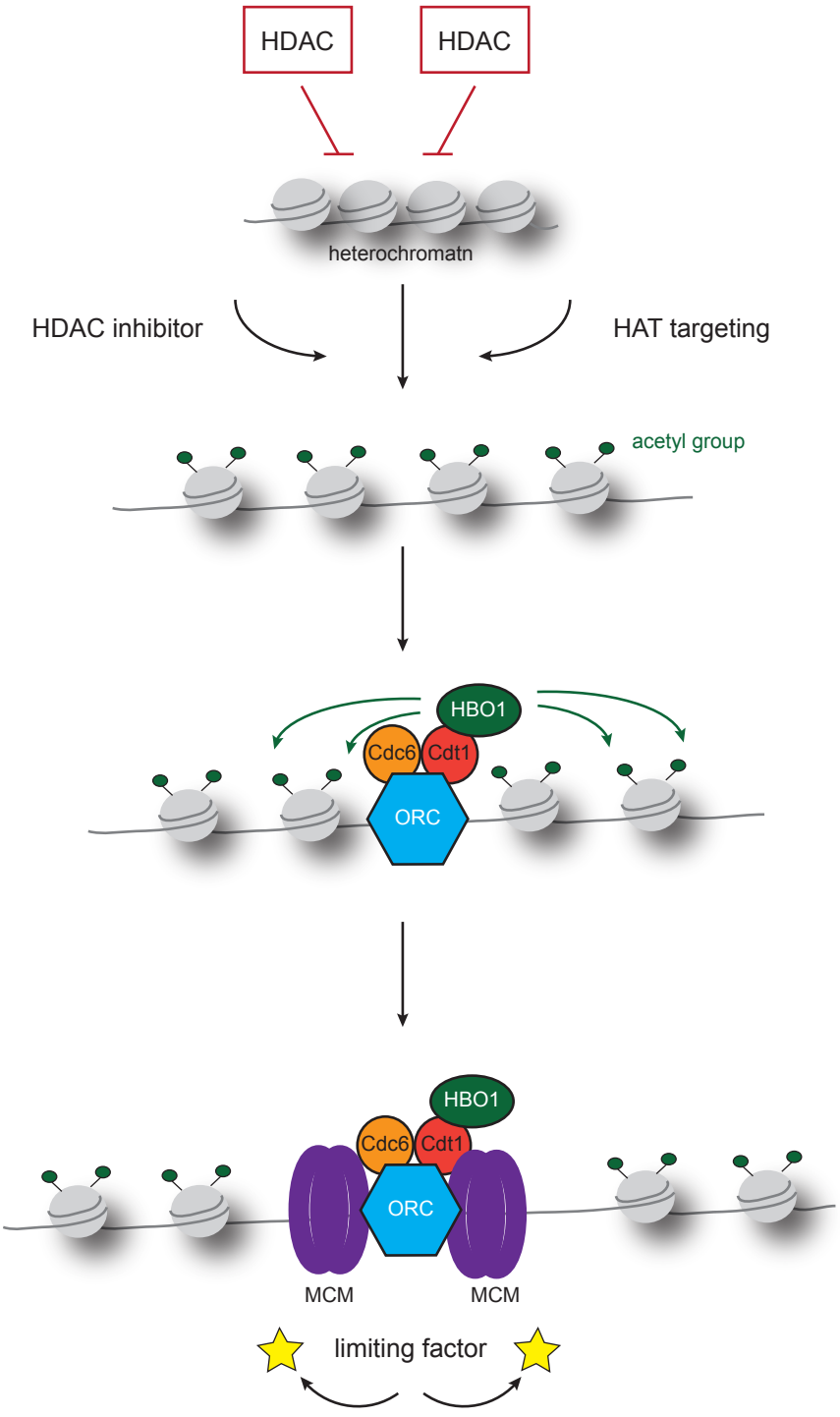

Figure 4.4.: Schematic representation of local ratio of HDAC vs. HAT as a potential regulator of origin efficiency. A high concentration of HDACs induces high compaction and hypoacetylation of heterochromatin. Upon HDAC inhibition or HAT targeting, acetyl groups are added to the chromatin, resulting in its hyperacetylation and a decondensed structure. Upon decondensation the access to chromatin for ORC is enhanced and facilitated, leading to binding of pre-RC. Replication origins are determined, licensed and activated. With the binding of a limiting factor, like Cdc45, the entry into S-phase is achieved.

5 Perspectives

The results presented in this work lead to new exciting questions that will be the basis for future experiments. The mechanism by which the nuclear position influences the DNA replication timing of distinct regions (see 4. Combined discussion and conclusion), can be verified by assessing the reproducibility in other cell lines. In the context of this model, it would be of upmost interest to target constitutive heterochromatin to the nuclear periphery in J1 embryonic stem cells [162] (Figure 5.1). Weber et al. (unpublished data) identified five distinct S-phase replication patterns in embryonic stem cells and detected major differences to somatic cells. For instance, constitutive heterochromatin is replicated in pattern II prior to the DNA at the nuclear periphery, which is replicated in pattern III. This is in contrast to somatic cells, where the nuclear periphery is replicated in mid S-phase concomitantly with facultative heterochromatin and prior to constitutive heterochromatin (Figure 1.1). To understand, whether nuclear position of DNA also has an impact on DNA replication timing in embryonic stem cells, I would target constitutive heterochromatin with the help of a sequence-specific major Satellite (ms) TALE [163] (Figures II.S1, II.S4) to the nuclear periphery. Following my proposal (Chapter II) [14] that the domino model is not only working in *cis* along the chromosome fiber, but also in *trans* across different chromosomes within the 3D nuclear space, the consequences from repositioned constitutive heterochromatin on DNA replication timing will be an rewarding subject. This targeting should lead to delayed DNA replication onset in embryonic stem cells and therefore, repositioned constitutive heterochromatin should replicate concomitantly with pattern III. This outcome would confirm the reproducibility of nuclear position as a potential regulator of DNA replication timing.

The proposed concentration of (regulatory) replication factors (Chapter II) [14] at the nuclear periphery during mid S-phase creates a microenvironment that enhances origin firing efficiency/ probability of origins in the nearby repositioned constitutive heterochromatin. The accompanying gradients of (regulatory) replication factors are potentially enriched at the nuclear periphery during mid S-phase, decreasing in the direction to the center (Figure II.S12). This reveals factors involved in setting up and activating DNA replication (Figure 1.2), such as MCM, Cdc45, GINS, DDK, as promising candidates for a gradient distribution from the nuclear periphery to the center in mid S-phase. Immunostainings for these factors in combination with the usage of our user-independent analysis (Figure II.S9) should allow the intensity measurements at peripheral and internal constitutive heterochromatin in different S-phase stages to identify potential regulatory factors.

The limiting factor(s) of DNA replication is/are not yet clearly characterized, but phosphorylated forms of MCM2 or Cdc45 are likely candidates for a rate-limiting factor for origin activation. The universal targeting approach (Chapter I) could target these factors to prominent structures, such as facultative and constitutive heterochromatin to reveal their effect on DNA replication activation and progression. In addition, an inducible system constructed by fusing constructs to estrogen receptors, could be used to manually control the targeting. The targeting would be prevented to take place until the hormone ligand is supplied to the medium. This should demonstrate a shift to earlier DNA replication timing, caused by the artificial recruitment of (limiting) factor(s) for origin activation. Although some potential DNA replication origins sequences were found [23, 94, 164–174], there is no major consensus sequence characterized. As soon as origin sequences were clearly identified, one could use such sequences as targets. With the help of the targeting approach (Chapter I), potential sequences should be targeted by the usage of a sequence-specific recognizer thereof to artificially recruit (regulatory) replication factors to them.

In Chapter II the experimental setup was based on the transient transfection of plasmids, carrying the GFP- tagged constitutive heterochromatin-binding/recognizing part and the GBP- tagged LaminB1. These transient transfections had the major advantage that targeted cells showed two targeting phenotypes, one with completely repositioned chromocenters and the second phenotype showed an intermediate targeting state (Figure II.2).

This intermediate targeting state was of upmost interest as internal chromocenters served as an internal control directly in targeted cells and could, therefore, be used to measure different DNA replication onsets in the very same cell (Figure II.6). Nevertheless, these transient transfections had some limitations and excluded potential additional experiments.

Stable cell lines that carry at least one targeting construct, like the constitutive heterochromatin recognizing/binding part (Figure II.S1), should significantly increase the amount of transfected cells. With the transfection of the remaining construct part, repositioning could be achieved and cells could be FACS sorted and RT-qPCR for major satellite RNA transcript levels could be performed.

This attempt would further demonstrate potential effects of nuclear position of DNA on other chromatin-based processes like transcription. Furthermore, Western Blot analysis or ChIp-Seq could give further insights into changes of

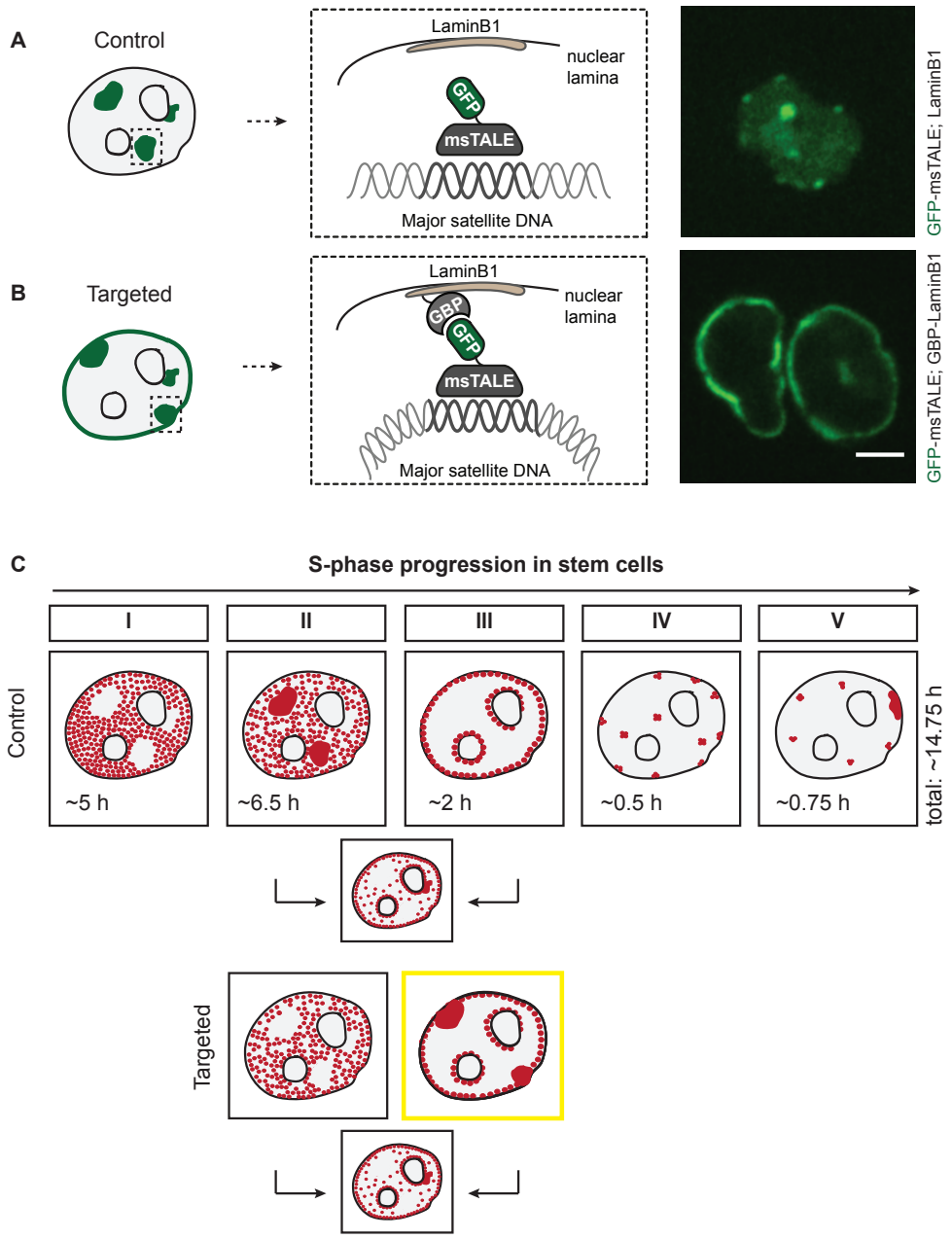

Figure 5.1.: Targeting strategy to reposition constitutive heterochromatin in embryonic stem cells. (A) In an untargeted state, the fusion protein composed of the constitutive heterochromatin recognizer major Satellite (ms)- TALE and GFP is visible as multiple green fluorescent spots throughout the nucleus, corresponding to constitutive heterochromatin. Untagged LaminB1, a key component of the nuclear lamina, did not interact with GFP-msTALE, leading to original localized constitutive heterochromatin throughout the whole nucleus. Mid section of one nucleus of an untargeted state is shown: msTALE-GFP (green) and LaminB1. (B) Schematic presentation of the targeting approach in a J1 targeted cell. Upon co-expression of msTALE-GFP and Lamin-tagged GFP-binding protein (GBP), tagged constitutive heterochromatin is repositioned to the nuclear lamina. Because of the strong interaction of GFP and GBP with a K_D in the subnanomolar range, constitutive heterochromatin is translocated to the nuclear periphery, clearly visible as a green targeting ring. Mid section of one nucleus of an untargeted state is shown: msTALE-GFP (green) and GBP-LaminB1. (C) Schematic representation of DNA replication pattern in embryonic stem cells (adapted scheme from Weber et al., unpublished data). DNA replication foci (red) show five distinct patterns. In contrast to somatic cells, constitutive heterochromatin is replicated in pattern II, prior to DNA at the nuclear lamina in pattern III. Durations of each substage are indicated in the respective scheme on the left, bottom side (from Weber et al., unpublished data). According to the domino model, which is postulating a next-in-line activation of adjacent origins, I speculate that repositioned constitutive heterochromatin could show a delayed DNA replication onset triggered by adjacent origins of the nuclear periphery of pattern III.

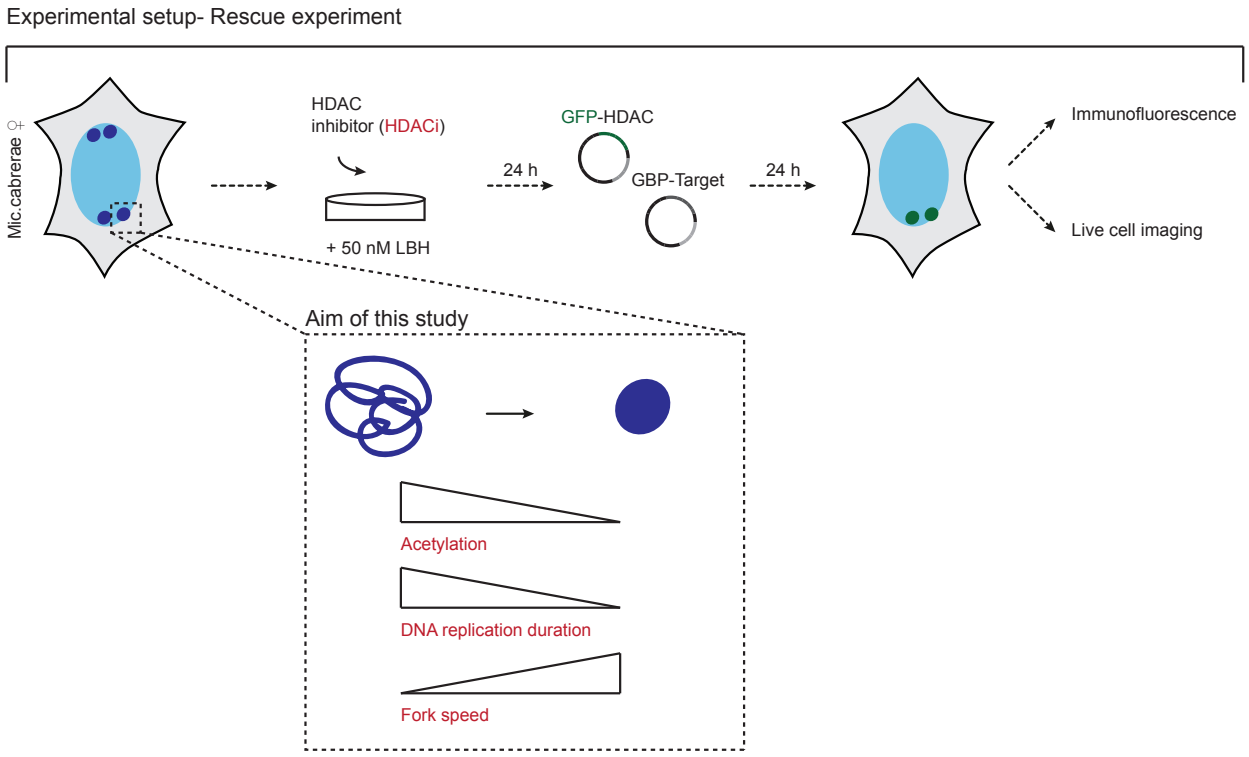

Figure 5.2.: Schematic representation of a rescue experiment to regain histone hypoacetylation after the induction of histone hyperacetylation by treatment with HDAC inhibitor. The level of histone acetylation has an impact on the DNA replication timing of heterochromatic blocks in *Microtus cabrerae* cells. Upon induction of hyperacetylation DNA replication timing is prolonged and the fork speed is decreased. With the treatment of the HDAC inhibitor and the following site-directed targeting of HDACs to the heterochromatic blocks, I would like to assess whether these effect on DNA replication timing can be rescued, leading to the natural shorter DNA replication timing and faster fork speeds.

histone modifications upon repositioning.

As shown in Chapter III, histone acetylation level is a regulator of DNA replication timing in the vole rodent. As HAT vs. HDAC activity might be an additional limiting factor (see 4. Combined discussion and conclusion) for determining the efficiency of origin firing, one could further manipulate the ratio of HATs to HDACs at specific genomic regions via the targeting strategy (Chapter I).

Especially the targeting of chromatin modifiers at defined cell cycle stages should allow the determination whether origin firing can be manipulated by tuning histone acetylation at specific origin maturation stages. The observed effects induced by HDAC inhibition (prolongation of S-phase duration, slower fork speed) (Figure III.6, III.7, III.8, III.S5) might even be rescued to the original DNA replication timing by targeting HDACs after their inhibition by drug-treatment (Figure 5.2). The induced targeted decrease of histone acetylation should exhibit direct effects on DNA replication dynamics, reverting back to shorter DNA replication durations and higher fork speed. Effects on replicated fork speed should be further determined with DNA combing, with and without treatment/targeting.

The predictions arising from my model on the mechanisms by which histone acetylation is likely to influence DNA replication timing (see 4. Combined discussion and conclusion) will be tested experimentally by assessing chromatin binding kinetics. Potential aims and experiment setups include the study of pre-RC formation kinetics, the level and duration of HBO1 binding as well as transient increase of histone acetylation level at DNA replication origins. The assessment of time and level of MCM loading, the availability and recruitment of Cdc45 and other firing factors, such as Mcm10 and GINS, as well as their recycling from early to late origins will shine light on their role, function and involvement in origin determination and firing in mammalian origins. Targeting of HBO1 to heterochromatic blocks, the study of pre-RC formation kinetics and the staining of components involved in determination and firing of origins should answer the question whether the availability and recruitment of Cdc45 or other firing factors, such as MCM10 and GINS are affected by the targeting.

Accompanying the quest for answers to our biological questions, there is a need to continue the development of tools for

an user-independent S-phase pattern recognition and classification program while directly implementing a colocalization analysis. This should allow a higher throughout analysis of imaging, enabling whole genome screening for S-phase progression regulators.

6 General references

1. Watson, J. D. & Crick, F. H. Molecular structure of nucleic acids; a structure for deoxyribose nucleic acid. *Nature* **171,** 737–8 (1953).
2. Meselson, M. & Stahl, F. W. The Replication of DNA in Escherichia Coli. *Proc Natl Acad Sci U S A* **44,** 671–82 (1958).
3. Kornberg, A. Biologic synthesis of deoxyribonucleic acid. *Science* **131,** 1503–8 (1960).
4. Chagin, V. O., Stear, J. H. & Cardoso, M. C. Organization of DNA replication. *Cold Spring Harb Perspect Biol* **2,** a000737 (2010).
5. Milner, G. R. Changes in chromatin structure during interphase in human normoblasts. *Nature* **221,** 71–2 (1969).
6. Aten, J. A., Bakker, P. J., Stap, J., Boschman, G. A. & Veenhof, C. H. DNA double labelling with IdUrd and CldUrd for spatial and temporal analysis of cell proliferation and DNA replication. *Histochem J* **24,** 251–9 (1992).
7. Gratzner, H. G. Monoclonal antibody to 5-bromo- and 5-iododeoxyuridine: A new reagent for detection of DNA replication. *Science* **218,** 474–5 (1982).
8. Nakamura, H., Morita, T. & Sato, C. Structural organizations of replicon domains during DNA synthetic phase in the mammalian nucleus. *Exp Cell Res* **165,** 291–7 (1986).
9. Nakayasu, H. & Berezney, R. Mapping replicational sites in the eucaryotic cell nucleus. *J Cell Biol* **108,** 1–11 (1989).
10. O'Keefe, R. T., Henderson, S. C. & Spector, D. L. Dynamic organization of DNA replication in mammalian cell nuclei: spatially and temporally defined replication of chromosome-specific alpha-satellite DNA sequences. *J Cell Biol* **116,** 1095–110 (1992).
11. Cardoso, M. C. *et al.* Mapping and use of a sequence that targets DNA ligase I to sites of DNA replication in vivo. *J Cell Biol* **139,** 579–87 (1997).
12. Leonhardt, H. *et al.* Dynamics of DNA replication factories in living cells. *J Cell Biol* **149,** 271–80 (2000).
13. Cardoso, M. C., Leonhardt, H. & Nadal-Ginard, B. Reversal of terminal differentiation and control of DNA replication: cyclin A and Cdk2 specifically localize at subnuclear sites of DNA replication. *Cell* **74,** 979–92 (1993).
14. Heinz, K. S. *et al.* Peripheral re-localization of constitutive heterochromatin advances its replication timing and impairs maintenance of silencing marks. *Nucleic Acids Res* **46,** 6112–6128 (2018).
15. Baddeley, D. *et al.* Measurement of replication structures at the nanometer scale using super-resolution light microscopy. *Nucleic Acids Res* **38,** e8 (2010).
16. Alexandrova, O., Solovei, I., Cremer, T. & David, C. N. Replication labeling patterns and chromosome territories typical of mammalian nuclei are conserved in the early metazoan Hydra. *Chromosoma* **112,** 190–200 (2003).
17. Pope, B. D., Hiratani, I. & Gilbert, D. M. Domain-wide regulation of DNA replication timing during mammalian development. *Chromosome Res* **18,** 127–36 (2010).
18. Cremer, T. & Cremer, C. Chromosome territories, nuclear architecture and gene regulation in mammalian cells. *Nat Rev Genet* **2,** 292–301 (2001).
19. Sadoni, N., Cardoso, M. C., Stelzer, E. H., Leonhardt, H. & Zink, D. Stable chromosomal units determine the spatial and temporal organization of DNA replication. *J Cell Sci* **117,** 5353–65 (2004).
20. Craig, J. M. & Bickmore, W. A. Chromosome bands–flavours to savour. *Bioessays* **15,** 349–54 (1993).
21. Huberman, J. A. & Riggs, A. D. Autoradiography of chromosomal DNA fibers from Chinese hamster cells. *Proc Natl Acad Sci U S A* **55,** 599–606 (1966).
22. Cayrou, C. *et al.* New insights into replication origin characteristics in metazoans. *Cell Cycle* **11,** 658–67 (2012).
23. Cayrou, C. *et al.* Genome-scale analysis of metazoan replication origins reveals their organization in specific but flexible sites defined by conserved features. *Genome Res* **21,** 1438–49 (2011).
24. Gilbert, D. M. Making sense of eukaryotic DNA replication origins. *Science* **294,** 96–100 (2001).
25. Hyrien, O. Peaks cloaked in the mist: the landscape of mammalian replication origins. *J Cell Biol* **208,** 147–60 (2015).
26. Vashee, S. *et al.* Sequence-independent DNA binding and replication initiation by the human origin recognition complex. *Genes Dev* **17,** 1894–908 (2003).

27. Schwaiger, M. & Schubeler, D. A question of timing: emerging links between transcription and replication. *Curr Opin Genet Dev* **16,** 177–83 (2006).

28. Li, J. J. & Kelly, T. J. Simian virus 40 DNA replication in vitro. *Proc Natl Acad Sci U S A* **81,** 6973–7 (1984).

29. Nossal, N. G. Protein-protein interactions at a DNA replication fork: bacteriophage T4 as a model. *FASEB J* **6,** 871–8 (1992).

30. Bell, S. P. & Dutta, A. DNA replication in eukaryotic cells. *Annu Rev Biochem* **71,** 333–74 (2002).

31. Dutta, A. & Bell, S. P. Initiation of DNA replication in eukaryotic cells. *Annu Rev Cell Dev Biol* **13,** 293–332 (1997).

32. Casas-Delucchi, C. S. & Cardoso, M. C. Epigenetic control of DNA replication dynamics in mammals. *Nucleus* **2,** 370–82 (2011).

33. Chesnokov, I. N. Multiple functions of the origin recognition complex. *Int Rev Cytol* **256,** 69–109 (2007).

34. Ohta, S., Tatsumi, Y., Fujita, M., Tsurimoto, T. & Obuse, C. The ORC1 cycle in human cells: II. Dynamic changes in the human ORC complex during the cell cycle. *J Biol Chem* **278,** 41535–40 (2003).

35. Mizushima, T., Takahashi, N. & Stillman, B. Cdc6p modulates the structure and DNA binding activity of the origin recognition complex in vitro. *Genes Dev* **14,** 1631–41 (2000).

36. Harvey, K. J. & Newport, J. Metazoan origin selection: origin recognition complex chromatin binding is regulated by CDC6 recruitment and ATP hydrolysis. *J Biol Chem* **278,** 48524–8 (2003).

37. Maiorano, D., Lemaitre, J. M. & Mechali, M. Stepwise regulated chromatin assembly of MCM2-7 proteins. *J Biol Chem* **275,** 8426–31 (2000).

38. Shin, J. H., Grabowski, B., Kasiviswanathan, R., Bell, S. D. & Kelman, Z. Regulation of minichromosome maintenance helicase activity by Cdc6. *J Biol Chem* **278,** 38059–67 (2003).

39. Miotto, B. & Struhl, K. HBO1 histone acetylase activity is essential for DNA replication licensing and inhibited by Geminin. *Mol Cell* **37,** 57–66 (2010).

40. Labib, K. & Diffley, J. F. Is the MCM2-7 complex the eukaryotic DNA replication fork helicase? *Curr Opin Genet Dev* **11,** 64–70 (2001).

41. Walter, J. & Newport, J. Initiation of eukaryotic DNA replication: origin unwinding and sequential chromatin association of Cdc45, RPA, and DNA polymerase alpha. *Mol Cell* **5,** 617–27 (2000).

42. Hyrien, O., Marheineke, K. & Goldar, A. Paradoxes of eukaryotic DNA replication: MCM proteins and the random completion problem. *Bioessays* **25,** 116–25 (2003).

43. Laskey, R. A. & Madine, M. A. A rotary pumping model for helicase function of MCM proteins at a distance from replication forks. *EMBO Rep* **4,** 26–30 (2003).

44. Masata, M., Juda, P., Raska, O., Cardoso, M. C. & Raska, I. A fraction of MCM 2 proteins remain associated with replication foci during a major part of S phase. *Folia Biol (Praha)* **57,** 3–11 (2011).

45. Bousset, K. & Diffley, J. F. The Cdc7 protein kinase is required for origin firing during S phase. *Genes Dev* **12,** 480–90 (1998).

46. Donaldson, A. D., Fangman, W. L. & Brewer, B. J. Cdc7 is required throughout the yeast S phase to activate replication origins. *Genes Dev* **12,** 491–501 (1998).

47. Pasero, P., Duncker, B. P., Schwob, E. & Gasser, S. M. A role for the Cdc7 kinase regulatory subunit Dbf4p in the formation of initiation-competent origins of replication. *Genes Dev* **13,** 2159–76 (1999).

48. Sheu, Y. J. & Stillman, B. The Dbf4-Cdc7 kinase promotes S phase by alleviating an inhibitory activity in Mcm4. *Nature* **463,** 113–7 (2010).

49. Gambus, A. *et al.* GINS maintains association of Cdc45 with MCM in replisome progression complexes at eukaryotic DNA replication forks. *Nat Cell Biol* **8,** 358–66 (2006).

50. Kamimura, Y., Tak, Y. S., Sugino, A. & Araki, H. Sld3, which interacts with Cdc45 (Sld4), functions for chromosomal DNA replication in Saccharomyces cerevisiae. *EMBO J* **20,** 2097–107 (2001).

51. Kanemaki, M. & Labib, K. Distinct roles for Sld3 and GINS during establishment and progression of eukaryotic DNA replication forks. *EMBO J* **25,** 1753–63 (2006).

52. Homesley, L. *et al.* Mcm10 and the MCM2-7 complex interact to initiate DNA synthesis and to release replication factors from origins. *Genes Dev* **14,** 913–26 (2000).

53. Merchant A.M., K. Y. C. Y. L. M. & Tye, B. K. A lesion in the DNA replication initiation factor Mcm10 induces pausing of elongation forks through chromosomal replication origins in Saccharomyces cerevisiae. *Molecular and cellular biology* **17,** 3261–3271 (1997).

54. Aparicio, O. M., Stout, A. M. & Bell, S. P. Differential assembly of Cdc45p and DNA polymerases at early and late origins of DNA replication. *Proc Natl Acad Sci U S A* **96,** 9130–5 (1999).

55. Aparicio, O. M., Weinstein, D. M. & Bell, S. P. Components and dynamics of DNA replication complexes in S. cerevisiae: redistribution of MCM proteins and Cdc45p during S phase. *Cell* **91,** 59–69 (1997).

56. Pacek, M., Tutter, A. V., Kubota, Y., Takisawa, H. & Walter, J. C. Localization of MCM2-7, Cdc45, and GINS to the site of DNA unwinding during eukaryotic DNA replication. *Mol Cell* **21,** 581–7 (2006).

57. Zou, L. & Stillman, B. Assembly of a complex containing Cdc45p, replication protein A, and Mcm2p at replication origins controlled by S-phase cyclin-dependent kinases and Cdc7p-Dbf4p kinase. *Mol Cell Biol* **20,** 3086–96 (2000).

58. Masumoto, H., Sugino, A. & Araki, H. Dpb11 controls the association between DNA polymerases alpha and epsilon and the autonomously replicating sequence region of budding yeast. *Mol Cell Biol* **20,** 2809–17 (2000).

59. Hubscher, U., Maga, G. & Spadari, S. Eukaryotic DNA polymerases. *Annu Rev Biochem* **71,** 133–63 (2002).

60. Moldovan, G. L., Pfander, B. & Jentsch, S. PCNA, the maestro of the replication fork. *Cell* **129,** 665–79 (2007).

61. Campbell, J. L. Eukaryotic DNA replication. *Annu Rev Biochem* **55,** 733–71 (1986).

62. Goldar, A., Labit, H., Marheineke, K. & Hyrien, O. A dynamic stochastic model for DNA replication initiation in early embryos. *PLoS One* **3,** e2919 (2008).

63. Rhind, N. DNA replication timing: random thoughts about origin firing. *Nat Cell Biol* **8,** 1313–6 (2006).

64. Shermoen, A. W., McCleland, M. L. & O'Farrell, P. H. Developmental control of late replication and S phase length. *Curr Biol* **20,** 2067–77 (2010).

65. Stinchcomb, D. T., Struhl, K. & Davis, R. W. Isolation and characterisation of a yeast chromosomal replicator. *Nature* **282,** 39–43 (1979).

66. Theis, J. F. *et al.* Identification of mutations that decrease the stability of a fragment of Saccharomyces cerevisiae chromosome III lacking efficient replicators. *Genetics* **177,** 1445–58 (2007).

67. Eaton, M. L., Galani, K., Kang, S., Bell, S. P. & MacAlpine, D. M. Conserved nucleosome positioning defines replication origins. *Genes Dev* **24,** 748–53 (2010).

68. Diffley, J. F. & Stillman, B. Similarity between the transcriptional silencer binding proteins ABF1 and RAP1. *Science* **246,** 1034–1038 (1989).

69. Rodriguez-Navarro, S. Insights into SAGA function during gene expression. *EMBO Rep* **10,** 843–50 (2009).

70. Vogelauer, M., Rubbi, L., Lucas, I., Brewer, B. J. & Grunstein, M. Histone acetylation regulates the time of replication origin firing. *Mol Cell* **10,** 1223–33 (2002).

71. Mechali, M. Eukaryotic DNA replication origins: many choices for appropriate answers. *Nat Rev Mol Cell Biol* **11,** 728–38 (2010).

72. Sporbert, A., Gahl, A., Ankerhold, R., Leonhardt, H. & Cardoso, M. C. DNA polymerase clamp shows little turnover at established replication sites but sequential de novo assembly at adjacent origin clusters. *Mol Cell* **10,** 1355–65 (2002).

73. Patel, P. K., Arcangioli, B., Baker, S. P., Bensimon, A. & Rhind, N. DNA replication origins fire stochastically in fission yeast. *Mol Biol Cell* **17,** 308–16 (2006).

74. Eshaghi, M. *et al.* Global profiling of DNA replication timing and efficiency reveals that efficient replication/firing occurs late during S-phase in S. pombe. *PLoS One* **2,** e722 (2007).

75. Maya-Mendoza, A., Olivares-Chauvet, P., Shaw, A. & Jackson, D. A. S phase progression in human cells is dictated by the genetic continuity of DNA foci. *PLoS Genet* **6,** e1000900 (2010).

76. Woodfine, K. *et al.* Replication timing of the human genome. *Hum Mol Genet* **13,** 191–202 (2004).

77. Braunstein, J. D., Schulze, D., DelGiudice, T., Furst, A. & Schildkraut, C. L. The temporal order of replication of murine immunoglobulin heavy chain constant region sequences corresponds to their linear order in the genome. *Nucleic Acids Res* **10,** 6887–902 (1982).

78. Raghuraman, M. K. *et al.* Replication dynamics of the yeast genome. *Science* **294,** 115–21 (2001).

79. Calvi, B. R., Lilly, M. A. & Spradling, A. C. Cell cycle control of chorion gene amplification. *Genes Dev* **12,** 734–44 (1998).

80. Hatton, K. S. *et al.* Replication program of active and inactive multigene families in mammalian cells. *Mol Cell Biol* **8,** 2149–58 (1988).

81. Hiratani, I. & Gilbert, D. M. Replication timing as an epigenetic mark. *Epigenetics* **4,** 93–7 (2009).

82. Hyrien, O., Maric, C. & Mechali, M. Transition in specification of embryonic metazoan DNA replication origins. *Science* **270,** 994–7 (1995).

83. Norio, P. *et al.* Progressive activation of DNA replication initiation in large domains of the immunoglobulin heavy chain locus during B cell development. *Mol Cell* **20,** 575–87 (2005).

84. Hyrien, O. & Mechali, M. Chromosomal replication initiates and terminates at random sequences but at regular intervals in the ribosomal DNA of Xenopus early embryos. *EMBO J* **12,** 4511–20 (1993).

85. Hiratani, I. *et al.* Global reorganization of replication domains during embryonic stem cell differentiation. *PLoS Biol* **6,** e245 (2008).

86. Courbet, S. *et al.* Replication fork movement sets chromatin loop size and origin choice in mammalian cells. *Nature* **455,** 557–60 (2008).

87. Lemaitre, J. M., Danis, E., Pasero, P., Vassetzky, Y. & Mechali, M. Mitotic remodeling of the replicon and chromosome structure. *Cell* **123,** 787–801 (2005).

88. Rhind, N. & Gilbert, D. M. DNA replication timing. *Cold Spring Harb Perspect Biol* **5,** a010132 (2013).

89. Drouin, R., Lemieux, N. & Richer, C. L. Analysis of DNA replication during S-phase by means of dynamic chromosome banding at high resolution. *Chromosoma* **99,** 273–80 (1990).

90. MacAlpine, D. M., Rodriguez, H. K. & Bell, S. P. Coordination of replication and transcription along a Drosophila chromosome. *Genes Dev* **18,** 3094–105 (2004).

91. Aran, D., Toperoff, G., Rosenberg, M. & Hellman, A. Replication timing-related and gene body-specific methylation of active human genes. *Hum Mol Genet* **20,** 670–80 (2011).

92. Eaton, M. L. *et al.* Chromatin signatures of the Drosophila replication program. *Genome Res* **21,** 164–74 (2011).

93. Karnani, N., Taylor, C., Malhotra, A. & Dutta, A. Pan-S replication patterns and chromosomal domains defined by genome-tiling arrays of ENCODE genomic areas. *Genome Res* **17,** 865–76 (2007).

94. Lucas, I. *et al.* High-throughput mapping of origins of replication in human cells. *EMBO Rep* **8,** 770–7 (2007).

95. Bartova, E., Krejci, J., Harnicarova, A., Galiova, G. & Kozubek, S. Histone modifications and nuclear architecture: a review. *J Histochem Cytochem* **56,** 711–21 (2008).

96. Casas-Delucchi, C. S. *et al.* Histone acetylation controls the inactive X chromosome replication dynamics. *Nat Commun* **2,** 222 (2011).

97. Lyon, M. F. Gene action in the X-chromosome of the mouse (Mus musculus L.) *Nature* **190,** 372–3 (1961).

98. Plath, K. *et al.* Role of histone H3 lysine 27 methylation in X inactivation. *Science* **300,** 131–5 (2003).

99. Kouzarides, T. Chromatin modifications and their function. *Cell* **128,** 693–705 (2007).

100. Donaldson, A. D. Shaping time: chromatin structure and the DNA replication programme. *Trends Genet* **21,** 444–9 (2005).

101. Iizuka, M., Matsui, T., Takisawa, H. & Smith, M. M. Regulation of replication licensing by acetyltransferase Hbo1. *Mol Cell Biol* **26,** 1098–108 (2006).

102. Cheng, L. Z., Workman, J. L., Kingston, R. E. & Kelly, T. J. Regulation of DNA replication in vitro by the transcriptional activation domain of GAL4-VP16. *Proc Natl Acad Sci U S A* **89,** 589–93 (1992).

103. Danis, E. *et al.* Specification of a DNA replication origin by a transcription complex. *Nat Cell Biol* **6,** 721–30 (2004).

104. Ghosh, D. Nonparametric methods for analyzing replication origins in genomewide data. *Funct Integr Genomics* **5,** 28–31 (2005).

105. Maric, C., Benard, M. & Pierron, G. Developmentally regulated usage of Physarum DNA replication origins. *EMBO Rep* **4,** 474–8 (2003).

106. Minami, H., Takahashi, J., Suto, A., Saitoh, Y. & Tsutsumi, K. Binding of AlF-C, an Orc1-binding transcriptional regulator, enhances replicator activity of the rat aldolase B origin. *Mol Cell Biol* **26,** 8770–80 (2006).

107. Kohzaki, H. & Murakami, Y. Transcription factors and DNA replication origin selection. *Bioessays* **27,** 1107–16 (2005).

108. Audit, B. *et al.* Open chromatin encoded in DNA sequence is the signature of 'master' replication origins in human cells. *Nucleic Acids Res* **37,** 6064–75 (2009).

109. Field, Y. *et al.* Distinct modes of regulation by chromatin encoded through nucleosome positioning signals. *PLoS Comput Biol* **4,** e1000216 (2008).

110. Zhou, J. *et al.* Cell cycle regulation of chromatin at an origin of DNA replication. *EMBO J* **24,** 1406–17 (2005).

111. Berger, S. L. The complex language of chromatin regulation during transcription. *Nature* **447,** 407–12 (2007).

112. Aggarwal, B. D. & Calvi, B. R. Chromatin regulates origin activity in Drosophila follicle cells. *Nature* **430,** 372–6 (2004).

113. Casas-Delucchi, C. S. *et al.* Histone hypoacetylation is required to maintain late replication timing of constitutive heterochromatin. *Nucleic Acids Res* **40,** 159–69 (2012).

114. Zappulla, D. C., Sternglanz, R. & Leatherwood, J. Control of replication timing by a transcriptional silencer. *Curr Biol* **12,** 869–75 (2002).

115. Knott, S. R., Viggiani, C. J., Tavare, S. & Aparicio, O. M. Genome-wide replication profiles indicate an expansive role for Rpd3L in regulating replication initiation timing or efficiency, and reveal genomic loci of Rpd3 function in Saccharomyces cerevisiae. *Genes Dev* **23,** 1077–90 (2009).

116. Crampton, A., Chang, F., Pappas D. L., J., Frisch, R. L. & Weinreich, M. An ARS element inhibits DNA replication through a SIR2-dependent mechanism. *Mol Cell* **30,** 156–66 (2008).

117. Unnikrishnan, A., Gafken, P. R. & Tsukiyama, T. Dynamic changes in histone acetylation regulate origins of DNA replication. *Nat Struct Mol Biol* **17,** 430–7 (2010).

118. Pryde, F. *et al.* H3 k36 methylation helps determine the timing of cdc45 association with replication origins. *PLoS One* **4,** e5882 (2009).

119. Schwaiger, M., Kohler, H., Oakeley, E. J., Stadler, M. B. & Schubeler, D. Heterochromatin protein 1 (HP1) modulates replication timing of the Drosophila genome. *Genome Res* **20,** 771–80 (2010).

120. Carothers, A. D. & Bickmore, W. A. Models of DNA replication timing in interphase nuclei: an exercise in inferring process from state. *Biometrics* **51,** 750–5 (1995).

121. Bickmore, W. A. & Carothers, A. D. Factors affecting the timing and imprinting of replication on a mammalian chromosome. *J Cell Sci* **108,** 2801–9 (1995).

122. Wong, P. G. *et al.* Chromatin unfolding by Cdt1 regulates MCM loading via opposing functions of HBO1 and HDAC11-geminin. *Cell Cycle* **9,** 4351–63 (2010).

123. Goren, A., Tabib, A., Hecht, M. & Cedar, H. DNA replication timing of the human beta-globin domain is controlled by histone modification at the origin. *Genes Dev* **22,** 1319–24 (2008).

124. Clouaire, T. & Stancheva, I. Methyl-CpG binding proteins: specialized transcriptional repressors or structural components of chromatin? *Cell Mol Life Sci* **65,** 1509–22 (2008).

125. Gribnau, J., Hochedlinger, K., Hata, K., Li, E. & Jaenisch, R. Asynchronous replication timing of imprinted loci is independent of DNA methylation, but consistent with differential subnuclear localization. *Genes Dev* **17,** 759–73 (2003).

126. Schubeler, D. *et al.* Genomic targeting of methylated DNA: influence of methylation on transcription, replication, chromatin structure, and histone acetylation. *Mol Cell Biol* **20,** 9103–12 (2000).

127. Blow, J. J., Gillespie, P. J., Francis, D. & Jackson, D. A. Replication origins in Xenopus egg extract Are 5-15 kilobases apart and are activated in clusters that fire at different times. *J Cell Biol* **152,** 15–25 (2001).

128. Simon, I. *et al.* Asynchronous replication of imprinted genes is established in the gametes and maintained during development. *Nature* **401,** 929–32 (1999).

129. Rothbauer, U. *et al.* A versatile nanotrap for biochemical and functional studies with fluorescent fusion proteins. *Mol Cell Proteomics* **7,** 282–9 (2008).

130. Rothbauer, U. *et al.* Targeting and tracing antigens in live cells with fluorescent nanobodies. *Nat Methods* **3,** 887–9 (2006).

131. Jimenez, R., Carnero, A., Burgos, M., Sanchez, A. & Diaz de la Guardia, R. Achiasmatic giant sex chromosomes in the vole Microtus cabrerae (Rodentia, Microtidae). *Cytogenet Cell Genet* **57,** 56–8 (1991).

132. Marchal, J. A., Acosta, M. J., Bullejos, M., Diaz de la Guardia, R. & Sanchez, A. Sex chromosomes, sex determination, and sex-linked sequences in Microtidae. *Cytogenet Genome Res* **101,** 266–73 (2003).

133. Lob, D. *et al.* 3D replicon distributions arise from stochastic initiation and domino-like DNA replication progression. *Nat Commun* **7,** 11207 (2016).

134. Chagin, V. O. *et al.* 4D Visualization of replication foci in mammalian cells corresponding to individual replicons. *Nat Commun* **7,** 11231 (2016).

135. Wu, R., Singh, P. B. & Gilbert, D. M. Uncoupling global and fine-tuning replication timing determinants for mouse pericentric heterochromatin. *J Cell Biol* **174,** 185–94 (2006).

136. Lebofsky, R., Heilig, R., Sonnleitner, M., Weissenbach, J. & Bensimon, A. DNA replication origin interference increases the spacing between initiation events in human cells. *Mol Biol Cell* **17,** 5337–45 (2006).

137. Letessier, A. *et al.* Cell-type-specific replication initiation programs set fragility of the FRA3B fragile site. *Nature* **470,** 120–3 (2011).

138. Katsuno, Y. *et al.* Cyclin A-Cdk1 regulates the origin firing program in mammalian cells. *Proc Natl Acad Sci U S A* **106,** 3184–9 (2009).

139. Krasinska, L. *et al.* Cdk1 and Cdk2 activity levels determine the efficiency of replication origin firing in Xenopus. *EMBO J* **27,** 758–69 (2008).

140. Thomson, A. M., Gillespie, P. J. & Blow, J. J. Replication factory activation can be decoupled from the replication timing program by modulating Cdk levels. *J Cell Biol* **188,** 209–21 (2010).

141. Ferguson, B. M. & Fangman, W. L. A position effect on the time of replication origin activation in yeast. *Cell* **68,** 333–9 (1992).

142. Friedman, K. L. *et al.* Multiple determinants controlling activation of yeast replication origins late in S phase. *Genes Dev* **10,** 1595–607 (1996).

143. Rhind, N., Yang, S. C. & Bechhoefer, J. Reconciling stochastic origin firing with defined replication timing. *Chromosome Res* **18,** 35–43 (2010).

144. Yang, S. C., Rhind, N. & Bechhoefer, J. Modeling genome-wide replication kinetics reveals a mechanism for regulation of replication timing. *Mol Syst Biol* **6,** 404 (2010).

145. Hamlin, J. L. *et al.* A revisionist replicon model for higher eukaryotic genomes. *J Cell Biochem* **105,** 321–9 (2008).

146. Heichinger, C., Penkett, C. J., Bahler, J. & Nurse, P. Genome-wide characterization of fission yeast DNA replication origins. *EMBO J* **25,** 5171–9 (2006).

147. Stanojcic, S., Lemaitre, J. M., Brodolin, K., Danis, E. & Mechali, M. In Xenopus egg extracts, DNA replication initiates preferentially at or near asymmetric AT sequences. *Mol Cell Biol* **28,** 5265–74 (2008).

148. Wu, P. Y. & Nurse, P. Establishing the program of origin firing during S phase in fission Yeast. *Cell* **136,** 852–64 (2009).

149. Edwards, M. C. *et al.* MCM2-7 complexes bind chromatin in a distributed pattern surrounding the origin recognition complex in Xenopus egg extracts. *J Biol Chem* **277,** 33049–57 (2002).

150. Wyrick, J. J. *et al.* Genome-wide distribution of ORC and MCM proteins in S. cerevisiae: high-resolution mapping of replication origins. *Science* **294,** 2357–60 (2001).

151. Mechali, M. & Kearsey, S. Lack of specific sequence requirement for DNA replication in Xenopus eggs compared with high sequence specificity in yeast. *Cell* **38,** 55–64 (1984).

152. Pollok, S., Bauerschmidt, C., Sanger, J., Nasheuer, H. P. & Grosse, F. Human Cdc45 is a proliferation-associated antigen. *FEBS J* **274,** 3669–3684 (2007).

153. Kohler, C. *et al.* Cdc45 is limiting for replication initiation in humans. *Cell Cycle* **15,** 974–85 (2016).

154. Gorisch, S. M., Wachsmuth, M., Toth, K. F., Lichter, P. & Rippe, K. Histone acetylation increases chromatin accessibility. *J Cell Sci* **118,** 5825–34 (2005).

155. Nan, X. *et al.* Transcriptional repression by the methyl-CpG-binding protein MeCP2 involves a histone deacetylase complex. *Nature* **393,** 386–9 (1998).

156. Kemp, M. G., Ghosh, M., Liu, G. & Leffak, M. The histone deacetylase inhibitor trichostatin A alters the pattern of DNA replication origin activity in human cells. *Nucleic Acids Res* **33,** 325–36 (2005).

157. Simpson, R. T. Nucleosome positioning can affect the function of a cis-acting DNA element in vivo. *Nature* **343,** 387–9 (1990).

158. Bhaskara, S. *et al.* Histone deacetylases 1 and 2 maintain S-phase chromatin and DNA replication fork progression. *Epigenetics Chromatin* **6,** 27 (2013).

159. Mantiero, D., Mackenzie, A., Donaldson, A. & Zegerman, P. Limiting replication initiation factors execute the temporal programme of origin firing in budding yeast. *EMBO J* **30,** 4805–14 (2011).

160. Patel, P. K. *et al.* The Hsk1(Cdc7) replication kinase regulates origin efficiency. *Mol Biol Cell* **19,** 5550–8 (2008).

161. Tanaka, S., Nakato, R., Katou, Y., Shirahige, K. & Araki, H. Origin association of Sld3, Sld7, and Cdc45 proteins is a key step for determination of origin-firing timing. *Curr Biol* **21,** 2055–63 (2011).

162. Li, E., Bestor, T. H. & Jaenisch, R. Targeted mutation of the DNA methyltransferase gene results in embryonic lethality. *Cell* **69,** 915–26 (1992).

163. Thanisch, K. *et al.* Targeting and tracing of specific DNA sequences with dTALEs in living cells. *Nucleic Acids Res* **42,** e38 (2014).

164. Besnard, E. *et al.* Unraveling cell type-specific and reprogrammable human replication origin signatures associated with G-quadruplex consensus motifs. *Nat Struct Mol Biol* **19,** 837–44 (2012).

165. Cadoret, J. C. *et al.* Genome-wide studies highlight indirect links between human replication origins and gene regulation. *Proc Natl Acad Sci U S A* **105,** 15837–42 (2008).

166. Dellino, G. I. *et al.* Genome-wide mapping of human DNA-replication origins: levels of transcription at ORC1 sites regulate origin selection and replication timing. *Genome Res* **23,** 1–11 (2013).

167. Karnani, N., Taylor, C. M., Malhotra, A. & Dutta, A. Genomic study of replication initiation in human chromosomes reveals the influence of transcription regulation and chromatin structure on origin selection. *Mol Biol Cell* **21,** 393–404 (2010).

168. Martin, M. M. *et al.* Genome-wide depletion of replication initiation events in highly transcribed regions. *Genome Res* **21,** 1822–32 (2011).

169. Mesner, L. D. *et al.* Bubble-seq analysis of the human genome reveals distinct chromatin-mediated mechanisms for regulating early- and late-firing origins. *Genome Res* **23,** 1774–88 (2013).

170. Mesner, L. D. *et al.* Bubble-chip analysis of human origin distributions demonstrates on a genomic scale significant clustering into zones and significant association with transcription. *Genome Res* **21,** 377–89 (2011).

171. Mukhopadhyay, R. *et al.* Allele-specific genome-wide profiling in human primary erythroblasts reveal replication program organization. *PLoS Genet* **10,** e1004319 (2014).

172. Picard, F. *et al.* The spatiotemporal program of DNA replication is associated with specific combinations of chromatin marks in human cells. *PLoS Genet* **10,** e1004282 (2014).

173. Sequeira-Mendes, J. *et al.* Transcription initiation activity sets replication origin efficiency in mammalian cells. *PLoS Genet* **5,** e1000446 (2009).

174. Valenzuela, M. S. *et al.* Preferential localization of human origins of DNA replication at the 5'-ends of expressed genes and at evolutionarily conserved DNA sequences. *PLoS One* **6,** e17308 (2011).

7 Annex

7.1 List of abbreviations

ac	acetylated
ACS	autonomous consensus sequence
ARS	autonomous replication sequence
BrdU	5'-bromo-2'-deoxyuridine
C	control
C2C12	mouse myoblast cell line
CAG	Hybrid construct consisting of the cytomegalovirus (CMV) enhancer fused to the chicken beta-actin promoter
Cdc	cell division control protein
CDK	cyclin dependent kinase
Cdt1	chromatin licensing and DNA replication factor 1
CFP	cyan fluorecent protein
ChIP-Seq	Chromatin Immuno- Precipiation and DNA-Sequencing
CI	confidence interval
CMV	cyromegalovirus promoter
CpG	CpG site/island, cytosine nucleotide is followed by a guanine
CRISPR	Clustered Regularly Interspaced Short Palindromic Repeats
DAPI	4'-6-Diamidin-2-phenylindol
dCas9	dead Cas9 enzyme
DDK	Dbf4-dependent kinase
DMEM	Dulbecco's Modified Eagle Medium
DMSO	dimethyl sulfoxide
DNA	deoxyribonucleic acid
DsRed	Discosoma red fluorescent protein
EDTA	Ethylenediaminetetraacetic acid
EdU	5'-ethynyl-2'-deoxyuridine
em	emission
ex	excitation
FACS	fluorescence-activated cell sorting
FISH	fluorescent *In situ* hybridization
GBP	green fluorescent protein binding nanonbody
Gcn5	histone acetyltransferase
GFP	green fluorecent protein
GINS	Go, Ichi, Nii, San replication complex (Japanese for five,one,two,three)
h	hour
H3	Histone H3
H4	Histone H4
HAT	histone acetyl tranferase
HBO1	human acetylase binding to ORC1, H4 specific
HDAC	histone deacetylase
HDACi	HDAC inhibitor
HP1	heterochromatin protein 1
IOD	inter-origin distance
J1	embryonic stem cells
K_D	dissociation constant
LBH	panobinostat, pan-HDAC inhibitor
macroH2a	histone variant
MaSat	major satellite repeat binder

MBD	5’ methycytosine binding domain
MBT	mid-blastula transition
MCM	Mcm2-7 complex
Mcm	minichromosome maintenance protein
me	methylated
Mecp2	methyl-cytosine binding protein 2
MEF	mouse embryonic fibroblasts
Mic.cabrerae	*Microtus cabrerae*, female cell line
min	minute
ms	major satellite
n	sample size
n.s.	not significant
NPC	nuclear pore complex
ORC	origin recognition complex
ORF	open reading frame
Ori	origin of replication
p	probability value
pc	plasmid collection number
PCNA	proliferating cell nuclear antigen
Pol	polymerase
pre-IC	pre-initiation complex
pre-RC	pre-replicative complex
PTM	post-translational modification
PZF	zinc finger protein
RFC	replication factor C
RFP	red fluorecent protein
RNA	ribonucleic acid
ROI	region of interest
RPA	replication protein A
Rpd3	histone deacetylase
RT	room temperature
S-phase	Synthesis phase
Se	early S-phase
Sir2	silent information regulator, histone deacetylase
Sl	late S-phase
Sld3	synthetic lethal mutations with dbp11-1
Sm	mid S-phase
T	targeted
TALE	transcription activator-like effector
TSA	trichostatin A
V_HH	nanobody
Xa	active X chromosome
Xi	inactive X chromosome
3D	three dimensional

7.2 Acknowledgments

In the first place, I would like to thank Prof. Dr. M. Cristina Cardoso, my doctoral supervisor. I am very grateful for your constant support, your advice and your enthusiasm. Thanks for always having an open ear, for your patience and for your confidence. Thanks for taking care of me for all these years, starting already ten years ago as my mentor during my bachelor studies.

For agreeing to be my second referee of this thesis, I would like to thank Prof. Dr. Bodo Laube.

My thanks also belong to Corella for introducing me to the field of targeted manipulations and for doing an excellent job in supervising me during my master's thesis, which laid the foundation to this thesis. Thanks also for the collaboration over the last years.

Furthermore, I would like to thank Prof. Dr. Dusan Cmarko, Prof. Dr. Ivan Raska, Prof. Dr. Juan Alberto and Dr. Ismael Romero-Fernández for their collaboration during my PhD studies.

Also, I'd like to say thanks to Timea, for her collaboration, for her enthusiasm and her good heart.

I thank Bianca, who I already met in my first semester. From the first moment on, it was a pleasure to learn from her, resulting in supervising the BB2 course together.

I like to thank Alex for his support and advice at any time, irrespective of how many microscopes were broken and of how many tasks he was dealing in parallel.

My warmest thanks goes to Anne, who is not only facilitating the daily lab routine, but also for her constant support, her open ear and for being the 'lab mummy'.

Henry taught me that there are no problems and that there are only challenges. I will try to keep this in mind not only for science, but also for my whole life.

For a great working atmosphere, I would like to express my special thanks to all past and present members of the lab: Anica, Annette, Annika, Annina, Beata, Christopher, Daniel, Diana, Emilia, Francesco, Franziska, Hadassah, Hui, Janine, Kai, Katrin, Ksenia, Laurence, Lena, Malini, Nicola, Peng, Simon, Stefania, Steffi, Stephan, Susi, Sven, Wei.

I am grateful for her good heart and for always just being, who she is: Manu.

For everything, especially endless support, input, discussion and valued friendship, I would like to thank the 'Lieblingsbiologen' aka Anne, Cathia, Paddy and Flori. I did not only have colleagues in this lab, I met friends for life, like Anne. Furthermore, I cannot imagine anymore that Cathia wasn't there from the very first moment on. Thanks for becoming such a good friend. Boys- PW and Flori- long time every day see and we managed now for more than 10 years. Thanks for being always there.

I would also like to thank Britta and Marius, not only for proofreading my thesis, but also for being good friends for many years. Marius introduced me to the group and laid the foundation for wonderful years in the lab.

Unfortunately, I cannot name everyone now, but I also would like to thank all the people, who helped me after my accident with all of their support, patience and love.

Special thanks also goes to Uli, Gitta, Ulla and Christoph for their support and help. Thanks for diversion and for valuable friendship: Anna, Betina, Christoph, Eileen, Gregor, Jasmin, Laura, Mailin, Marcus, Patrick and Sarah.

Last but not least, I would like to try to put into words my immense gratitude and love for my family, especially my mum, my dad and my sister. Thanks for your unconditional support, your belief in me and your motivation!

And finally, for Thomas, my best friend and my major support. I can count on you no matter what. I am glad you are there, thanks for all and everything.

7.3 Declaration - Ehrenwörtliche Erklärung

Ich erkläre hiermit ehrenwörtlich, dass ich die vorliegende Arbeit entsprechend den Regeln guter wissenschaftlicher Praxis selbstständig und ohne unzulässige Hilfe Dritter angefertigt habe.

Sämtliche aus fremden Quellen direkt oder indirekt übernommenen Gedanken sowie sämtliche von Anderen direkt oder indirekt übernommenen Daten, Techniken und Materialien sind als solche kenntlich gemacht. Die Arbeit wurde bisher bei keiner anderen Hochschule zu Prüfungszwecken eingereicht.

Darmstadt, den 31. August 2018

_____

(Kathrin Sarah Heinz)

7.4 Curriculum vitæ

Personal Information

Name:	Kathrin Sarah Heinz
Address:	Schnittspahnstrasse 10, 64287 Darmstadt, Germany
Date of birth:	05.10.1988
Place of birth:	Darmstadt

Doctoral studies

09/2013 - 08/2018	**PhD thesis** Technische Universität Darmstadt, Department of Biology Cell Biology and Epigenetics Prof. Dr. M. Cristina Cardoso ”Effect of heterochromatin (com)position on DNA replication timing”

Academic education

01/2011 - 07/2013	**Master thesis** Technische Universität Darmstadt, Department of Biology Cell Biology and Epigenetics Prof. Dr. M. Cristina Cardoso ”Effect of heterochromatin (com)position on DNA replication timing”
10/2011 - 07/2013	**Master of Science:** Technical Biology Technische Universität Darmstadt, Department of Biology Majors: Cell biology and Epigenetics, Microbiology, Neurobiology, Plant technology
04/2011 - 07/2011	**Bachelor thesis** Technische Universität Darmstadt, Department of Biology Cell Biology and Epigenetics Prof. Dr. M. Cristina Cardoso ”Physiological effects of peptides derived from p53 and p21 transported by Cell-penetrating peptides”
10/2008 - 07/2011	**Bachelor of Science:** Biology Technische Universität Darmstadt, Department of Biology Majors: Cell Biology and Epigenetics, Developmental Biology, Genetics, Radiation Biology

Conferences

09/2017	Eukaryotic DNA Replication & Genome Maintenance Cold Spring Harbor Laboratories, New York Oral presentation
03/2016	International Meeting of the German Society for Cell Biology Ludwig-Maximilians-Universität München Poster
03/2016	Chromatin Dynamics Symposium Ludwig-Maximilians-Universität, München Poster

Publications

Heinz, K. S., Casas-Delucchi, C. S., Török, T., Cmarko, D., Rapp, A., Raska, I. and Cardoso, M. C. (2018). Peripheral re-localization of constitutive heterochromatin advances its replication timing and impairs maintenance of silencing marks. Nucleic Acids Res **46**, 6112–6128

Heinz, K. S., Casas-Delucchi,C.S., Alexander Rapp, Romero-Fernandez, I., Marchal, J.A. and Cardoso, M.C. DNA replication dynamics of vole genome and its epigenetic regulation (in submission to ‘Epigenetics and Chromatin’)

Heinz, K. S. and Cardoso, M.C. Targeted manipulation/repositioning of subcellular structures and molecules (submitted to ‘Methods in Molecular Biology’)